



# NORTHWEST GEOLOGY

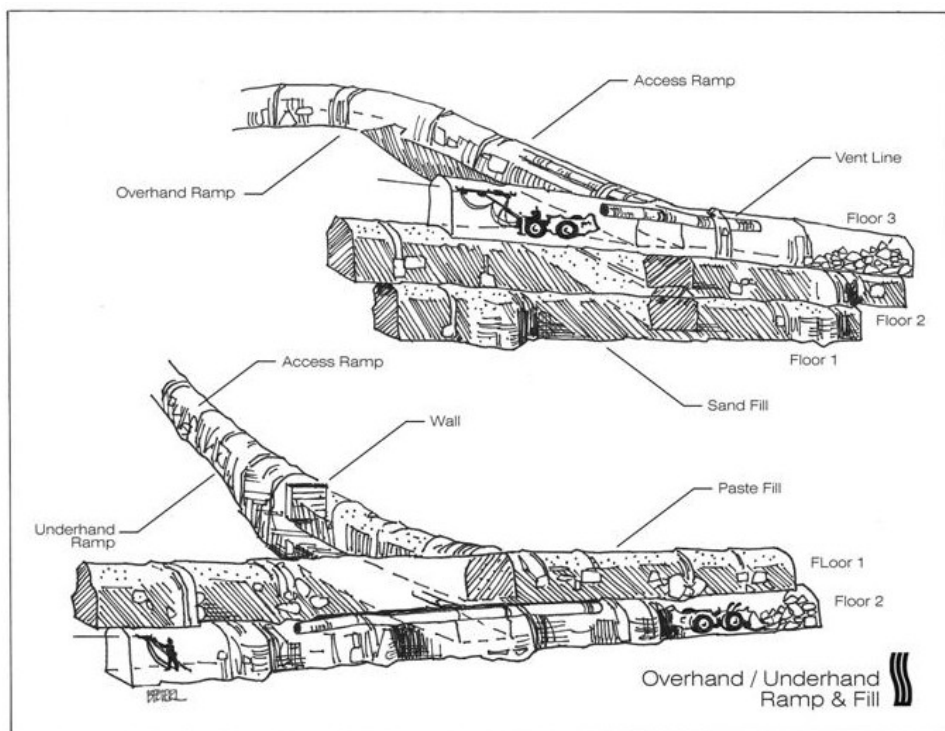
*The Journal of The Tobacco Root Geological Society*

Volume 37, August 2008

33rd Annual Field Conference

## The Red Lodge Area, Montana

July 31—August 3, 2008



Published by The Tobacco Root Geological Society, Inc.

P.O. Box 2734

Missoula, Montana 59806

<http://trgs.org>

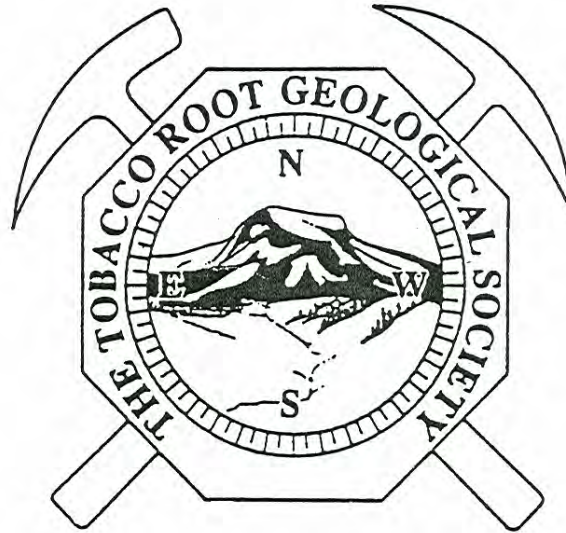
Edited by: Robert C. Thomas and Richard I. Gibson

*Cover: Beartooth Butte (see Thomas, this volume)*

*Above: Overhand ramp and fill mining method at Stillwater Mine (see Koski et al., this volume).*

# The Tobacco Root Geological Society, Inc.

P.O. Box 2734  
Missoula, Montana 59806



## Officers, 2008:

**President: Mike Stickney, Montana Bureau of Mines and Geology, Butte**

**Vice-President: Robert C. Thomas, Dept. of Environmental Sciences,  
U. of Montana-Western, Dillon, MT**

**Treasurer: Ted Antonioli, Montana Mining Association**

**Secretary: Ted Antonioli, Montana Mining Association**

**Webmaster: Dick Gibson, Consultant, Butte**

## Board of Directors, 2008:

**Richard B. Berg, Montana Bureau of Mines and Geology, Butte, MT**

**Bruce E. Cox, Stillwater Mining Co., Nye, MT**

**Marie Marshall Garsjo, Natural Resources Conservation Service, Ft. Worth, TX**

**Richard I. Gibson, Gibson Consulting, Butte, MT**

**Larry Johnson, Consultant, Missoula, MT**

**Larry Smith, Montana Bureau of Mines and Geology, Butte**

**Robert C. Thomas, Dept. of Environmental Sciences, U. of Montana-Western, Dillon, MT**

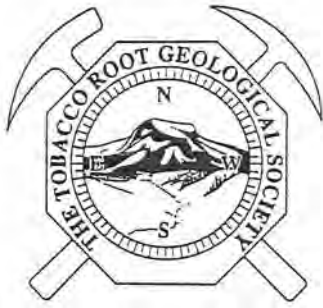
## Conference Organizer, Red Lodge Field Conference:

**Robert C. Thomas, Dept. of Environmental Sciences,  
U. of Montana-Western, Dillon, MT**

**ISSN: 0096-7769**

**© 2008 The Tobacco Root Geological Society, Inc.**

**<http://trgs.org>**



# NORTHWEST GEOLOGY

*The Journal of The Tobacco Root Geological Society*

Volume 37, August 2008

The Red Lodge Area

and other papers

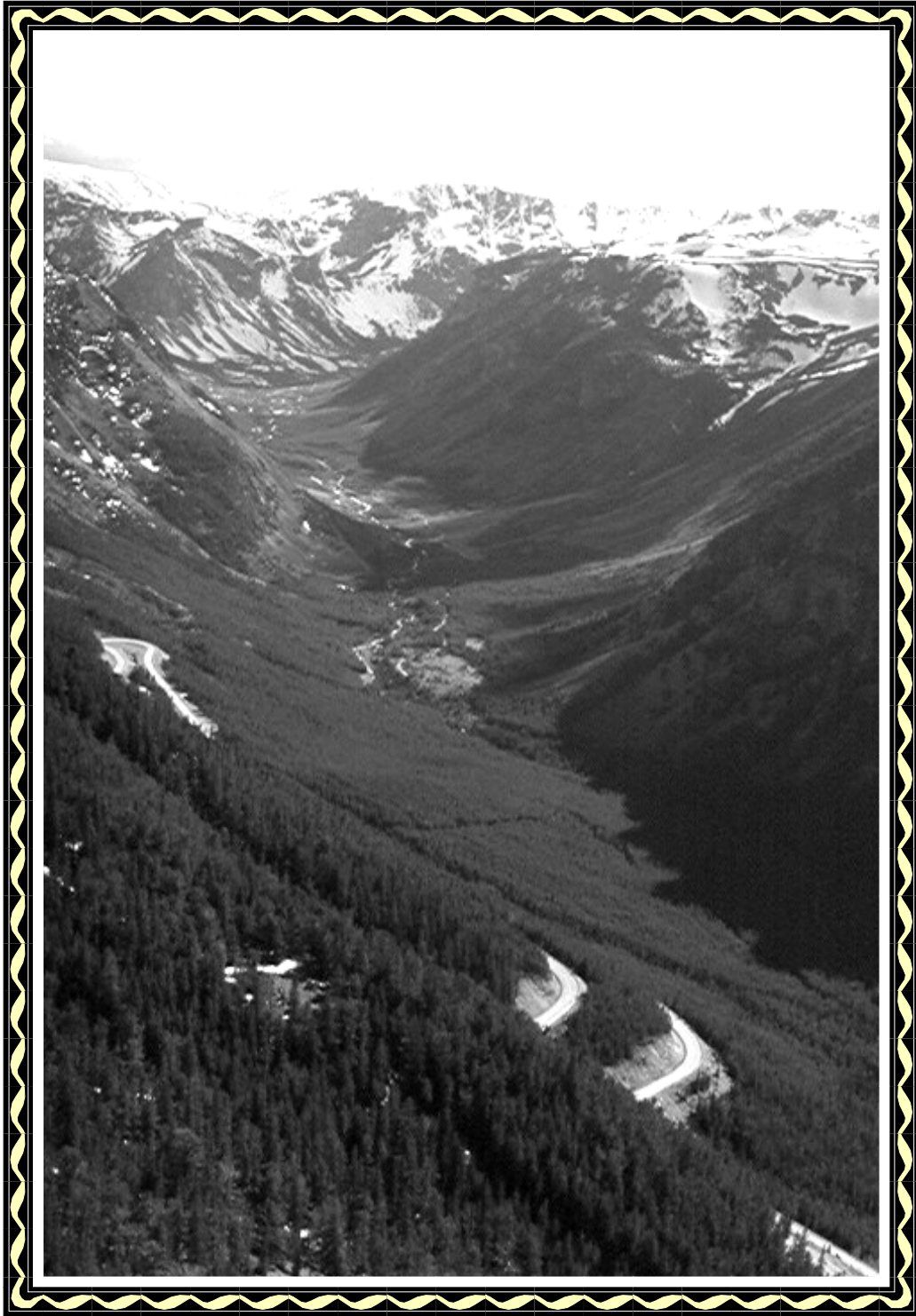
## Table of Contents

Author	Page	Title
Marv Kauffman	1	A brief history of the Yellowstone-Bighorn Research Association (YBRA) geologic field camp, Red Lodge, Montana
Paul A. Mueller, David W. Mogk, Darrell J. Henry, Joseph L. Wooden, David A. Foster	5	Geologic Evolution of the Beartooth Mountains: Insights from Petrology and Geochemistry
David H. Malone, John P. Craddock	21	Recent contributions to the understanding of the Heart Mountain Detachment, Wyoming
Bruce E. Cox, Paul Holick	41	Reverse fault duplication of the J-M Pd/Pt Reef—opportunities for enhanced mine production in the Stillwater Complex, Montana
Kelly R. Probst, Paul A. Mueller, George Kamenov	45	Geochemistry of Cretaceous and Tertiary plutons of the Great Falls Tectonic Zone: Implications for crustal evolution
Paul Mueller, David Foster, Jennifer Gifford, Joseph Wooden, David Mogk	61	Tectonic and stratigraphic implications of detrital zircon suites in Cambrian and Precambrian sandstones from the eastern margin of the Belt Basin
Caleb N. Stroup, Paul K. Link, C. Mark Fanning	69	Provenance of Late Miocene fluvial strata of the Sixmile Creek Formation, southwest Montana: Evidence from detrital zircon
Kevin Lielke	85	The Butcher Creek conglomerate: an enigmatic Paleogene deposit from the northern Gravelly Range of southwestern Montana
David W. Baker, Katelyn E. Gibbs, Allen West	97	Nanodiamonds at the Indian Creek archaeological site near Townsend, Montana: Evidence of an extra-terrestrial impact event
Rich Gaschnig, Jeff Vervoort, Reed S. Lewis, Andy Dufrane	101	Utilizing U-Pb geochronology of inherited zircon in the Atlanta lobe of the Idaho batholith as a probe of the deep crust in southern Idaho: a progress report

**FIELD GUIDES**

Ennis P. Geraghty	111	Field guide to the Benbow Area, Beartooth Mountains Front: Dean to the Golf Course, Stillwater County, Montana
Mike Koski, Mike Pasecznyk, Matt Knight, Ennis Geraghty	123	General geology and mining practices on the J-M Reef, Stillwater Mine, Nye, MT
Mervin J. Bartholomew, Kevin G. Stewart, Donald U. Wise, Heather A. Ballantyne	135	Paleoseismites: Indicators of Laramide tectonism and other events near the Bighorn Basin, Montana and Wyoming
Robert C. Thomas	159	A field guide to the Cambrian section at Beartooth Butte, northwestern Wyoming





Rock Creek and Beartooth Mountains  
—*Photo by Richard I. Gibson*

# A BRIEF HISTORY OF THE YELLOWSTONE-BIGHORN RESEARCH ASSOCIATION (YBRA) GEOLOGIC FIELD CAMP, RED LODGE, MONTANA

**Marv Kauffman**

*Department of Environmental Sciences, The University of Montana Western, Dillon, MT 59725*

---

Prof. Taylor Thom and Richard Field of Princeton's Geology Department initiated the "Red Lodge Project" in 1930 for the "furthering of fundamental geological science and the training of students under exceptionally favorable conditions." There were 19 active participants that first year.

Red Lodge was chosen because of its superb geologic setting in an area that was then relatively unknown. Dr. J. C. Fred Siegfriedt, a Red Lodge doctor and mayor, known as an amateur paleontologist, owned some land near Piney Dell, about five miles southwest of Red Lodge, which he rented as a field station to Taylor Thom in 1931. That year 35 participants and the following year 42, together with family members, occupied the one old house, small cabins, and tents at Piney Dell.

For the next 30 years, Roy Wadsworth, a giant of a coal miner/carpenter, and his wife Florence served as repairman, caretaker, and cook. Participation by many geologists and students from 17 colleges and universities during the first three years of the Red Lodge Project forced the search for new quarters. A dude ranch, Camp Senia, 12 miles up the West Fork valley provided space for the 1933-1935 field seasons.

In searching for a permanent location closer to Red Lodge, Thom learned through the Northern Pacific Railway Company in 1934 of a canceled grazing lease available on the slopes of Mount Maurice. The total price for the 120 acres would be \$420. A newly formed Princeton Geological Association (PGA) raised enough money to purchase



Fanshawe Lodge at YBRA Field Camp.

the site (although there is some question whether the funds were ever paid) and in 1935 construction on the new camp was begun. By the summer of 1936 Roy Wadsworth and his helpers had finished the lodge, a shower house, and fourteen other cabins. A reservoir was built along Howell Gulch, named for Benjamin F. Howell of Princeton, who assisted Thom in choosing this site. According to archival records, the total cost was just over fourteen thousand dollars, including lumber, labor, furnishings, and materials. To celebrate the opening, the 75 camp residents hosted 175 Red Lodge guests to a pig roast on July 17, 1936.

On July 14, 1936, the Yellowstone-Bighorn Research Association (YBRA) was incorporated as a not-for-profit organization in

the state of Montana. Although it never has exercised the option to do so, YBRA is authorized to grant degrees. On November 21, 1936, a five-year lease on the camp was granted to the YBRA by the Princeton Geological Association.

During the early years financial support came from Princeton University, Carter Oil Company, the Northern Pacific Railway, other universities, and many private individuals. In June, 1941, the PGA gave the YBRA an option to buy the camp for \$4000. That option was accepted and on April 24, 1942 the camp property was transferred to YBRA. A resolution was passed by the PGA to reduce the selling price to \$1.00 because of efforts already made by participants during past years.



Interior of Fanshawe Lodge.

During the first 50 years there were at least three dozen doctoral theses produced out of this area by students from Cincinnati, Columbia, Johns Hopkins, Minnesota, Princeton, Wisconsin, and Yale, among others. Undergraduate students participated as field assistants in most of these projects. Since the mid-1950s, undergraduate field courses have been conducted at YBRA by numerous schools, including the Princeton-YBRA field course (now the Penn-YBRA field course), Southern Illinois geology and botany courses, the Penn State University geology program, the Harvard/Yale geology program, and others.

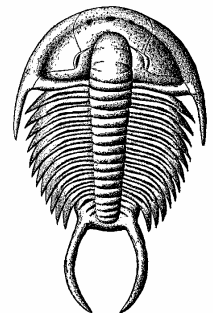
Since the late 1970s, several universities have conducted alumni colleges for their graduates and friends. These week-long programs have introduced many non-geologists to the area's geology and natural history. Begun by Princeton, alumni colleges have now been run by Amherst, Franklin and Marshall, Southern Illinois, and Johns Hopkins universities. In addition to their academic and social values, these programs have made outstanding contributions to maintaining the financial integrity of YBRA.

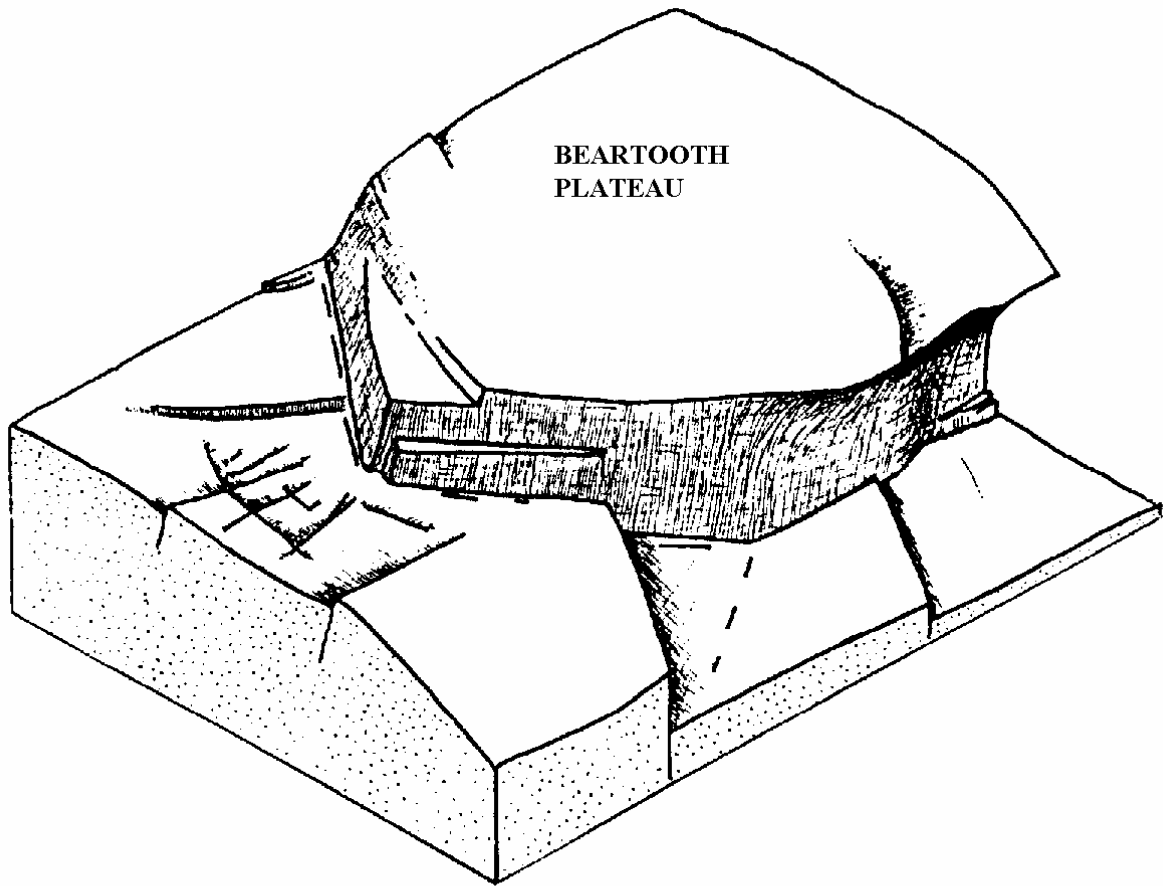
Although research has taken a secondary place to education during the last few decades, numerous graduate and faculty research programs continue to use the YBRA facilities for parts of every field season. Summer institutes for teachers have been held at YBRA, conducted during the 1970s and 1980s primarily by Prof. Erling Dorf of Princeton, and Prof. Will Parsons of Wayne State University. Other uses of the camp have included a writing conference by the American Geological Institute, an NSF-supported Research Experience for Undergraduates (REU) program, and field conferences and symposium meetings of International Geological Congresses and the Bill-

ings and Montana Geological Societies. This will be the first year that the Tobacco Root Geological Society has utilized the YBRA facility.

## REFERENCES

This article was summarized by Marv Kauffman from oral history and various articles, especially "The Red Lodge Project and the YBRA: The Early Years, 1930-1942" by William E. Bonini, Stephen K. Fox, and Sheldon Judson; MGS-YBRA Joint Field Conference and Symposium, 1986





Cambrian surface as mapped and inferred—by Don U. Wise  
in Billings Geological Society, 9th Annual Field Conference  
*Beartooth Uplift and Sunlight Basin* (1958)

# GEOLOGIC EVOLUTION OF THE BEARTOOTH MOUNTAINS: INSIGHTS FROM PETROLOGY AND GEOCHEMISTRY

**Paul A. Mueller**

*Department of Geological Sciences, University of Florida Gainesville, FL 332611*

**David W. Mogk**

*Department of Earth Sciences, Montana State University, Bozeman, MT 59717*

**Darrell J. Henry, Joseph L. Wooden, David A. Foster**

*Department of Geological Sciences, University of Florida Gainesville, FL 332611*

---

## Introduction

The Beartooth Mountains of Montana and Wyoming lie within the Beartooth-Big Horn magmatic zone (BBMZ), a major sub-province of the Wyoming province (Fig. 1; Condie, 1976; Mogk et al., 1992; Mueller et al., 1996; Chamberlain et al., 2003; Mueller and Frost, 2006). The range is dominated by Late Archean igneous and metamorphic rocks of the TTG association (tonalite, trondhjemite, and granodiorite) exhumed by erosion concomitant with and subsequent to movement on a Laramide, high-angle, reverse fault along the eastern margin of the range. Phanerozoic cover is preserved in only a few localities; hence, the range offers an excellent opportunity to examine the Precambrian basement of the northern Rocky Mountains. The eastern part of the Beartooth Range, however, is distinct within the BBMZ and the Wyoming province because of its diversity and the extent of its Archean rock record. Early work by Poldervaart and students (e.g., Eckelmann and Poldervaart, 1957; Harris, 1959; Larsen et al., 1966; Rowan, 1969; Skinner, 1969; Spencer, 1969; Butler, 1969) described and mapped the varied lithologies and structures throughout the eastern Beartooth Mountains, but they did not have adequate geochemical and geochronologic support to accurately ascertain the true ages and petrologic relationships among the lithologies they mapped (e.g., Gast et al., 1958; Giletti, 1966). Application of modern analytical approaches, primarily

ion probe (specifically SHRIMP), however, have led to the recognition of a substantial Middle to Early Archean rock record, which extends to 3.5 Ga for rock ages and 4.0 Ga for detrital zircon ages. In addition to the preservation of older Archean rocks, the Beartooth range is distinguished by the presence of the Late Archean Stillwater layered igneous intrusion (2.7 Ga), which lies on the northeastern border of the Range. The Stillwater Complex was an important resource of chromite in the previous century and of platinum group metals today.

In this paper we provide a general overview (with selected references) of the major events and periods of time that shaped the unique record of crustal evolution preserved in the Beartooth Mountains. The most detailed discussion, however, is reserved for the late Archean magmatic rocks exposed extensively along U.S. Highway 212 (Beartooth Highway) between Red Lodge, MT and the Lamar River Valley in Yellowstone National Park. Although more detailed information on specific outcrops and mileages along Highway 212 are available in numerous guidebooks available from the Montana Bureau of Mines and Geology and in the G.S.A. Field Guide Series volume devoted to the northern Rocky Mountains (e.g., Mueller et al., 1987), Figure 2 depicts specific outcrop locations noted in the text.

**1. The earliest record.** The earliest record of

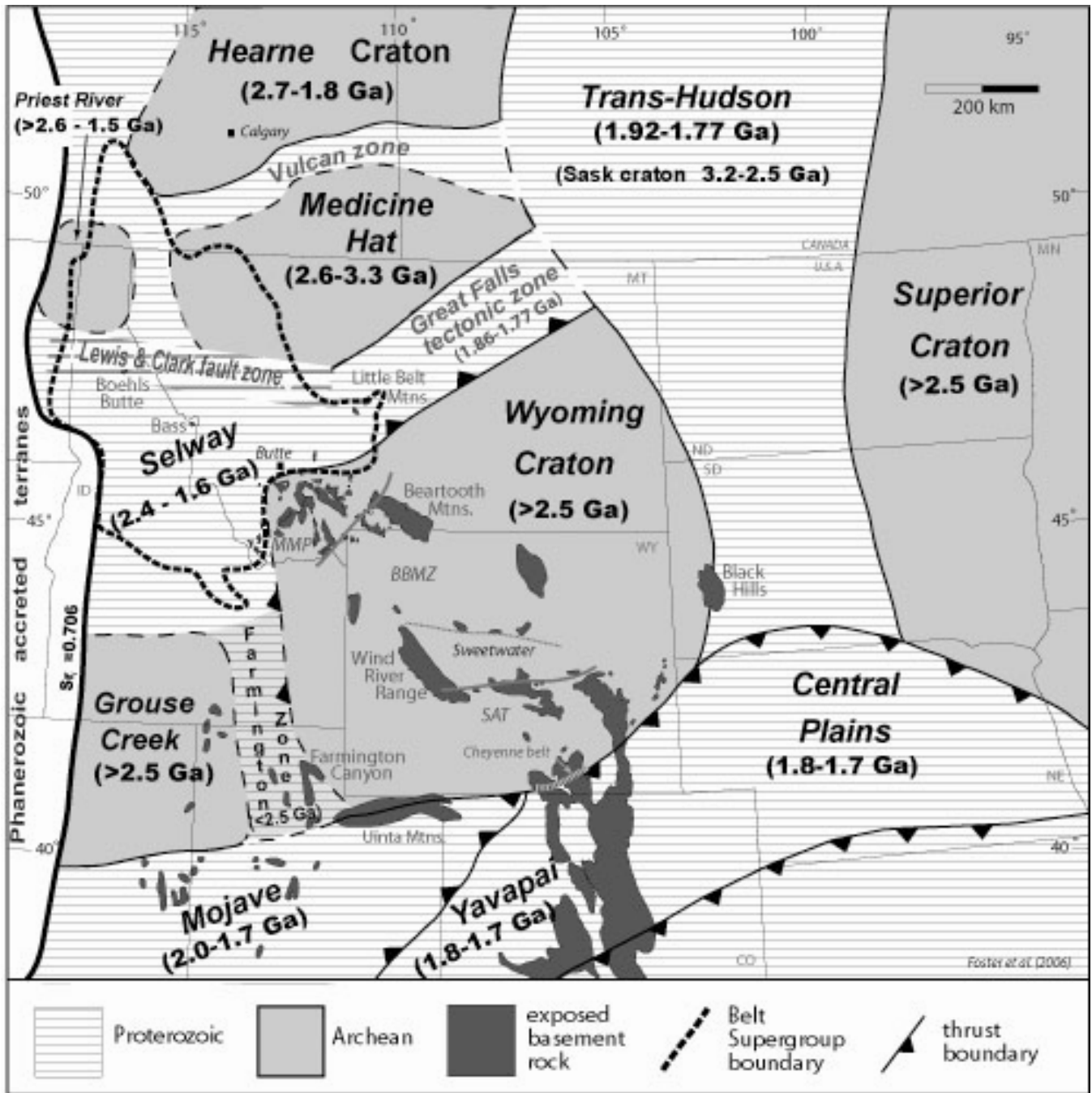
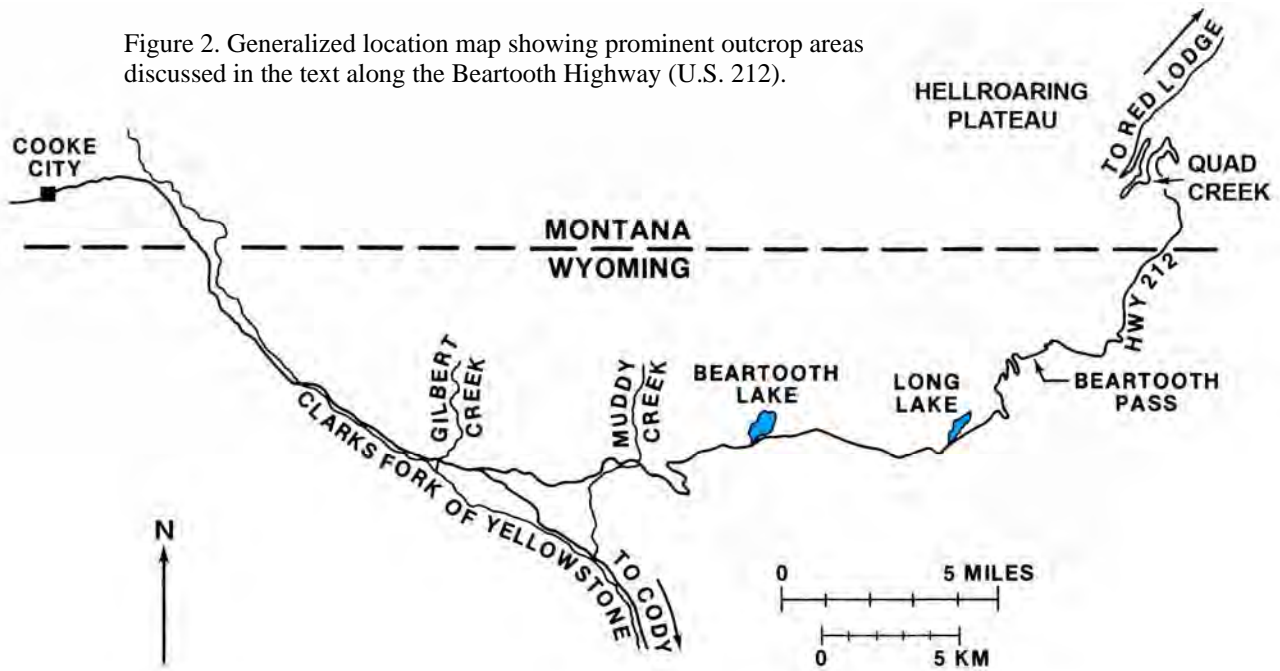


Figure 1. A generalized geologic map showing the relationship of the Beartooth Mountains to the Wyoming Province and its sub-provinces as well as other structural and age provinces of the northern Rocky Mountains.

Figure 2. Generalized location map showing prominent outcrop areas discussed in the text along the Beartooth Highway (U.S. 212).



crustal evolution preserved in the Beartooth Mountains is derived from detrital zircons. Mueller et al. (1996, 1998), for example, analyzed zircons extracted from quartzites interpreted to be Archean based on the nature of the metamorphism and deformation, and the ages of intercalated metasupracrustal rocks. U-Pb ages determined for detrital grains via ion microprobe (SHRIMP) are dominated by 3.2-3.4 Ga grains in all samples. Detrital grains younger than 3.2 Ga were not documented, which suggests deposition after 3.2 Ga. These quartzites are exposed in the southeastern part of the Range as components within strongly deformed and metamorphosed supracrustal sequences described below. The critical observations derived from the detrital record and pertinent to Early Archean crustal evolution are: 1) roughly 25% of the zircons analyzed are >3.5 Ga and ages extend to 4.0 Ga (Fig. 3), and this strongly supports the proposition that rocks in this age range were present in the Beartooth area, as proposed by Wooden and Mueller (1988) based on modeling of common Pb isotopic compositions in the Late Archean felsic rocks; 2) Valley et al. (2005) examined zircons from quartzites from the eastern Beartooths for their O-isotopic compositions and found that oxygen-isotope values of detrital zircons are i) slightly elevated relative to zircons from mantle-derived melts, ii) are similar

to those found in the ancient 4.2-4.4 Ga zircons from Australia, and iii) are consistent with very limited intracrustal recycling of surface materials into the magmas that generated the igneous rocks that were the source of the detrital zircons, and 3) Hf isotopic data for several multi-grain zircons separates for these rocks (Stevenson and Patchett, 1990) also support the presence of older Archean crust in the Beartooth area, as indicated by the Pb isotopic data. These quartzites are well exposed along U.S. Highway 212 as discussed below.

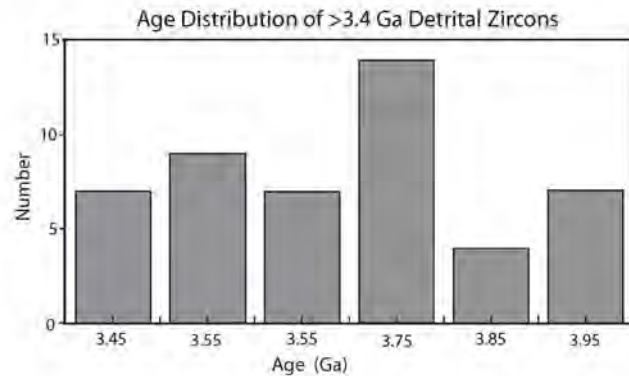


Figure 3. Histogram showing the distribution of the ages (3.4 Ga and older) of detrital zircons reported by Mueller et al. (1998).

## 2. The 3.0-3.5 Ga magmatic and metamorphic record.

Gneissic rocks that are dominantly tonalitic to granodioritic to trondhjemitic in composition (TTG suite) are preserved at varying scales within the volumetrically dominant Late Archean rocks found throughout the range. A wide variety of metasupracrustal rocks (metagneous and metasedimentary) are intercalated with the Late Archean rocks in some locations. Two prominent locations are near U.S. Highway 212 along the switchbacks leading to the Beartooth Plateau (where the highway first crosses Quad Creek near the summit and on Hellroaring Plateau (Fig. 2; Henry et al., 1982; Mueller et al., 1982a, b; Mogk and Henry, 1988). The metamorphosed supracrustal rocks of the Hellroaring Plateau include metabasites, peraluminous gneisses (migmatites), metaironstones, metatramafic rocks, quartzites and quartzofeldspathic gneisses (e.g., James, 1946) last deformed in the late Archean (Rowan and Mueller, 1971). Many of these lithologies preserve petrologic evidence of one, and possibly two, stages of granulite facies metamorphic overprints with an amphibolite facies overprint that is commonly associated with local mylonitization.

Although several of these lithologies provide useful information on the metamorphic evolution of the area, the most instructive lithology is the migmatitic peraluminous gneiss (Fig. 4). The aluminous migmatites of the Hellroaring Plateau and Quad Creek areas can be classified as both metatexites and diatexites, and have typical metamorphic assemblages of quartz + plagioclase + K-feldspar + biotite + sillimanite ± garnet ± cordierite. The peak metamorphic conditions are calculated to be 750-800 C and 6-8 kbar using a variety of independent mineralogical geothermobarometers. Melting appears to be primarily the result of dehydration melting of biotite via reactions such as biotite + sillimanite = garnet + K-feldspar + melt and biotite + sillimanite + quartz = garnet + cordierite + K-feldspar + melt (e.g., Maas and Henry, 2002). It is relatively common to find migmatites with well-

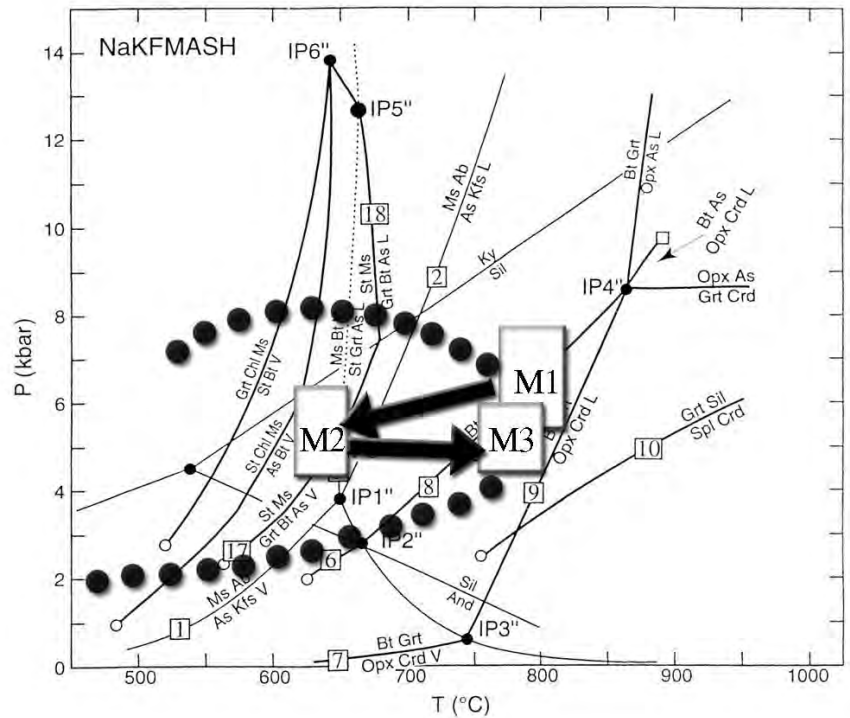


Figure 4. Phase diagram depicting critical relationships of metamorphic mineral parageneses found in Middle Archean lithologies preserved in the Hellroaring Plateau and Quad Creek areas.

developed leucosomes and biotite- and sillimanite-rich melanosomes. These melanosomes are interpreted to be the consequence of crystallization via back reactions from the locally derived granitic melts. As the system cools and the melt crystallizes, the water and alkalis are released allowing many reactions to operate in a retrograde sense. This series of retrograde reactions resulted in the initial stabilization of sillimanite and biotite, and later, local sillimanite dissolution where muscovite develops at lower temperature.

Ages for these rocks are difficult to determine because of the multiple metamorphic overprints (e.g., Mueller, 1979). Quartzofeldspathic gneisses and migmatites that have been examined for their U-Pb zircon systematics suggest a range of ages from 3.5 Ga to 3.0 Ga. Whole-rock Sm-Nd data indicate a range of depleted mantle model ages generally compatible with the ages suggested by U-Pb zircon systematics, but do extend to 4.0 Ga. Common Pb (Pb-Pb) isotopic relations are more cohesive and show a general correlation on an isochron diagram along a reference line corresponding to an age of ~3.4 Ga. This "age" is clearly the result of mixing

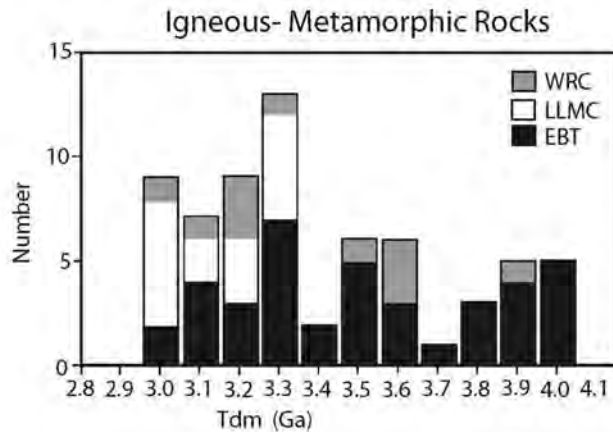


Figure 5. Depleted mantle model ages (Sm-Nd) for metaigneous rocks from the northern Wyoming province. LLMC (Late Archean) and EBT (Middle Archean Hellroaring and Quad Creek rocks) are from the eastern Beartooth Mountains as described in the text. WR samples are from the bimodal metavolcanic (basalt-dacite) sequence in Wind River canyon (Owl Creek Mountains) to demonstrate that the most ancient crustal components in the Beartooth crust apparently influenced magma compositions throughout at least the northern Wyoming Province.

among rocks of different ages as well as re-equilibration during metamorphisms. The observation that the “ages” from these whole rock systems (Pb-Pb and Sm-Nd) lie within the range of rock ages measured by U-Pb zircon geochronology strongly suggests the whole-rock systems were not greatly disturbed by the late Archean magmatic and metamorphic events. It is also clear that this crust interacted strongly with some Late Archean magmatic rocks as evidenced by the presence of Sm-Nd model ages of  $>3.5$  Ga.

**3. Late Archean evolution.** The Late Archean TTG suite of rocks (Wooden et al., 1988a, b) that volumetrically dominate the Beartooth Mountains are the basis for designating this region as part of the BBMZ (e.g., Mogk et al., 1992). Tonalitic to trondhjemitic rocks and gneisses formed in the range 2.8 to 2.9 Ga (U-Pb zircon ages) are exposed extensively throughout the Range. A typical example in the eastern Beartooth Mountains is the Long Lake magmatic complex (LLMC). The LLMC constitutes a diverse assemblage of Late Archean

amphibolitic andesites (AA) to TTG suite rocks that include the Long Lake granite (LLG) and the Long Lake granodiorite (LLGd). These rocks were intruded during the waning stages of a protracted tectonothermal event that imparted gneissic textures to some rocks, while others show few signs of metamorphism or deformation, i.e., dynamothermal metamorphism overlapped in part with this Late Archean magmatic event. Metamorphism was generally in the amphibolite facies and etamorphic foliations and lineations were imparted on the AA and LLGd units as described below. Structurally, studies near Long Lake on U.S. Highway 212 show the rocks exhibit a NW-SE fabric that reflects the dominant structural trend of most of the Archean rocks of the Beartooth Mountains (Warner et al., 1982). Casella (1964, 1969) suggests that this is indicative of regional scale open folds. The dominant lineation plunges 45SE. Some later NNW-SSE basaltic dikes also intrude the LLMC and related rocks throughout the range.

Lithologies range from dioritic to granitic in composition and have quite complex field and geochemical relationships that resulted in their designation as the Long Lake magmatic complex (LLMC), i.e., they do not constitute a single homogeneous batholith. The most common rocks belong to a series of tonalitic to granitic rocks referred to as the Long Lake granite (LLG). The LLG carries inclusions of two other distinguishable units: the Long Lake granodiorite (LLGd) and the andesitic amphibolite (AA). Each of these units has distinctive major-element, trace-element, structural, and petrographic features (e.g., Wooden et al., 1988b; Fig. 6). [Additional compositional data are available in the papers of Warner et al. (1982), Wooden et al. (1982) and Mueller et al. (1985, 1988).]

The area near Long Lake along U.S. Highway 212 is an excellent place to view the weakly foliated, slightly gneissose Long Lake granite (LLG) that locally intrudes the lineated Long Lake granodioritic (LLGd) gneiss. Both units include blocks of strongly-lineated and foliated amphibolite that has basaltic andesite to ande-

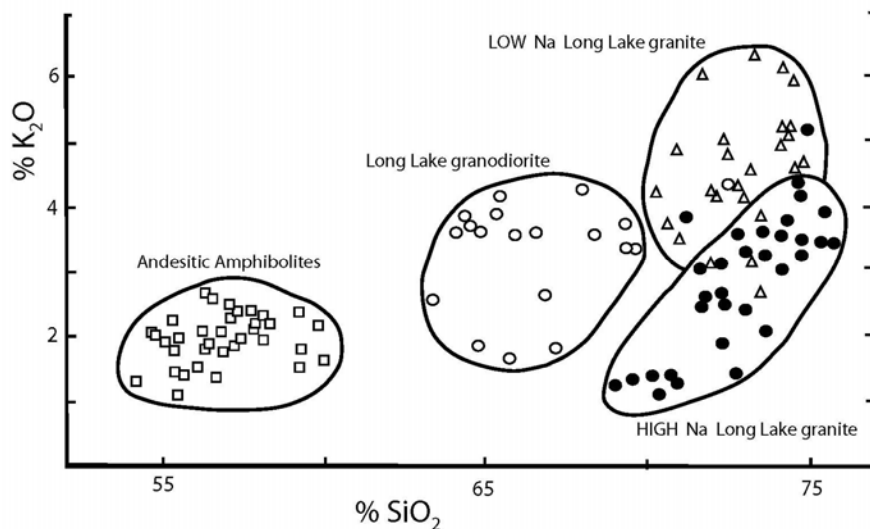


Figure 6. Plot of whole-rock  $K_2O$  vs.  $SiO_2$  as wt. % for members of the Late Archean rocks referred to as the Long Lake magmatic complex (LLMC).

sitic compositions similar to modern orogenic andesites (Wooden et al., 1982; Mueller et al., 1985, Wooden et al., 1988; Mueller et al., 1988) as well as inclusions of apparently older supracrustal rocks (Warner et al., 1982). U-Pb zircon isotopic studies establish a range of ages for all LLMC rock types from ~2.8 Ga to 2.9 Ga (Mueller et al., 1988 and unpubl.). The local gneissic banding, lineation, and granoblastic texture of the recrystallized quartz and feldspars suggests that deformation and recrystallization must have developed at relatively high temperature to allow ductile deformation. This tectonothermal event must have taken place after the Long Lake granodiorite emplacement, but prior to, or coeval with, the massive intrusion of the Long Lake granite. Post metamorphic cooling probably began about 2.75 Ga based on composite whole-rock Rb-Sr and Pb-Pb isochrons for all members of the LLMC (Fig. 7; Mueller et al., 1988). There are some minor amounts of unmetamorphosed quartz-microcline pegmatites with local development of coarse-grained allanite (Warner et

al., 1982); however, ages have not been determined for these veins.

*Long Lake Granite (LLG):* The LLG is a gray to pink plagioclase + K-feldspar + quartz + biotite rock that is medium to coarse-grained (Mueller et al., 1988). On a mesoscopic scale, the LLG is relatively homogeneous with locally abundant inclusions of LLGd and amphibolite. Foliation and gneissic banding are generally poorly developed except near large inclusions. Compositionally, the LLG ranges from tonalite to granite and has a magmatic assemblage of quartz + K-feldspar + plagioclase

(An<sub>24-25</sub>) + biotite + zircon + magnetite + ilmenite + apatite. The rock has an igneous, hypidiomorphic texture consisting predominantly of strained phenocrysts of quartz, cryp-

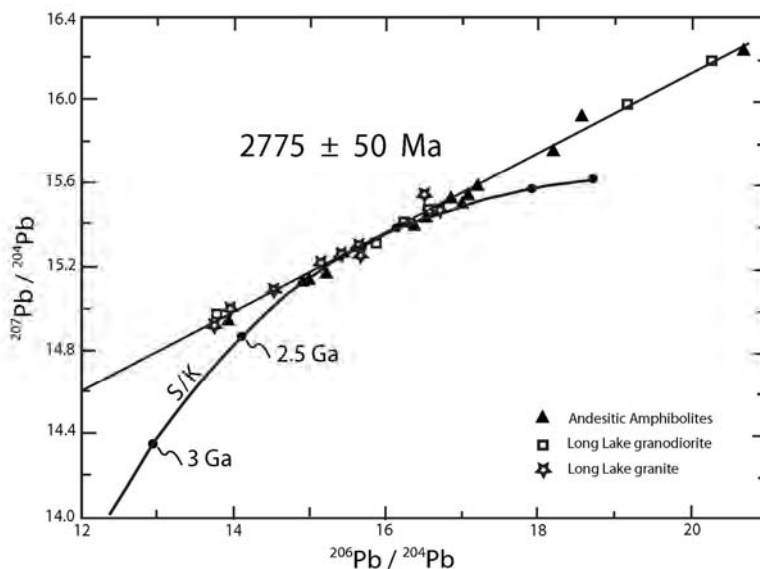


Figure 7. Common Pb compositions for Late Archean (LLMC) rocks showing an age (2.77 Ga) younger than crystallization ages (2.8-2.9 Ga U-Pb zircon ages) and, therefore, indicative of cooling of the LLMC subsequent to the termination of late Archean metamorphism and deformation (often referred to as the Beartooth Orogeny).

toperthitic microcline, antiperthitic plagioclase, and brown-green biotite. The quartz and microcline phenocrysts are locally recrystallized to unstrained quartz and microcline granoblastic aggregates at the margins of phenocrysts. Furthermore, unstrained plagioclase/quartz myrmekitic intergrowths commonly develop between plagioclase and microcline. Trace amounts of magnetite, zircon, apatite, pyrite, and monazite are found in both phenocrysts and recrystallized grains and are considered early-formed magmatic minerals. Medium- to coarse-grained allanite is well developed, especially along late fractures and within recrystallized areas, presumably reflecting the influence of late hydrothermal fluids. Plagioclase is locally altered to sericite and biotite is altered to chlorite + muscovite + rutile + epidote. The LLG retains much of its magmatic character, but is partially recrystallized with several stages of alteration.

Chemically, rocks of the LLG have calc-alkaline to sodic major element patterns with high  $\text{SiO}_2$  (>70%), strongly depleted HREE ( $\text{Lu}=1\text{-}2\times$  chondrites), and moderately enriched LREE ( $\text{La}=100\times$  chondrites) (Fig. 6, 8). These rocks are chemically distinct from the older units in terms of fractionation patterns and potential sources (Wooden et al., 1982;

Mueller et al., 1988). Chemical analyses suggest the presence of two distinct groups, one relatively richer in  $\text{Na}_2\text{O}$  than the other group for a given  $\text{SiO}_2$  or  $\text{K}_2\text{O}$  content (Fig. 6). However, these groups have no distinct areal distribution and cannot be mapped as separate units. Nonetheless, both the high- and low-Na groups exhibit a negative correlation between  $\text{SiO}_2$  and  $\text{Na}_2\text{O}$ , similar to patterns reported in other Archean suites (Wooden et al., 1982). The LLG is relatively low in Sr and Rb, but high in Ba. Mueller et al. (1985) propose the source must have been relatively sodic and siliceous, and contained some garnet or amphibole to accommodate the major- and trace-element constraints.

*Long Lake Granodiorite (LLGd)* The LLGd is a lineated, gray rock that ranges from granite to tonalite (e.g., Wooden et al., 1982). Petrographically, the LLGd is typically an igneous rock with a hypidiomorphic texture. The magmatic assemblage was assemblage quartz + K-feldspar + Plagioclase(An28-32) + biotite + zircon + magnetite + ilmenite + apatite + allanite. The LLGd is a geochemically distinct rock type, despite the mineralogical and grain size similarity to the LLG (Fig. 6, 8). Texturally, the LLGd exhibits a more pronounced lineation and gneissic appearance, and can be recognized as inclusions in LLG in some areas.

The LLGd can be described as a calc-alkaline granodiorite lower in  $\text{SiO}_2$  (65-70%) and  $\text{Na}_2\text{O}$  relative to  $\text{K}_2\text{O}$  than the LLG (Fig. 6). Based on the distinctive trace-element abundances that include higher Sr, Ba, and REE contents, the LLGd is clearly separate from LLG (Fig. 6, 8; Wooden and Mueller, 1988). It is not likely, therefore, that the LLG and LLGd are derived from the same source because the source of the LLGd is not likely to

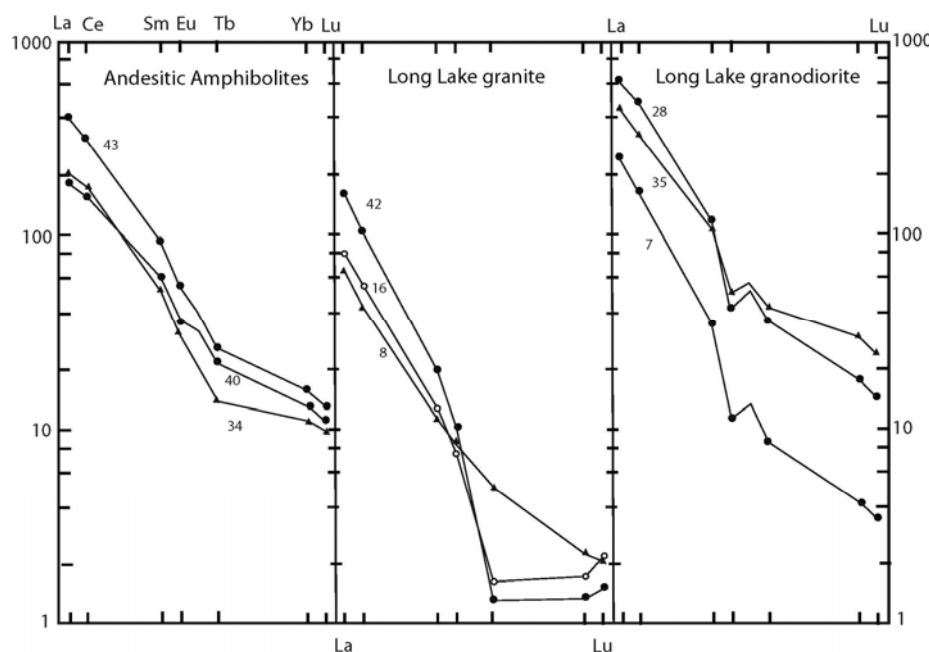


Figure 8. Chondrite-normalized rare earth element abundances for the three main rock units in the Long Lake Magmatic Complex (abbreviations as in text).

contain garnet or amphibole, or be as sodic or siliceous as the source for LLG.

*Andesitic amphibolite (AA)* The AA is a medium to fine-grained metamorphic rock. It is the most abundant and recognizable rock type included within the LLG. Inclusions of the AA vary in size from less than 1 m to more than a km throughout the eastern and central Bear-tooth Mountains. These rocks are generally linedated with aligned hornblende (pargasitic to edenitic hornblendes) and biotite. Warner et al. (1982) note an agglomeratic phase with numerous clasts of metasedimentary rock and gneisses. The clasts, in turn, have random foliations relative to the surrounding AA. The dominant lineation plunges 45° to the SE. Hornblende-plagioclase geothermometry typically yields 750-820°C. Its major element chemistry is clearly distinct from the more granitic member of the LLMC (Fig. 6).

The AA ranges from basaltic andesite to andesite in composition and is comprised of plagioclase, amphibole, biotite, and epidote. Geochemically, major element abundances indicate the AA can be divided into tholeiitic and calc-alkaline groups that both exhibit highly distinctive trace element contents (Mueller et al., 1983), though the tholeiitic rocks are generally characterized by higher incompatible-element contents. The LREE abundances in these rocks vary widely, i.e., 50-500 times chondrites (Fig. 8, 9). The positive correlation between Ce and Sr suggest that both elements are behaving incompatibly and the relative depletion of high field strength elements (HFSE; Ti, Zr, Hf, Nb, etc)) parallels that found in modern convergent margins magmas (Fig. 9). Based on the relatively high levels and wide ranges of the incompatible trace elements, Mueller et al. (1983, 1988) suggest that these rocks were formed in a convergent margin environment, but could not have been produced by conventional partial

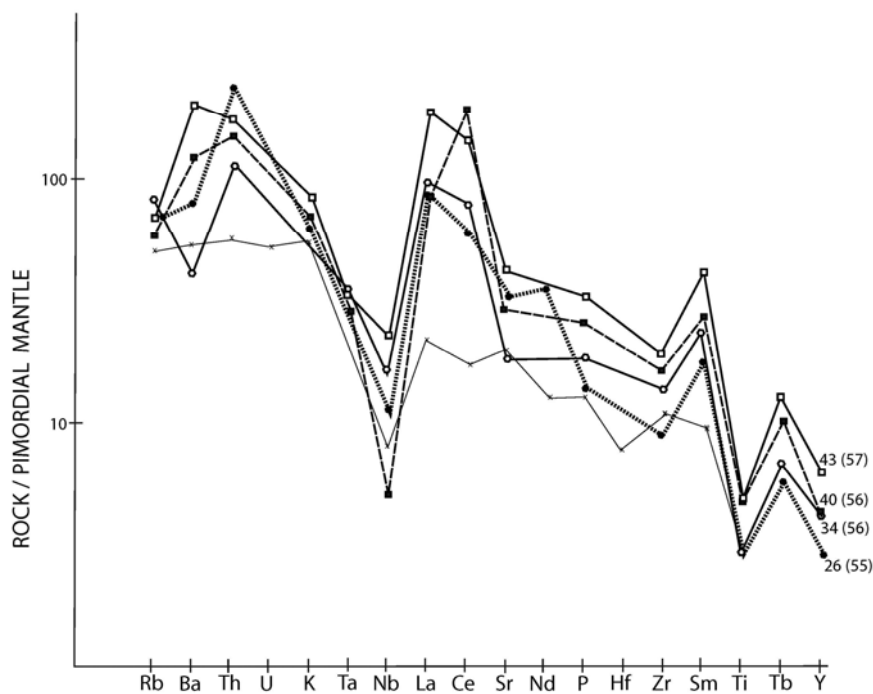


Figure 9. Normalized plot of incompatible elements utilizing element abundances and sequence from Wood et al. (1979). Numbers adjacent to individual patterns (e.g., 43, 57, etc.) refer to sample numbers from Mueller et al. (1983); numbers in parentheses are wt. % SiO<sub>2</sub>. Samples 43 and 40 are tholeiitic; samples 26 and 34 are of calc-alkaline affinity. X indicates the average basaltic andesite of Java and Bali (Whitford et al., 1979) as an example of modern subduction-related rocks of comparable overall chemistry.

melting and fractional crystallization processes in the mantle without a contribution of another phase(s) enriched in incompatible elements. They further indicate that the source of the magmas was metasomatically altered mantle with metasomatism occurring immediately prior to melting based on Sm-Nd isotopic systematics. Relative to the AA, the distinctive Ba and Sr contents, and the Eu anomaly of the LLGd make it difficult to produce the LLGd from the same source as that which formed the more mafic AA or to derive it by fractional crystallization from the AA. It has been suggested that incompatible-enriched fluids were likely involved in the formation of both rocks, but interacted with fundamentally different sources.

**4. Stillwater complex.** The Stillwater layered igneous complex was emplaced along the eastern margin of the Range in latest Archean time (~2.7 Ga), subsequent to the emplacement of the ubiquitous, Late Archean tonalitic and trondhjemitic rock sequences (Nunes and Tilton, 1971; Mueller and Wooden, 1976). The complex was intruded into a diverse suite of apparently undeformed metasupracrustal rocks, including quartzites, schists, and banded iron formation. The hornfels aureole of the Stillwater complex has variously been described by Page (1977), Labotka et al (1982), Labotka and Kath (2001), Vaniman et al., 1980; and Thomson (2008). Hornfelsed schists dominate and include orthopyroxene-cordierite and anthophyllite-cordierite hornfelses, with evidence of local partial melting (Thomson, 2008). Metamorphic conditions in the aureole have been estimated in the range of 700°-800°C and 2-3.7 Kbar (Labotka and Kath, 2001; Thomson, 2008). The metasupracrustal rocks in the aureole have typical major-element compositions, but possess distinctively high transition metal contents (e.g., Beltrame et al., 1982; Geissman and Mogk, 1988) that distinguish them from other metasupracrustal rocks in the range, such as those immediately across the Mill Creek-Stillwater Fault Zone (MCSFZ) on Lake Plateau area immediately to the south. Discontinuities in structural style, metamorphic grade (garnet-cordierite-sillimanite schists in the Lake Plateau area have estimated metamorphic conditions of 650°-680°C and ~8 Kbar), age of the adjacent granitic gneisses (~2.8 Ga), and distinct whole-rock compositions of metasupracrustal rocks on either side of the MCSFZ led to the interpretation by Geissman and Mogk (1988) that the Stillwater Complex along with its aureole was tectonically emplaced against the main Beartooth massif after it crystallized, about 2.7 Ga ago.

**5. Proterozoic activity.** Proterozoic deformation and magmatic activity was largely limited to intrusion of mafic dikes (Prinz, 1964; Condie et al., 1969; Mueller and Rogers, 1973; Mueller and Baadsgaard, 1973; Armbrustmacher and Simons, 1977; Harlan et al., 1997). These rocks have not been dated successfully in many in-

stances, however, ages currently reported range from Archean to Proterozoic, including relatively alkaline compositions that appear confined to a single event at ~1.4 Ga and a group of quartz tholeiites at ~700 Ma (Baadsgaard and Mueller, 1971; see also: [http://serc.carleton.edu/files/NAGTWorkshops/petrology03/Mafic\\_dykes.doc](http://serc.carleton.edu/files/NAGTWorkshops/petrology03/Mafic_dykes.doc)). Most dikes, however, are of tholeiitic composition and appear to be Archean. Other Proterozoic activity is largely confined to the western margin of the range (e.g., Montgomery and Lytwyn, 1984), which borders on the Montana metasedimentary province, a region strongly affected by orogenesis at ~1.8 Ga (e.g., Mueller et al, 2005; Foster et al., 2006).

**6. Phanerozoic History.** Following emplacement of mafic dikes at various times in the Proterozoic, K-Ar mineral ages of 2470 and 2520 Ma for muscovite in pegmatites and of 2290 and 2340 Ma for biotite (Gast et al., 1958) indicate that the Precambrian rocks of the range had cooled to less than 300°C by 2290 Ma and have not been subsequently heated above that temperature. In terms of the Range's most recent exhumation history, some Precambrian rocks were exposed by the Paleocene (66-57 Ma) and large amounts of Precambrian detritus was deposited in the Wasatch Formation along the northeast mountain front in the early Eocene (57-50 Ma) (Foote et al., 1961). Simons and Armbrustmacher (1976) argue that the sub-Cambrian surface in the northeastern Beartooth Mountains may have been exposed for up to 30-40 Ma longer than the southwestern part of the range, resulting in the greater erosional rounding. Present topography of the southeastern portion of the Beartooth Mountains (Main Beartooth Massif) is a high altitude flat or gently rolling plateau that has a few patches of Paleozoic sedimentary rocks (e.g., Flathead sandstone along U.S. 212 and at Beartooth Butte/Beartooth Lake; Simons and Armbrustmacher, 1976). The extensive, modern plateau surface is apparently very close to the sub-Cambrian depositional surface (i.e., the Precambrian basement was at the surface in early Cambrian times), which requires that it has been cycled to the surface at least twice during the Phanero-

zoic, once to erode the basement and deposit the Paleozoic sequence and then again to remove the Paleozoic sequence (an ongoing process).

Low temperature thermochronological data can be used to quantify the exhumation history of the Precambrian basement rocks. Omar et al. (1994), for example, presented a comprehensive apatite fission track study of samples from exposures along the Beartooth highway and from an exploration borehole in the basin adjacent to the mountain range. The surface samples span from current elevations of about 3300-1800 meters. The borehole penetrated Phanerozoic clastic sediments and crystalline rocks and at greater depth the Beartooth thrust underlying the sedimentary rocks. The com-

plete profile comprises about 3800 meters of paleocrustal section and provides an excellent snapshot into the Mesozoic and Cenozoic exhumation history of the Beartooth Block (Fig. 10).

The fission track data form two groups. Samples from above about 3100 m elevation give apparent ages of ca. 101-282 Ma with mean fission track lengths of ca. 12-10 microns, which show bimodal or strongly skewed distributions indicating very slow cooling during Phanerozoic time (Fig. 10). Samples collected from elevations below about 3100 m give apparent ages between ca. 57 and 48 Ma with unimodal track length distributions and mean track lengths as long as 13.9 microns, indicating more rapid cooling. Track length correction of the Paleocene apparent ages indicates apparent ages of ca. 60 Ma for the samples from just below 3100 m (Omar et al., 1994). The steep age vs. elevation slope for the younger group of samples indicates that the more rapid Paleocene-Eocene cooling was due to erosional exhumation of the Beartooth block that commenced at ca. 60 Ma. The break in slope between the older and younger groups of samples marks the position of the base of the apatite partial annealing zone prior to exhumation, or a temperature of about 110 degrees C. At least 3.5 km of exhumation occurred starting in Laramide time based on the section of crust with Cenozoic apatite cooling ages. Mean track lengths on the order of 13.8 to 13.2 microns for the samples in this interval indicate cooling rates of about 6-10 degrees C per million years, when we modeled the fission track parameters (Fig. 11). This cooling rate corresponds to an erosion rate of about 0.33-0.5 km/m.y. between about 60 and 50 Ma or upwards of 3.3-5 km of erosion

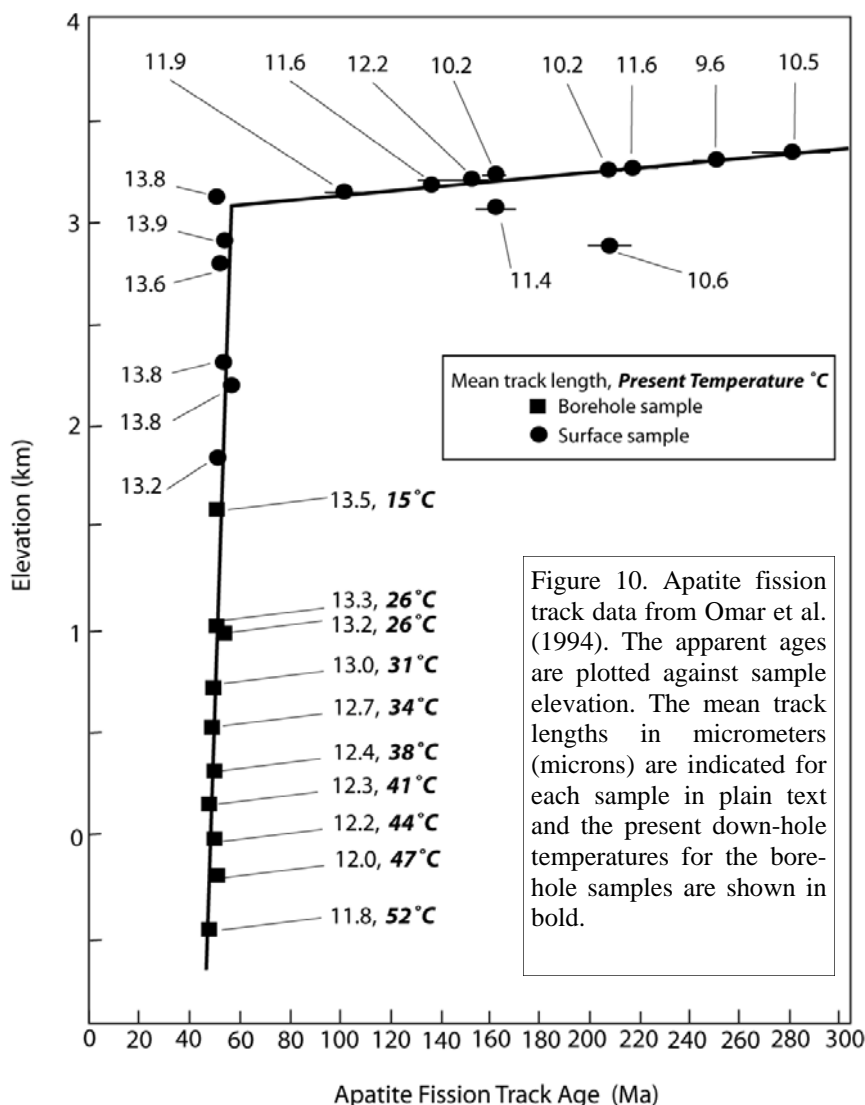
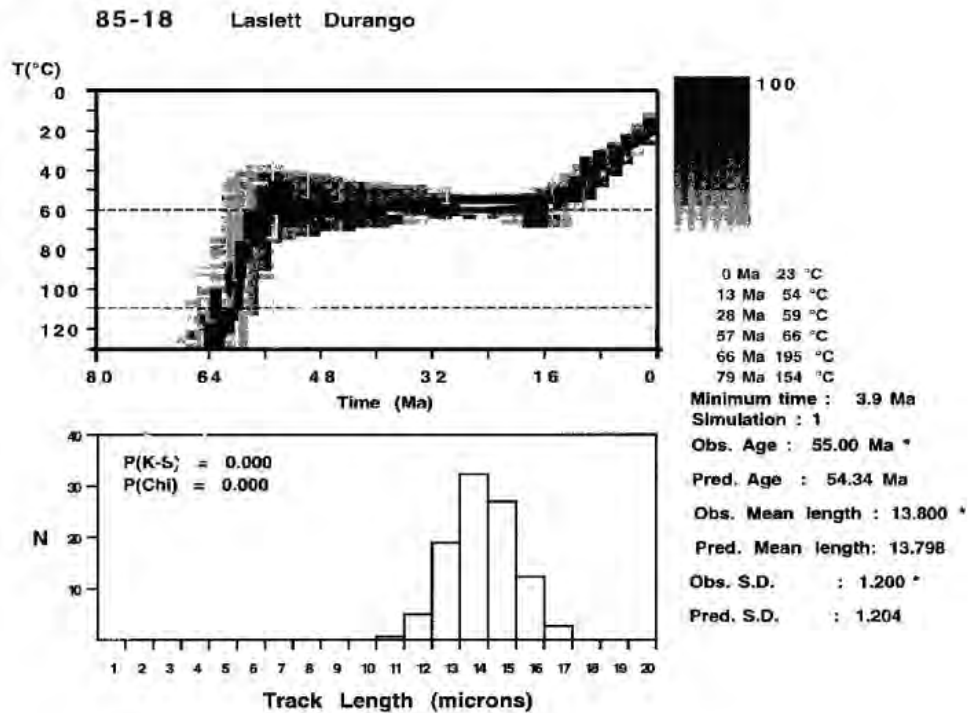


Figure 10. Apatite fission track data from Omar et al. (1994). The apparent ages are plotted against sample elevation. The mean track lengths in micrometers (microns) are indicated for each sample in plain text and the present down-hole temperatures for the borehole samples are shown in bold.

(A)



(B)

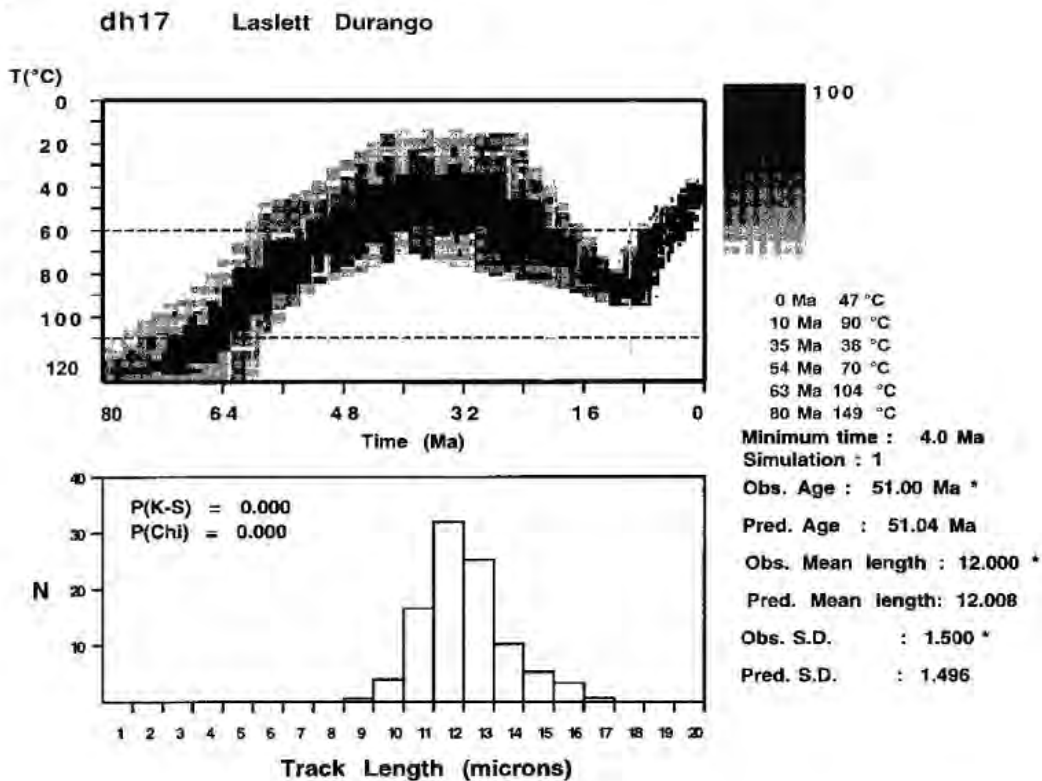


Figure 11.(A) Model cooling paths consistent with the fission track parameters for a typical sample from about 2800 m elevation. (B) Model cooling path consistent with the fission track parameters for a typical sample from intermediate depths in the borehole profile.

assuming an average geothermal gradient of 20 degrees C/km. Presumably this is the time interval when most of the Phanerozoic strata were eroded off of the Precambrian basement (Fig. 11).

Laramide erosional exhumation of the Beartooth basement was due to uplift of the block on the Beartooth Thrust and the development of significant topography. Laramide shortening and uplift of the Beartooth block does not, however, explain all of the fission track data. The shorter mean track lengths of samples from the borehole, and even from the lower elevation outcrop samples, requires a period of heating in Eocene time (due to the deposition of sediments or change in the geothermal gradient) followed by cooling during the last 10 Ma. Our modeling of the fission track parameters shows about 60 degrees of post-Miocene cooling for some samples (Fig. 11). The Miocene to Recent phase of cooling was most likely due to erosional exhumation associated with a Miocene and younger uplift of the plateau due to the migration of the Yellowstone Hot spot into SW Montana. The current high elevation of the Beartooth Plateau, therefore, is most likely due to the presence of the Yellowstone Hot Spot and not residual Laramide topography.

Apatite (U-Th)/He data from samples collected along the Beartooth highway gives a cooling age of ca. 115 Ma for one sample collected from an elevation above 3000 m, and apparent ages of ca. 70-64 Ma below 2800 m to 52-38 Ma at lower elevations (Fig. 12). These data indicate that the base of the apatite He partial retention zone (about 70 degrees C) prior to Laramide exhumation was between modern elevations of 2800 and 3000 meters and support the results of the fission-track data. The fact that younger

(Miocene) ages are not found from the surface samples suggests that the glacial and fluvial incision of the Plateau is very recent and not related to Laramide tectonics.

**Summary.** Precambrian basement exposed along the Beartooth Highway provides a glimpse into some the earliest parts of earth history, particularly the process of “cratonization”. The BBMZ and Wyoming Province in general have been resilient structural entities for billions of years. While Proterozoic and Phanerozoic subduction and resultant magmatism and deformation have strongly affected neighboring provinces, little to no evidence of such processes is preserved with the Wyoming province proper (e.g., Mueller et al., 2005; Mueller and Frost, 2006). In the Beartooth area, K-Ar ages of ~2300 Ma from crystalline basement strongly suggests these rocks have not been above ~350 degrees C for over 2 billion years, equivalent to the history of many greenstone belts around the world. Today, however, the northwestern Wyoming province is encountering a unique event—the interaction with the Yellowstone plume. This interaction offers a unique opportunity to understand the forces that are capable of disrupting such a formidable and long-lived craton.

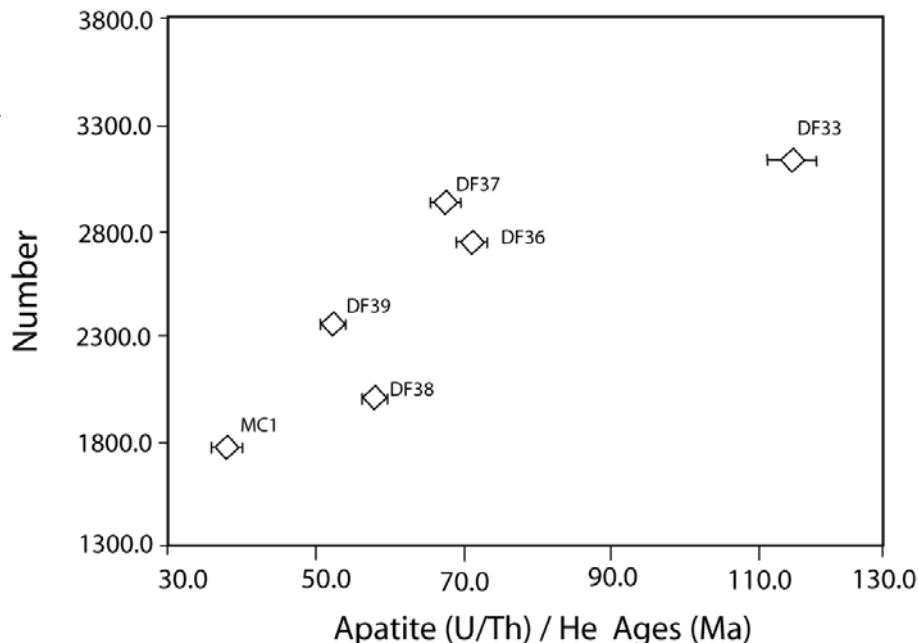


Figure 12. He age vs. sample elevation plot for apatites from the Beartooth Highway section. These data were generated at the University of Melbourne, Australia.

**Acknowledgements.** In a brief overview such as presented here, it is impossible to properly credit all of those who have collaborated with us over the years and helped us reach our present understanding of Beartooth Precambrian geology. Nonetheless many thanks to those who have kibbitzed on field trips, to students who have completed theses, and to those who have provided the devil's advocacy to our theories in numerous meetings and workshops. In addition, we acknowledge the financial support of the N.S.F. (EAR-0609948) and the U.S.G.S.

## References Cited

- Armbrustmacher, T.J., and Simons, F.S., 1977, Geochemistry of amphibolites from the central Beartooth Mountains, Montana-Wyoming: U.S. Geologic Survey, Journal of Research, v. 5, p. 53-60.
- Baadsgaard, H., and Mueller, P.A., 1973, K-Ar and Rb-Sr ages of intrusive Precambrian mafic rocks, southern Beartooth Mountains, Montana and Wyoming: Geological Society of America Bulletin, v. 84, p. 3635-3644.
- Beltrame, R., 1982, Systematic variations in hornfels at the base of the Stillwater Complex, Montana and Wyoming: Montana Bureau of Mines and Geology Special Publication 84, p. 107-130.
- Butler, J.R., 1969, Origin of Precambrian granite gneisses in the Beartooth Mountains, Montana and Wyoming: *in* Larsen, L.H., ed., Igneous and Metamorphic Geology: Geological Society of America Memoir 115, p. 73-101.
- Casella, C.J., 1964, Geologic evolution of the Beartooth Mountains, Montana and Wyoming, Part 4: Relationship between Precambrian and Laramide structures in the Line Creek area: Geological Society of America Bulletin, v. 75, p. 969-984.
- Casella, C.J., 1969, A review of the Precambrian geology in the eastern Beartooth Mountains, Montana and Wyoming: *in* Larsen, L.H., ed., Igneous and Metamorphic Geology: Geological Society of America Memoir 115, p. 53-71.
- Chamberlain, K.R., Frost, C.D., and Frost, B.R., 2003, Early Archean to Mesoproterozoic evolution of the Wyoming province: Archean origins to modern lithospheric structure: Canadian Journal of Earth Sciences, v. 40, p. 1357-1374.
- Condie, K.C., 1976, The Wyoming Archean Province in the western United States: *in* Windley, B.F., ed., The Early History of the Earth, Wiley, London, p. 499-511.
- Condie, K.C., Leech, A.P., and Baadsgaard, H., 1969, Potassium-argon ages of Precambrian mafic dikes in Wyoming: Geological Society of America Bulletin, v. 80, p. 899-905.
- Eckelmann, F.D., and Poldervaart, A., 1957, Geologic evolution of the Beartooth Mountains, Montana and Wyoming, Part 1: Archean history of the Quad Creek area: Geological Society of America Bulletin, v. 68, p.1225-1262.
- Foose, R.M., Wise, D.U., and Garbarini, G.S., 1961, Structural Geology of the Beartooth Mountains, Montana and Wyoming: Geological Society of America Bulletin, v. 72, p. 1143-1172.
- Foster, D., Mueller, P., Vogl, J., Mogk, D., and Wooden, J., 2006, Proterozoic evolution of the western margin of the Wyoming Craton: Implications for the tectonic and magmatic evolution of the northern Rocky Mountains: Canadian Journal of Earth Science, v. 43, p. 1601-1619.
- Gast, P., Kulp, J., and Long, L., 1958, Absolute age of the early Precambrian rocks in the Bighorn basin of Wyoming and Montana, and southeastern Manitoba: American Geophysical Union Transactions, v. 9, p. 322.
- Geissman, J.G., and Mogk, D., 1986, Late Archean tectonic emplacement of the Stillwater Complex along reactivated basement structures, northern Beartooth Mountains, southern Montana, U.S.A.: *in* Aldrich, J.J. Jr., and Laughlin, A.W., eds., 6th International Conference on Basement Tectonics, p. 25-44.
- Giletti, B.J., 1966, Isotopic ages from southwestern Montana: Journal of Geophysical Research, v. 71, p. 4029-4036.
- Harlan, S.S., Geissman, J.W., and Snee, L.W., 1997, Paleomagnetic and <sup>40</sup>Ar/<sup>39</sup>Ar geochronologic data from Late Paleozoic mafic dikes and sills, Montana and Wyoming: U.S. Geological Survey Professional Paper 1580, 16 p.
- Harris, R.L., Jr., 1959, Geologic evolution of the Beartooth Mountains, Montana and Wyoming, Part 3: Gardner Lake Area, Wyoming: Geological Society of America Bulletin, v. 70, p. 1185-1216.
- Henry, D.J., Mueller, P.A., Wooden, J.L., Warner, J.L., and Lee-Berman, R., 1982, Granulite grade supracrustal assemblages of the Quad Creek area, eastern Beartooth Mountains, Montana: *in* Mueller, P.A., and Wooden, J.L., eds., Precambrian Geology of the Beartooth Mountains, Montana and Wyoming: Montana Bureau of Mines and Geology Special Publication 84, p. 147-159.
- James, H.L., 1946, Chromite deposits near Red Lodge, Carbon County, Montana: US Geological Survey Bulletin 945-F, p. 151-189.
- Khoury, S., and Ghaly, T., 1973, Geological evolution of the Archean basement in the Long Lake area, Beartooth

- Mountains, Wyoming: Earth Research, v. 1, p.1-15.
- Labotka, T.C., and Kath, R.L., 2001, Petrogenesis of the contact metamorphic rocks beneath the Stillwater Complex, Montana: Geological Society of America Bulletin, v. 113, p. 1312-1323.
- Labotka, T.C., Vaniman, D.T., and Papike, J.J., 1982, Contact metamorphic effects of the Stillwater Complex, Montana - the concordant iron-formation - a reply to the role of buffering in metamorphism of iron-formation: American Mineralogist, v. 67, p. 149-152.
- Larsen, L.H., Poldervaart, A., and Kirchmeyer, M., 1966, Geologic evolution of the Beartooth Mountains, Montana and Wyoming, Part 7: Structural homogeneity of gneisses in the Lonesome Mountain area: Geological Society of America Bulletin, v. 77, p. 1277-1292.
- Maas, A.T., and Henry, D.J., 2002, Heterogeneous growth and dissolution of sillimanite in migmatites: Evidence from cathodoluminescence imaging: Geological Society of America Abstracts with Program, v. 34.
- Mogk, D.W., and Henry, D.J., 1988, Metamorphic petrology of the northern Archean Wyoming Province, SW Montana: evidence for Archean collisional tectonics: *in* Metamorphism and crustal evolution in the western United States, Ernest, W., ed., Proceedings of the VII Rubey Colloquium on Metamorphic Terranes, Prentice Hall, NY, p. 362-382.
- Mogk, D.W., Mueller, P.A., and Wooden, J.L., 1992, The nature of Archean terrane boundaries: an example from the northern Wyoming Province: Precambrian Geology, v. 55, p. 155-168.
- Montgomery, C., and Lytwyn, J., 1984, Rb-Sr systematics and ages of principal Precambrian lithologies in the South Snowy block: Journal of Geology, v. 92, p. 103-112
- Mueller, P.A., and Wooden, J.L., 1976, Rb-Sr age of the contact aureole of the Stillwater igneous complex, Montana: Earth Planetary Science Letters, v. 29, p. 384-388.
- Mueller, P.A., 1979, Ages of deformation in the Hellroaring Plateau area, eastern Beartooth Mountains, Montana: Canadian Journal of Earth Sciences, v. 16, p. 1124-1129.
- Mueller, P.A., Wooden, J.L., Odom, A.L., and Bowes, D.R., 1982a, Geochemistry of the Archean rocks of the Quad Creek and Hellroaring Plateau areas of the eastern Beartooth Mountains: *in* Mueller, P.A. and Wooden, J.L., eds., Precambrian Geology of the Beartooth Mountains, Montana and Wyoming: Montana Bureau of Mines and Geology Special Publication 84, p. 69-82.
- Mueller, P.A., Wooden, J.L., and Bowes, D.R., 1982b, Precambrian evolution of the Beartooth Mountains, Montana-Wyoming, U.S.A: Revista Brasileira de Geociencias, v. 12, p. 216-222.
- Mueller, P.A., Wooden, J.L., Schulz, K., and Bowes, D.R., 1983, Incompatible-element-rich andesitic amphibolites from the Archean of Montana and Wyoming: Evidence for mantle metasomatism: Geology, v. 11, p. 203-206.
- Mueller, P.A., Wooden, J.L., Henry, D.J., and Bowes, D.R., 1985, Archean crustal evolution of the eastern Beartooth Mountains, Montana and Wyoming: *in* Czamanske, O.K., and Zientek, M.L., eds., Stillwater Complex: Montana Bureau of Mines and Geology Special Publication 92, p. 9-20.
- Mueller, P.A., Locke, W.W., and Wooden, J.L., 1987, A study in contrasts: Archean and Quaternary geology of the Beartooth Highway: Geological Society of America Centennial Field Guide, Rocky Mountain Section, p. 75-78.
- Mueller, P.A., Shuster, R.D., Graves, M.A., Wooden, J.L., and Bowes, D.R., 1988, Age and composition of a late Archean magmatic complex, Beartooth Mountains: Montana Bureau of Mines Special Publication 96, p. 7-22.
- Mueller, P.A., Wooden, J.L. and Nutman, A.P., 1992, 3.96 Ga zircons from an Archean quartzite, Beartooth Mountains, Montana: Geology, v. 20, p. 327-330.
- Mueller, P.A., Wooden, J.L., Mogk, D.W., Nutman, A.P., and Williams, I.S., 1996, Extended history of a 3 Ga trondhjemitic gneiss, Wyoming Province, USA: evidence from U-Pb systematics in zircon: Precambrian Research, v. 78, p. 41-52.
- Mueller, P.A., Wooden, J.L., Nutman, A.P., and Mogk, D.W., 1998, Early Archean crust in the northern Wyoming province – Evidence from U-Pb ages of detrital zircons: Precambrian Research, v. 91, p. 297-307.
- Mueller, P., Burger, H., Wooden, J., Brady, J., Cheney, J., Harms, T., Heatherington, A., and Mogk, D., 2005, Age and tectonic implications of Paleoproterozoic metamorphism in the northern Wyoming Province: Journal of Geology, v. 111, p. 169-179.
- Mueller, P., and Frost, C., 2006, The Wyoming Province: A distinctive Archean craton in Laurentian North America: Canadian Journal of Earth Science, v. 43, p. 1391-97.
- Nunes, P., and Tilton, G., 1971, Uranium-lead ages of minerals from the Stillwater igneous complex and associated rocks, Montana: Geological Society of America Bulletin, v. 82, p. 2231-2249.
- Omar, G.I., Lutz, T.M., and Giegenback, R., 1994, Apatite fission-track evidence for Laramide and post Laramide uplift and anomalous thermal regime at the Beartooth Overthrust, Montana-Wyoming: Geological Society of America Bulletin, v. 106, p. 74-85.
- Page, N.J., 1977, The Stillwater Complex, Montana: rock succession, metamorphism and structure of the complex and adjacent rocks: U. S. Geological Survey Professional Paper 999.

- Prinz, M.J., 1964, Geologic evolution of the Beartooth Mountains, Montana and Wyoming, Part 5: Mafic dike swarms of the southern Beartooth Mountains: Geological Society of America Bulletin, v. 75, p. 1217-1248.
- Rowan, L.C., 1969, Structural geology of the Quad-Wyoming-Line Creeks area, Beartooth Mountains, Montana: Geological Society of America Memoir 115, p. 1-18.
- Rowan, L.C., and Mueller, P.A., 1971, Relations of folded dikes and Precambrian polyphase deformation, Gardner Lake area, Beartooth Mountains, Wyoming: Geological Society of America Bulletin, v. 82, p. 2177-2186.
- Simons, F.S., and Armbrustmacher, T.J., 1976, High-level plateaus of the southeastern Beartooth Mountains, Montana and Wyoming - Remnants of an exhumed sub-Cambrian marine plain: U.S. Geological Survey, Journal of Research, v. 4, p. 387-396.
- Skinner, W.R., 1969, Geologic evolution of the Beartooth Mountains, Montana and Wyoming: Part 8: Ultramafic rocks in the Highline Trail Lakes area, Wyoming: Geological Society of America Memoir 115, p. 19-52.
- Spencer, E.W., 1959, Geologic evolution of the Beartooth Mountains, Montana and Wyoming, Part 2: Fracture Patterns: Geological Society of America Bulletin, v. 70, p. 467-508.
- Stevenson, R.K., and Patchett, P.J., 1990, Implications for the evolution of continental crust from the Hf isotope systematics of Archean detrital zircons: *Geochimica et Cosmochimica Acta*, v. 54, p. 1683-1698.
- Thomson, J.A., 2008, Beneath the Stillwater Complex: Petrology and geochemistry of quartz-plagioclase-cordierite (or garnet)-orthopyroxene-biotite  $\pm$  spinel hornfels, Mountain View area, Montana: *Amer. Mineralogist*, v. 93, p. 438-450.
- Valley, J., Lackey, J., Cavosie, A., Clechenko, C., Spicuzza, M., Basei, M., Bindeman, I., Ferreira, V., Sial, A., King, E., Peck, W., Sinha, A., and Wei, C., 2005, 4.4 billion years of crustal maturation: oxygen isotope ratios of magmatic zircons: *Contributions to Mineralogy and Petrology*, v. 150, p. 561-580.
- Vaniman, D.T., Papike, J.J., and Labotka, T.C., 1980, Contact metamorphic effects of the Stillwater Complex, Montana, the concordant iron formation: *American Mineralogist*, v. 65, p. 1087-1102.
- Warner, J.L., Lee-Berman, R., and Simonds, C.H., 1982, Field and petrologic relations of some Archean rocks near Long Lake, eastern Beartooth Mountains, Montana and Wyoming: *in* Mueller, P.A., and Wooden, J.L., eds., *Precambrian Geology of the Beartooth Mountains, Montana and Wyoming*, Montana Bureau of Mines and Geology Special Publication 84, p. 57-68.
- Whitford, D., Nicholls, I., and Taylor, S., 1979, Spatial variations in the geochemistry of Quaternary lavas across the Sunda Arc in Java and Bali: *Contributions to Mineralogy and Petrology*, v. 70, p. 341-356.
- Wood, D., Joron, J., Treuil, M., Norry, M., and Tarney, J., 1979, Elemental and Sr isotope variations in basic lavas from Iceland and the surrounding ocean floor: *Contributions to Mineralogy and Petrology*, v. 70, p. 319-339.
- Wooden, J.L., and Mueller, P.A., 1988, Pb, Sr, and Nd isotopic compositions of a suite of Late Archean igneous rocks, eastern Beartooth Mountains: implications for crust-mantle evolution: *Earth Planetary Science Letters*, v. 87, p. 59-72.
- Wooden, J.L., Mueller, P.A., Hunt, D.K., and Bowes, D.R., 1982, Geochemistry and Rb-Sr geochronology of Archean rocks from the interior of the southeastern Beartooth Mountains, Montana and Wyoming: *in* Mueller, P.A., and Wooden, J.L., eds., *Precambrian Geology of the Beartooth Mountains, Montana and Wyoming*: Montana Bureau of Mines and Geology Special Publication 84, p. 45-56.
- Wooden, J.L., Mueller, P.A., and Mogk, D.W., 1988, A review of the geochemistry and geochronology of the Archean rocks of the northern part of the Wyoming Province: *in* Ernst, W.G., ed., *Metamorphism and Crustal Evolution of the Western United States*, v. 7, p. 383-410.
- Wooden, J.L., Mueller, P.A., Mogk, D.W., and Bowes, D.R., 1988, A review of the geochemistry and geochronology of Archean rocks of the Beartooth Mountains, Montana and Wyoming: *in* Lewis, S.E., and Berg, R.B., eds., *Precambrian and Mesozoic Plate Margins*: Montana Bureau of Mines and Geology Special Publication, 96, 23-42.
- Zeitler, P.K., 1985, Closure temperature implications of concordant Ar-40 Ar-39 potassium-feldspar and zircon fission-track ages from high-grade terranes: *Nuclear Tracks and Radiation Measurements*, v. 10, p. 441-442.



# RECENT CONTRIBUTIONS TO THE UNDERSTANDING OF THE HEART MOUNTAIN DETACHMENT, WYOMING

**David H. Malone**

*Dept. of Geography-Geology, Illinois State University, Campus Box 4400, Normal, IL 61790  
dhmalon@ilstu.edu*

**John P. Craddock**

*Geology Dept., Macalester College, St. Paul, MN 55105 Craddock@Macalester.edu*

---

## ABSTRACT

For more than a century, the Heart Mountain Detachment has attracted the attention of researchers and students from around the world. The development of the continuous allochthon model for Heart Mountain Faulting about 20 years ago as an alternative to the long-standing concept of Tectonic denudation has provided the context for the latest generation of work on the origin and emplacement of allochthonous upper plate rocks.

The consensus of work in the last 15 years indicates that volcanic rocks overlying the HMD are everywhere allochthonous. The upper plate was emplaced catastrophically (>150 m/sec) through the collapse of a volcanic edifice in the northern Absaroka Range at about 49.5 Ma. In the proximal areas of the Detachment, vent facies volcanic rocks were down-dropped and translated to the SE. During the edifice collapse, the underlying sheet of Paleozoic rocks was dismembered, and the various blocks were rotated independently around a vertical axes of rotation. To the southeast, in the adjacent Big Horn and Absaroka Basins, the upper plate was emplaced upon an Eocene land surface. Here, the upper plate has the characteristics of a large debris avalanche deposit, which is similar to those that are found at the base of younger stratovolcanoes around the world. Several 100 km to the south, in the Green River Basin, where lacustrine conditions dominated, the effect of the emplacement of the upper plate was evidenced by a significant desiccation event as the upper plate dammed drainage upstream.

Prior to collapse, active hydrothermal systems

were present at several volcanic centers. The collapse was initiated by the injection of volcanic gas and glass, and the heating of pore waters through volcanic intrusion, which caused the reduction of friction that enable the mass of rock to move. Continued movement (i.e., friction reduction) was facilitated by mechanical fluidization and the frictional dissociation of carbonate rocks and the consequent generation of CO<sub>2</sub>. Thus, the idea of a gravitational collapse of the continuous allochthon, and the catastrophic emplacement rates required of tectonic denudation, are best supported by the available data.

## INTRODUCTION

The Heart Mountain Detachment in northwest Wyoming has been the focus intense geologic research for more than a century. Literally dozens of papers, maps and conference presentations authored by scores of scientists of diverse backgrounds have been published on the Heart Mountain problem over the years. Despite this level of attention, many of the aspects of the geometry, origin, and deformational history of the Heart Mountain Detachment remain problematic and controversial. Hauge (1993) provides an excellent summary of the general characteristics of the Heart Mountain Detachment; he also provides a detailed review of the history of research and an insightful historical discussion of the important points of controversy. Readers are strongly encouraged to read this important paper as this is the basis for the summary presented herein. The most recent field guide for the Heart Mountain Detachment area is provided by Malone and others (1999).

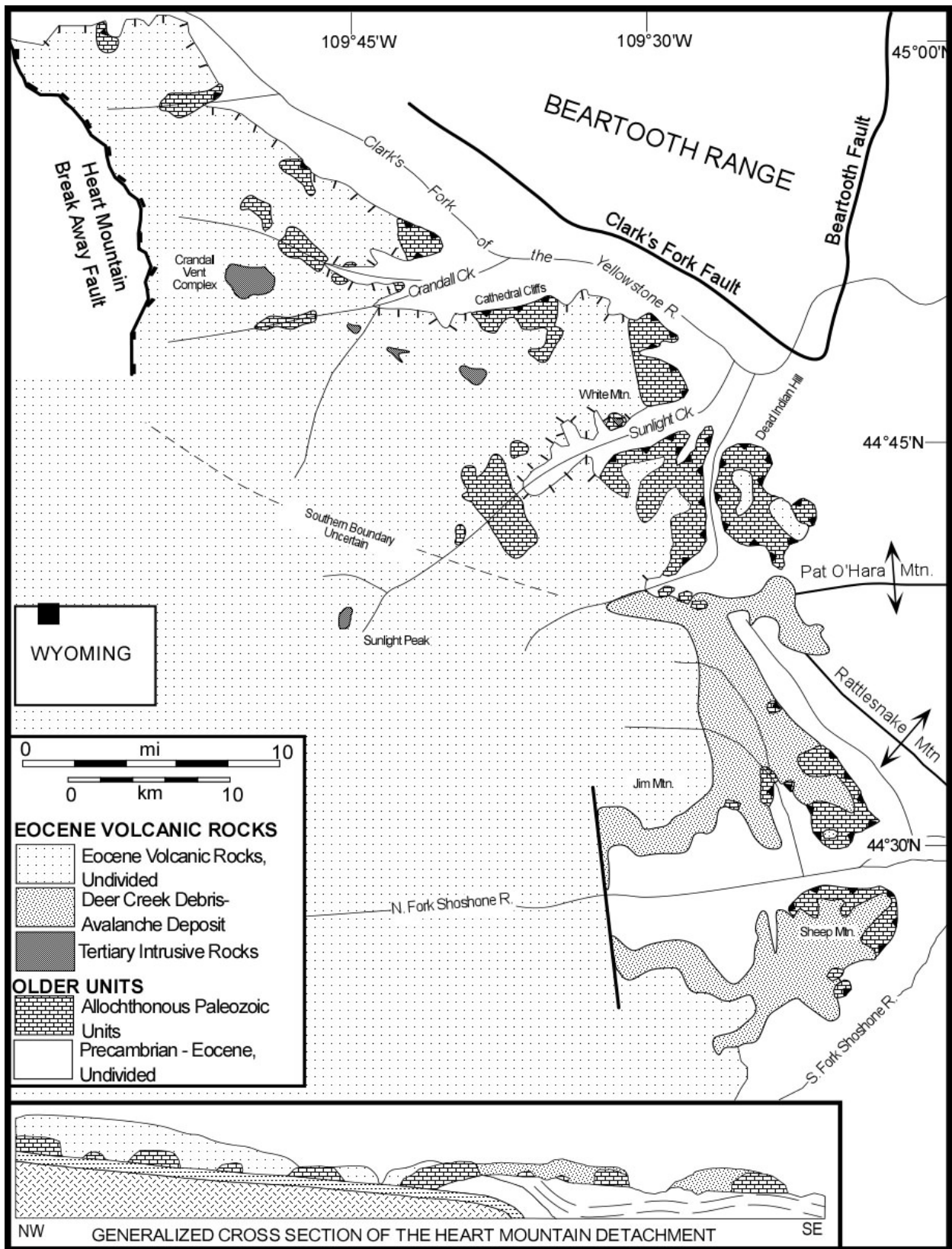


Figure 1. Geologic map and schematic cross section of the Heart Mountain Detachment and surrounding areas (modified from Pierce, 1987; Haugue, 1993; and Malone and others, 1999).

At Heart Mountain, just north of Cody, Wyoming, the more than 230 m of Paleozoic limestone and dolomite beds that form the summit overlie with no apparent discordance early Eocene and older, pre-Laramide strata. Heart Mountain is an erosional remnant of a much more extensive upper plate the Heart Mountain Detachment (Figure 1). The major characteristics of the Heart Mountain Detachment (HMD) as summarized by Hauge (1993) and Malone (2000) are:

- 1) an extended (>3400 km<sup>2</sup> in area) upper plate with transported distances of as much as 50 km;
- 2) a detachment horizon in the proximal areas that consistently occurs along a lower Ordovician bedding plane;
- 3) an average dip of the detachment horizon at the time of emplacement of less than 2°;
- 4) a breakaway, bedding plane, and ramp components, with a younger-over-older age relation in the proximal areas and an older-over-younger age relation in the distal areas. Part of the upper plate, at least the distal toe, most likely was transported over an Eocene land surface; and
- 5) a maximum time frame for emplacement of <2.0 Ma during middle Eocene time, and perhaps as little as 0.2 Ma.

#### *Tectonic Denudation vs. Continuous Allochthon*

Two fundamentally different models describing the geometry, kinematic pattern, and emplacement of the upper plate of the HMD were described by Hauge (1993). For many years, the upper plate was viewed to have been emplaced catastrophically as numerous independent slide blocks (Figure 2a; Pierce 1973, 1987), and as a result of this detachment faulting, a tectonically denuded surface was formed. Immediately after faulting had ceased, massive outpourings of Wapiti Formation volcanic rocks were deposited on the detached blocks as well as on the

tectonically denuded surface (Pierce, 1973, 1987). The most compelling line of evidence for this interpretation is the complete lack of erosion on the exposed fault plane, indicating that the time interval between slide block emplacement and the deposition of the Wapiti Formation must have been very short.

During the 1980s, a different model for the emplacement of the HMD upper plate was advanced. In this view, the upper plate is interpreted to have been a continuous allochthon rather than a series of individual slide blocks (Figure 2b; Hauge, 1985, 1990, 1993). Volcanic rocks overlying the detachment, originally viewed as in depositional contact, were reinterpreted as allochthonous, and as such comprising much of the upper plate (Hauge, 1990). Thus, the continuous allochthon model requires no tectonic denudation or catastrophic emplacement of numerous slide blocks, and the model eliminates the mechanical enigma that tectonic denudation poses.

It is important to note that the tectonic denudation model was developed initially in the distal areas of the detachment, before the existence and geologic characteristics of the proximal areas were discovered. Conversely the continuous allochthon model was developed from work that was almost exclusive to the proximal areas, that is along the break-away and bedding plane areas of the Detachment.

#### *Dominant Problem, circa 1993*

Hauge (1993) reported the following dominant problems at the time of his writing: What is the structure and stratigraphy of Eocene volcanic rocks overlying the detachment? Are they in depositional contact, or are they allochthonous? If allochthonous, what mechanism transported them to their present position, and what does that relationship reveal about the emplacement mechanism, kinematic pattern and emplacement rate of the upper plate?

The purpose of this report is to summarize the contributions of the current generation of works to the understanding of the Heart Mountain

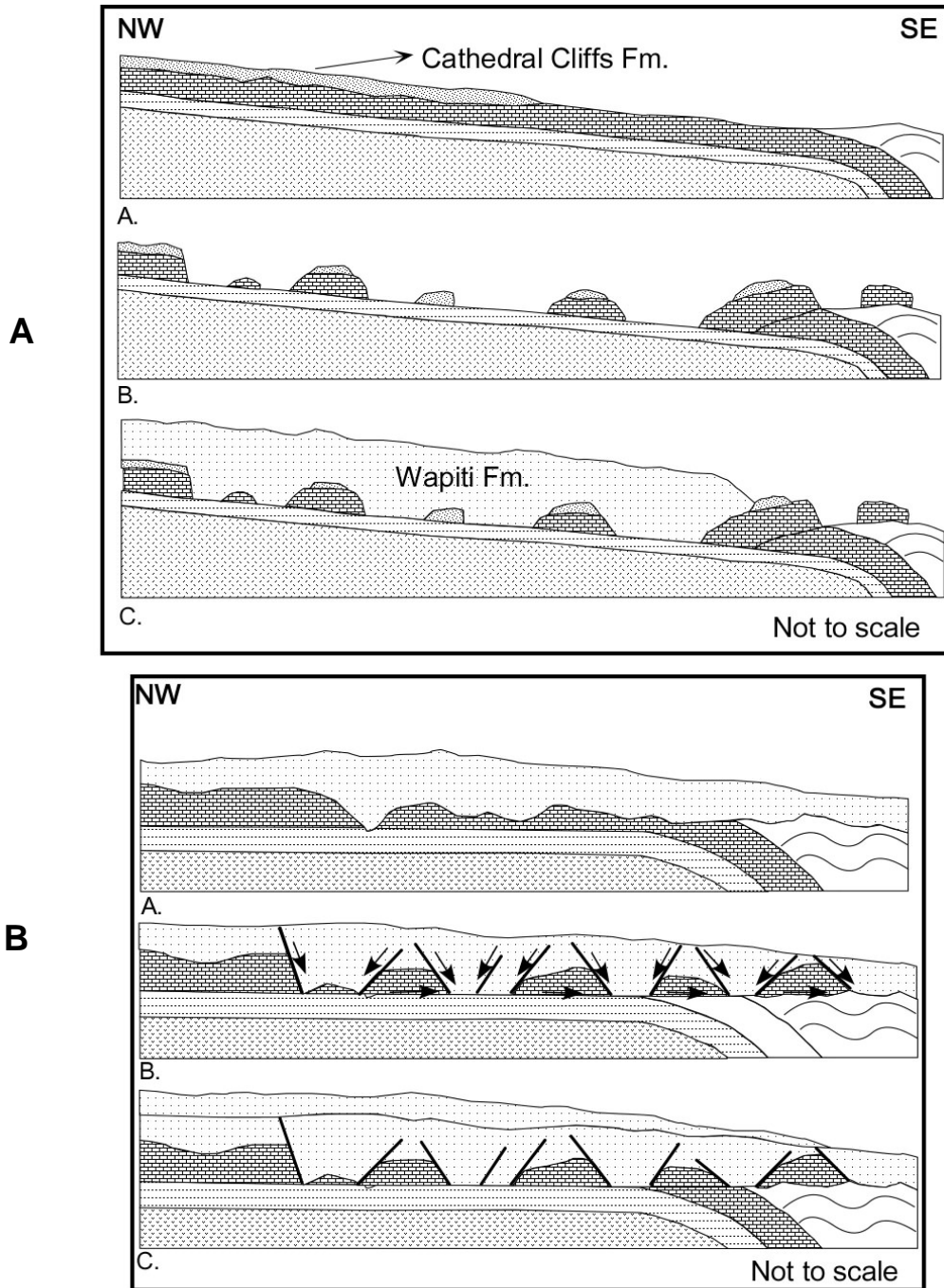


Figure 2. **A.** Tectonic Denudation Model of Heart Mountain Faulting (from Pierce, 1987). Before faulting, Eocene volcanic rocks of the Cathedral Cliffs formation rest upon a dip slope of Paleozoic rocks on the flank of the Laramide Beartooth Uplift. A detachment formed along a basal Ordovician bedding plane, and individual, mountain size blocks were catastrophically emplaced along the detachment, and out into the adjacent Big Horn Basin. Immediately after faulting, massive eruptions of Wapiti Formation volcanic rocks buried the disrupted terrain, and preserved its features. Gravity sliding was the dominant emplacement mechanism.

**B.** Continuous Allochthon Model of Heart Mountain Faulting (from Hauge, 1990). Before faulting a thick succession of undivided Eocene volcanic rocks rest upon a dip slope of Paleozoic Rocks on the flank of the Laramide Beartooth Uplift. During building, the volcanic pile became gravitationally unstable, and began to collapse. During this collapse, a detachment formed along a basal Ordovician bedding plane, and volcanic rocks were down-dropped, rotated, and translated into a series of grabens. Thus, the upper plate was comprised of volcanic and Paleozoic rocks, with volcanic rocks comprising most of its volume. This collapse event was gradual, and occurred over as much as 2 million years. After the allochthon stabilized, younger volcanic rocks were deposited on to the disrupted terrain. Gravity spreading was the dominant emplacement mechanism.

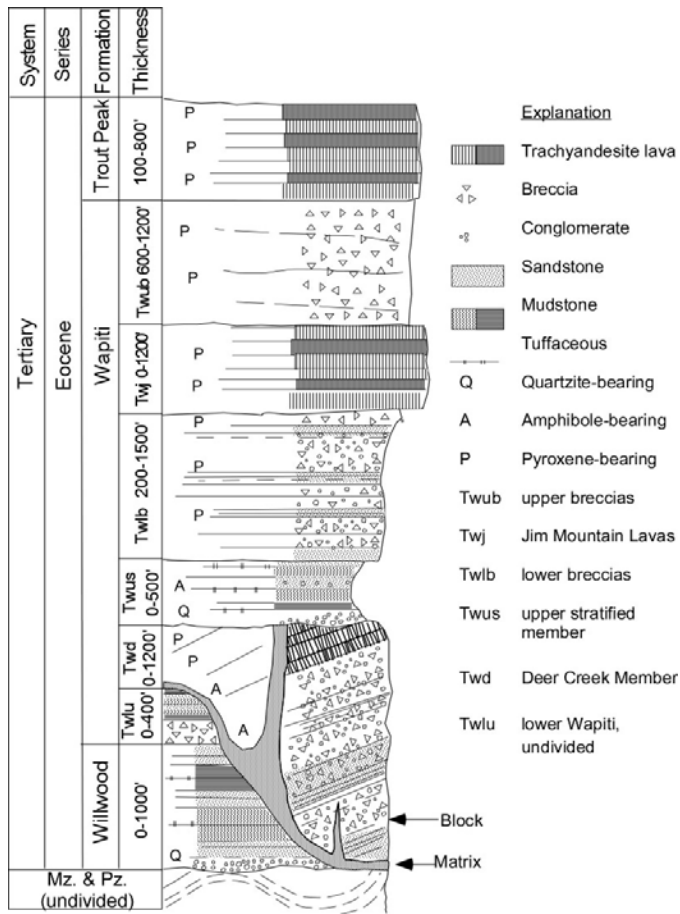


Figure 3. Stratigraphic column of Eocene volcanic rocks exposed in the North Fork of the Shoshone River valley (distal areas of the Heart Mountain Detachment; modified from Malone, 1996, and Malone and others, 1999).

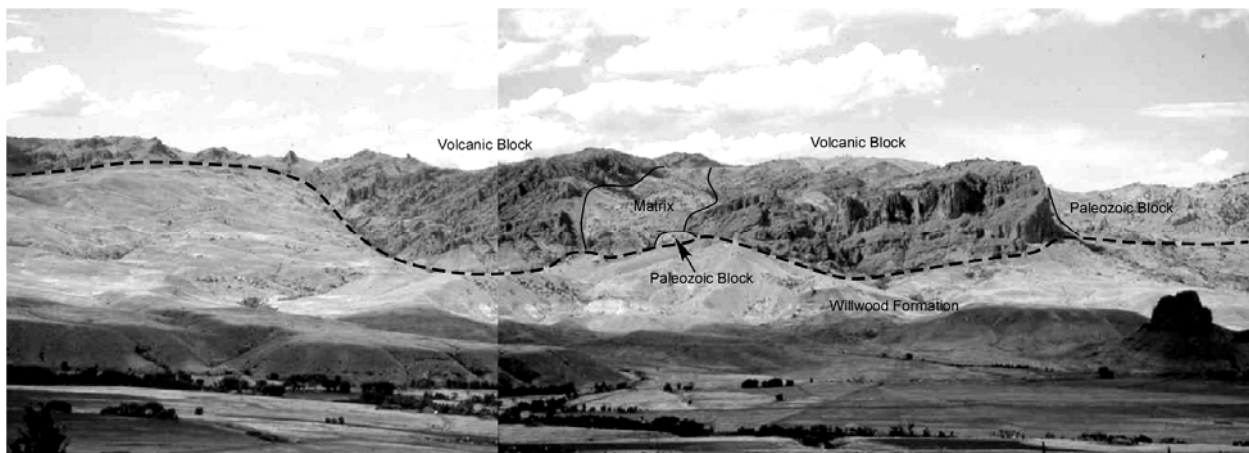


Figure 4a. Panoramic view to the north of the type area of the Deer Creek Member of the Wapiti Formation from the South Fork Shoshone River Valley, about 3 mi (5 km) away. The light-colored, grassy foothills are underlain by the Willwood Formation (Twl) and Cody Shale (Kc). The heavy dashed line is the early middle Eocene land surface with more than 1000 ft (321 m) of relief. In this scene, two blocks (>1 km in diameter) are visible (Twdb). The block to the right (east) consists of about 800 ft of interbedded breccias, sandstones, and conglomerates, and dips about 25° to the north. The two blocks are bounded by a poorly exposed, lighter-colored interval of matrix. Matrix (Twdm) also occurs beneath each block but is too thin to be resolved from this distance. From Malone (1996).

Detachment. Eighteen peer-reviewed papers that address various aspects of the Heart Mountain problem have been published between 1993 and 2008. More than thirty conference presentations, three PhD dissertations, one MS thesis, and more than a dozen BS research projects, largely through Keck supported efforts in the late 1990s also have been completed. In the sections that follow, we will focus mainly on the peer reviewed publications.

## DISCUSSION

### *Stratigraphy of Eocene Volcanic Rocks*

As indicated by Hauge (1993), the key to understanding the dynamics of the emplacement of the upper plate of the HMD rests squarely on further study of the associated Eocene volcanic rocks of the Absaroka Volcanic Supergroup (see Sundell, 1990, for a detailed overview of these rocks). Unfortunately, because of the abundance of vent facies rocks, the local intense deformation of these rocks, and the generally poor exposure and access, no viable and widely accepted volcanic stratigraphy has ever been established in the proximal areas of the HMD. Hauge (1990, 1993) recommended that the units defined by Pierce (i.e. the Wapiti and Cathedral Cliffs Formation) be abandoned, and that general or informal terminology be used instead. No significant progress has been made to the understanding of the stratigraphy of Eocene volcanic rocks in the proximal areas of the HMD.

Further to the south, in the distal areas of the HMD and beyond, vent facies rocks grade into epiclastic vol-

canic rocks, where defining a working, valid stratigraphy is possible. As part of his PhD research, Malone conducted detailed stratigraphic studies and geologic mapping at a scale of 1:24,000 was carried out in a 250 mi<sup>2</sup> (650 km<sup>2</sup>) area in the North and South Fork Shoshone River valleys in the northeastern Absaroka Range, an area roughly corresponding with the former-land-surface phase of the Heart Mountain detachment as defined by Pierce (1987). Figure 3 is a composite stratigraphic column for volcanic rocks that occur in this area. Here described blocks (individually as large as several km<sup>2</sup> in area) of vent-medial-facies lava flows, breccias, and sandstones within a thin, heterogeneous matrix of boulder- to sand-sized volcanoclastic material are observed (Figure 4). The blocks and matrix together comprise a laterally continuous and mappable lithostratigraphic unit within the volcanic succession. He designated this unit the Deer Creek Member of the Wapiti Formation. Further work by Malone (1997) indicated that the unit also occurs throughout the upper South Fork Shoshone River valley.

The Deer Creek Member is interpreted as the deposit of a debris avalanche, formed by the collapse of a large stratovolcano within the northern

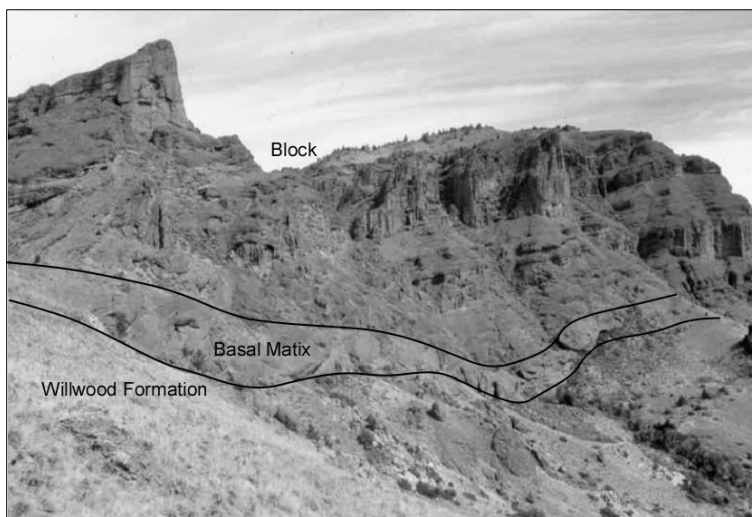


Figure 4b. Closer view to the east of the type area of the Deer Creek Member. This locality is the southerly known limit of the unit, and is more than 25 mi (40 km) from the center of the inferred source area near Sunlight Peak. The steep slopes consist of dark brown breccias, sandstones, and conglomerates within the Deer Creek Member block (Twdb). The beds within the block dip about 30° to the northwest. At the base, a 25 ft (8 m) zone of matrix is present (Twdm). The unit here fills a local Eocene paleotopography with as much as 400 ft (125 m) of relief. From Malone (1996).

Absaroka Range during the early middle Eocene time. The currently documented areal extent and volume of the Deer Creek Member are ~175 mi<sup>2</sup> (450 km<sup>2</sup>) and ~24 mi<sup>3</sup> (80 km<sup>3</sup>), respectively. These numbers are similar to younger debris-avalanche deposits reported in many Quaternary volcanic successions. The Deer Creek Member is temporally and spatially associated with allochthonous Paleozoic Rocks of the Heart Mountain Detachment. Initially, Malone (1994) advocated a two-stage

retrogressive collapse of a volcanic edifice in the Sunlight Peak area. Later work by Beutner and Craven (1996) indicated that the Crandall intrusive center was a more likely source area for this collapse, Malone (2003) and Rhodes and others (2007) argued for a single collapse with the Eocene volcanic and Paleozoic carbonate rocks that comprise the Deer Creek member represent the distal toe and debris-avalanche deposit that resulted from the edifice collapse.

### Timing of Emplacement

In the early 1990s, the best estimate for the timing of the emplacement of the upper plate of the HMD was based on vertebrate paleontology of Willwood and Wapiti Formation rocks at the base of Jim Mountain. Stratigraphic evidence from Eocene sedimentary and volcanic rocks (Pierce 1973, 1987; Torres and Gingerich, 1983) indicates that the emplacement of the upper plate of the HMD occurred within a two-million-year window during the early middle Eocene (49.5-47.5 million years ago). This two-million-year window enabled Hauge (1985, 1990) the time needed for slow, gravity spreading of a continuous allochthon.

Feeley and Cosca (2003) provide an excellent summary of the petrology, geochemistry, and geochronology of the Sunlight Peak vent complex at Jim Mountain (Figure 5). The timing of Heart Mountain faulting is now well constrained in the distal areas of the HMD where upper plate rocks overlay Eocene strata of the Willwood formation. Feeley and Cosca (2003) report an  $^{40}\text{Ar}/^{39}\text{Ar}$  age of  $49.5 \pm 0.16$  Ma for basal Jim Mountain lava at Jim Mountain, which is about 100 m above the Heart Mountain interval. Based on paleontological evidence in the North Fork Shoshone River Valley (Torres, 1985; Gunnell and others, 1992), Heart Mountain faulting must have occurred during the earliest middle Eocene (Bridgerian age, Blackforkian subage; North American Land Mammal Age) between 50-49 Ma. Figure 5 illustrates these age relationships at Jim Mountain.

Heart Mountain faulting correlates with a major desiccation horizon in the Laney Member. Rhodes and others (2007) recognized mudcracks as much as 2 m deep superimposed on lacustrine mudstones of the lower LaCledé Bed of the Green River Formation in the Washakie Basin.

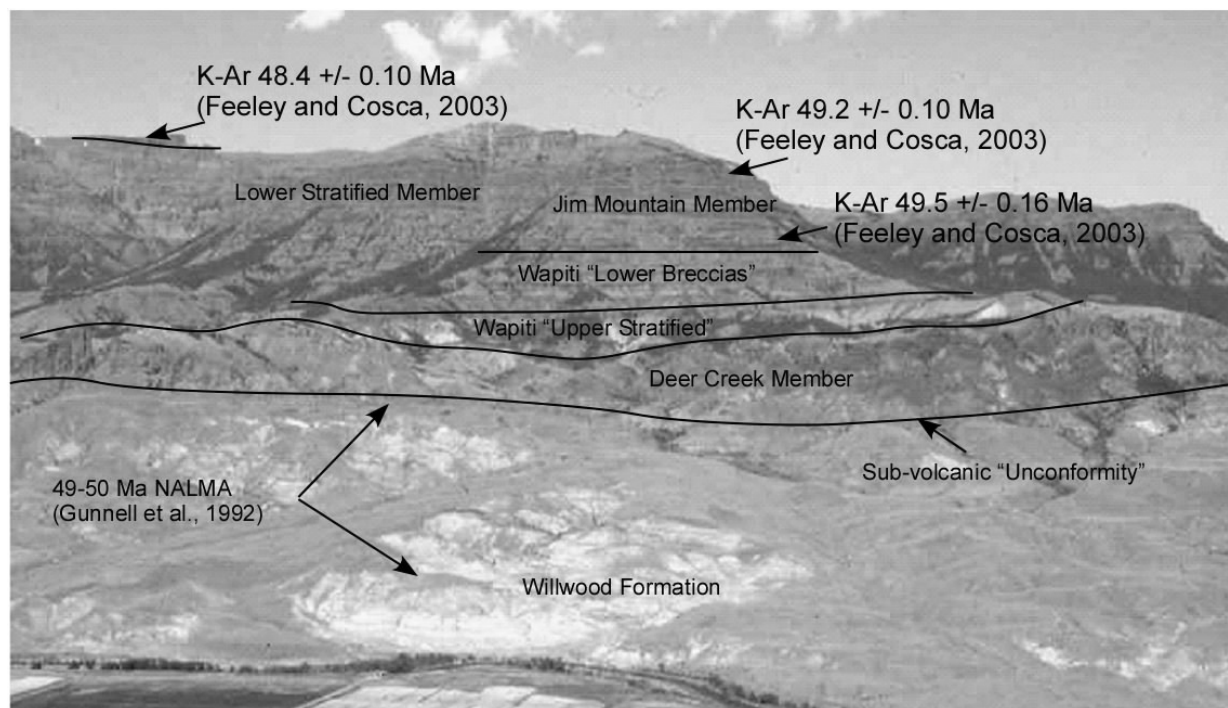


Figure 5. Summary of age control in the North Fork Shoshone River Valley at Jim Mountain.

These mudcracks reflect a sudden and intense desiccation of Eocene Lake Gosiute. In a related study of Eocene stratigraphy of Wyoming, Smith and others (2003) reported  $^{40}\text{Ar}/^{39}\text{Ar}$  weighted mean ages of tuffs overlying and underlying the desiccation horizon to be  $49.70 \pm 0.10$  and  $48.94 \pm 0.12$  Ma, respectively, which correlates well with the timing of the Heart Mountain event further to the north. Thus, Rhodes and others (2007) proposed a unique cause-effect relationship, where the emplacement of the upper plate caused the drainage to Lake Gosiute to be impounded, which resulted in the reduction of the water supply to the lake and the development of the large mud cracks.

Based on the geochronologic evidence provided by Feeley and Cosca (2003) and Smith and others (2003), the time interval for Heart Mountain faulting has been reduced by an order of magnitude. Assuming a maximum error in the reported geochronologic data the time frame for Heart Mountain faulting is 49.34-49.80 Ma. Assuming all reported dates are reliable, Heart Mountain faulting would have had to have occurred between 49.70 and 49.50 Ma, which leaves 200 Ka as the time available for faulting and the deposition of some overlying and underlying rocks. A catastrophic emplacement of the upper plate is therefore likely.

New absolute ages are available in the proximal areas of the HMD as well. Near the break-away area, Douglas and others (2003) report  $^{40}\text{Ar}/^{39}\text{Ar}$  ages on a variety of small plutons between  $48.1 \pm 0.5$  to  $50.1 \pm 0.3$  Ma, within the age range of HMD tectonism.

In an abstract, Hiza (1999) reported an age of  $48.21 \pm 0.08$  ka on a deformed dike (presumably transported as part of the upper plate), but noted that the field relations were ambiguous at that locality. Furthermore she reported an age of  $50.01 \pm 0.14$  for an undeformed tuff that overlies the breakaway (presumably from the Trout Peak Trachyandesite). This age would seem a bit old, as all other work suggests younger ages for rocks overlying the HMD upper plate. In any case, Hiza advo-

cated that this data supported the protracted deformation associated with the Continuous Allochthon Model.

In an abstract, Beutner and others (2004) reports two  $^{40}\text{Ar}/^{39}\text{Ar}$  ages of 48.34 and 48.59 Ma from rootless plutons in the upper plate (no location or errors given). If these plutons are indeed allochthonous, this would suggest an emplacement event at least a million years later than what is indicated to the south. Assuming such, the upper plate would need to have been emplaced sequentially as multiple events.

#### *Emplacement Rate of the Upper Plate Observations from the Detachment Breccia*

Aside from Eocene volcanic rocks, the “breccias” along the detachment horizon have received the lion’s share of attention over the past 15 years as clues about the initiation and transport mechanisms of the upper plate were sought. What has been described as “detachment breccia” is composed largely of carbonate material up to 1-2 m in thickness, which occurs at the base of the upper plate at most localities in the proximal areas of the HMD (Pierce 1973; Beutner and Gerbi, 2005). Because lower plate rocks are undeformed, this breccia was interpreted by Pierce (1973, 1979) to have been derived from the upper plate as a “tectonic carpet” during its emplacement. Because little or no volcanic material was originally found in this breccia where it is overlain by volcanic rocks, Pierce (1973, 1987) argued that these volcanic rocks were deposited after emplacement of the upper plate and a period of tectonic denudation. In a number of areas, this breccia intrudes upper plate rocks as clastic dikes (Pierce 1979). In addition to the all-carbonate breccia, breccia of mixed-volcanic carbonate and all-volcanic (Hauge 1985) compositions have been reported. Hauge (1985) reported lineations (interpreted as fault striae with kinematic significance) at most exposures, and used the term microbreccia to describe these rocks.

Beutner and Craven (1996) and Beutner and Gerbi (2005) reported the occurrence of ac-

creted, rolled and mantled grains, volcanic and delicate glass shards within the microbreccia at White Mountain and many other localities within the HMD region (Figure 6a-c). The glassy grains are variable in composition, may contain phenocrysts, and have shard-like shapes and cusped margins. The presence of glass indicates that a volcanic event was intimately associated with the development of the detachment breccias, and that the injection of a “sill-like mass of volcanic gasses, glass, and finely broken carbonates” initiated the catastrophic movement of the upper plate.

The accreted grains typically have a central core of volcanic or carbonate rock, which are armored by concentric rims that are as much as a mm in thickness. These accreted grains bear a strong resemblance to accretionary lapilli in volcanic settings and impact sites. Buetner and Gerbi (2005) interpret these accreted grains as being formed in some type of gaseous suspension, and that the gas was derived through dissociation of carbonate through frictional heating during catastrophic emplacement of the upper plate. These volcanic and friction derived fluids contributed to the mechanism that enabled the upper plate to move down such a gentle slope.

Anders and others (2000) examined the bot-

toms of many large slide blocks, including the breccias of the HMD, and found layers of well rounded, coarse grained, granular material which bears a strong resemblance to fluvial sandstones or conglomerate. They believe that these fabrics were formed through mechanical sieving in a high energy, fluidized environment during catastrophic emplacement of the upper plate.

Investigations of the HMD at White Mountain have redefined the “breccia” as a carbonate ultracataclasite (CUC; Craddock and others, In Press). This one meter thick unit is well-lithified (“welded”) and composed of calcite, dolomite, aragonite and lizardite, has a density of 3.01 gm/cc and a melting temperature of 1330°C. Geochemically, the CUC is 7.5% SiO<sub>2</sub>, something confirmed by the presence of volcanic fragments and mafic minerals (e.g., hornblende) and the contemporaneous nature of volcanism to faulting along the HMD. We also observed calcite and quartz (and combinations of both) spheroids (100-micron-diameter melt droplets?), and a variety of zeolite minerals as reaction rims. Some components of the CUC

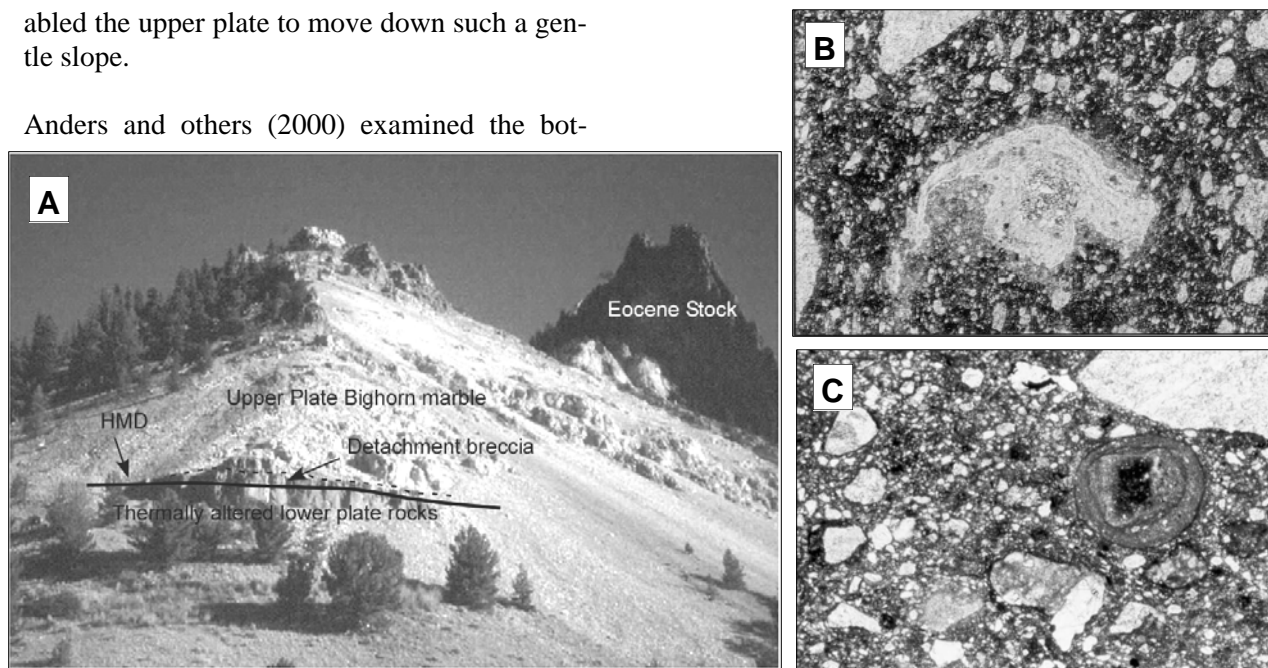


Figure 6. A: Exposure of HMD at White Mountain. B: Delicate volcanic glass shard from White Mountain, field of view, 0.7 cm (from Beutner and Craven, 1996). C: Accreted grain from White Mountain, field of view, 0.7 cm (from Malone and others, 1999).

were in liquid form as the HMD became active (volcanic source?), and some underwent phase changes during faulting, and fluids were present during faulting. Anisotropy of magnetic susceptibility (AMS) measurements preserve a clean magnetic fabric with the long axis ( $K_{\max}$ ) of the magnetic ellipsoid parallel to the upper plate transport direction. Similarly, paleomagnetic results confirm magnetite as the primary magnetic carrier mineral (Curie  $T^{\circ}$  580 $^{\circ}$ ) and as the paleomagnetic paleopole is down and westward, and not up and southerly as would be expected for the Eocene, the CUC rocks are remagnetized.

#### *Calcite Twinning Strain*

Craddock and others (2000) conducted a detailed analysis of calcite twinning strain fabrics in upper and lower plate carbonate rocks in order to better understand the emplacement rate and kinematic pattern of the HMD event. Lower plate rocks revealed an E-W shortening axis that formed during the Laramide Orogeny. No post-Laramide strain overprint was observed in upper or lower plate rocks. As twinning is a strain-rate dependent process, the absence of any twinning strain overprint indicates that the emplacement of the upper plate was likely catastrophic.

#### *Physical Constraints and Mechanical Modeling*

Craddock and others (in press) were the first to objectively quantify the emplacement rate of the upper plate. They offer thermodynamic and mechanical calculations based on frictional melting of calcite and other minerals, geochemical data, and the characteristics of the HMD breccias at White Mountain. This calculation reveals an upper plate emplacement rate of 126-340 m/sec and that the duration of the emplacement event was on the order of a few minutes, too brief a time to develop an emplacement-related calcite twinning strain overprint in upper or lower plate carbonates. This brief and catastrophic detachment event produced a significant amount of  $CO_2$  by flash heating.

#### *Detachment Fluids*

Templeton and others (1995) reported systematic C and O isotope depletions from the break-away fault to the ramp. They interpreted that hot meteoric waters, generated by Eocene intrusive centers circulated along the HMD during the gradual emplacement of a continuous allochthon, and thus supported Hauge's model. One major flaw in this study is that only allochthonous carbonate rocks were analyzed. No data is reported from associated volcanic rocks. Furthermore, no data was collected from nearby autochthonous rocks west of the break away or at Beartooth Butte.

Douglas and others (2003) expanded the isotopic data set of Templeton and others (1995) and included some isotopic dates (mentioned above) and fluid inclusion data. They noted that isotopic depletions were more significant near the break-away, and that the fluids were associated with hydrothermal activity at the New World Mining district north of Silver Gate. Thus, although it is clear that a fluid phase did indeed interact with the rocks above and below the HMD horizon, these fluids may have circulated here before, through intrusion fluid interaction, during through frictional heating during upper plate emplacement, or after movement using the newly formed, high porosity fault zone as a pathway (Aharanov and Anders, 2006).

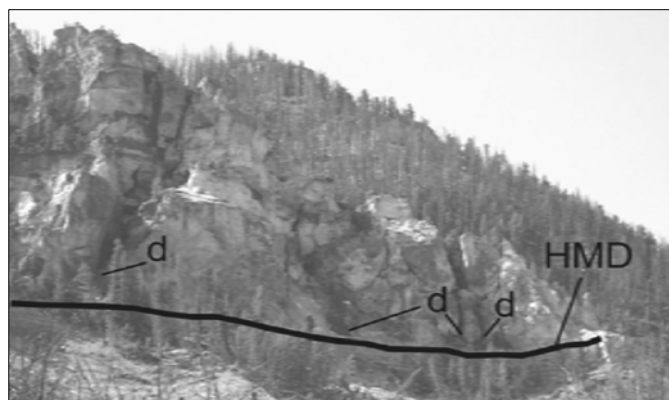


Figure 7. Field relations at the base of Cathedral Cliffs. Eocene igneous dikes (d) terminate along the HMD (from DeFrates and others, 2006).

*Detachment Kinematics  
Eocene Dikes at Cathedral Cliffs*

One extensional mechanism of Hauge's continuous allochthon is the intrusion of an igneous dike swarm that he interpreted to be coeval with faulting, and thus accommodate part of the dilation of the upper plate. These dikes are spectacularly exposed at Cathedral Cliffs (Figure 7), where dozens of dikes pervade allochthonous Paleozoic rocks. DeFrates and others (2006) analyzed the magnetic fabrics of 32 mafic dikes at Cathedral Cliffs using low-field anisotropy of magnetic susceptibility (AMS) as a proxy for flow. These dikes intrude Ordovician-Mississippian carbonate and overlying Eocene volcanic rocks and are truncated along the nearly horizontal HMD. The dikes trend between N10°W and N20°E, are all steeply dipping, and range in width between 0.5 to 3 m. Flow directions for the dikes were determined by the bearing and plunge of the  $K_{\max}$  (maximum principal susceptibility) axes relative to the dike orientation. About 70% of the dikes sampled show typical dike AMS patterns with  $K_{\max}$  and  $K_{\text{int}}$  in the plane of the dike and  $K_{\min}$  normal to the dike plane. As no dikes exist locally in the lower plate, the most reasonable explanation for these dikes is that they are older than, and unrelated to, Heart Mountain faulting, and are thus not kinematically related to the emplacement of the upper plate. The roots of the dikes studied here are likely buried beneath younger volcanic rocks northwest or west of Cathedral Cliffs. It is possible and perhaps likely that dike intrusion occurred immediately prior to the emplacement of the upper plate, and that volcanic processes were involved in the emplacement event.

*Hot Water*

Aharanov and Anders (2006) proposed that the diking at Cathedral Cliffs and elsewhere in the area was essential to the initial movement of the upper plate. In their view, extensive dike intrusion into the upper plate before faulting created a

special condition that allowed horizontal stresses to increase, and thus contributed to elevated pore fluid pressures in the basal Bighorn Dolomite. Simultaneously, the heating caused by the diking event caused the trapped pore waters to expand. These high pore fluid pressures caused the reduction in normal stress needed for initial movement. Once movement was initiated, other mechanisms (volcanic injection, mechanical fluidization, etc.) could have contributed to continued movement of the upper plate.

*Calcite Twinning Strain*

Footwall limestones preserve a layer-parallel shortening strain normal to the subduction margin of North America and maintain this E-W orientation in their original depositional position. Upper plate Madison Limestones preserve this same layer-parallel shortening strain but, as the upper plate blocks are allochthonous, the orientation of the shortening axes is quite varied (Figure 8) thereby documenting the chaotic downslope motion of limestone blocks (Craddock and others, 2000). Many of the blocks rotated about vertical axis as they slid

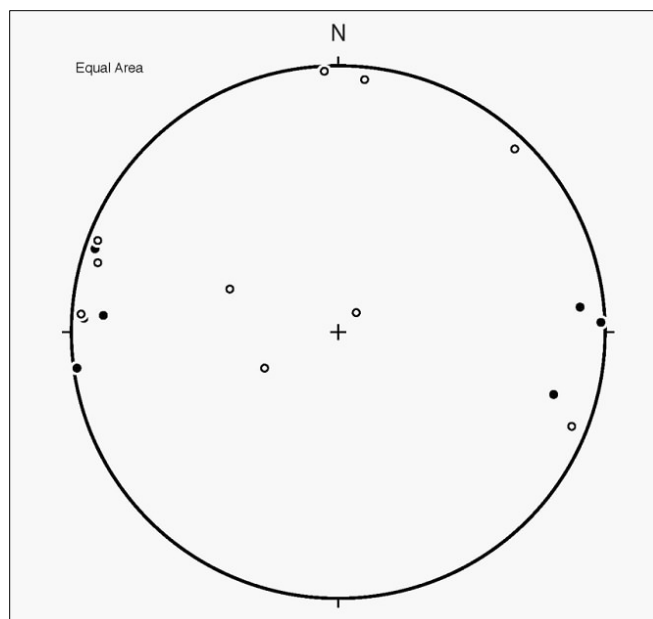


Figure 8. Lower hemisphere projection of pre-detachment, Laramide shortening strains derived from mechanically twinned calcite. Solid circles are footwall limestones which preserve the regional, E-W sub-horizontal shortening whereas allochthonous upper plate limestones (open circles) preserve the same layer-parallel shortening strain but with no pattern (Craddock and others, 2000).

down the detachment. At White Mountain the upper plate marbles have a layer-parallel shortening axis oriented at  $203^\circ$  that constrains the block rotation to be either  $113^\circ$  counterclockwise or  $247^\circ$  clockwise, as compared to the  $90^\circ$  layer-parallel shortening strain in the footwall limestones. We do not have a means to know if there was one rotation or many. White Mountain preserves striations on the detachment that are oriented at  $154^\circ$  so the upper plate block was already rotated as it slid to rest toward  $154^\circ$ . White Mountain is so named because the upper plate rocks are Madison Group limestones that are now marbles; both the marbles and detachment-parallel calcite veins record a vertical shortening strain that is likely the result of post-HMD burial (Craddock and others, in press).

## SUMMARY

### *The fate of tectonic denudation*

The sum of all research over the past 15 years overwhelmingly indicates that Eocene volcanic rocks overlying the HMD are everywhere allochthonous. Also, the preponderance of the evidence suggests that these rocks were emplaced catastrophically during the collapse of part or all of one or more volcanic edifices in the northern Absaroka Range. Thus, the interpretations by Pierce and his colleagues at the U.S. Geological Survey that were developed in the 1960s-1980s of independently emplaced blocks via gravity sliding has attracted little attention by the current generation of workers. Pierce's model of catastrophic emplacement, albeit of a continuous allochthon or large landslide/debris avalanche, has however, been supported by most of the recent work.

### *The fate of the continuous allochthon*

Much of the work done over the past 15 years was stimulated by Hauge's continuous allochthon model, and many of the various aspects of the model were rigorously tested. His idea of all volcanic rocks overlying the HMD being allochthonous rather than being in depositional contact thus far has stood the test of time. Fur-

thermore, all workers today agree that the upper plate was emplaced as part of an intact sheet that was comprised of Paleozoic and volcanic rocks. His observations of faults within upper plate rocks, brecciated lower plate rocks, and lineations along the fault plane have gone unchallenged.

His interpretation of the rate of emplacement, and the kinematics of extension have however been challenged, and the new data that is now available requires modification to the continuous allochthon model. There is now ample subjective and objective evidence that suggest that the upper plate was emplaced catastrophically rather than gradually. Also, volcanic processes, both directly and indirectly, likely led to the initiation of the upper plate, and its continued movement down a gentle slope. Rather than gravity spreading associated with a building volcanic pile, workers today envision the emplacement event as the collapse of a one or more existing volcanic edifices.

How then, can the great many faults described by Hauge (1985) be explained? Certainly, some of these faults could have formed during the catastrophic collapse. Others could have formed prior to the collapse during an earlier episode of gravity spreading (see Beutner and others, 2004). Finally, some could have formed after the collapse event during a later phase of gravitational collapse (see Malone, 1994, for a discussion of some normal faults near Logan Mountain).

### *Did the upper plate override an Eocene land surface?*

One question that has arose since the advent of the continuous allochthon model concerns whether or not the upper plate emplaced onto a land surface in its distal areas (south and west). Another way to couch this question is: Is the basal contact of the upper plate in the distal areas of the HMD a fault, unconformity, or some sort of hybrid? In the proximal areas of the HMD, the answer to this question is clear, and all workers refer to the contact as a fault. In the distal areas of the HMD (i.e., south and east

of Rattlesnake and Pat O'Hara Mountains), the answer to this question is more ambiguous, and dependent on the context of how the upper plate is considered.

Pierce (1957, 1975) in the development of the Tectonic Denudation model for Heart Mountain faulting, interpreted that upper plate of the HMD was emplaced upon an Eocene land surface, and that adjacent/overlying volcanic rocks were later deposited on this same land surface. Hauge (1985, 1990) argues that the upper plate of the HMD may not have transgressed an Eocene land surface. He recommended that the term former-land-surface be avoided, and the descriptive term "detachment ramp" to be used instead. Based on structural and stratigraphic data gathered during my research and earlier investigations by other workers, there is ample evidence that an Eocene land surface did indeed exist, and that this land surface was overridden by allochthonous Paleozoic and volcanic rocks. These lines of evidence include:

1) Sundell (1990) reports the existence of a regional unconformity at the base of the volcanic succession throughout the Absaroka Range. The entire Eocene succession was deposited in a wide range of terrestrial (e.g., Willwood Formation), volcanogenic environments (e.g., AVS units), and consequently, numerous breaks in deposition (unconformities) must exist. The contact at the base of the DCM represents a sharp contrast in sedimentation. The Willwood Formation consists of basin-fill sandstones and mudstones, and the Wapiti Formation consists of volcanogenic strata, thus a break in deposition must occur between these two successions.

2) There is a younger over older age relationship beneath all volcanic rocks in the distal areas of the Detachment. If the volcanic and carbonate rocks were indeed emplaced together as part of the same catastrophic event, this age relationship is more consistent with an unconformity rather than a fault.

3) Petrified wood is present in the matrix of the DCM, suggesting that a forest was overridden

and that debris from this forest was incorporated during the emplacement of the debris avalanche.

4) The complex local relief on the lower surface is more likely to be the result of fluvial-geomorphic rather than structural processes (Malone, 1996, 1997).

5) Elsewhere in the eastern Absaroka Range, as much as 300 m of distal facies volcanic rocks (the lower stratified and tuff breccia members of the Wapiti Formation of Malone, 1996, and 1997) occur between the DCM and underlying Willwood Formation. These rocks are absent where DCM rests directly upon the Willwood Formation and older units. The absence of these older volcanic rocks requires erosion and/or no deposition of volcanic strata prior to the emplacement of the DCM, thus indicating an unconformity.

6) If this contact were some sort of a low-angle fault that did not "daylight" and where the upper plate did not transgress a sizeable land surface which includes a number of foot wall ramps, there would need to be an identical number of hanging wall (upper plate) ramps in order to construct a viable and admissible cross section, according to thin-skin geometric theory. Furthermore, the entire Mississippian-Eocene section that is present within the foot-wall ramp would need to be found in the hanging wall somewhere. A few small blocks of the Willwood formation are present, much less than a fraction of a percent of the entire upper plate, but there are no rocks in the upper plate between the age of Mississippian and Eocene. The simplest explanation is that these rocks never existed in the upper plate and that they were removed by erosion during the Laramide Orogeny rather than first being incorporated in the upper plate, transported to the Big Horn Basin, and then eroded away since Eocene time without a trace. To take this a step further, it is even simpler to state that a hanging wall ramp never existed at all, and the pre-faulting situation included an erosional surface to the south and east of the footwall ramp.

7) A few small fragments, some more than 100 m in maximum dimension, of the Willwood Formation occur at structurally high positions within the DCM (Malone, 1996). The simplest explanation for these enigmatic features is that they were incorporated from the underlying strata, perhaps small hilltops, during emplacement of the DCM.

Based on the above lines of evidence, it is almost certain that the distal toe of the allochthon did indeed cross an Eocene land surface during emplacement, as originally envisioned by Pierce (1973).

#### *Semantics and Research Context Issues*

The Heart Mountain Detachment is enigmatic, complex, well studied, controversial, and unfortunately still poorly understood. In our view, a major part of the problem here is the enormous volume of literature from a variety of sub-disciplines within geology that has been produced over the years. Such a volume makes it very difficult to write simple, short paper that will honor all of the past research. Similarly, this large amount of work has resulted in at least two different contexts in which the present generation of workers is operating; this makes it very difficult and in some cases impossible for these workers to communicate. For example, some workers (e.g., Hauge) view the HMD purely in the context of structural geology. In the context of structural geology, deformed volcanic and Paleozoic rocks are allochthonous and part of an upper plate. The boundaries between components of the upper plate are faults. The lower contact of allochthonous rocks is everywhere a detachment. Relief on the detachment in the distal areas is interpreted to be attributed to footwall and side wall ramps. Figure 9 is a photograph of the Detachment at Jim Smith Creek, which is in the proximal areas of the HMD. Here the contact is razor sharp. Hauge (1985) reported brecciated volcanic and Paleozoic rocks along the detachment, an igneous dike that terminates on the HMD, and a striated microbreccia just above the contact. Here, volcanic rocks are allochthonous in the traditional sense, and they were downfaulted

and translated during the emplacement of the upper plate.

A second context is to view the allochthonous rocks in a geomorphic/stratigraphic context. For example, at Mount St Helens, there is a body of rocks on the north side of the mountain that has a distinct lower contact with some relief, covers a several 10s of km<sup>2</sup>, is more than 100 m in thickness in places, consists of blocks and matrix, has a hummocky upper surface, was observed to be associated with an eruption and blocked the drainage of a river system. We can easily call this a debris-avalanche deposit because the debris avalanche that formed the deposit was observed as it was emplaced in 1981. A similar body of sediment and rock exists at the base of a number of volcanic edifices around the world. These can comfortably be called debris-avalanche deposits as well, even though the debris avalanche was not observed, it was inferred, which is uniformitarianism in the most simple form. If a body of rock of similar texture, thickness, structure, composition, areal extent, etc. as part of an Eocene volcanic succession in Wyoming, this geomorphic/stratigraphic context could still apply. The geomorphic/stratigraphic context is the basis for the work of Malone, Sundell, Anders, and Craddock. In this context, the body of allochthonous Paleozoic and Eocene rocks in the distal regions of the HMD as a lithostratigraphic unit within the Eocene volcanic succession of the Absaroka Range. Instead of fault-bounded



Figure 9. Field relations at Jim Smith Creek. For a detailed description and interpretation of this locality, see Malone and others, 1999.

blocks, these are blocks separated by matrix. Some blocks are volcanic, some are limestone. Some are big (>10 km across), some are small. The basal contact is an unconformity, which is a sedimentary rather than tectonic contact. Figure 10 provides a photograph and geologic map of the Bear Creek area on the southwest side of Sheep Mountain. Figure 11 is a cartoon that illustrates the issue of where or not the basal contact in the distal areas of the HMD

Thus, is there a fundamental difference between a catastrophically emplaced extensional allochthon and a large landslide/debris avalanche?

Future workers are advised to use appropriate, non-genetic terminology as possible, and should appreciate that a feature as large and complex as the Heart Mountain Detachment requires input from many subdisciplines of geology.

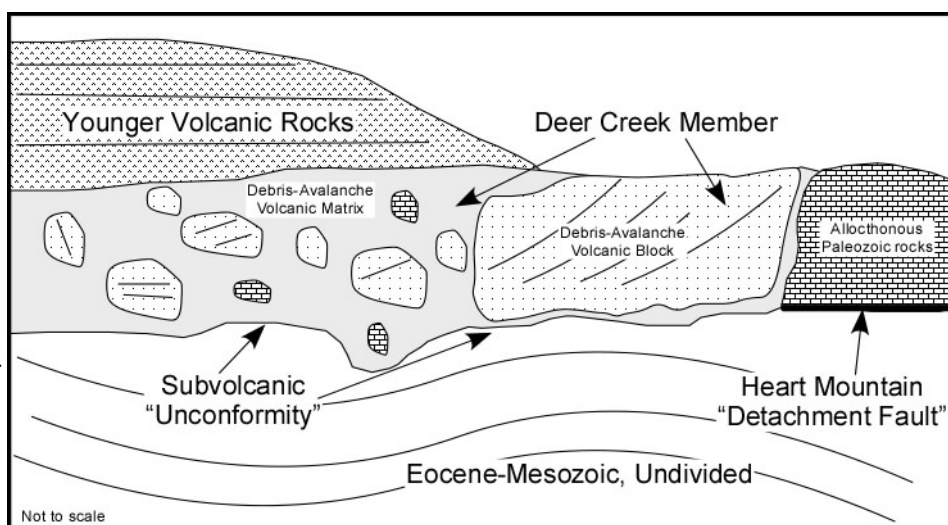


Figure 11. Cartoon of the structural relationship between volcanic and Paleozoic rocks in the distal areas of the HMD. Paleozoic rocks rest upon younger strata; it is easy to consider this contact a detachment fault. However, where Eocene volcanic rocks overlie the same strata, which are older, a more reasonable interpretation would be an unconformity. As volcanic rocks and Paleozoic rocks comprise a laterally and mappable lithostratigraphic unit within the Absaroka Volcanic succession, and because these rocks are interpreted to be the product of an edifice collapse (i.e., debris-avalanche deposit), we believe it is more appropriate to consider the basal contact everywhere in the distal areas of the HMD an unconformity.

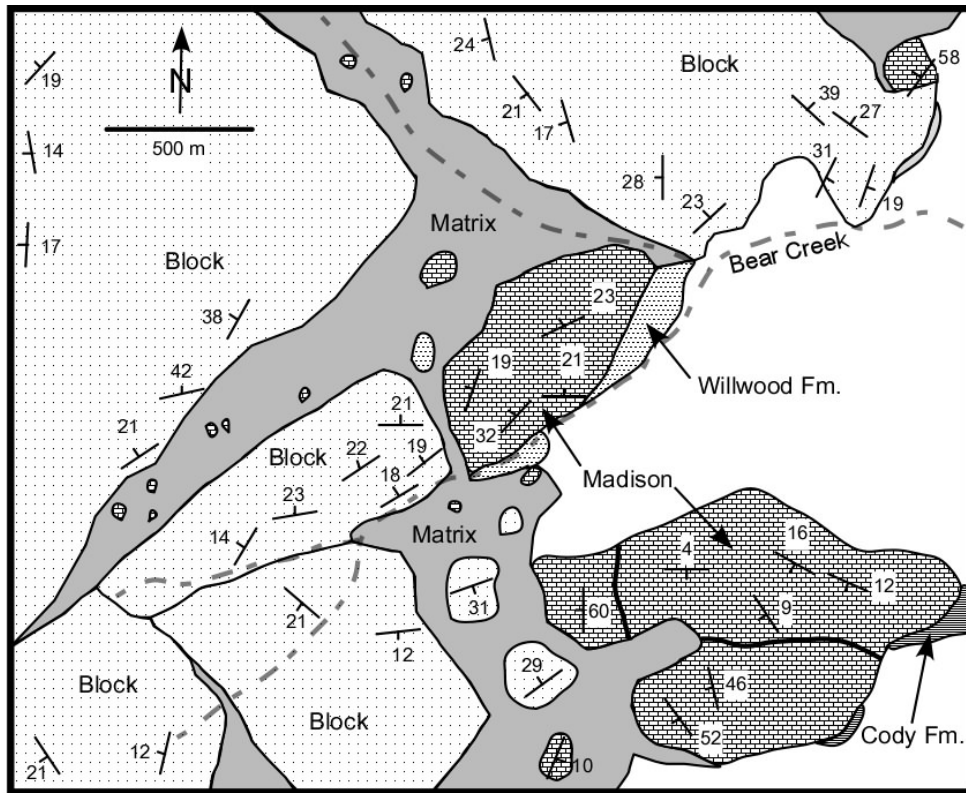
### *Summary of the Emplacement of the Upper Plate*

Most workers over the past 15 years agree that the best explanation now for the emplacement of the upper plate of the HMD is some sort of catastrophic gravitational collapse of part of the Absaroka volcanic pile about 50 million years ago (e.g., Malone, 1994, 1995, 1996, 2000; Buetner and Craven, 1996; Beutner and Gerbi, 2005, Aharanov and Anders, 2006; Craddock and others, 2000; Craddock and others, in

press). In light of this work, the following is proposed sequence of events for tectonism along the Heart Mountain fault (please compare with Malone, 1996, Figure 25; and Beutner and Gerbi, 2005, Figure 16).

1) Prior to Absaroka volcanism, Laramide tectonism created the surrounding structural features including the Beartooth Uplift, Pat O'Hara and Rattlesnake Mountain anticlines, and the Absaroka and Big Horn basins (Figure 12; Figure 13a). Uplift of the anticline features was coincident with the deposition of Willwood Formation sandstones and mudstones in the

adjacent basins. The boundary between the Beartooth Uplift to the north and the Absaroka Basin to the south is structurally complex and probably consisted of two northwest-trending fault/monocline systems, each displaying several thousand feet of structural relief. The northern fault zone is the Clarks Fork fault system, and the southern fault zone is buried beneath younger volcanic rocks, but is probably along strike with the Pat O'Hara Mountain anticline. The evidence for this southern fault/monocline is clearly indicated by the sub volcanic rocks that occur within the region. To the



A.



B.

Figure 10. A. Geologic map of the Bear Creek area on the south side of Sheep Mountain in the distal areas of the Detachment. This area is an excellent place to view the relationship between allochthonous Paleozoic and Eocene volcanic rocks. Here, four or five volcanic blocks, each more than 500 m in maximum dimension, rest beside a like number of allochthonous Paleozoic Blocks. Each block has a unique internal structure. Debris-avalanche matrix occurs between the various blocks. Several smaller blocks of volcanic and Paleozoic rocks and Eocene Willwood Formation occur within the matrix. B. View to the north of the Bear Creek area, illustrating the field relations between allochthonous Paleozoic rocks and Eocene volcanic rocks.

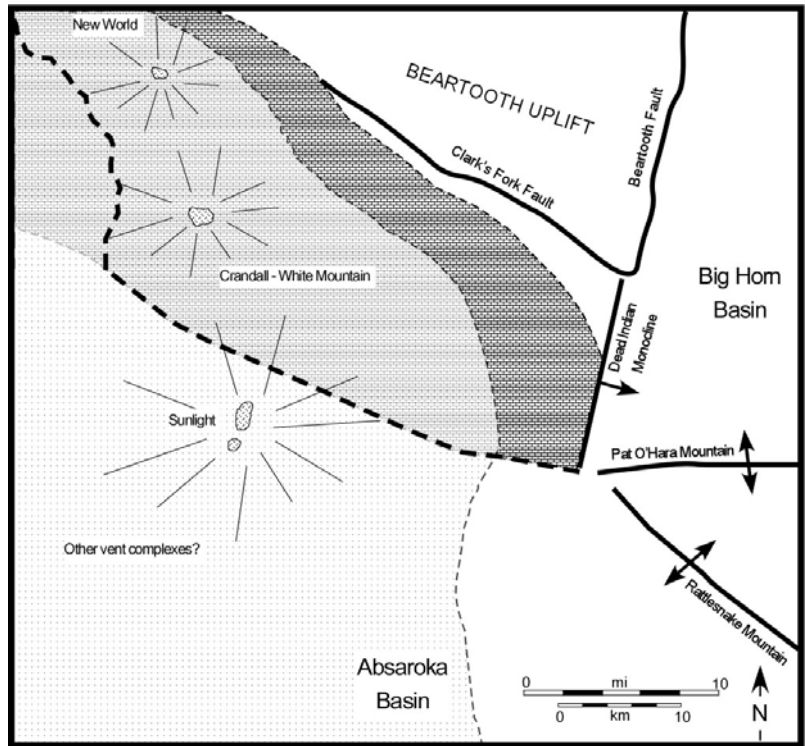


Figure 12. Paleogeographic reconstruction of the HMD area immediately before the emplacement of the upper plate at about 50 Ma (Modified from Malone, 1996).

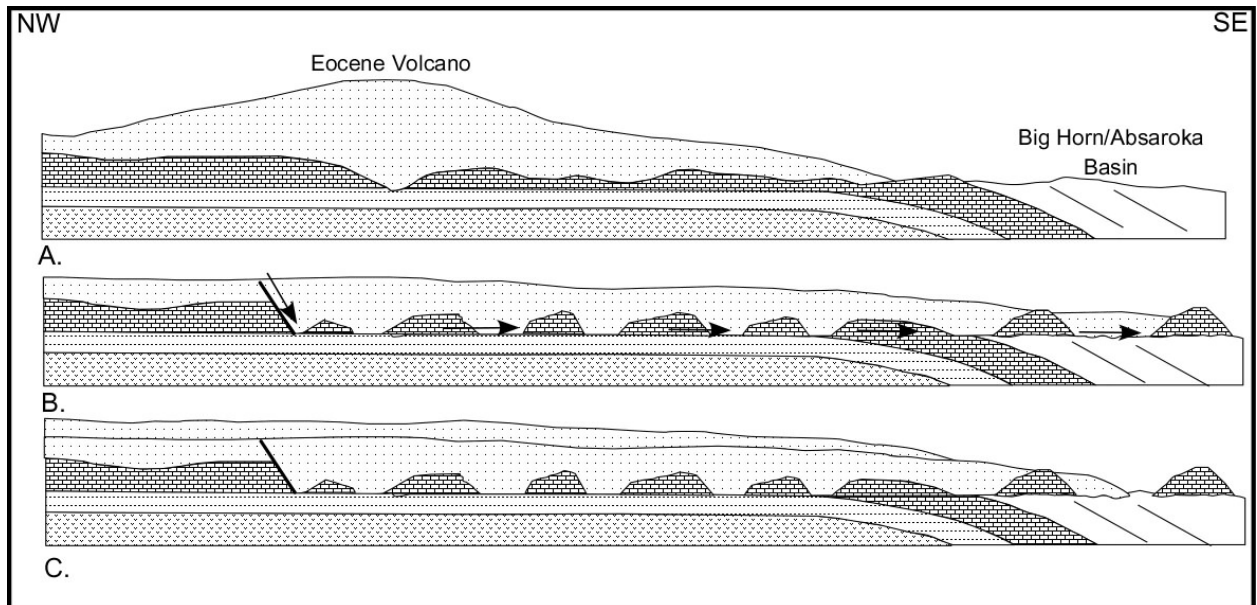


Figure 13. Reconstruction of the edifice collapse that led to the development of the HMD (Modified from Malone, 1996, Malone and others, 1999, and Beutner and Gerbi, 2005).

north, in the Clark's Fork drainage, the sub-volcanic rocks are everywhere Paleozoic in age. In the Shoshone River drainage west of Rattlesnake Mountain >25 km to the south, the sub volcanic rocks are everywhere Mesozoic and Tertiary in age (Malone 1996, 1997). A major structural discontinuity with several thousand meters of relief is needed to account for these field relations. A buried Laramide fault zone/monocline is the simplest explanation for this structural discontinuity.

Between these two Laramide fault zones, Paleozoic rocks dip gently off of the Beartooth Uplift to the south and southeast. These rocks comprise most of the future bedding plane and ramp phases of the HMD.

2) The waning stage of Laramide tectonism was accompanied by the inception of igneous activity in the Absaroka Volcanic Province. In the northern Absaroka Range, several large stratovolcanoes developed likely in the vicinity of the younger New World, Crandall, and Sunlight vent complexes. Relief between the tops of the volcanoes and the basin floors at this time, and throughout Absaroka volcanism, probably exceeded 20,000 ft (6230 m). To the south, in the present Shoshone River valleys, basinal conditions persisted, and the Absaroka Basin was filled with more than 1000 ft (300 m) of light-colored distal-facies sandstones, mudstones, and conglomerates.

3) Ongoing tectonism during the waning stages of the Laramide orogeny, active erosion of along the toe of the volcanic pile, the rapid deposition of loosely consolidated volcanoclastic material, and volcanic-plutonic-hydrothermal activity in the Absaroka Range created an unstable gravitational situation for the region.

4) The injection of volcanic gas and glass (Beutner and Gerbi, 2005; Douglass and others, 2003) and/or the reduction of normal stress through igneous diking and the consequent heating of pore fluids, cause the initial movement of the upper plate. The upper plate contained volcanic rocks, Paleozoic rocks, and many small intrusions.

5) Initial and subsequent movement was catastrophic, with the entire event taking less than an hour. This catastrophic movement along the HMD created significant frictional heat, which caused the dissociation of CO<sub>2</sub> and development of the unique textures and structures found in the detachment breccia (Anders and others, 2000, Beutner and Craven, 2005; Craddock and others, in press). The presence of this supercritical fluid reduced friction, and enabled the upper plate to be emplaced along a gentle slope. Mechanical fluidization described by Anders and others (2000) and other workers may have aided in the mobility of the upper plate (Figure 13b).

6) The proximal areas of the HMD are dominated by vent facies volcanic rocks. These rocks were down-faulted during the emplacement event. The geometry and kinematics described by Hauge may still apply, but at a faster rate than he proposed. In the distal areas of the HMD, the upper plate was emplaced onto an Eocene land surface as a gigantic debris-avalanche that contained both carbonate and volcanic components. The Rattlesnake Mountain/Pat O'Hara Mountain structures served as a wedge, funneling some of the debris avalanche to the east into the Big Horn Basin, and some to the South into the Absaroka Basin. The debris avalanche came to a rest once fluidization dissipated. The debris avalanche dammed the paleodrainage system, causing desiccation in Lake Gosuite, several hundred kilometers to the south.

7) After emplacement, minor gravitational adjustments occurred, and eventually volcanism resumed, burying the upper plate. Eventually, the upper plate was dissected by stream erosion, leaving remnants of resistant rocks (e.g., Heart Mountain; Figure 13b).

#### *Recommendations for the next phase of research*

During the past 15 years, significant advancements have been made to the understanding of the emplacement of the upper plate of the HMD. The stratigraphy of volcanic rocks, at

least in the distal areas of the HMD, the timing of movement, the rate of upper plate movement, the kinematic pattern of the upper plate, and the mechanism for fluidization are better understood now than ever before. However, many significant problems remain:

In light of the available geochronology data, is the emplacement of the upper plate better explained as a single event, or are multiple events required?

Where was the volcanic edifice that collapsed? Can the emplacement rate of the upper plate at White Mountain as determined by Craddock and others (in press) be supported by similar calculations elsewhere?

Can a viable volcanic stratigraphy be developed in the proximal areas of the HMD where vent facies rocks dominate? If so, can the edifice collapse event be reconstructed in better detail, including the kinematics of volcanic rock movements?

These questions, and others that arise, will be answered by additional detailed geologic mapping of Eocene volcanic and plutonic rocks. This mapping should be supported by paleomagnetic analyses and extensive isotopic age determinations.

## REFERENCES CITED

Aharonov, E., and Anders, M.H., 2006, Hot water: a solution to the Heart Mountain detachment problem?: *Geology*, v. 34, p. 165-168.

Anders, M.H., Aharonov, E., and Walsh, J.J., 2000, Stratified granular media beneath large slide blocks: Implications for mode of emplacement: *Geology*, v. 28, p. 971-974.

Beutner, E.C., and Craven, A.E., 1996, Volcanic fluidization and the Heart Mountain detachment, Wyoming: *Geology*, v. 24, p. 595-598.

Beutner, E.C., Hauge, T.A., Colgan, J.P., and Oesleby, T.W., 2004, Two stage emplacement of the South Fork-Heart Mountain fault system, NW Wyoming: *Geological Society of America, Abstracts with Programs*, v. 36, no. 4, p. 34.

Beutner, E.C., and Gerbi, G.P., 2005, Catastrophic emplacement of the Heart Mountain block slide, Wyoming and Montana, USA: *Geological Society of America Bulletin*, v. 117, p. 724-35.

Craddock, J.P., Neilson, K.J., and Malone, D.H., 2000, Calcite twinning strain constraints on Heart Mountain detachment kinematics, Wyoming: *Journal of Structural Geology*, v. 22, p. 983-991.

Craddock, John P., Malone, David H., Magloughlin, Jerry, Cook, Avery L., Reiser, Michael E., and Doyle, James R., *in press*, Dynamics of the emplacement of the Heart Mountain allochthon at White Mountain: Constraints from calcite twinning strains, anhysteretic magnetic susceptibility and thermodynamic calculations: *Geological Society of America Bulletin*.

DeFrates, J., Malone, D.H., and Craddock, J.P., 2006, Anisotropic magnetic susceptibility (AMS) analysis of basalt dikes at Cathedral Cliffs, WY: Implications for Heart Mountain Faulting: *Journal of Structural Geology*, v. 28, p. 9-18.

Douglas, T.A. Chamberlain, C.P., Poage, M.A., Abruzzese, M., Schultz, S., Henneberry, J., and Layer, P., 2003, Fluid flow and the Heart Mountain Fault; a stable isotopic, fluid inclusion, and geochronologic study: *Geofluids*, v. 3, p. 13-32.

Feeley, T.C., and Cosca, M.A., 2003, Time vs. Composition Trends of magmatism at Sunlight Volcano, Absaroka Volcanic Province, Wyoming: *Geological Society of America Bulletin*, v. 115, p. 714-728.

Gunnell, G.F., Bartels, W.S., Gingerich, P.D., and Torres, V., 1992, Wapiti Valley faunas, early and middle Eocene fossil vertebrates from the North Fork Shoshone River Valley, Park County, Wyoming: Cont. from the Museum of Paleontology, University of Michigan, v. 28, p. 247-287.

Hauge, T.A., 1985, Gravity-spreading origin of the Heart Mountain Allochthon, northwestern Wyoming: *Geological Society of America Bulletin*, v. 96, p. 1440-1456.

Hauge, T.A., 1990, Kinematic model of a continuous Heart Mountain allochthon: *Geological Society of America Bulletin*, v. 102, p. 1174-1188.

Hauge, T.A., 1993, The Heart Mountain detachment, northwestern Wyoming: 100 years of contro-

versy: *in* Snoke, A.W., Steidtmann, J.R., and Roberts, S.M., eds., *Geology of Wyoming: Wyoming Geological Survey Memoir #5*, p. 530-571.

Hiza, Margaret M., and Snee, Lawrence W., 1999, Protracted deformation (> 2 Ma) of the Heart Mountain detachment, Absaroka Volcanic Province, Wyoming: *Geological Society of America, Abstracts with Programs*, v. 31, p. 428.

Malone, D.H., 1994, A debris-avalanche origin for Absaroka volcanic rocks overlying the Heart Mountain detachment, northwest Wyoming: Unpublished Ph.D. dissertation, The University of Wisconsin, 292 p.

Malone, D.H., 1995, A very large debris-avalanche deposit within the Eocene volcanic succession of the Northeastern Absaroka Range, Wyoming: *Geology*, v. 23, p.661-664.

Malone, D.H., 1996, A revised interpretation of Eocene volcanic stratigraphy in the lower North and South Fork Shoshone River Valleys, Wyoming: Wyoming Geological Association, 47th Annual Field Conference Guidebook, p. 109-138.

Malone, D.H., 1997, Recognition of a distal facies greatly extends the domain of the Deer Creek debris-avalanche deposit (Eocene), Absaroka Range, Wyoming: Wyoming Geological Association, Annual Field Conference Guidebook, v. 48, p. 1-9.

Malone, D.H., 2000, Structure and stratigraphy of Eocene volcanic rocks in the proximal areas of the Heart Mountain detachment: Wyoming Geological Association, Field Conference Guidebook, v. 51, p. 109-131.

Malone, D.H., Hauge, T.A. and Beutner, E.L., 1999, Field guide for the Heart Mountain detachment and associated structure: *Geological Society of America Field Guide*, v. 1, p. 177-203.

Pierce, W.G., 1957, Heart Mountain and South Fork detachment thrusts of Wyoming: *American Association of Petroleum Geologists Bulletin*, v. 41, p. 591-626.

Pierce, W.G., 1973, Principal features of the Heart Mountain fault and the mechanism problem: *in* DeJong, K., ed., *Gravity and Tectonics*, John Wiley & Sons, New York, p. 457-471.

Pierce, W.G., 1979, Clastic dikes of Heart Mountain fault breccia, northwestern Wyoming, and their sig-

nificance: U.S. Geological Survey Professional Paper 1133, 25 p.

Pierce, W.G., 1987, The case for tectonic denudation by the Heart Mountain Fault; a response: *Geological Society of America Bulletin*, v. 99, p. 552-568.

Rhodes, M.K., Malone, D.H., Carroll, A.R., and Smith, M., 2007, Sudden desiccation of Lake Gosiute at 49 Ma: A downstream effect of Heart Mountain Faulting?: *The Mountain Geologist*, no. 1, p 1-10.

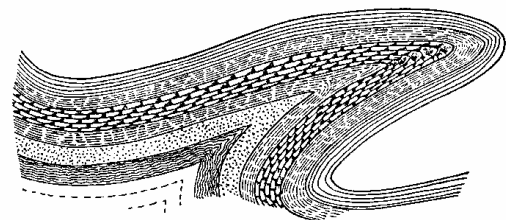
Smith, M.E., Singer, B., and Carroll, A.R., 2003,  $^{40}\text{Ar}/^{39}\text{Ar}$  geochronology of the Green River Formation, Wyoming: *Geological Society of America Bulletin*, v. 115, p. 549-565.

Sundell, K.A., 1990, Sedimentation and tectonics of the Absaroka Basin of northwestern Wyoming: Wyoming Geological Association, 41st Annual Field Conference Guidebook, p. 105-122.

Templeton, A.S., Sweeny, J., Jr., Manske, H., Tilghman, J.F., Calhoun, S.C., Violich, A., and Chamberlain, C.P., 1995, Fluids and the Heart Mountain fault revisited: *Geology*, v. 23, p. 929-932.

Torres, V., and Gingerich, P.D., 1983, Summary of Eocene stratigraphy at the base of Jim Mountain, North Fork of the Shoshone River, northwestern Wyoming: Wyoming Geological Association, 34th Annual Field Conference Guidebook, p. 205-208.

Torres, V., 1985, Stratigraphy of the Eocene Willwood, Aycross, and Wapiti formations along the north fork of the Shoshone River, north-central Wyoming: *University of Wyoming Contributions to Geology*, 1985, v. 23 no. 2, p.83-97.



# REVERSE FAULT DUPLICATION OF THE J-M Pd/Pt REEF - OPPORTUNITIES FOR ENHANCED MINE PRODUCTION IN THE STILLWATER COMPLEX, MONTANA

**Bruce E. Cox**

Missoula, Montana - Hecla Mining Company, Lucky Friday Mine  
Stillwater mine geologist 2001-2006

**Paul Holick**

Columbus, Montana - Stillwater mine production geologist

## INTRODUCTION

Stillwater Mining Company operates two palladium-platinum mines within the Stillwater mafic layered intrusive complex in south-central Montana. The mines at Nye and East Boulder are developed within the J-M (Johns-Manville) Reef, a discrete PGE-mineralized horizon in the lower Banded Series on the north flank of the Beartooth Mountains.

The Beartooth uplift, associated with the Laramide Orogeny, rotated Stillwater complex strata into their current steeply north-dipping position (Figure 1). Uplift mechanics produced an array of faults that displace the J-M reef in strike-slip, oblique-slip and reverse style with displacements ranging from a few feet to a few miles. A four-dimensional understanding of this complex series of faults has been enabled by the

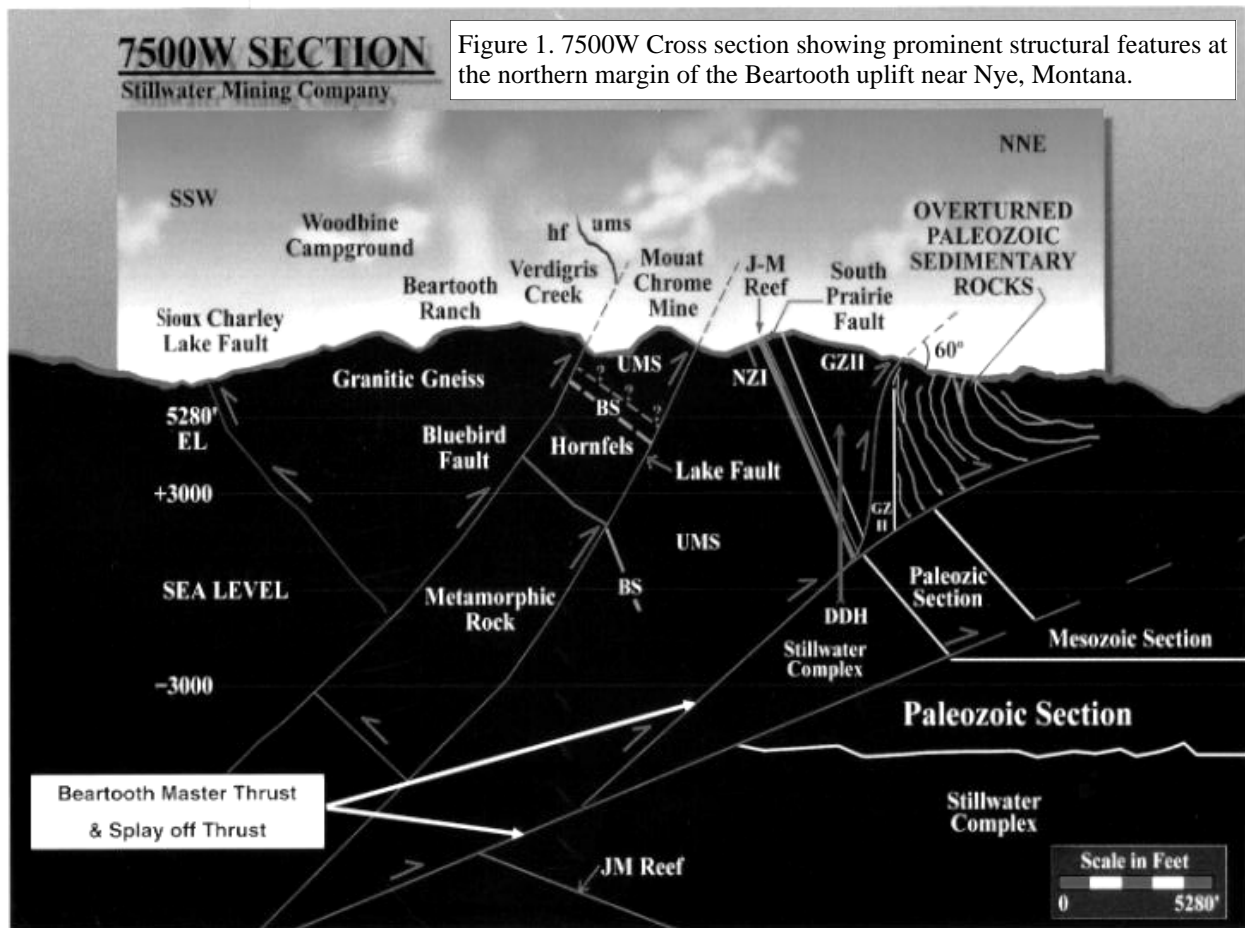


Figure 1. 7500W Cross section showing prominent structural features at the northern margin of the Beartooth uplift near Nye, Montana.

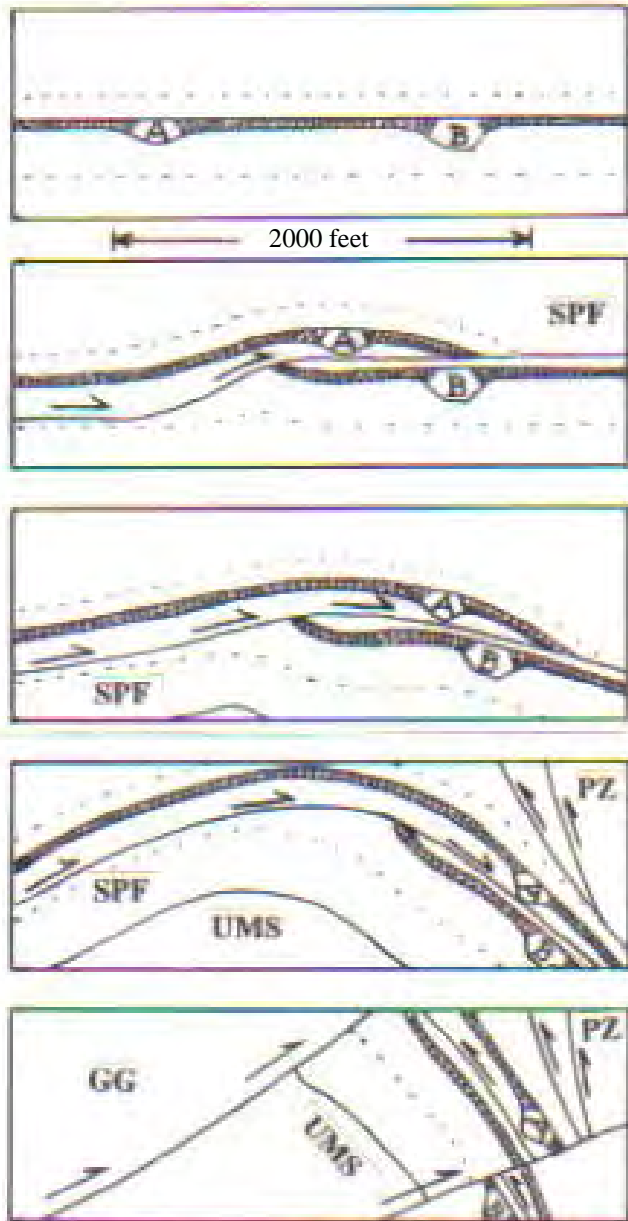


Figure 2. Schematic cross-sections (view west) depicting hypothetical sequential development of repeated sections of J-M Reef. A and B represent reef ballrooms for tracking relative displacements. SPF = South Prairie fault, UMS = Stillwater ultramafic series, GG = granitic gneiss, PZ = Paleozoic strata. Vertical exaggeration ~ 7X.

high density of development core drilling, over two decades of underground production geology and by several generations of surface geologic mapping (Czamanske and Zientek, 1985).

## REVERSE FAULTS

The South Prairie fault (SPF) is one of several long-lived regional structures oriented roughly parallel to Banded Series stratigraphy and traceable for about 13 miles along strike. The close proximity of SPF to the J-M Reef hangingwall and local convergence of these two features suggest that initial displacement along the SPF may have occurred during the earliest stages of the Beartooth uplift as a low-angle, north-directed reverse fault which ramped across J-M Reef strata (Figure 2). Most of the displacement along the SPF probably occurred during the main stages of Laramide tectonism as south-directed high-angle reverse movement (refer to Geraghty, 2008, this volume).

The resultant fault is commonly a few inches thick but locally is greater than 10 feet thick. The SPF is rarely, if ever, seen in surface outcrops but underground exposures display a range of shear features including protomylonite, cataclasite, elaborate slickenside surfaces, strongly contorted clayey gouge and lenses of plucked wallrock. The fault locally exploits one of several thin strata of buckshot-textured olivine cumulate (oCBS) which occur in the immediate hangingwall of the reef. Alteration and ore mineral character within the fault suggest local remobilization and possible enrichment of ore-bearing sulfides. Daily sampling in several South Prairie fault-hosted stopes has documented that the dark green-to-black gouge at the sole of the fault contains PGM grades equal to or greater than immediately adjacent unfaulted reef strata.

## PRODUCTION IN DUPLEX ZONES

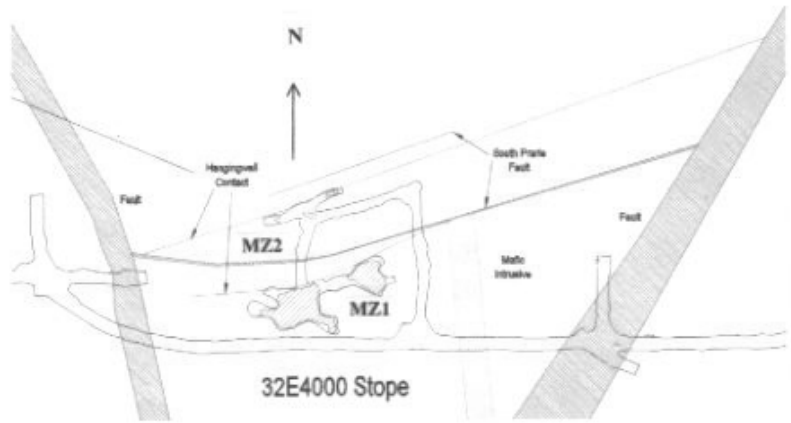
The JM Reef at the Nye operation is locally duplicated across (occurs on both sides of) the SPF. Within duplex packages, mineralized reef strata on the south side of the SPF are commonly different from those on the north side, suggesting that the duplicated section has been displaced a few hundred feet to >2,500 feet from its original position. In these sectors of the mine, development drilling and mapping along the footwall laterals show that the convergence

of SPF and JM Reef has a scoop-like geometry in which the duplexed package is flanked by strike-slip faults (Figure 3).

Duplex features can contain two or more slices of ore-grade JM Reef. Defining the geometry and grade of duplex zones can yield improved efficiency in the mining process by providing access from a single development crosscut to mine multiple ore headings or stacked reef slices within a single heading (Figure 4).

Duplex packages commonly have shorter strike and dip extent than unfaulted sections of mineralized reef and can pose engineering challenges for the location of access crosscuts, methods of ground support and overall stope sequencing. However, mining several faces concurrently from the same access crosscut can reduce the

Figure 3. Plan view of 32E4000 Stope. MZ1 is in-place mineralized reef and MZ2 is fault-repeated mineralized reef.



development cost per ton of ore extracted and appears to outweigh the greater care required for stope planning.

Production from sectors of repeated reef historically represent approximately 5% of all production at the Nye operation. Several other duplex targets have been identified and may eventually be mined as alternative ground support methods prove viable or as narrow width mining methods are given greater emphasis.

The authors appreciate the willingness of Stillwater Mining Company to allow access to data for this paper.

**REFERENCES CITED**

Czamanske, G.K., and Zientek, M.L., editors, 1985, The Stillwater Complex, Montana: Geology and Guide: Montana Bureau of Mines and Geology, Special Publication 92, 396 p.

Geraghty, E.P., 2008, Laramide structural features in the Stillwater Complex portion of the Beartooth Mountains front: forethrusts, backthrusts, duplexes, an "evolved" triangle zone: Northwest Geology, vol. 37 (*this volume*).

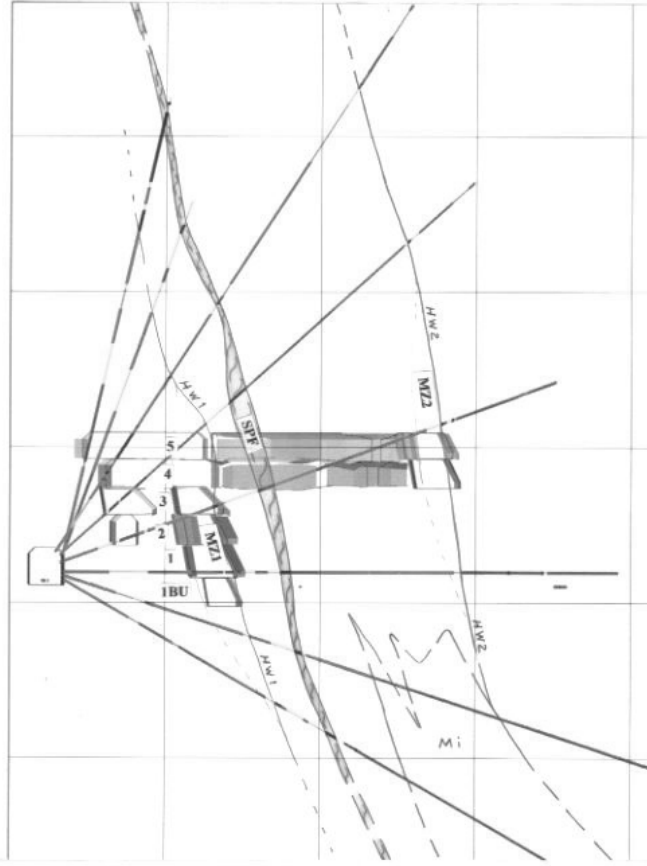
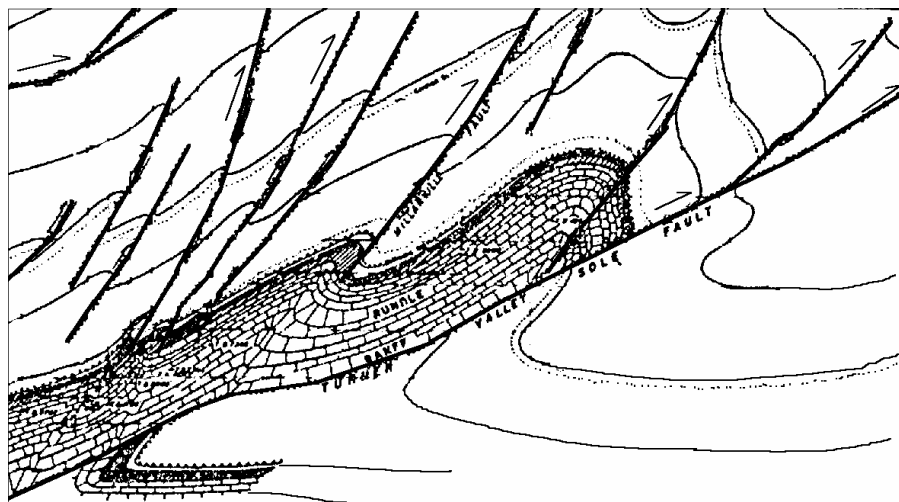


Figure 4. Cross-section through 32E4000 Stope showing geologic interpretation from drill core logs and mined floor 1 bottom-up and floors 1-5. Floors 6 and 7 are not shown. 50-foot square grid, view west.



# GEOCHEMISTRY OF CRETACEOUS AND TERTIARY PLUTONS OF THE GREAT FALLS TECTONIC ZONE: IMPLICATIONS FOR CRUSTAL EVOLUTION

Kelly R. Probst, Paul A. Mueller, and George Kamenov

*Department of Geological Sciences, University of Florida, Gainesville, FL 32611*

---

## Abstract

Constraining the age and tectonic origin of the crust in the Great Falls tectonic zone (GFTZ) is important to understanding the accretionary history of Laurentia. Because the basement of the GFTZ is not well exposed, isotopic and elemental studies of the Cretaceous and Tertiary plutons intruded into this zone provide constraints on the age and composition of this crust. Trace element, Sr, Nd, and Pb isotopic compositions of these magmatic rocks show several important characteristics: 1) LREE enrichment with minimal Eu anomalies and HREE contents < 10x chondrites indicate a mafic lower crustal source containing garnet, amphibole, and/or pyroxene with little or no plagioclase, 2) Depletion in HFSE (e.g., Nb) suggests this source was originally formed in a convergent margin, 3) Sm-Nd model ages (TDM) range from 1.1-1.9 Ga and whole rock Pb isotopes provide a nearly linear array at ~2.1 Ga, indicating that Archean crust is unlikely to be directly involved. Lu/Hf isotopic systematics preserved in zircon grains from individual plutons reveal Paleoproterozoic model ages in all cases. The western Highland Mountains contain an additional zircon population characterized by an Archean model age (~3.0 Ga); there is no evidence of Archean grains within the eastern study area. These observations support models that suggest the GFTZ formed as part of a convergent margin, possibly related to a collision between the Wyoming Province and Medicine Hat block.

*Editors' note:* Tables 1 and 2 are Excel spreadsheets, available for download at [www.trgs.org/TOC-7.htm#2008](http://www.trgs.org/TOC-7.htm#2008)

## INTRODUCTION

### Background

Many aspects of the evolution of Laurentia remain unclear because the geologic evolution of boundary zones between many basement age provinces is not well constrained. One outstanding example of this problem is exemplified by the number of extant proposals for the identity of the craton(s) that separated from SW Laurentia during the Neoproterozoic breakup of Rodinia. Australia, South China, and Siberia have been proposed as this conjugate, but the paucity of high resolution geologic and paleomagnetic data prevent the development of a unique solution (Burrett and Berry, 2000; Karlstrom et al., 2001; Wingate et al., 2002; Gallet et al., 2000; Sears and Price, 2003; Meert and Torsvik, 2003). One key area that is critical to reconstructing the evolution of western Laurentia is the Precambrian basement of the Great Falls tectonic zone (GFTZ). This zone remains poorly characterized because of the lack of basement exposure due to the accumulation of a thick sedimentary cover (e.g., Belt-Purcell), Mesozoic terrane accretion, and plutonism (O'Neill and Lopez, 1985; Mueller, et al., 1995; Boerner et al., 1998). A potential window into this largely buried basement is available via study of the numerous Mesozoic and Cenozoic plutons within the GFTZ. Extensive plutonism marked the Mesozoic and Cenozoic of the western United States, including the GFTZ, which was probably the result of Farallon/Kula Plate subduction beneath the Cordilleran margin (Dickinson, 1981; Humphreys et al., 2003). The composition of these mostly felsic plutons provides an indirect sample of the Precambrian basement, as suggested by DePaolo (1988). DePaolo (1988) showed that granitoid rocks can provide a reliable means of sampling the iso-

topic composition of the deeper parts of the crust. Identifying the petrogenetic processes involved in forming these plutons provides invaluable information about source material and/or interactions of mantle-derived magmas with the intervening crust.

Systematic variations of trace element and isotopic systems provide highly sensitive tools in correlating the chemistry of these young plutonic rocks to their petrogenetic processes and sources within mantle and crustal reservoirs (e.g., Farmer and DePaolo, 1983; Zartman, 1988). Early isotopic mapping in the western United States was conducted in the 1970's using  $^{87}\text{Sr}/^{86}\text{Sr}$  as the primary tool. Kistler and Peterman (1973) identified the proposed boundary between cratonic North America and Phanerozoic accreted terranes by mapping Sr isotopic ratios of young plutonic rocks and identified this boundary as the  $^{87}\text{Sr}/^{86}\text{Sr}$  0.706 line. They demonstrated that the initial stron-

tium isotopic ratios in young rocks located in central California were dependent on geographic location, reflecting the distribution of basement rocks of differing ages and compositions (Kistler and Peterman, 1973). This approach was expanded by Farmer and DePaolo (1983), who used Sm-Nd systematics to propose that the interactions of mantle and crust during the genesis of continental granitic magmas are influenced by their distance from the continental margin. They conducted a comparative Nd and Sr isotopic study across the northern half of the Great Basin of Nevada and Utah (e.g., spanning from the continental margin to the cratonic interior). They interpreted isotopic signatures of plutons east of the Roberts Mountain Thrust (RMT) to be predominantly influenced by the Precambrian crystalline basement, whereas plutons west of the RMT are primarily derived from mantle and/or younger crustal sources (Farmer and DePaolo, 1983). This observation led to their identification of the western edge of the Precambrian basement as the RMT, 100-200 km east of the  $^{87}\text{Sr}/^{86}\text{Sr}$  0.706 line of Kistler and Peterman (1973).

Bennet and DePaolo (1987) extended this approach and recognized that identifying the boundary between different crustal age-provinces can provide information about the formation and subsequent modification of the continents. Bennet and DePaolo (1987) used Sm-Nd systematics to compare Nd age provinces to the isotopic Pb provinces of the southwestern United States, previously identified by Zartman (1984). Although there are a total of four lead isotopic provinces in the southwestern United States (Zartman, 1974), Nd isotopic mapping delineates only three. In the Wyoming Province, one of the oldest elements of Laurentia, Wooden and Mueller (1988) used a combination of Sr, Nd, and Pb systematics and trace element compositions of late Archean igneous rocks of the Beartooth Mountains to postulate a subduction origin for the voluminous late Archean crust of the northern Wyoming Province along with contemporaneous metasomatism of the accompanying mantle wedge.

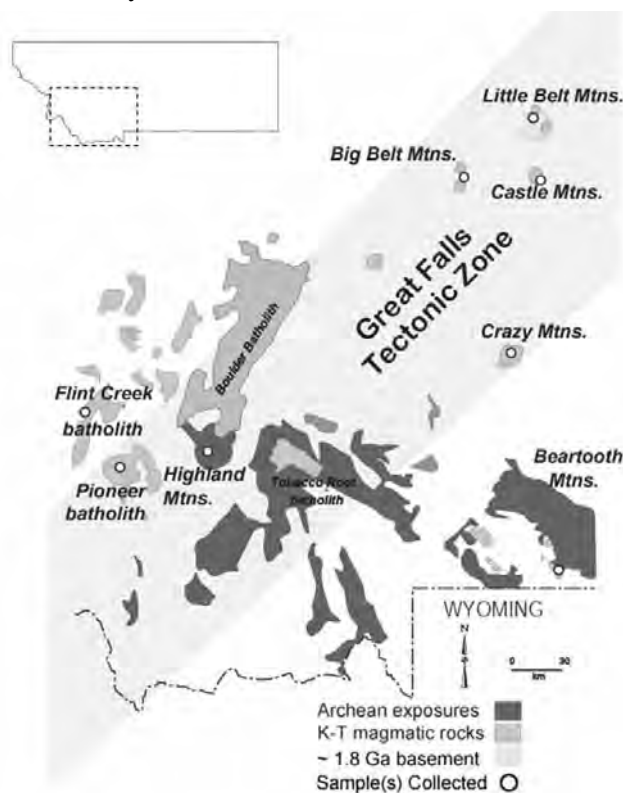


Figure 1. Simplified geologic map modified from Mueller, et al., (2005) of the study area with generalized sample locations. The inset shows the study area (dotted box) in relation to the 0.706 Sr line (dashed line) of Kistler and Peterman (1973).

## **Regional Setting**

Several workers have proposed that the Wyoming Province collided with the southern edge of the Rae-Hearne craton and/or the intervening Medicine Hat block as part of a series of orogenic events that led to the assembly of Laurentia's main components during the Paleoproterozoic (e.g., O'Neil and Lopez, 1985; Hoffman, 1988; Mueller et al., 2005; Dahl et al., 1999). This collision resulted in the formation of a suture zone, incorporating both juvenile crust formed during convergence as well as reworked Archean crustal elements, and has been labeled the Great Falls tectonic zone (GFTZ; O'Neil and Lopez, 1985; Mueller et al., 2002) (Figure 1). The proportion of these disparate elements, however, is unclear. Juvenile Paleoproterozoic crustal products are documented only in the Little Belt Mountains of southwestern Montana (Mueller, et al., 2002). A contrasting interpretation of the GFTZ suggests that the belt of NE-SW trending features of the GFTZ, including magnetotelluric patterns, end abruptly at the intersection with the Trans-Hudson orogen in southwestern-most Saskatchewan, Canada. These authors (Boerner et al., 1998) concluded that the GFTZ is an Archean structure that was later reactivated as an intracratonic shear zone during the Paleoproterozoic.

In this study we use major and trace element, Sr, Nd, and Pb isotopic values of Cretaceous and Tertiary magmatic rocks of intermediate composition (i.e., those likely derived from lower crustal sources; Table 1) and Lu-Hf systematics of zircons (Table 2) to gain insight into the age and nature of the lower crust within the GFTZ and constrain the tectonic origin of the GFTZ. Although isotopic mapping has been conducted on a large scale throughout western North America (Kistler and Peterman, 1973; Farmer and DePaolo, 1983; Bennet and DePaolo, 1987), little work has been done to define smaller scale boundaries within this region. The northwestern edge of the Wyoming craton represents one area where detailed spatial resolution is required to assess the role it played during the amalgamation of Laurentia and as a consequence, its importance for testing models for the Rodinia configuration of Laurentia (e.g., Gunn, 1991, Mogk et al., 1992). Using K-T plutons that have been intruded

into the GFTZ as probes of the lower crust will produce a high resolution image of lower crustal composition in this region and provide possibly valuable constraints for both Proterozoic paleogeographic/paleotectonic reconstructions and for testing proposed conjugate cratons in Rodinia reconstructions (e.g., AUSWUS (Burrett and Berry, 2000; Karlstrom et al., 2001), AUSMEX (Wingate et al., 2002), SIBCOR (Gallet et al., 2000; Sears and Price, 1978, 2000, 2003; Meert and Torsvik, 2003), SWEAT (Jefferson, 1978; Moores, 1991; Hoffman, 1991; Ross et al., 1992)).

## **METHODS**

### **Sampling Strategy**

Phanerozoic plutons were sampled in two areas of known or suspected Proterozoic crust (Figure 1). An eastern group was collected from units near the Paleoproterozoic crust in the Little Belt Mountains and within the general confines of the Montana alkali province (MAP). This group contains three samples from the Castle Mountains, three samples from the Crazy Mountains, two samples from the Little Belt Mountains, and one sample from the Big Belt Range. The western group comes from an area of suspected mixed Archean and Proterozoic crust in the western GFTZ (e.g., Mueller et al., 1996; Foster et al., 2006). Samples were collected in the Flint Creek Range, the Highland Mountains, and the Pioneer Mountains. Due to the exposure of well documented Archean lithologies within the Beartooth Mountains, a sample, (BT 03), was collected to provide an Archean reference for Hf isotopic ratios.

### **Geochemical Preparation**

Rock samples were crushed using a steel jaw crusher and then ground using a tungsten carbide ball mill to generate homogeneous fine powders for geochemical analysis. Whole rock major element data were obtained via XRF analysis (at the Northern Ontario Division of Mines). All other geochemical analyses were conducted at the University of Florida. Trace element data were collected after the whole rock powders were dissolved using a HF-HNO<sub>3</sub> mixture and analyzed using the Element-2 ICP-MS calibrated using the

following standards: ENDV, QLO-1, BCR-2, AGV-1, RGM-1, and G-2. Sm-Nd, Rb-Sr, and Pb were separated from whole rock samples using standard column chemistry methods (e.g., Heatherington et al., 1991). Rb-Sr and Sm-Nd spikes were added prior to dissolution in order to determine the elemental concentrations. Rb-Sr, Sm-Nd, and Pb isotopic compositions were measured on a “Nu-Plasma” MC-ICP-MS. Isotopic ratios of Sr are reported relative to a NBS 987 value of  $^{87}\text{Sr}/^{86}\text{Sr}=0.71025$  ( $\pm 0.00003$ ,  $2\sigma$ ), which is applicable to all samples. The measured  $^{144}\text{Nd}$ ,  $^{148}\text{Nd}$ , and  $^{150}\text{Nd}$  beams were corrected for isobaric interference from Sm using  $^{147}\text{Sm}/^{144}\text{Sm} = 4.88$ ,  $^{147}\text{Sm}/^{148}\text{Sm} = 1.33$ , and  $^{147}\text{Sm}/^{150}\text{Sm} = 2.03$ . All measured ratios were normalized to  $^{146}\text{Nd}/^{144}\text{Nd} = 0.7219$  using an exponential law for mass-bias correction. The data are reported relative to a JNdi-1 value of  $^{143}\text{Nd}/^{144}\text{Nd}=0.512099$  ( $\pm 0.000018$ ,  $2s$ ), which is applicable to all samples. Pb isotopic analyses were also conducted on the Nu-Plasma MC-ICP-MS using the Tl normalization technique of Kamenov et al. (2004). The Pb isotopic compositions are reported relative to the following NBS 981 values:  $^{206}\text{Pb}/^{204}\text{Pb}=16.937$  ( $\pm 0.004$ ,  $2\sigma$ ),  $^{207}\text{Pb}/^{204}\text{Pb}=15.491$  ( $\pm 0.004$ ,  $2\sigma$ ),  $^{208}\text{Pb}/^{204}\text{Pb}=36.695$  ( $\pm 0.009$ ,  $2s$ ), and are applicable to all samples.

### Mineral Separation and Analysis

Samples were pulverized in a jaw crusher and

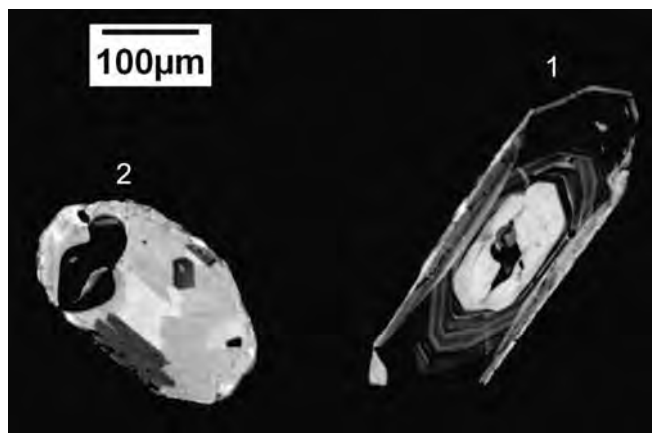


Figure 2. CL image of “typical” zircon grains from the Highland Mountains (HM 02) showing igneous zoning.

ground in a disc mill to ensure the disaggregation of rock fragments. The pulverized material was then sieved, passed across the Gemini water table to generate a heavy mineral separate and followed by density separation using tetrabromoethane (TBE) and methylene iodine (MI) and magnetic separation. The separates were then hand picked to isolate representative zircons (Figure 2), which were mounted in epoxy plugs to facilitate LA-ICP-MS analysis. A zircon standard, FC-1, separated from the Duluth gabbro was also mounted together with the sample zircons (Mueller et al., 2007). The mounted zircons were analyzed using a 213 nm laser ablation (LA) system connected to the “Nu-Plasma” MC-ICP-MS. Prior to ablation, the grains were subjected to cathode luminescence imaging by D. Henry at Louisiana State University to identify any zonation or other heterogeneities. For both standards and samples, ion beams were simultaneously collected for Lu, Hf, and Yb following methods in Mueller et al. (2007). The reported Hf isotope data are relative to the following values of the FC-1 standard:  $^{176}\text{Hf}/^{177}\text{Hf} = 0.282168$  ( $\pm 0.000026$ ,  $2n=155$ ), and is applicable to all samples. In order to verify the LA protocol one of the zircon samples were dissolved in HF-HNO<sub>3</sub> using Teflon-lined bombs under high-pressure and temperature and Hf was separated from the REE elements following a method described in Coyner et al. (2004). Hf isotopes were also measured on the “Nu-Plasma” MC-ICP-MS via wet plasma to confirm results from the LA method (Table 2).

## **RESULTS**

### Major Elements

Major element data (Table 1) show that samples have SiO<sub>2</sub> weight percents between 55 and 73. Based on normative mineralogy this sample set includes monzogabbro to syenite (Figures 3, 4). Estimated modal mineralogy and petrographic analysis, however, suggest the samples are more accurately described as granite to monzogranite, with the exception of sample CZ 05 from the Crazy Mountains. This sample contains no quartz and is best described as an amphibole-plagioclase cumulate (Table 3). Due

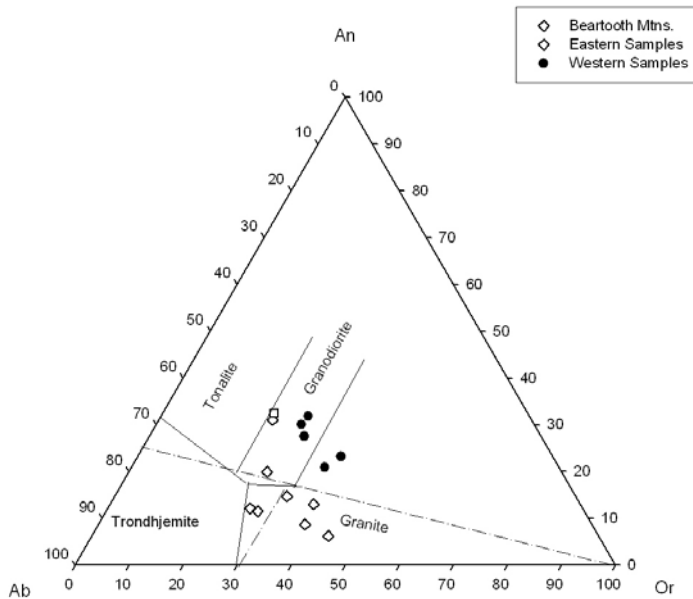


Figure 3. The classification of granitoids based on their molecular normative An-Ab-Or composition after Barker (1979) (heavy lines) and O'Connor (1965) (dotted lines) from Rollinson (1991).

to its anomalous major elemental chemistry, it will be excluded from any further discussion of major and trace elements. It is also important to note that sample BT03, from the Beartooth Mountains, is an Archean basement sample, not a Mesozoic plutonic sample. The Flint Creek pluton (samples FC 01 and FC 02) is more specifically described and mapped as granodiorite by Lewis, (1998). The samples collected from the Highland Mountains are from units described and mapped by Ruppel et al. (1993). Highland Mountain sample HM01 is described as a monzogranite and HM02 is described as a granodiorite. The extent of alteration (Table 3) is determined based on a qualitative assessment, primarily on the extent of seritization of plagioclase.

With the exception of two samples from the Crazy Mountains (CZ 03 and CZ 05), the eastern locations are more enriched in total alkalis ( $\text{Na}_2\text{O} + \text{K}_2\text{O}$ ), ranging from 8 to 10%, than their western, more calc-alkaline counterparts, that range from 6 to 8% (Figure 4). This overall trend correlates well with published data, (i.e., the eastern group lies largely within the Montana alkali province (MAP) and the western group lies within the slightly older, calc-

alkaline magmatic province of the Cordilleran orogenic belt. It is worth noting that the  $\text{Al}_2\text{O}_3$  contents are low enough that muscovite is not present in any of the samples. This implies that the samples are likely to be classified as I-type granitoids (Chappell and White, 1974).

### Trace Elements

Trace element data are presented in Table 1 and plotted normalized to the composition of N-MORB using values of Sun and McDonough (1989) (Figure 5). The normalized data show clear depletion in high field strength elements (HFSE) such as Nb, Zr, and Hf, a positive anomaly in Pb concentrations, and no obvious Eu anomalies. All samples have LREE-enriched rare earth patterns exceeding 100x chondrites (Figure 6). None of the samples show strong depletions in HREE (<10x chondrites) that would be expected for melts equilibrated with garnet.  $(\text{La}/\text{Yb})_N$  ratios are enriched in the east, with samples ranging from 13.45 to 66.68 with an average of 32.45 whereas the western samples have a much more restricted range of 7.75 to 14.71 with a mean of 12.25, suggesting a more homogeneous source and/or set of petrogenetic processes. Overall, the eastern samples are more enriched in the highly

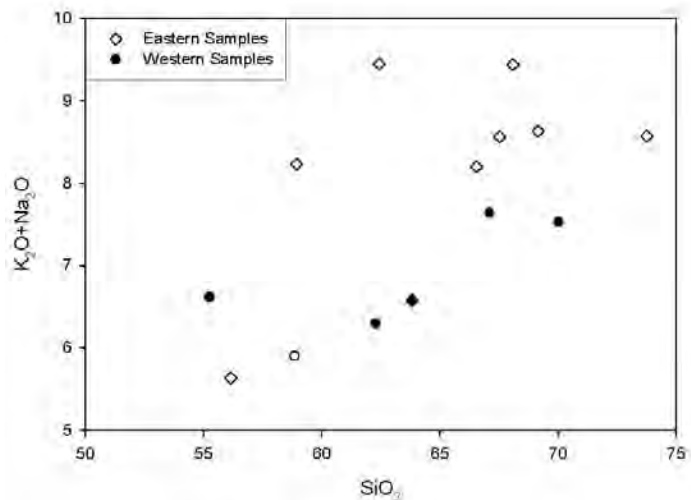


Figure 4. Total alkali vs.  $\text{SiO}_2$ , shows the chemical variation within the dataset. Note that the eastern samples are alkaline and the western samples are calc-alkaline. The plagioclase-amphibole cumulate from the Crazy Mountains (CZ 05) has been excluded.

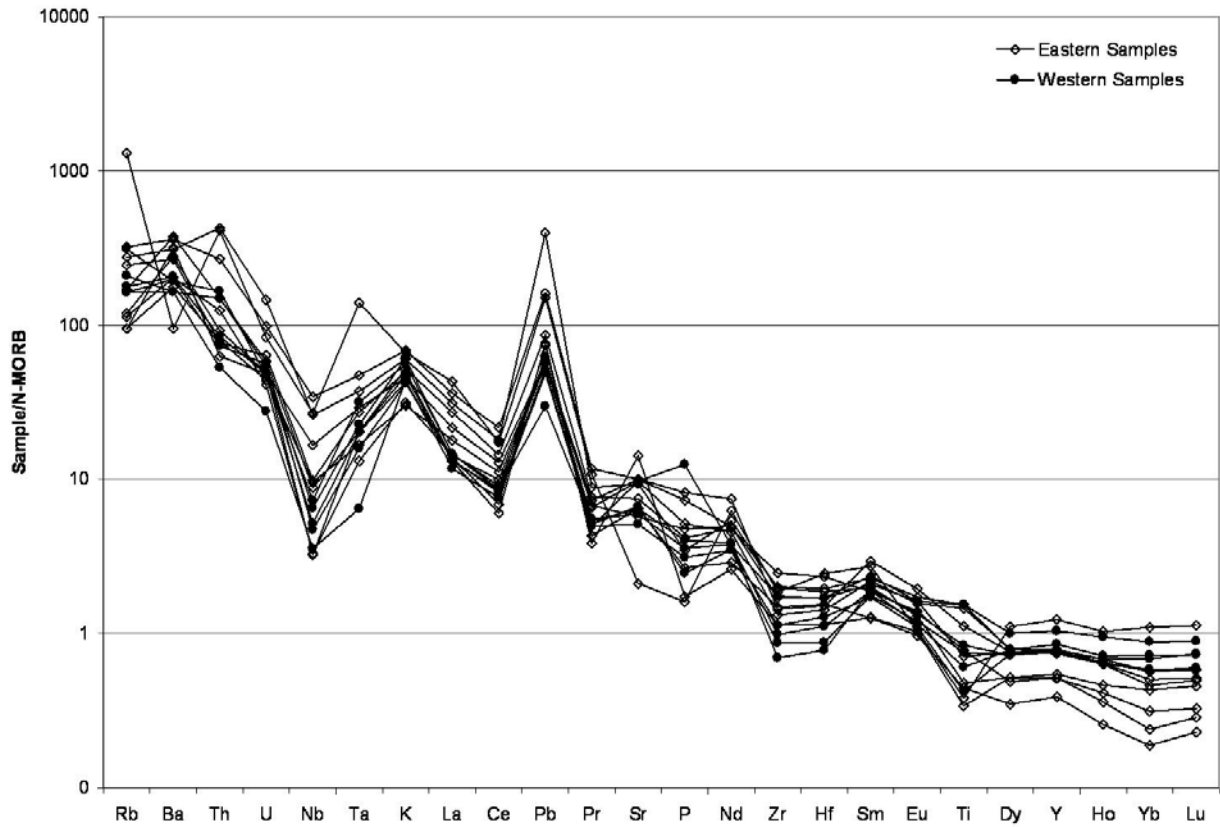
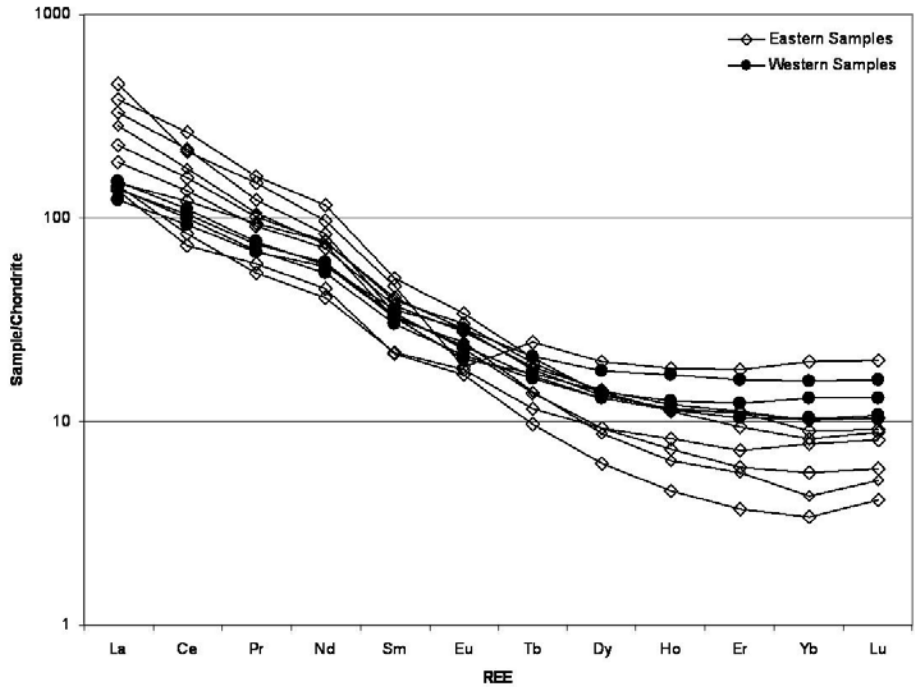


Figure 5. Trace element abundance diagrams, normalized to N-MORB (Sun and McDonough, 1989). The plagioclase-amphibole cumulate from the Crazy Mountains (CZ 05) has been excluded. The depletion in HFSE such as Nb indicate that the magmas were likely generated in a convergent margin setting and/or were derived from an ancient subduction environment.

Figure 6. Rare earth element (REE) abundances normalized to chondritic meteorite values (Sun and McDonough, 1989). The plagioclase-amphibole cumulate from the Crazy Mountains (CZ 05) has been excluded. The enrichment in HREE is less than 10x chondrites and suggests a lower crustal source containing garnet, amphibole, and possibly pyroxene. The lack of Eu anomalies also indicates that the source material was not in equilibrium with plagioclase.



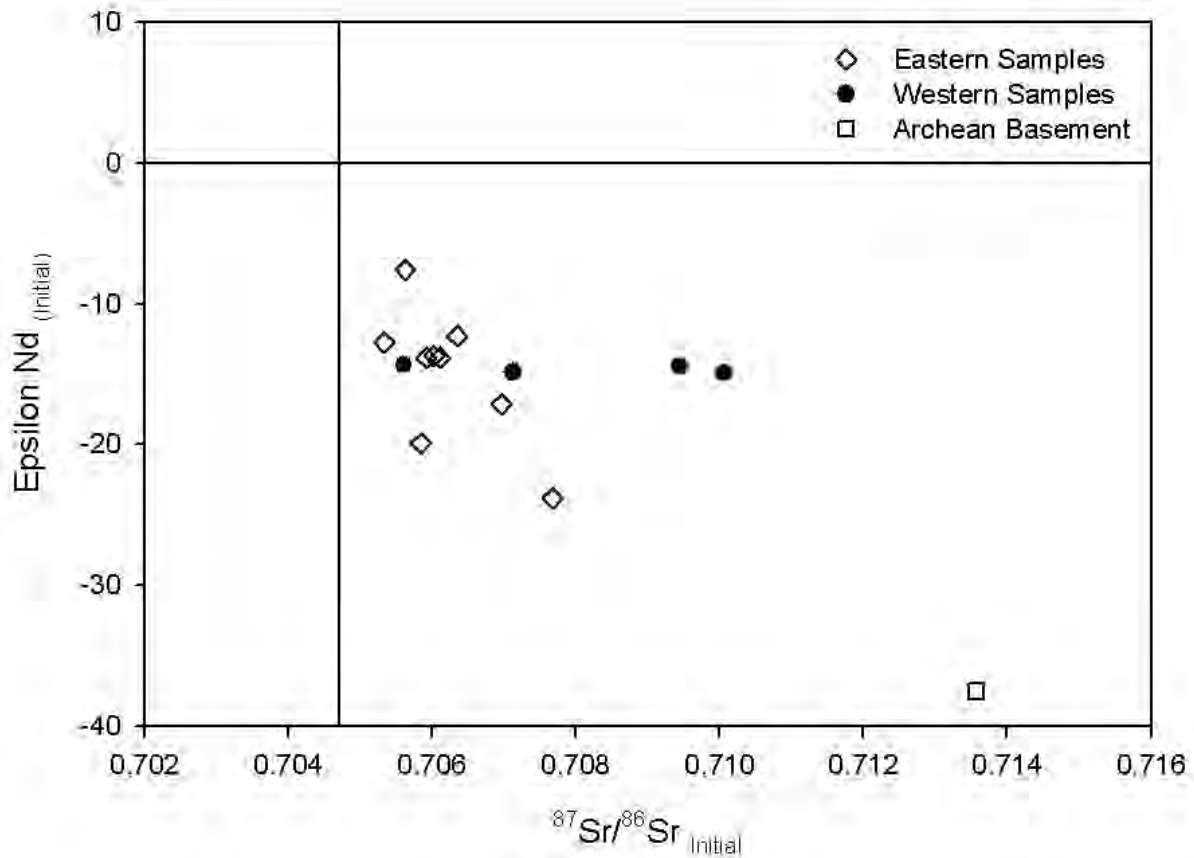


Figure 7. Initial  $^{87}\text{Sr}/^{86}\text{Sr}$  and  $\epsilon\text{Nd}$  variation diagram calculated at 50 Ma for the eastern samples and at 70 Ma for the western samples; the value for the Beartooth gneiss sample is calculated at 50 Ma.

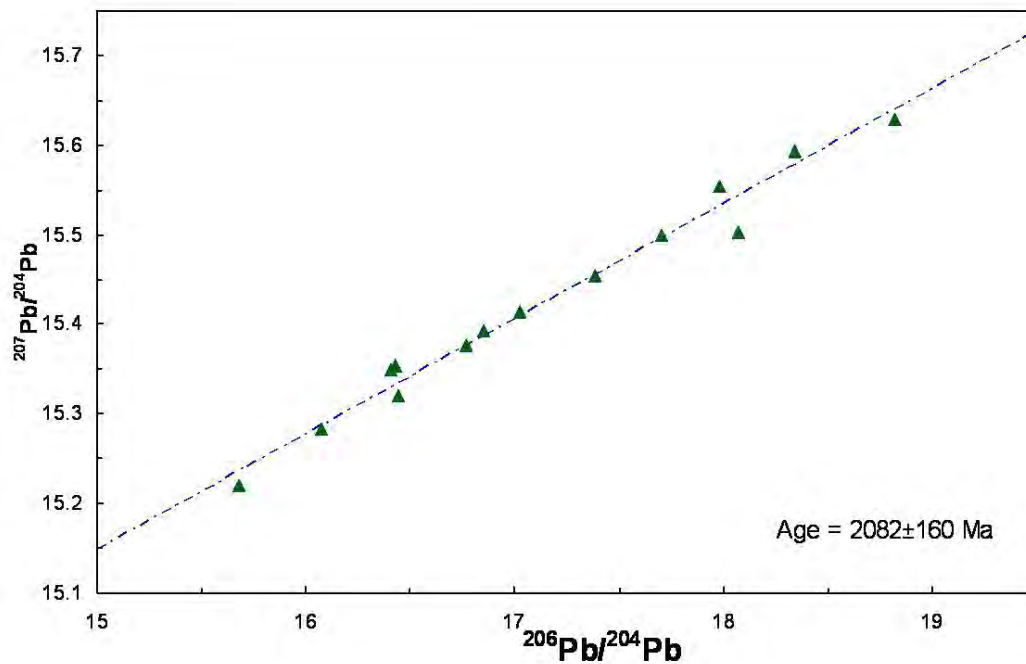


Figure 8. Whole rock Pb isotopic plot showing linear array of sample data from eastern and western sample sets. Linearity of the array can be interpreted in terms of a common age of ~2.0 Ga for the source of all samples. The “age” of the source is essentially the same as the oldest Proterozoic ages of the exposed basement in the Little Belt Mountains (Mueller et al., 2002).

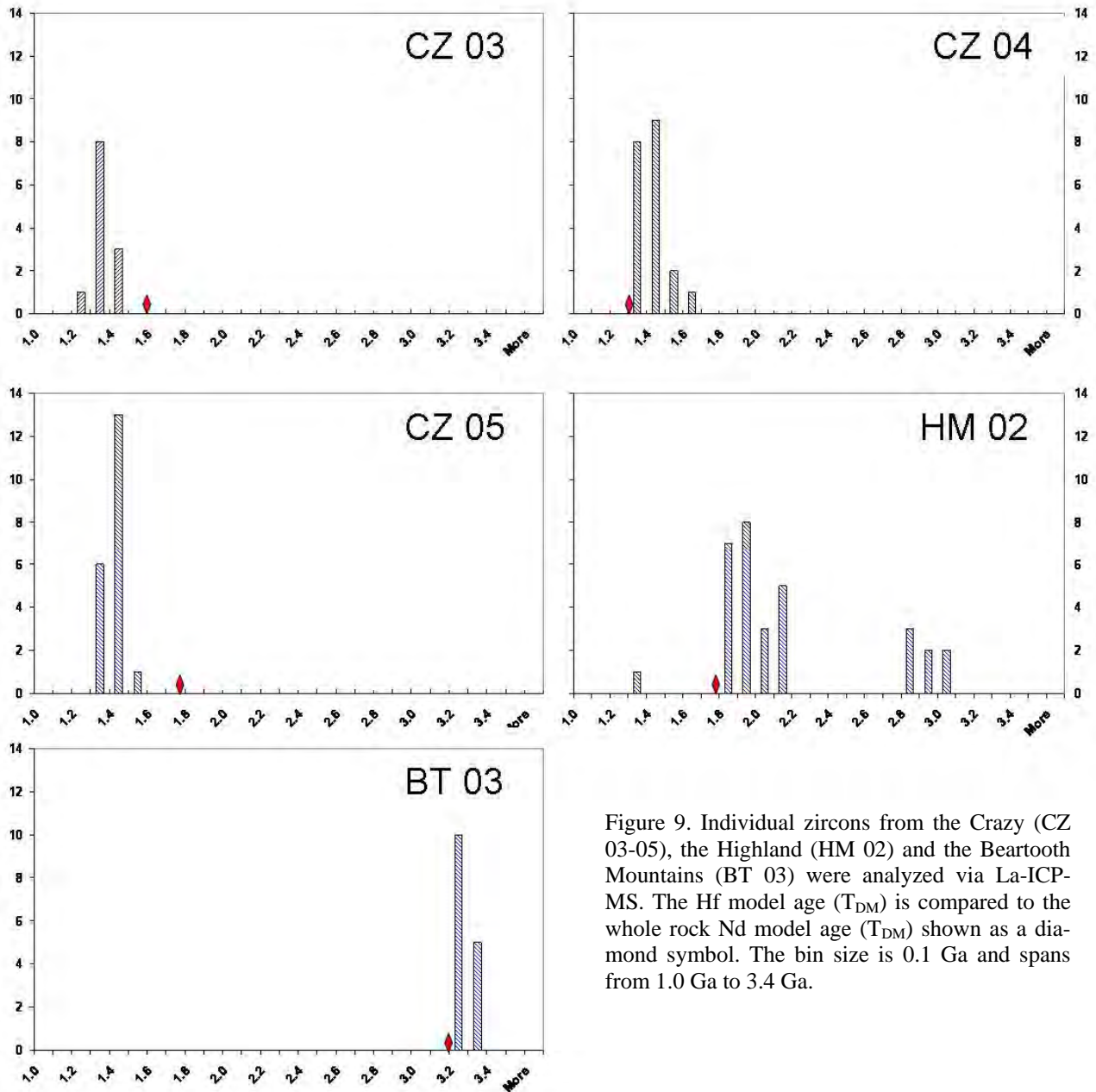


Figure 9. Individual zircons from the Crazy (CZ 03-05), the Highland (HM 02) and the Beartooth Mountains (BT 03) were analyzed via La-ICP-MS. The Hf model age ( $T_{DM}$ ) is compared to the whole rock Nd model age ( $T_{DM}$ ) shown as a diamond symbol. The bin size is 0.1 Ga and spans from 1.0 Ga to 3.4 Ga.

incompatible elements such as Ce, Pb, Y, and Nb. For example, there is a geographic contrast in Y+Nb contents, with the easternmost samples ranging from 18 to 100, with an average of 57 and the western samples have much lower, more limited range of concentrations ranging from 29 to 39 with an average of 35, which reflects the general compositional contrasts between the more alkaline MAP suites and the more calc-alkaline rocks of the western group.

### Isotopes

The Sr, Nd, and Pb isotopic data are presented in Table 2. The amphibole-plagioclase cumulate (CZ 05) is included in the isotopic discussion due to its isotopic similarity to the granitoids, i.e., its cumulate nature only affects its elemental composition. The initial values were calculated using an average age estimate of 70 Ma for the western samples and 50 Ma for the eastern, MAP samples (Dudas et al., 1987;

Harlan et al., 1988). The range of calculated initial  $^{87}\text{Sr}/^{86}\text{Sr}$  is 0.7053 to 0.7101, with an average of 0.7068. The range of initial strontium isotopic compositions is greater in the western portion of the study area (0.7056 to 0.7101) compared to the eastern study area (0.7053 to 0.7077). The difference is likely due to, the presence of Archean crust (in situ or as detritus in younger sedimentary rocks) in the western area.

Present day  $^{144}\text{Nd}/^{143}\text{Nd}$  ratios range from 0.511381 to 0.5121219, and correspond to  $\epsilon\text{Nd}$  values of -24.52 to -8.17 and  $T_{\text{DM}}$  (depleted mantle model age) of 1.97 to 1.1 Ga respectively. The western portion of the study area typically has more restricted  $\epsilon\text{Nd}$  values ranging from -18.2 to -15.0 and  $T_{\text{DM}}$  of 1.94 to 1.5 Ga compared to the wide range of -24.5 to -8.2 and  $T_{\text{DM}}$  ages of 1.97 to 1.1 Ga observed in the eastern group. On the  $^{87}\text{Sr}/^{86}\text{Sr}$  and  $\epsilon\text{Nd}$  correlation diagram (Figure 7) the data plot in the lower right quadrant, but do not form a coherent array. The Archean basement sample from the Beartooth Mountains, calculated for 50 Ma, is provided for reference.

Whole rock Pb isotopic compositions show a range of values, i.e.,  $^{206}\text{Pb}/^{204}\text{Pb}$  varies from 15.68 to 18.82,  $^{207}\text{Pb}/^{204}\text{Pb}$  from 15.22 to 15.63, and  $^{208}\text{Pb}/^{204}\text{Pb}$  from 36.44 to 38.86. These data form a well correlated linear array on a  $^{207}\text{Pb}/^{204}\text{Pb}$  vs.  $^{206}\text{Pb}/^{204}\text{Pb}$  diagram that corresponds to an age of  $2082 \pm 160$  Ma calculated with Isoplot (Ludwig, 2003) (Figure 8). This array includes samples from both geographic

and geochemical groups and, in particular, samples that contain Pb elemental abundances ranging from 11.9 to 111.9 ppm (Table 1).

### Zircons

At least twenty grains from selected samples were analyzed and their Lu-Hf model ages ( $T_{\text{DM}}$ ) are summarized in Figure 9 and in Table 2. The mean  $^{176}\text{Hf}/^{177}\text{Hf}$  ratio of 20 grains from CZ 04 is 0.282320 (+/-0.000080,  $2\sigma$ ), which corresponds to an epsilon Hf value of -16.0 and a  $T_{\text{DM}}$  of 1.3 Ga. The mean  $^{176}\text{Hf}/^{177}\text{Hf}$  ratio for three analyses of the dissolved grains from this sample is 0.282345 (+/-0.000015,  $2\sigma$ ), which corresponds to an epsilon Hf value of -15.3 and a  $T_{\text{DM}}$  of 1.2 Ga (Table 2). The similarity of the Hf isotopic compositions suggests that both methods produced statistically indistinguishable results. The advantage of using the in-situ laser ablation technique is that it allows for numerous grains to be assessed individually, providing multiple model ages for a single whole rock sample, thereby yielding better resolution of magmatic and source heterogeneity compared to a single whole-rock measurement. Laser ablation analyses of zircon were conducted on five samples: HM 02 from the Highland Mountains in the western portion of the study area, CZ 03, 04, 05 from the Crazy Mountains in the eastern portion of the study area, and BT03 from the Beartooth Mountains (Archean basement). Samples from the Crazy Mountains (eastern area) yield average  $\epsilon\text{Hf}$  values of -16.0 (CZ03), -16.0 (CZ04), and -16.9 (CZ05) with ranges from -17.4 to -13.6 (CZ03), -19.7 to -

Sample	Modal T.S.	Modal H.S.	Normative	Mineral Assemblages	Alteration
BB01	Granite	Granite	syenite	Plag, qtz, k-spar, amph	little-none
LB01	Granite	Granite	granite/syenogranite	K-spar, plag, qtz	little-none
LB02	Quartz monzonite	Granite	alkali-feldspar syenite	Plag, k-spar, qtz, amph, bt	little-none
CZ03	Tonalite	Tonalite	monzogabbro	Plag, amph, qtz	little-none
CZ04	Tonalite	Granodiorite	monzonite	Plag, qtz, bt	little-none
CZ05	?		nepheline-bearing alkali-feldspar syenite	Plag, bt, amph	none
CA01	Granite	Granite	Alkali-feldspar granite	Plag, k-spar, qtz, bt	moderate
CA02	Granite	Granite	quartz syenite	K-spar, plag, qtz	moderate
CA03	Granite	Granite	quartz monzonite	Plag, qtz, k-spar, amph	litte-moderate
BT03	Granite	Granite	monzogabbro	Plag, k-spa, qtz, amph, bt	litte-moderate
HM01	Granite	Granite	alkali-feldspar granite	Plag, k-spar, qtz, bt, amph	little-none
HM02	Granite	Granite	alkali-feldspar granite or granite/monzogranite	Qtz, plag, k-spar, bt	little-none
PM01	Granite	Granite	quartz monzodiorite	Plag, qtz, k-par, bt, amph	none
FC01	Granodiorite	Granite	alkali-feldspar quartz syenite	Plag, qtz, k-spar, bt, amph	little-none
FC02	Quartz monzonite	Quartz monzonite	nepheline-bearing alkali-feldspar syenite	Plag, k-spar, qtz, amph, bt, pyr	moderate

Table 3. Petrographic data

13.8 (CZ04), and -19.0 to -14.2 (CZ05). The Highland Mountains (western area) reveal more variability, with an average  $\epsilon$  Hf of -36.0 and a range from -57.7 to -15.7. This wide range includes two distinct model age populations: ~1.9 Ga and ~2.8 Ga, which may indicate a degree of Archean crustal involvement in this sample (Figure 9). The lower values are not substantially from Archean basement sample (BT 03), which yielded an average  $\epsilon$  Hf of -65.3, with values falling between -66.6 and -63.8.

## **DISCUSSION**

### **Major Elements**

Major element abundances and petrographic analysis are essential for rock classification, as well as for providing insight into petrogenesis and source. These rocks exhibit many of the mineralogical and chemical characteristics of I-Type granites as defined by Chappell and White (1974). Mineralogically, the relative abundance of amphibole compared to biotite and the observed lack of muscovite, support the I-type classification of these samples. S-type granites are characterized by higher mica abundance, especially muscovite. I-Type granites also yield abundant magnetite (instead of ilmenite) and pink and white alkali feldspars, both of which are present in the sample set. Additionally, the presence of mafic enclaves in outcrops in the Big Belt Range, Highland Mountains, and the Pioneer Mountains indicate a non S-type source.

Chemically, these samples also correspond to I-type granites in CaO, Na<sub>2</sub>O, and Sr concentrations (Table 1). The average values of 3.68 weight percent, 4.06 weight percent, and 711 ppm respectively are too high to correspond to S-type granites (Bowden, 1984). In addition, the CIPW normative mineralogy demonstrates that the average amount of quartz is below the amounts typically found in S-type rocks, and that the amount of corundum is within the limits (below 1.0) of an I-type granite (Table 3). This evidence is compatible with petrogenesis involving a mafic, meta-igneous source.

### **Trace Elements**

Trace element concentrations help provide estimates of the source material composition, the residual minerals left behind by melt extraction, and the extent of melt-mixing and source variability. The REE patterns in all rocks show enrichment in LREE and a corresponding less enriched distribution of HREE, characteristic of continental granitoids (Pearce, et al., 1984; Winter, 2001). The enrichments in HREEs are less than 10x chondrites, suggesting a lower crustal (mafic) source potentially containing one or more of the following: garnet, amphibole, and/or pyroxene. Y and Yb, however, are concentrated in garnet, and the lack of any negative Y or Yb anomaly again suggests that the magma source(s) was not garnet-bearing (Figures 3-3 and 3-4). The lack of Eu anomalies indicate that plagioclase was absent from the source, that the source had not previously undergone a significant feldspar fractionation cycle (Halliday and Stephens, 1984), and that plagioclase fractionation had very limited impact on magmatic evolution in these samples. This provides further evidence of a mantle and/or lower crust source that lacked an upper crustal history. LILEs (large ion lithophile elements) are also incompatible and behave similarly to the HFSE in solid-melt exchange, but behave differently in the presence of an aqueous fluid. Given that this dataset shows enrichment in Rb, Ba, and Pb, but lesser enrichments in the HFSE, a high LILE/HFSE ratio results (Figure 5). The decoupling of these two chemical groups is best explained by the participation of water-rich fluids in the genesis of subduction zone magmas (e.g., Hanson, 1978; Winter, 2001). Depletion in HFSEs and Nb in particular indicate that the magmas were likely generated in a convergent margin setting, were derived from rocks produced in an ancient subduction environment (Morris and Hart, 1983; Saunders et al., 1991), or some combination of the ancient subducted material and the younger Cretaceous/Tertiary subduction.

Major and trace element abundances for these intermediate granitoids, therefore, strongly suggest that the samples were derived primarily, if

not exclusively, from a mafic, meta-igneous, lower crustal source. The stimulus for melting in both the eastern and western regions is likely related to Farallon/Kula plate subduction, despite the alkalic vs. calc-alkalic nature of the rocks from the eastern and western groups respectively (Coney & Reynolds, 1977; Humphreys et al., 2003). An alternate option is that the lower crustal source formed in a subduction environment related to the collision between the Wyoming Province and the Medicine Hat Block. This ambiguity of the age of the source and potential mixing of Farallon/Kula-derived fluids or magmas derived from an ancient subduction generated mafic lower crust cannot be resolved with trace element data alone.

### **Age of the Lower Crust**

Regardless of their petrochemical composition, contemporaneous intrusions emplaced in similar country-rocks and derived from similar sources can be expected to show very similar Sr-Nd-Pb-Hf isotopic systematics. Measurements of present day isotopic values, particularly for Sr, Nd, and Pb, can be used to calculate the initial isotopic ratios for the source material. These calculated initial values are useful for determining both petrogenetic and model age information about the source. Initial Sr isotopic values range from 0.705-0.710, generally compatible with an ancient crustal origin (e.g., Arth et al., 1986, Mueller, et al., 1997), but extend to lower values than expected for felsic magmas east of the 0.706 line. Figure 7 shows initial  $^{87}\text{Sr}/^{86}\text{Sr}$  and  $\epsilon\text{Nd}$  ratios fall in the region of most continental crust and the negative  $\epsilon\text{Nd}$  values strongly indicate that there was involvement of much older crust.

Sm and Nd are far less susceptible to fractionation during melting and subsequent alteration than are Rb and Sr and, as a result, the  $^{143}\text{Nd}/^{144}\text{Nd}$  ratio can be used to provide a more reliable indicator of the age of the material in the source region(s). The range of Sm/Nd model ages for these rocks suggests that the source(s) are likely to be both compositionally and chronologically heterogeneous. Although the actual  $T_{\text{DM}}$  are scattered from 1.1-1.9 Ga,

this range is well within the temporal boundaries of the Proterozoic, indicating that there is not likely to be significant, direct involvement of Archean crust. It is important to note that the upper limit of this range corresponds with the oldest basement rock U/Pb zircon age-dates determined for the Little Belt Mountains at ~1.9 Ga (Mueller et al., 2002) and is, therefore, unlikely to be a fortuitous mixture of Archean and younger crust.

The heterogeneity seen in the Rb-Sr and Sm-Nd systematics is not evident in the Pb-Pb system. A whole rock Pb isotopic plot (Figure 8) produces a linear array that suggests a Paleoproterozoic source with limited age heterogeneity. Extensive recent mixing to produce a homogenous array for individual plutons over this large of an area seems unlikely; therefore, mixing and establishment of the diverse U/Pb ratios needed to form the array was more likely to have been in the Proterozoic. These whole rock Pb isotopic data, therefore, suggest that this lower crustal source is likely Proterozoic and that ~2.0 Ga is a reasonable approximation of its apparently limited range of ages (Figure 8). An “age” of ~2.1 Ga compares favorably with the age of the oldest Proterozoic rocks in the area (~1.9 Ga; Mueller et al., 2002) and the oldest Sm-Nd model ages.

As noted above, the Sm-Nd model ages are not consistently Paleoproterozoic. Some of this variability is likely due to heterogeneities in the source region, variable fractionation of Sm and Nd, and/or mixing between sources (Mueller et al., 1995, 1996). Sm-Nd model ages suggest some mixing of the Proterozoic source(s) characteristic of the Pb array with a younger asthenospheric Nd component. The older component may approximate the ~1.9 Ga basement age from the Little Belt Mountains and the other may be derived from fluids liberated by Farallon/Kula subduction. The primary reason for the difference in response of the Sm-Nd and Pb-Pb systems during petrogenesis of individual rocks is directly related to the smaller differences in the elemental abundances of Sm and Nd compared to Pb elemental abundances between the mantle and crust. This differential

makes for a more homogeneous, more crust-dominated response of the Pb system than the Sm-Nd system in crustal environments.

Further constraints on the age of the source are provided by Lu/Hf isotopic ratios preserved in zircon crystals formed during the crystallization of the granitoid melts or directly inherited from the source. The Lu/Hf system is similar to the Sm/Nd system in providing insight into petrogenetic and crustal processes, with the advantage of yielding numerous analyses from zircon crystals rather than the averaging represented by whole-rock Sm-Nd data. These Hf values provide a “snapshot” of the isotopic composition of the melt (and hence source region) itself and, in some cases, zircons inherited from that source or sources are likely to remain largely undisturbed by incorporation in the melt or subsequent weathering and/or hydrothermal or other alteration processes. This effect is observed in the Highland Mountains (sample HM02), where the Nd model age ( $T_{DM}$ ) is ~1.8 Ga and correlates well with the primary Hf model age ( $T_{DM}$ ) data, but fails to identify two additional Hf model age populations detected at ~1.4 Ga and ~2.8 Ga (Figure 9), which may indicate a more heterogeneous source for this magma. The fact that the Highland sample falls on the overall Pb array suggests limited involvement of these older and younger sources.

## CONCLUSIONS

Detailed geochemical analyses conducted on Cretaceous-Tertiary granitic plutons within the GFTZ provide valuable insight into the composition of the lower crust in the GFTZ and its tectonic origin. These plutons are all I-type granites, derived from the melting of a predominantly mafic, ancient, lower crustal source (s) that originally formed as the result of subduction. Isotopic data (Sr, Nd, Pb, and Hf) suggest that the lower crust is Paleoproterozoic in age, indicating that new lower crust was being generated during this time interval, which is conducive to viewing the GFTZ as a collisional suture zone. Paleotectonic reconstructions that require identifying the Neoproterozoic conjugate to western Laurentia should take in account the dominantly Paleoproterozoic character of the GFTZ.

## ACKNOWLEDGMENTS

This research was funded by the Tobacco Root Geologic Society, the Colorado Scientific Society, National Science Foundation (EAR 0106592), and the USGS (05HQGR0156). We thank Jim Vogl, David Foster, David Mogk, and Josh Richards for their assistance in sample collection and helpful discussions, Sam Coyner for his guidance in sample preparation, Darryl Henry for CL and SEM images of the zircons, and to David Foster, Joe Meert, and Shawn Malone for their insightful reviews.

## REFERENCES

- Arth, J.G., Zen, E-an, Sellers, F., and Hammarstrom, J., 1986, High initial Sr isotopic ratios and evidence for magma mixing in the Pioneer batholith of southwest Montana: *Journal of Geology*, v. 94, p. 419-430.
- Barker, F., 1979, Trondhjemite: Definition, environment and hypotheses of origin: *in* Trondhjemites, dacites, and related rocks: Barker, F., ed., Elsevier, Amsterdam, p. 1-12
- Bennet, V., and DePaolo, D.J., 1987, Proterozoic crustal history of the western United States as determined by neodymium isotopic mapping: *Geological Society of America Bulletin*, v. 99, p. 674-685.
- Boerner, D., Craven, J., Kurtz, R., Ross, G., and Jones, F., 1998, The Great Falls tectonic zone: Suture or intracontinental shear zone?: *Canadian Journal of Earth Science*, v. 35, p. 175-183.
- Borg, S.G., and DePaolo, D.J., 1994, Laurentia, Australia, and Antarctica as a late Proterozoic supercontinent: constraints from isotopic mapping: *Geology*, v. 22, p. 307-310.
- Bowden, P., Batchelor, R.A., Chappell, B.W., Didier, J., and Lameyre, J., 1984, Petrological, geochemical, and source criteria for the classification of granitic rocks: A discussion: *Physics of the Earth and Planetary Interiors*, no. 35, p 1-11.
- Burrett, C., and Berry, R., 2000, Proterozoic Australia-Western United States (AUSWUS) fit between Laurentia and Australia: *Geology*, v. 28, p. 103-106.
- Chappell, B.W., White, A.J.R., 1974, Two contrast-

- ing granite types: *Pacific Geology*, v. 8, p. 173-174.
- Coney, P.J., and Reynolds, S.J., 1977, Flattening of the Farallon slab: *Nature*, v. 270, p. 403-406.
- Coyner, S.J., Kamenov, G.D., Mueller, P.A., Rao, V., Foster, D.A., 2004, FC-1: A zircon reference standard for the determination of Hf isotopic compositions via laser ablation ICP-MS: *Eos Trans., AGU*, 85 (47), Fall Meeting Suppl., V51C-0584.
- Dahl, P.S., Holm, D.K., Gardner, E.T., Hubacher, F.A., and Foland, K.A., 1999, New constraints on the timing of Early Proterozoic tectonism in the Black Hills (South Dakota), with implications for docking of the Wyoming province with Laurentia: *Geological Society of America Bulletin*, v. 111, p. 1335-1349.
- DePaolo, D.J., 1988, Age dependence of the composition of continental crust: Evidence from Nd isotopic variations in granitic rocks: *Earth and Planetary Science Letters*, v. 90, p. 263-271.
- Dickinson, W.R., 1981, Plate tectonics of the continental margin of California: *in* The Geotectonic Development of California, W.G. Ernst, ed., Prentice-Hall, Englewood Cliffs, N.J., 706 p.
- Dudás, F.Ö.; Carlson, R.W.; and Eggler, D.H., 1987, Regional middle Proterozoic enrichment of the subcontinental mantle source of igneous rocks from central Montana: *Geology*, v. 15, p. 22-25.
- Farmer, G.L. and DePaolo, D.J., 1983, Origin of Mesozoic and Tertiary granite in the western United States and implications for pre-Mesozoic crustal structure I. Nd and Sr isotopic studies in the geocline of the northern Great Basin: *Journal of Geophysical Research*, v. 88, no. B4, p. 3379-3401.
- Foster, D.A., Mueller, P.A., Mogk, D.W., Wooden, J.L., and Vogl, J.J., 2006, Proterozoic evolution of the western margin of the Wyoming Craton: Implications for the tectonic and magmatic evolution of the northern Rocky Mountains: *Canadian Journal of Earth Sciences*, v. 43, p. 1601-1619.
- Gallet, Y., Pavlov, V.E., Semikhatov, M.A., and Ptrov, P.Y., 2000, Late Mesoproterozoic magnetostratigraphic results from Siberia: Paleogeographic implications and magnetic field behaviour: *Journal of Geophysical Research*, v. 105, p. 16481-16499.
- Gunn, S.H., 1991, Isotopic constraints on the crustal evolution of southwestern Montana: Ph.D. dissertation, University of California at Santa Cruz, 204 p.
- Halliday, A.N., and Stephens, W.E., 1984, Crustal controls on the genesis of the 400 Ma old Caledonian granites: *Physics of Earth and Planetary Interiors*, v. 35, p. 89-104.
- Hanson, G.N., 1978, The application of trace elements to the petrogenesis of igneous rocks of granitic composition: *Earth and Planetary Science Letters*, v. 38, p. 26-43.
- Harlan, S.S., Geissman, J.W., Lageson, D.R., and Snee, L.W., 1988, Paleomagnetic and isotopic dating of thrust belt deformation along the eastern edge of the Helena salient, northern Crazy Mountains, Montana: *Geological Society of America Bulletin*, v. 100, p. 492-499.
- Heatherington, A., and Mueller, P.A., 1991, Geochemical evidence for Triassic rifting in southwestern Florida: *Tectonophysics*, v. 188, p. 291-302.
- Hoffman, P., 1988, United Plates of America, the birth of a craton: *Annual Review of Earth and Planetary Science*, p. 16543-16603.
- Hoffman, P.J., 1991, Did the breakout of Laurentia turn Gondwanaland inside-out?: *Science*, v. 252, p. 1409-1412.
- Humphreys, E., Hessler, E., Dueker, K., Farmer, G.L., Erslev, E., and Atwater, T., 2003, How Laramide-age hydration of North American lithosphere by the Farallon slab controlled subsequent activity in the western United States: *International Geology Review*, v. 45, p. 575-595.
- Jefferson, C.W., 1978, Correlation of middle and upper Proterozoic strata between northwestern Canada and south and central Australia [abs.]: *Geological Association of Canada Program with Abstracts*, v. 13, p. 429.
- Kamenov, G.D., Mueller, P., and Perfit, M., 2004, Optimization of mixed Pb-Tl solutions for high precision isotopic analyses by MC-ICP-MS: *Journal of Analytical Atomic Spectrometry*, v.19, no. 9, p. 1262-1267.
- Karlstrom, K.E., Ahall, K.L., Harlan, S.S., Williams, M.L., McLelland, J., and Geissman, J.W., 2001, Long-lived (1.8-1.0 Ga) convergent orogen in southern Laurentia, its extensions to Australia and

- Baltica, and implications for refining Rodinia: *Precambrian Research*, v. 111, p. 5-30.
- Kistler, R.W., and Peterman, Z.E., 1973, Variations in Sr, Rb, K, Na, and initial  $^{87}\text{Sr}/^{86}\text{Sr}$  in Mesozoic granitic rocks and intruded wall rocks in central California: *Geological Society of America Bulletin*, v. 84, p. 3489-3512.
- Lewis, R.S., 1998, Geologic map of the Butte 1° x 2° quadrangle, Montana: Montana Bureau of Mines and Geology Open File Report MBMG 363.
- Ludwig, K. R., 2003, User's manual for Isoplot 3.00: Berkeley Geochronology Center Special Publication 4. Berkeley Geochronology Center.
- Meert, J.G. and Torsvik, T.H., 2003. The making and unmaking of a supercontinent: Rodinia Revisited: *Tectonophysics*, v. 375, p. 261-288.
- Mogk, D.W., Mueller, P.A., and Wooden, J.L., 1992, The nature of Archean terrane boundaries: An example from the northern Wyoming Province: *Precambrian Research*, v. 55, p. 155-168.
- Moore, E.M., 1991, Southwest U.S.-East Antarctic (SWEAT) connection: A hypothesis: *Geology*, v. 19, p. 425-428.
- Morris, J.D., and Hart, S.R., 1983, Isotopic and incompatible trace element constraints on the genesis of island arc volcanics from Cold Bay and Amak Island, Aleutians, and implications for mantle structure: *Geochimica et Cosmochimica Acta*, v. 47, p. 2051-2030.
- Mueller, P.A., Shuster, R.D., D'Arcy, K.A., Heatherington, A.L., Nutman, A.P., and Williams, I.S., 1995, Source of the northeastern Idaho Batholith: Isotopic evidence for a Paleoproterozoic terrane in the northwestern U.S.: *Journal of Geology*, v. 103, p. 63-72.
- Mueller, P.A., Heatherington, A.L., D'Arcy, K.A., Wooden, J.L., and Nutman, A.P., 1996, Contrasts between Sm-Nd whole rock and U-Pb zircon systematics in the Tobacco Root batholith, Montana: Implications for the determination of crustal age provinces: *Tectonophysics*, v. 265, p. 169-179.
- Mueller, P., Wooden, J., Heatherington, A., and Nutman, A., 1997, Distribution of Proterozoic crust along the NW margin of cratonic North America: evidence from U-Pb zircon ages and isotopic systematics in young granitoids: *Geological Society of America Abstracts with Programs*, v. 29, p. A-70.
- Mueller, P., Heatherington, A., Kelley, D., Wooden, J., Mogk, D., 2002, Paleoproterozoic crust within the Great Falls Tectonic Zone: Implications for the assembly of southern Laurentia: *Geology*, v. 30, p. 127-130.
- Mueller, P.A., Burger, H.R., Wooden, J.L., Brady, J.B., Cheney, J.T., Harms, T.A., Heatherington, A.L., Mogk, D.W., 2005, Paleoproterozoic metamorphism in the northern Wyoming Province: Implications for the assembly of Laurentia: *Journal of Geology*, v. 113, p. 169-179.
- Mueller, P., Foster, D., Mogk, D., Wooden, J., and Vogl, J., 2007, Provenance of the Uinta Mountain Group from Pb and Hf isotopic compositions of detrital zircons: *Geology*, v. 35, n. 5, p.431-434.
- O'Connor, J.T., 1965, A classification for quartz-rich igneous rock based on feldspar ratios: USGS Professional paper 525B, p. B79-B84.
- O'Neill, J., and Lopez, D., 1985, Character and regional significance of Great Falls tectonic zone, East-Central Idaho and West-Central Montana: *American Association of Petroleum Geologists Bulletin*, v. 69, p. 437-447.
- Pearce, J.A., Harris, N.B.W., and Tindle, A.G., 1984, Trace element discrimination diagrams for the tectonic implications of granitic rocks: *Journal of Petrology*, v. 25, p. 956-983.
- Pesonen, L.J., Elming, S.A., Mertanen, S., Piskarevski, S., D'Agrella-Filho, M.S., Meert, J., Schmidt, P.W., Abrahamsen, N., and Bylund, G., 2003, Assemblies of continents during the Proterozoic: Rodinia and beyond: *Tectonophysics*, v. 375, p. 289-324.
- Ross, G.M., Parrish, R.R., and Winston, D., 1992, Provenance and U-Pb geochronology of the Mesoproterozoic Belt Supergroup (northwestern United States): Implications for age deposition and pre-Panthalassa plate reconstructions: *Earth and Planetary Science Letters*, v. 113, p. 57-76.
- Ruppel, E.T., O'Neill, J.M., and Lopez, D.A., 1993, Geologic Map of the Dillon 1° x 2° quadrangle, Idaho and Montana: U.S. Geological Survey Map I-1803-H.

Saunders, A.D., Norry, M.J., and Tarney, J., 1991, Fluid influence on the trace element composition of subduction zone magmas: *Philosophical Transactions of the Royal Society of London*, v. 335, p. 377-392.

Sears, J.W., and Price, R.A., 1978, The Siberian connection: A case for the Precambrian separation of the North American and Siberian cratons: *Geology*, v. 6, p. 267-270.

Sears, J.W., and Price, R.A., 2000, New look at the Siberian connection: No SWEAT: *Geology*, v 28, p. 423-426.

Sears, J.W., and Price, R.A., 2003, Tightening the Siberian connection to western Laurentia: *Geological Society of America Bulletin*, v. 115, no. 8, p. 943-953.

Sun, S.S., and McDonough, W.F., 1989, Chemical and isotopic systematics of oceanic basalts: implications for mantle composition and processes: *in* Saunders, A.D., and Norry, M.J., eds., *Magmatism in ocean basins: Geological Society of London Special Publication*, no.42, p. 313-345.

Wingate, M.T.D., Pisarevsky, S.A., and Evans, D.A.D., 2002, Rodinia connections between Australia and Laurentia: No SWEAT, no AUSWUS?: *Terra Nova*, v. 14, p. 121-128.

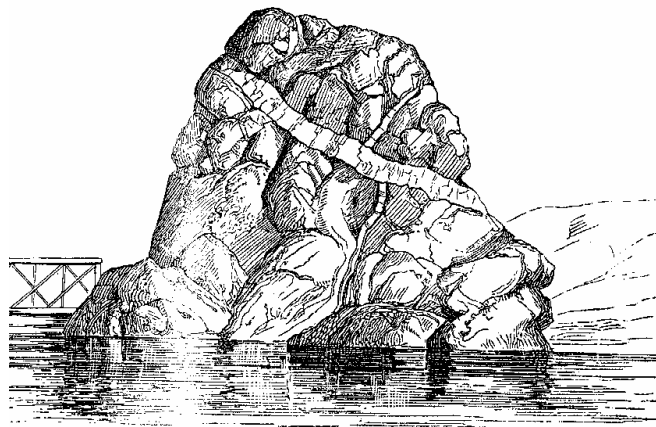
Winter, J.D., 2001, *An introduction to igneous and metamorphic petrology: Prentice Hall, Upper Saddle River, N.J.*, 697 p.

Wooden, J.L., and Mueller, P.A., 1988, Pb, Sr, and Nd isotopic compositions of a suite of late Archean igneous rocks, eastern Beartooth Mountains: Implications for crust-mantle evolution: *Earth and Planetary Science Letters*, v. 87, p. 59-72.

Wooden, J.L., and Miller, D.M., 1990, Chronologic and isotopic framework for early Proterozoic crustal evolution in the eastern Mojave Desert region, SE California: *Journal of Geophysical Research*, v. 95, no., B12, p. 20133-20146.

Zartman, R.E., 1974, Lead isotopic provinces in the Cordillera of the western United States and their geologic significance: *Economic Geology*, v. 69, p. 792-805.

Zartman, R.E., 1988, Proceedings of the international Conference on Basement Tectonics, v.8, p. 699-710.



# TECTONIC AND STRATIGRAPHIC IMPLICATIONS OF DETRITAL ZIRCON SUITES IN CAMBRIAN AND PRECAMBRIAN SANDSTONES FROM THE EASTERN MARGIN OF THE BELT BASIN

**Paul Mueller, David Foster and Jennifer Gifford**

*Department of Geological Sciences, University of Florida, Gainesville, Florida 32611 (mueller@geology.ufl.edu)*

**Joseph Wooden**

*U.S. Geological Survey, 345 Middlefield Road, Menlo Park, CA 94025*

**David Mogk**

*Department of Earth Sciences, Montana State University, Bozeman, MT 59717*

---

## ABSTRACT

U-Pb ages were determined by SHRIMP RG ion microprobe and laser ablation ICP-MS methods for individual detrital zircons extracted from quartz-rich (meta)sedimentary rocks that crop out along the eastern margin of the Belt basin. Units sampled include the Cambrian Flathead sandstone, the Proterozoic Niehart quartzite, and two distinct facies of the LaHood Formation of the Belt Supergroup (coarse conglomerate and siltstone). The age-distributions of zircons from the Neoproterozoic Niehart quartzite (basal Belt) and the Cambrian Flathead sandstone are nearly identical and dominated by grains with ages from 1.72 to 1.88 Ga. The total range of ages from these samples is extended by grains of both additional Proterozoic and Archean ages, and is compatible with derivation from known Laurentian tectonic units that occur within or adjacent to the Great Falls tectonic zone (GFTZ). Zircons from the LaHood samples exhibit a distinctly Archean signature dominated by 3.5 Ga grains; Proterozoic grains are present in only one of the two samples. The sample of Flathead sandstone from the Little Belt Mountains mimics the Niehart quartzite sample, including the lack of ~1.5-1.6 Ga grains characteristic of the lower two-thirds of the Belt Supergroup throughout most of the basin. This suggests that none of these lower units of the Belt section was being recycled along the ancient eastern margin of the basin at the time of Flathead sedimentation,

though similarity to the results from the nearby Niehart quartzite may indicate local recycling of Niehart material or, very improbably, that the two units had a very similar provenance. Collectively, all of the zircons in all samples analyzed can be related to ages determined for the Paleoproterozoic crust of the GFTZ and adjacent Archean rocks of the Wyoming province. The ~1.5-1.6 Ga zircons characteristic of the North American magmatic gap that are present in many lower Belt sedimentary rocks (i.e., pre-Missoula Group) and interpreted to indicate a southwestern-western source are not present in these early eastern Belt units (i.e., LaHood, Niehart). Consequently, these data provide a powerful argument that the Neoproterozoic, cratonic conjugate to western Laurentia is likely to contain an extension of the GFTZ, even if these pure quartz sandstones (Flathead and Niehart) developed as lag-type deposits on the craton and were then reworked in the marginal marine environment.

## INTRODUCTION

Many recent papers have utilized the age-spectra derived from U-Pb dates of detrital zircons to establish the ages of basement exposed in the provenance of individual sedimentary rocks (e.g., DeGraaff-Surpless et al., 2003; Van Wyck and Norman, 2004; Thomas et al., 2005; Mueller et al., 2007). For tectonic reconstructions, the inferred basement configuration can then be used to help identify the cratons that

contributed detritus to the sedimentary rock in question. This concept is not always applicable in a straightforward manner, however, because: 1) it is very difficult to distinguish grains derived directly from basement from grains that have passed through one or more sedimentary cycles and 2) the absence of grains of specific ages is not necessarily indicative of a lack of basement of that age in the source region. Recycling and lack of an age-signal may, but do not necessarily, lead to ambiguity in interpretation of age-spectra. Interpretative errors associated with recycled grains are typically “false positives”, i.e., interpreted incorrectly to indicate the presence of basement of a particular age. The lack of grains for a particular age-interval provides a temptation to infer that basement of that age-range was not in the

provenance, however, there can be many reasons, beginning with bulk compositions, which can result in “lack of signal”. Both of these problems, particularly lack of signal issues, are best addressed by analyzing multiple samples from individual formations or stratigraphic intervals (e.g., DeGraaff-Surpless et al., 2003).

Age-distributions (U-Pb) of detrital zircons from the Belt Supergroup were used by Ross and Villeneuve (2003) to identify distinct sources for many stratigraphic sections in the Belt Basin. In particular, they pointed out the relatively widespread spatial and temporal distribution of 1.7-1.8 Ga grains and the relatively unique presence of 1.5-1.6 Ga zircons in the lower two-thirds of the Belt succession (pre-Missoula Group). Basement of this age is rare

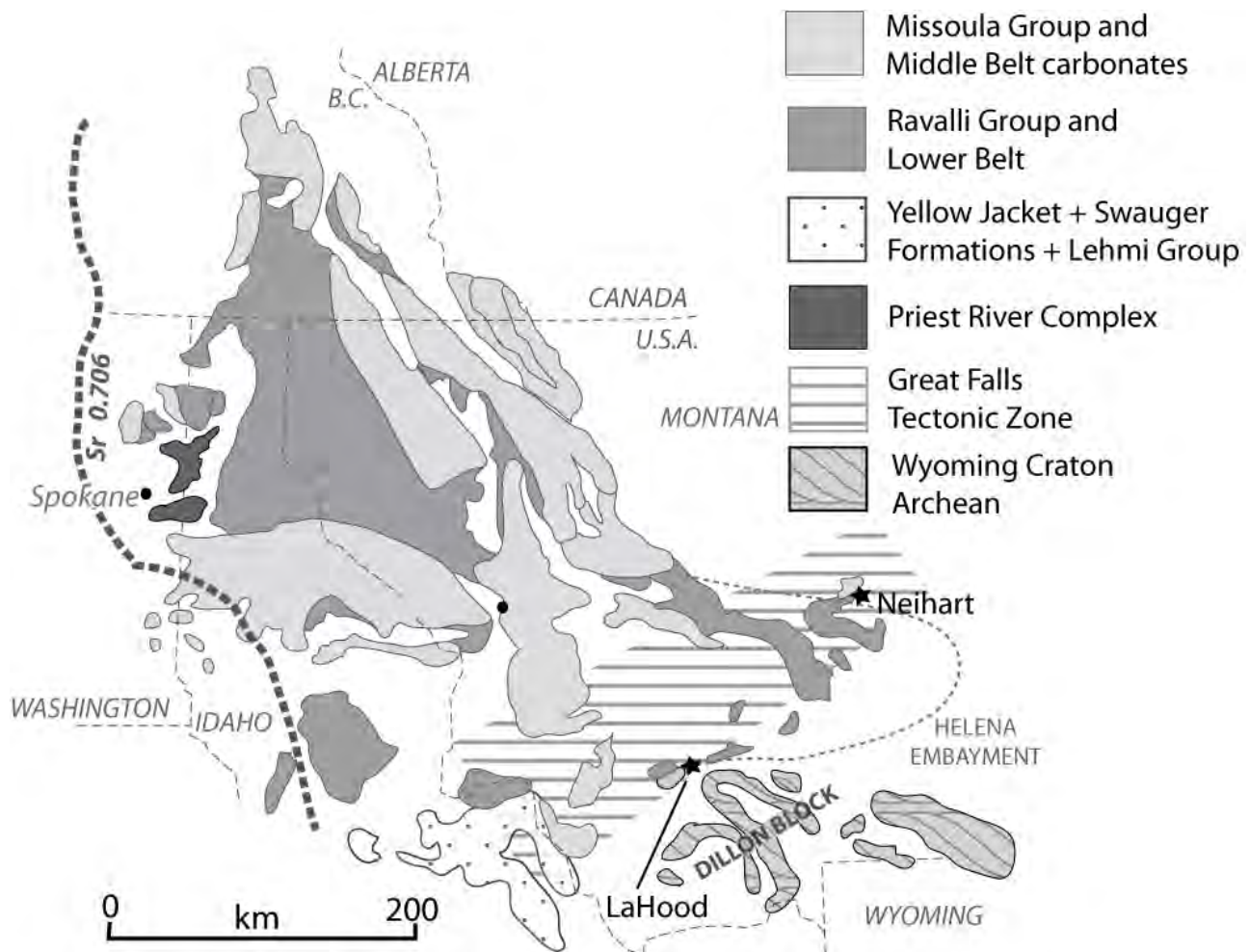


Figure 1. Schematic geologic map depicting regional geologic relations of Precambrian rocks in the study area with sample locations.

in North American Laurentia and led these authors to postulate a non-Laurentian source. Though the non-Laurentian source was not positively identified, these authors suggested that the Gawler craton of southern Australia was a likely candidate. If correct, this would imply that part of modern Australia comprised a portion of the Mesoproterozoic conjugate to this part of western Laurentia (Mueller et al., 2003). Lewis et al. (2007), Doughty and Chamberlain (2007), and Link et al. (2007) have also reported ages for detrital zircons from Belt strata that are generally compatible with the data presented by Ross and Villeneuve (2003).

In this paper we present new U-Pb ages of detrital zircons from a sandstone and from psammitic rocks that both pre-date and post-date the major period of sedimentation and deformation in the Belt basin. Early or pre-Belt sedimentation is represented by the Niehart quartzite that crops out near the eastern limit of the basin in the Little Belt Mountains (e.g., Schieber, 1989) and the LaHood formation (Schmitt, 1988) from the southeastern part of the basin (Jefferson Canyon). A sample from the basal Paleozoic section (Cambrian Flathead sandstone) from an outcrop within the spatial limits of the Belt basin in the Little Belt Mountains (Newlan reservoir) was also analyzed. In addition to providing insight into the source(s) of clastic detritus being shed into the basin during the earliest phase(s) of subsidence, data from these samples are used to evaluate to what extent Belt sedimentary material was locally active in the sedimentary cycle in the Cambrian. It is important to recognize that such recycled material could lead to a “false positive” in terms of the age of basement that was actively being eroded in the Cambrian, i.e., subsequent to Neoproterozoic rifting.

## SAMPLES AND METHODS

*Niehart quartzite.* This sample of meta-quartz arenite was collected from cliff-forming outcrops of along Little Belt creek in the Little Belt Mountains, where it rests unconformably on the ~1.79-1.86 Ga metamorphic rocks exposed in the core of the range (Mueller et al., 2002; Fig. 1). Despite its unconformable relation to the under-

lying quartzofeldspathic gneisses, the Niehart contains very little feldspar. The Niehart was proposed to have been deposited during an early phase of Belt sedimentation and to be intercalated with the Newland Formation as it pinches out to the south (Schieber, 1989). It may be a temporal equivalent of the LaHood Formation (e.g., Schmitt, 1988), but clearly accumulated mineralogically much more mature sediment than the LaHood.

*LaHood Formation.* Stratigraphically, the LaHood has been proposed as the basal member of the Belt Supergroup in the southeastern part of the basin, just as the Niehart has been proposed as the oldest unit in the Little Belt region. The LaHood represents the southernmost exposures of the Belt Supergroup adjacent to the Archean-cored Tobacco Root Mountains (e.g., Frost and Winston, 1987; Schmitt, 1988). Schmitt (1988) and others have suggested that the LaHood may be the lateral equivalent in part of the Newland, Chamberlain, and Grayson Formations and by extension the Niehart. Two distinct facies of the LaHood Formation (Fig. 1) were sampled: 1) coarse sandstone present as matrix within the conglomerate exposed in Jefferson Canyon along the Jefferson River near the town of La Hood and 2) a siltstone from approximately 3 miles north of Jefferson Canyon (Schmitt, 1988).

*Flathead sandstone.* The Flathead is a geographically widespread sandstone deposit, often a quartz arenite, which crops out throughout much of the northern Cordillera and represents the earliest phase of transgressive mid-Cambrian sedimentation (Poole et al., 1992). This sample is a typical quartz arenite and was collected from a small quarry near the dam at Newlan Reservoir (Fig. 1; Zieg et al., 2004). The quartz arenite at this location was mapped as Cambrian Flathead sandstone by Reynolds and Brandt (2006).

These samples were crushed and zircon separated by standard hydrodynamic, density, and magnetic methods. Magnetic separation was limited to 6° side-tilt at 1.5A and zircons were hand-picked for purity from the non-magnetic fraction. Individual grains were then mounted in epoxy, ground and polished, and imaged by optical and

CL (cathodoluminescence) methods prior to analysis on the SHRIMP-RG (ion probe) at the Stanford-U.S.G.S. Microanalytical Center (e.g., Compston and Williams, 1992). Laser ablation ICP-MS (Mueller et al., 2008) was used for some grains from sample LBF-1 (Flathead sandstone). Data are plotted as probability density distributions in Figure 2 using the ISOPLOT software (Ludwig, 2003); all samples plotted are <10% discordant.

## RESULTS AND DISCUSSION

*Niehart quartzite.* Figure 2A shows the distribution of U-Pb ages derived from zircons from this unit. Measured  $^{207}\text{Pb}/^{206}\text{Pb}$  ages range from 1708 to 3354 Ma, with younger grains generally more euhedral than older grains. Despite the wide range of ages determined, a vast majority of measured ages fall into limited spans of time. In particular, >50% of all analyses are between 1725 and 1875 Ma. Other prominent age ranges include ~2460-2530 Ma, ~2600-2700 Ma, ~2800-2840 Ma, and older ages to 3354 Ma. The most important characteristics are: 1) the sample is dominated by Paleoproterozoic grains between 1.72 and 1.88 Ga and contains a small fraction of Archean grains, 2) the sample does not contain 1.5-1.6 Ga grains corresponding to the North American magmatic gap reported from other lower Belt units (Ross and Villeneuve, 2003), and 3) it contains a minor, but significant, number of grains in the 2465-2528 Ma range, a range for which only a limited number of crustal age-provinces have been identified on a global scale, one of which does exist in SW Montana (Mueller et al., 1996; 2004). In fact all ages represented in this sample correspond to ages of basement from the Great Falls tectonic zone (GFTZ) and the northern Wyoming province (Wooden et al., 1982; Mueller et al., 2002).

*La Hood Formation.* Although the two La Hood samples differ in their relative proportions of middle and early Archean grains, both are devoid of Proterozoic grains. Sample BLH-1 from the conglomeratic phase of the La Hood in Jefferson Canyon, for example, has no Proterozoic grains and, in fact, is strongly dominated by ~3500 Ma

grains (14 of 16 grains analyzed). Ross and Villeneuve (2003) report results for a similar sample at this location, which also showed the presence of this ~3500 Ma component, though it was mixed with greater quantities of Late Archean detritus. This result emphasizes the disparities that can occur in short stratigraphic intervals. Certainly such a limited age range of detrital grain ages seems incongruous in light of the wide range of lithologies present in the numerous boulders and cobbles exposed at this location. Similarly, the age distribution for zircons from the siltstone facies (north of Jefferson Canyon; Schmitt, 1988) contains a mixture of both middle and late Archean components as well as some Paleoproterozoic grains typical of rock ages from the GFTZ (~1.8 Ga). The distribution in BLH-2, therefore, is more similar to the results of Ross and Villeneuve (2003) than BLH-1. Results reported here support the interpretation of Frost and Winston (1987), who used Sm-Nd systematics to support previous suggestions that the La Hood detritus was derived largely from nearby Wyoming province basement. The Tobacco Root Mountains, which contain 3.4-3.5 Ga gneisses as well as Late Archean rocks (e.g., Mueller et al., 2004), is proximal to the outcrops of conglomerate in Jefferson Canyon and a likely source of the Archean grains in both samples.

*Flathead sandstone.* U-Pb ages of zircons from this Cambrian sandstone define a pattern that suggests little recycling of Belt detritus (Fig. 2) because it contains no zircons from the 1.5-1.6 Ma population used by Ross and Villeneuve (2003) to suggest that the older sediments of the Belt basin had a western, perhaps Australian, source. The Flathead's detrital zircon age-spectrum does appear, however, to mimic that of the Niehart sample reported here and by Ross and Villeneuve (2003) to a significant degree. There are several implications to these data, including: 1) the lack of 1500-1600 Ma grains implies that pre-Missoula Group Belt sediment was not being actively recycled during the Cambrian transgression in the Little Belt area and 2) attempts to use the detrital zircon signatures of Belt and other non-fossiliferous rocks in the region as a correlation tool must be done cau-

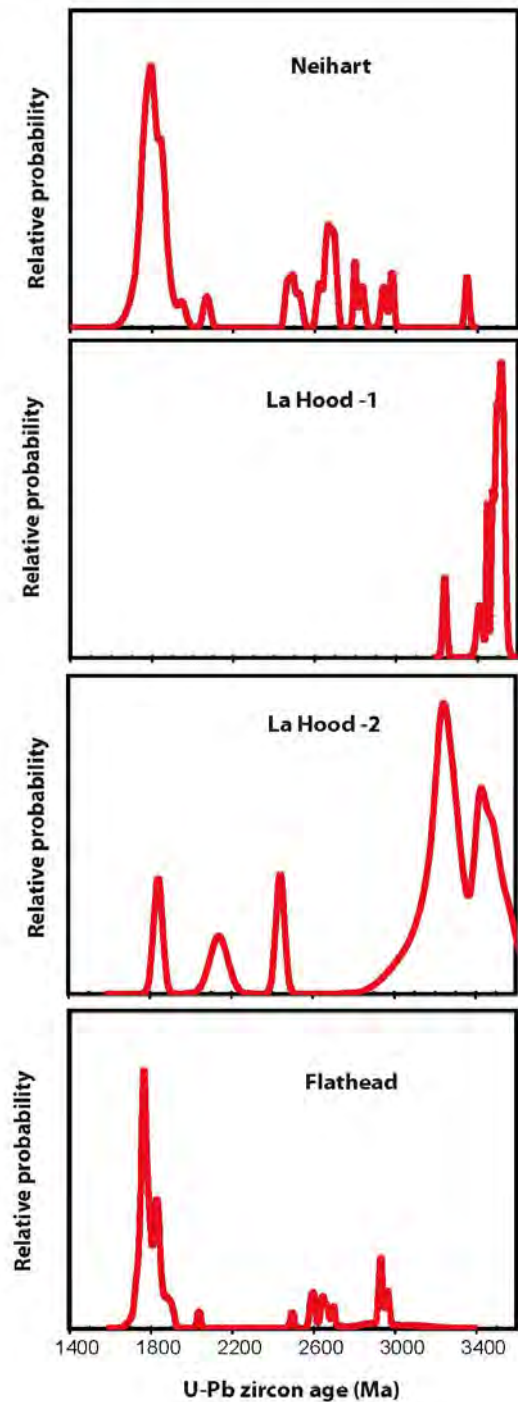


Figure 2. Probability density plots for  $^{207}\text{Pb}/^{206}\text{Pb}$  ages determined for detrital zircons from the Niehart Quartzite (40 grains), LaHood Formation (BLH-1, 12 grains; BLH-2, 12 grains, and Flathead (71 grains). These plots depict relative probabilities densities, which are dimensionless quantities used to capture the relative abundances of ages and are derived from quantifying probabilities of the specific age determined for an individual grain and the error associated with that measurement. On a random sampling basis, analysis of 21 grains yields a probability of 90% that a population of grains present at the 10% level would be detected; 63 grains are required for a 95% probability of detecting a population present at the 5% level.

## CONCLUSIONS

The U-Pb ages of detrital zircons in sedimentary and metasedimentary rocks are useful for constraining regional and large-scale tectonic and sedimentologic processes. In the Belt basin in southwestern Montana, data presented here provide several important insights into the provinciality of early Belt sedimentation. In particular, there is a strong contrast between the age-distributions in the two basal units (Niehart quartzite and LaHood Formation). The Niehart quartzite is dominated by 1.7-1.8 Ga grains, however, there are 1.7-1.8 Ga grains in only one of the LaHood samples, which are dominantly composed of Archean grains. In addition, the 1.5-1.6 Ga grains identified by Ross and Villeneuve (2003) as tectonically significant components in the lower 2/3 of the Belt section (largely pre-Missoula Group) are not present in either the LaHood or Niehart samples. The contrast between the age-distributions in these samples and younger successions as reported by Ross and Villeneuve (2003), including the lack of 1.5-1.6 Ga grains in both of these samples, suggests that initial sedimentation was into isolated, probably fault-bounded, smaller basins that received detritus from very limited eastern sources. This source material was very mature in the case of the Niehart, as opposed to the immature materials deposited in the fault-bounded depocenters of the LaHood Formation (e.g., Schmitt, 1988). It is also important to note that the two LaHood samples differ significantly from each other in that the siltstone facies contains the 1.7-1.8 Ga signal and the conglomeratic matrix does not. This

tiously, and 3) there is no evidence of magmatic rocks developed in response to Neoproterozoic rifting, i.e., no Neoproterozoic or younger grains are present in the Flathead sample.

change occurs over a distance of only a few kilometers. Consequently, the age-distributions of individual samples reported here are of little to no value in correlating the Niehart and LaHood Formations (or even within the LaHood), despite their likely temporal equivalence. Similarly, these results are of little value for correlating the Niehart and LaHood sections with units deposited in the central or western parts of the Belt basin. In short, these data demonstrate the inherent risks involved when attempting to test temporal equivalence of strata based on “missing signals”.

Data for the Flathead sample are puzzling in that the age-distribution for this sample is essentially identical to the age-distribution pattern from the ~900 Ma older Niehart quartzite. Deposition of such a pure quartz sandstone (Flathead) typically reflects a lag-type deposit (in this case on the Precambrian basement) that was then reworked in the marginal marine environment (e.g., Medaris et al., 2002; Van Wyck and Norman, 2004). This is clearly not the case for the Flathead sampled for this study. Instead, the detrital zircon age distribution for this sample is more compatible with accumulation in a restricted basin in which detritus was limited to, or overwhelmed by, contributions from the Niehart. The alternative is that the Flathead had a provenance nearly identical to that of the Niehart. The identical provenance option seems the least likely because the Flathead in this area was deposited over an angular unconformity involving a broad range of the Belt succession and older basement, which should have provided a more diverse provenance than that represented by the ages of detrital zircons. This Flathead sample, therefore, mimics the Niehart not only in its detrital zircon age-distribution, but also in its likely mode of deposition, i.e., accumulation in a small, fault-bounded basin that received mature, but locally derived sediment.

Tectonically, the distinctive 1580-1590 Ma population of zircons present in the lower Belt Supergroup (Ross and Villeneuve, 2003) is not represented in the Niehart, LaHood, or Flathead samples. A majority of the zircons in all samples represent ages determined for the Paleoproterozoic

and older crust of the Great Falls tectonic zone (GFTZ) and adjacent Wyoming province (WP), i.e., no western source is required. If the GFTZ is indeed the source of the Paleoproterozoic zircons along the eastern margin of the basin, then it appears that at least this part of the Belt Basin likely developed on GFTZ/WP crust and received detritus from this crust. The predominance of GFTZ-age zircons throughout Belt strata further suggests that GFTZ may underlie the majority of the basin (e.g., Foster et al., 2006). If so, the cratonic conjugate that separated from western Laurentia in the Neoproterozoic most likely contains an extension of the GFTZ and/or WP.

## ACKNOWLEDGEMENTS

Financial support was provided by the U.S.G.S. (#00057505) and the N.S.F. (EAR 01-06592 and 05-45751 and 05 45751). We also thank A. Heatherington and G. Kamenov for laboratory assistance and Linda Foster for assistance in manuscript preparation.

## REFERENCES CITED

- Compston, W., and Williams, I., 1992, Ion probe ages for the British Ordovician and Silurian stratotypes: *in* Webby, B., and Laurie, J., eds., *Global Perspectives on Ordovician Geology*: Rotterdam, Netherlands, Balkema, p. 59-67.
- DeGraaff-Surpless, K., Mahoney, J., Wooden, J., and McWilliams, M., 2003, Lithofacies control in detrital zircon provenance studies: Insights from the Cretaceous Methow basin, southern Canadian cordillera: *Geological Society of America Bulletin*, v. 115, p. 899-915.
- Doughty, P., and Chamberlain, K., 2007, Age of Paleoproterozoic basement and related rocks in the Clearwater complex, northern Idaho, U.S.A.: *in* Link, P., and Lewis, R., eds., *Proterozoic Geology of Western North America and Siberia*: Society of Economic Paleontologists and Mineralogists Special Publication 86, p. 9-35.
- Foster, D., Mueller, P., Vogl, J., Mogk, D., and Wooden, J., 2006, Proterozoic evolution of the western margin of the Wyoming Craton: Implications for the tectonic and magmatic evolution of the northern

Rocky Mountains: Canadian Journal of Earth Science, v. 43, p. 1601-19.

Frost, C.D., and Winston, D., 1987, Nd isotope systematics of coarse- and fine-grained sediments: examples from the middle Proterozoic Belt-Purcell Supergroup: *Journal of Geology*, v. 97, pp. 309–327.

Lewis, R., Vervoort, J., Burmester, R., McClelland, W., and Chang, Z., 2007, Geochronological constraints on Mesoproterozoic and Neoproterozoic(?) high-grade metasedimentary rocks of north-central Idaho, U.S.A.: *in* Link, P., and Lewis, R., eds., Proterozoic Geology of Western North America and Siberia: Society of Economic Paleontologists and Mineralogists Special Publication 86, p. 37-53.

Link, P., Fanning, M., Lund, K., and Alienikoff, J., 2007, Detrital-zircon populations and provenance of Mesoproterozoic strata of east-central Idaho, U.S.A.: Correlation with the Belt Supergroup of southwest Montana: *in* Link, P., and Lewis, R., eds., Proterozoic Geology of Western North America and Siberia: Society of Economic Paleontologists and Mineralogists Special Publication 86, p. 101-128.

Ludwig, K., 2003, Isoplot 3.00: Berkeley Geochronology Center Special Publication No. 4, 70 p.

Medaris, L., Singer, B., Dott, R., Naymark, A., Johnson, C., and Schoot, R., 2002, Late Paleoproterozoic climate, tectonics, and metamorphism in the southern Lake Superior region and proto-North America: Evidence from the Baraboo interval quartzites: *Journal of Geology*, v. 111, p. 243-257.

Mueller, P., Kamenov, G., Heatherington, A., and Richards, J., in press, Crustal evolution in the southern Appalachian orogen: Evidence from Hf isotopes in detrital zircons: *Journal of Geology*, v. 116.

Mueller, P., Foster, D., Mogk, D., Wooden, J., and Vogl, J., 2007, Detrital mineral chronology of the Uinta Mountain Group: Implications of the Grenville flood in southwestern Laurentia: *Geology*, v. 35, p. 431-434.

Mueller, P., Burger, H., Wooden, J., Brady, J., Cheney, J., Harms, T., Heatherington, A., and Mogk, D., 2005, Age and tectonic implications of Paleoproterozoic metamorphism in the northern Wyoming Province: *Journal of Geology*, v. 113, p. 169-179.

Mueller, P., Foster, D., Mogk, D., and Wooden, J., 2004, New insights into the Proterozoic evolution of

the western margin of Laurentia and their tectonic implications: Geological Society of America, Abstracts with Programs, v. 36, no. 5, p. 404.

Mueller, P., Foster, D., Wooden, J., Mogk, D., and Lewis, R., 2003, Archean and Proterozoic sources for basal quartzites from the eastern and western margins the Belt Basin: *Northwest Geology*, v. 32, p. 215-216.

Mueller, P., Heatherington, A., Kelley, D., Wooden, J., and Mogk, D., 2002, Paleoproterozoic crust within the Great Falls Tectonic Zone: Implications for the assembly of southern Laurentia. *Geology*, v. 30, p. 127-130.

Mueller, P., Heatherington, A., D'Arcy, K., Wooden, J., and Nutman, A., 1996, Contrasts between Sm-Nd and U-Pb zircon systematics in the Tobacco Root batholith, Montana: Implications for the determination of crustal age provinces: *Tectonophysics*, v. 265, p. 169-79.

Poole, F., Stewart, J., Palmer, A., Sandberg, C., Madrid, R., Ross, R., Hintze, L., Miller, M., and Wrucke, C., 1992, Latest Precambrian to latest Devonian time: Development of a continental margin: *in* Burchfiel, B., Lipman, P., and Zoback, M., eds., The Cordilleran Orogen: Conterminous U.S: Geological Society of America, *Geology of North America*, v. G-3, p. 9-56.

Reynolds, M., and Brandt, T., 2006, Preliminary geologic map of the White Sulphur Springs 30' x 60' quadrangle, Montana: U.S. Geological Survey Open-File Report 2006-1329.

Ross, G., and Villeneuve, M., 2003, Provenance of the Mesoproterozoic (1.45 Ga) Belt basin (western North America): Another piece in the pre-Rodanian paleogeographic puzzle: *Geological Society of America Bulletin*, v. 115, p. 1191-1217.

Schieber, J., 1989, The origin of the Niehart Quartzite, a basal deposit of the Mid-Proterozoic Belt Supergroup, Montana, U.S.A.: *Geological Magazine*, v. 126, p. 271-281.

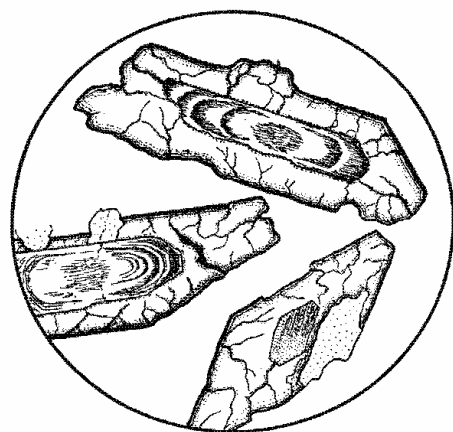
Schmitt, J., 1988, Sedimentation and tectonic setting of the Middle Proterozoic LaHood Formation, Belt Supergroup, southwestern Montana: *in* Lewis, S., and Berg, R., eds., *Montana Bureau of Mines and Geology Special Publication 96*, p. 89-96.

Thomas, W., Astini, R., Mueller, P., Gehrels, G., and Wooden, J., in review, Detrital zircon ages sustain

Laurentian affinities of the Argentine Precordillera terrane: submitted to *Geology*.

Van Wyck, N., and Norman, M., 2004, Detrital zircon ages from Early Proterozoic quartzites, Wisconsin, support rapid weathering and deposition of mature quartz arenites: *Journal of Geology*, v. 112, p. 305-315.

Zeig, G.A., Feeback, D.L., Vogl, J.J., Foster, D.A., Mueller, P.A., and Mogk, D.W., 2004, A field tour through the Proterozoic rocks of the southern Little Belt Mountains: *Northwest Geology*, v. 33, p. 100-110.



# PROVENANCE OF LATE MIOCENE FLUVIAL STRATA OF THE SIXMILE CREEK FORMATION, SOUTHWEST MONTANA: EVIDENCE FROM DETRITAL ZIRCON

Caleb N. Stroup, Paul K. Link

Idaho State University, Pocatello, Idaho, 83209

C. Mark Fanning

Australian National University, Canberra, Australia

## ABSTRACT

Detrital zircon age spectra from two samples of the Late Miocene Anderson Ranch member of the Sixmile Creek Formation in southwest Montana, one northeast of Lima and one east of Dillon, were used to test the hypothesis of Late Miocene drainage from central Idaho into the Ruby graben of southwest Montana. Both samples have defined Neogene detrital zircon grain populations with peaks at about 9-12 Ma. The southerly sample (SC1) also contains multiply recycled pre-Neogene zircons, including 1.5 – 1.75 Ga Paleoproterozoic populations recycled from Mesoproterozoic Belt Supergroup and Cretaceous foreland basins sandstones. Other small populations of Antler-age Mississippian-Devonian grains, ca. 700 Ma Neoproterozoic grains, and 1.8 to 2.0 Ga grains are also present. The absence of 45 to 50 Ma grains from the Challis Volcanic Group precludes the likelihood of first-cycle Late Miocene drainage from central Idaho, contrary to previous models for the provenance of the Sixmile Creek Formation.

Our data suggest that the Sixmile Creek Formation con-

tains fluviably transported zircon grains proximately derived from uplifts on the north side of the Late Miocene tumescent Heise volcanic field and the east flank of the adjacent Beaverhead Mountains near the Idaho-Montana border.

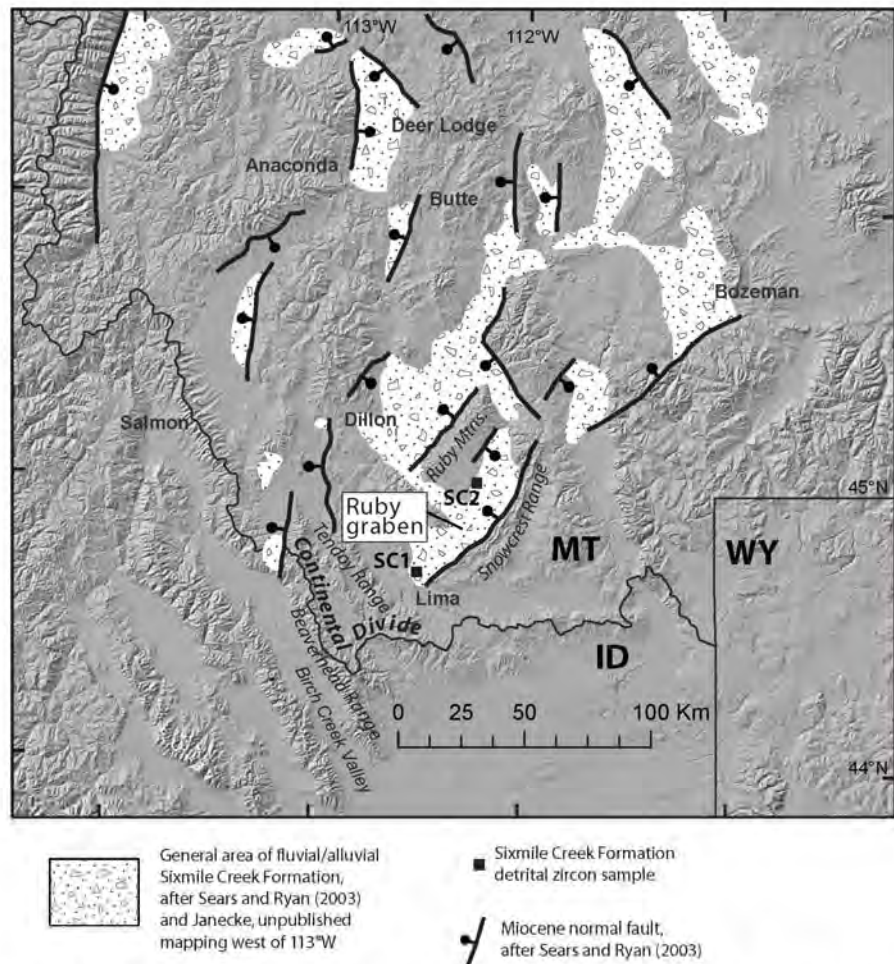


Figure 1: Map of sample location and general distribution of the Sixmile Creek Formation. See Table 1 for sample ages and location details.

## INTRODUCTION

Miocene to early Pliocene paleovalley fill preserved in the Sixmile Creek Formation in southwest Montana contains important information for reconstructing the topographic history of the region as related to the initiation of Basin and Range extension and Yellowstone hotspot tectonics (Fritz and Sears, 1993; Sears and Ryan, 2003; Sears and Thomas, 2007). Between the Ruby and Snowcrest Ranges of southwest Montana, fluvial facies of the Sixmile Creek Formation filled an Early to Late Miocene northeast-trending half graben, the Ruby graben (Fig. 1). Axial northeastward paleoflow is indicated in the Ruby graben by systematic clast imbrication, grain size trends, cross-bedding, and channel geometries (Fritz and Sears, 1993; Sears and Ryan, 2003).

The ca. 6 Ma Timber Hill basalt (Fritz et al., 2007) also occupied the Ruby graben and flowed northeast from at least as far south as Lima, Montana (Fritz and Sears, 1993). It is likely that the Timber Hill basalt is correlative with the ca. 6 Ma Indian Creek basalt (Hodges, 2006) in the Medicine Lodge Valley of eastern Idaho. The source vent for these basalts may have been on the eastern Snake River Plain, perhaps associated with the 6.0 Ma Blue Creek volcanic center (Fritz and Sears, 1993). Late Miocene drainage within this paleovalley system appears to have flowed north-northeastward from the eastern Snake River Plain, across what is currently the continental divide.

Paleodrainage reconstructions that invoke far-traveled streams from central Idaho flowing into the Ruby graben, delivering detritus to the Sixmile Creek Formation, have been proposed by Fritz and Sears (1993) and Sears and Ryan (2003). This model is based primarily on correlation of clast lithologies in conglomerate of the Sixmile Creek Formation with lithologies in central and eastern Idaho (Fritz and Sears, 1993; Sears and Ryan, 2003; Fritz et al., 2007; Sears and Thomas, 2007). This model, however, is seemingly at odds with other models of Late Miocene topography in eastern Idaho

(Rodgers and Anders, 1990) and northeastward migration of topographic divides with the Yellowstone hotspot system on the Snake River Plain (Pierce and Morgan, 1992; Beranek et al., 2006)

We use detrital zircon geochronology to identify the provenance of Sixmile Creek fluvial sands and to test paleodrainage models. Detrital zircon age spectra from modern streams draining central Idaho are well-documented (Link et al., 2005) and serve as modern analogs for paleo-streams which would have drained the same areas. Comparison of detrital zircon age spectra from fluvial sandstones of the Sixmile Creek Formation in the Ruby graben with modern stream sands from central Idaho allows the hypothesis of a south-central Idaho provenance (e.g., Fritz and Sears, 1993) to be evaluated.

## GEOLOGIC CONTEXT AND STRATIGRAPHY

The Eocene to Pliocene Bozeman Group records two discrete episodes of continental sedimentation. The Bozeman Group is composed of the middle Eocene to Early Miocene Renova Formation and the Miocene to early Pliocene Sixmile Creek Formation (Fields et al., 1985; Rasmussen, 2003; Fritz et al., 2007). In southwest Montana, the Sixmile Creek Formation unconformably overlies the Renova Formation, usually with angular relationships (Fields et al., 1985). This unconformity is commonly attributed to the tectonism associated with the initiation of Neogene crustal extension and the development of intermontane basins in southwest Montana. The timing of the unconformity varies regionally, but generally it initiated at about 18 Ma and spanned 1-2 m.y. (Barnosky and Labar, 1989; Burbank and Barnosky, 1990; Fritz and Sears, 1993; Sears and Fritz, 1998; Sears and Thomas, 2007).

Above the Early Miocene unconformity, the Sixmile Creek Formation accumulated in newly formed NE trending half grabens. Graben-fill deposits are up to 1,200 m thick (Hanneman, 1989) and composed of dominantly coarse conglomerate, intercalated ash fall tuffs, fluvially

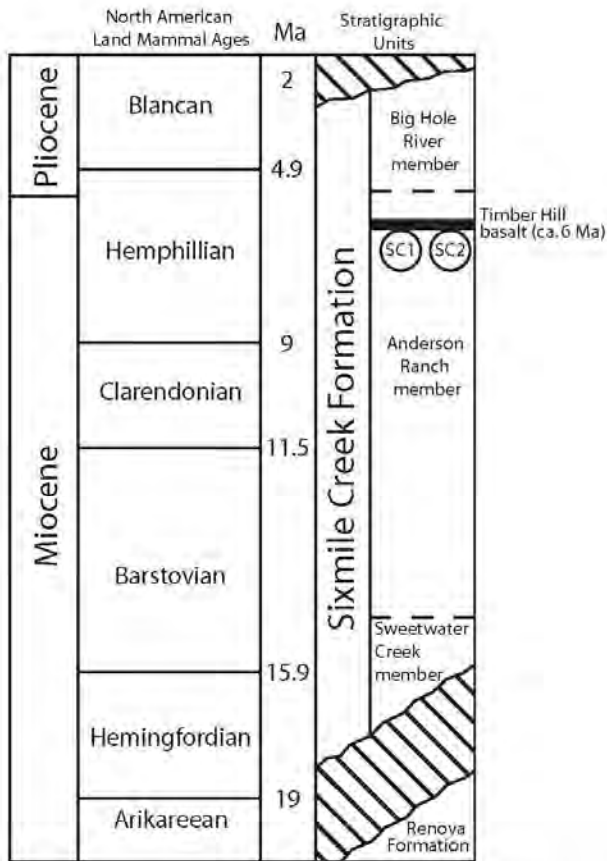


Figure 2: Generalized stratigraphy of the Sixmile Creek Formation in the Ruby graben (modified from Fritz and Sears, 1993). Circles represent general stratigraphic positions of samples. See Table 1 for sample description and age constraints. Land mammal ages from Woodburne and Swisher (1995).

reworked tuffs, and basalts (Kuenzi and Fields, 1971; Fields et al., 1985; Fritz and Sears, 1993; Fritz et al., 2007).

The Sixmile Creek Formation is informally subdivided into three members (Fig. 2): the basal Sweetwater Creek member, the Anderson Ranch member, and the capping Big Hole River member (Fritz and Sears, 1993). In the Ruby graben, the Sweetwater Creek Member consists of coarse, matrix-supported diamictite with fine-grained matrix. These coarse-grained rocks are interpreted subaerial debris flow deposits reworked from nearby Oligocene Renova Formation mudstone, with clasts sourced from local bedrock (Sears and Ryan, 2003). The Anderson Ranch member is composed predominantly of volcanic material, both primary ash fall and reworked epiclastic tuffs, and fluvial siltstone, sandstone and con-

glomerate. Individual tephra beds of the Anderson Ranch member range from 6-11.3 Ma (Shane and Sears, 1995). Much of the volcanic material is fluviually reworked ash fall with internal bedding and trough-cross stratification (Fritz et al., 2007). The ca. 6 Ma Timber Hill basalt is present within the Anderson Ranch member (Fritz et al., 2007). The detrital zircons analyzed in this study are from two samples collected from Anderson Ranch member fluvial sandstones below the Timber Hill basalt in the Ruby graben. The Big Hole River member of the Sixmile Creek Formation overlies the Anderson Ranch member and is composed of roundstone conglomerate, siltstone, and sandstone. This member is commonly poorly consolidated with cobbles and pebbles of red Belt Supergroup or Lemhi Group quartzite, white Paleozoic(?) quartzite, and black chert that has been interpreted to be derived from the Devonian Milligen Formation (Fritz and Sears, 1993; Fritz et al., 2007).

## PALEODRAINAGE MODELS

Some workers have suggested that fluvial strata of the Sixmile Creek Formation were deposited by a major stream system which flowed northeast from central Idaho through the axis of the Ruby graben (Fritz and Sears, 1993; Sears, 1995; Sears and Ryan, 2003; Sears and Thomas, 2007; Fritz et al., 2007). The northeast trending distribution of the valley-confined Timber Hill basalt records northeastward flow along the axis of the paleovalley of the Ruby graben. Clast imbrication, grain size trends, and sedimentary structures also suggest northeast directed paleoflow (Fritz and Sears, 1993).

### *Exotic Clasts*

The primary evidence used to argue for sourcing from Idaho, west of the Beaverhead Range, is the fact that Sixmile Creek fluvial conglomerates contain pebble and cobble lithologies interpreted to match distinct lithologies found in south-central Idaho. These lithologies include (1) pink, feldspathic, jasper-granule bearing quartzite interpreted as the Swauger Quartzite, (2) white quartzite interpreted as the Kinnikinic Quartzite, and (3) black chert with convolute white quartz veins interpreted as chert of the Milligen Formation (Fritz and Sears, 1993; Sears and Ryan, 2003; Fritz et al., 2007).

The Swauger Quartzite lies above the Lemhi Group (Belt Supergroup) near Salmon, Idaho and crops out in the Beaverhead Range (Fig. 1) near the Idaho-Montana border (Link et al., 2007a).

The Ordovician Kinnikinic Quartzite one of several regionally extensive orthoquartzites (e.g. Eureka Quartzite) deposited on the Paleozoic western North American passive margin. The Kinnikinic and the lithologically similar Ordovician Summerhouse Formation crop out in and west of the Beaverhead Range of eastern Idaho and southwestern Montana (Fig. 1) (Ruppel, 1998). If white quartzite clasts in the Sixmile Creek Formation are from the Kinnikinic, it is possible they were delivered, first-cycle, from western Montana or Idaho.

Although neither the Swauger nor the Kinnikinic Quartzite are present immediately adjacent to the Ruby Graben, both lithologies could have been supplied from the area of the Beaverhead Range in southwestern Montana and eastern Idaho (Fig. 1).

Clasts of black chert with several generations of white quartz veins in Sixmile Creek conglomerate have been interpreted as chert of the Milligen Formation (Fritz and Sears, 1993; Sears and Ryan, 2003; Fritz et al., 2007). The chert of the Milligen Formation only crops out in the hangingwall of the Pioneer thrust sheet (the Antler allochthon) (Turner and Otto, 1995). Chert clasts described by Sears and collaborators contain folded and cross-cutting white quartz veins, which is also a feature of the Milligen Formation resulting from deformation during the Antler orogeny (Link et al., 1987; Turner and Otto, 1995). If this correlation is correct, the ultimate source for black chert clasts in the Sixmile Creek Formation must have been in central Idaho.

These clasts could, however, have been recycled through a number of pre-Sixmile Creek deposits and do not necessarily require a direct Late Miocene drainage connection with central Idaho as suggested by Sears and collaborators.

It is also possible that black chert clasts in the Sixmile Creek Formation were actually derived first-cycle from the Mississippian Middle Canyon Formation which is locally composed of up to 60% black chert (Lonn et al., 2000). The Middle Canyon Formation is exposed across much of the Beaverhead Range in southwestern Montana and eastern Idaho (Fig. 1).

### *Volcanic detritus*

A large proportion of the sediment in the Sixmile Creek was ultimately derived from silicic eruptions of Yellowstone hotspot track calderas (Fritz and Sears, 1993; Stroup et al., 2008). Much of this tuffaceous sediment has been fluviually reworked and it is not clear what proportion was reworked from local ash fall and what proportion was derived first-cycle from rocks proximal to Snake River Plain calderas. Cobble-sized, rounded pumice clasts present in Sixmile Creek conglomerates, however, were not likely delivered to the system as volcanic ejecta and are evidence for fluvial transport from a primary volcanic source (Sears and Thomas, 2007; Fritz et al., 2007; Stroup et al., 2008). Individual pumice clasts have not been dated. Sears and Thomas (2007) and Fritz et al. (2007) suggested they may have been derived from Picabo and Twin Falls age rocks in central Idaho. These clasts could, however, have been sourced from more proximal primary volcanics of the Heise volcanic field, still indicating Late Miocene drainage from southwest of the modern continental divide.

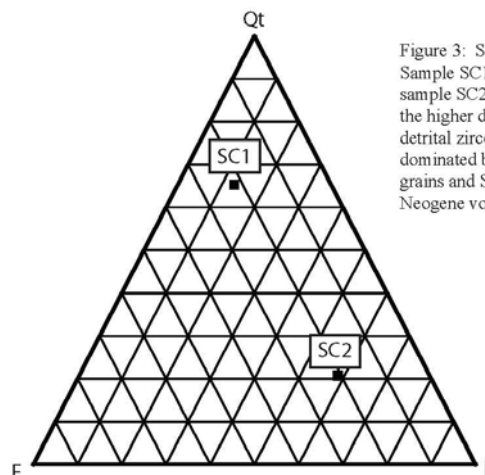


Figure 3: Standard Qt-F-L diagram. Sample SC1 is more mature than sample SC2. This is also reflected by the higher diversity observed in detrital zircon populations. SC1 is dominated by pre-Neogene recycled grains and SC2 is dominated by Neogene volcanic grains (Fig. 4).

**Table 1: Late Miocene detrital zircon samples with locations, southwest Montana**

Name	Fig.	Age	Youngest Detrital (Ma)	Description	UTM Zone	Easting	Northing	Sample Number
SC1	4a	~6 Ma	5.5 ± 0.4	Medium to coarse sub-arkosic fluvial sandstone	12	377312	4953874	58PL02
SC2	4b	~6 Ma	5.1 ± 2.0	Fine to coarse tuffaceous lithic fluvial sandstone	12	400784	4988842	37PL02

**DETRITAL ZIRCON GEOCHRONOLOGY**

*Sampling strategy and analytical techniques*

Fine- to medium-grained fluvial sandstones from well-exposed stratigraphic sections of Late Miocene rocks in the Ruby graben immediately below the ca. 6 Ma Timber Hill basalt (Fritz et al., 2007) were targeted for sampling. Samples were collected in 2002 by Link (Table 1). Stroup and Link revisited sample locations in 2007.

In general, the youngest rim or zone of about 60 randomly selected detrital zircon grains was analyzed with a sensitive high-resolution ion microprobe (SHRIMP) and a U-Pb age obtained using standard techniques (see Williams, 1998 and Link et al., 2008). Complete analytical data are presented in Appendix I. Precambrian grains that are greater than 20% discordant were not included in the probability-frequency plots presented in this paper. Ages used here are the <sup>207</sup>Pb/<sup>206</sup>Pb age for grains older than ca. 800 Ma and the <sup>206</sup>Pb/<sup>238</sup>U age for grains younger ca. 800 Ma (cf. Beranek et al., 2006).

Single youngest detrital zircon U-Pb ages were not used here as robust indicators of maximum depositional age. Only populations consisting of three grains or more were considered significant. Although single grain-ages may be meaningful in many situations (e.g., Dickinson and

Gehrels, 2008), the conservative approach taken here minimizes the risk of attaching significance to spurious ages.

Using the Gazzi-Dickinson method, detrital modes of sandstones were determined by point counting of thin sections. A minimum of 500 points were counted from each sample. The Gazzi-Dickinson method minimizes the effect of grain size on calculation of detrital modes

Possible grain source	Minimum age (Ma)	Maximum age (Ma)	Source regions
Yellowstone hotspot system	0	17	Snake River Plain and Yellowstone system, northeast Nevada to northwest Wyoming
Challis and Absaroka volcanics and related intrusions	42	55	South-central Idaho and southwest Montana, north of Snake River Plain
Devonian and Mississippian Antler orogenic belt volcanism	320	450	Antler allochthon, west of Pioneer thrust in central Idaho and northern Nevada
Neoproterozoic Bannock Volcanic Member	680	720	Pocatello, ID area (Fanning and Link, 2004)
Pioneer Mtns. Neoproterozoic gneiss	580	800	Pioneer Mountains Metamorphic core complex (Link et al., 2005; Durk et al., 2007)
Grenville orogen	950	1300	Central Idaho and Idaho-Wyoming thrust belts; Neoproterozoic to Paleozoic miogeocline
Recycled Yavapai-Mazatzal, non-North American grains, and syn-Belt volcanics	1380	1800	Recycled through the Missoula and Lemhi Groups of the Belt Supergroup (Link et al., 2007a)
Paleoproterozoic basement	1800	2500	Primary grains, exposed basement west of the Wyoming province (Kellogg et al., 2003; Foster et al., 2006)
Wyoming province	2500	2800	Primary grains from exposed basement or recycled through Proterozoic or Paleozoic sandstone

Table 2. Detrital zircon age populations in late Miocene sandstones of southwest Montana and selected possible source rocks. Modified from Link et al. (2005) and Beranek et al. (2006).

(Ingersoll et al., 1984). Sandstone compositions are summarized in Figure 3. Point count data are given in Appendix II.

### Interpreting provenance

Zircon is a heavy mineral resistant to chemical weathering that is a common component in siliciclastic sedimentary systems. Because zircons do not break down chemically in sedimentary systems, grains can be recycled through weathering of older sedimentary rocks (Link et al., 2005). Grains present in a sedimentary system can, therefore, be derived from older sources, stored in sedimentary strata, and put back in the system one or more times. Second-cycle zircons may be widely distributed and give information about the ultimate source, but not the proximate one. Conversely, first-cycle zircons are derived from weathering of igneous and metamorphic rocks.

The degree of reworking of a sandstone is reflected in the diversity of its detrital zircon populations, which may be grouped into defining, major, and minor components (Link et al., 2005). Populations of zircon grains can serve as precise provenance tracers in small (first- and second-order; Ingersoll et al., 1993) fluvial basins. If it can be reasonably demonstrated that zircon grains in a sedimentary system are first-cycle, start and end points for transport vectors can be inferred. This requires knowledge of the ages of possible source areas.

The geochronology of the northern Rocky Mountains is reasonably well defined, although in some areas little U-Pb geochronology has been done. Possible source areas for Late Miocene sedimentary rocks sampled here are given in Table 2. Many of the populations observed

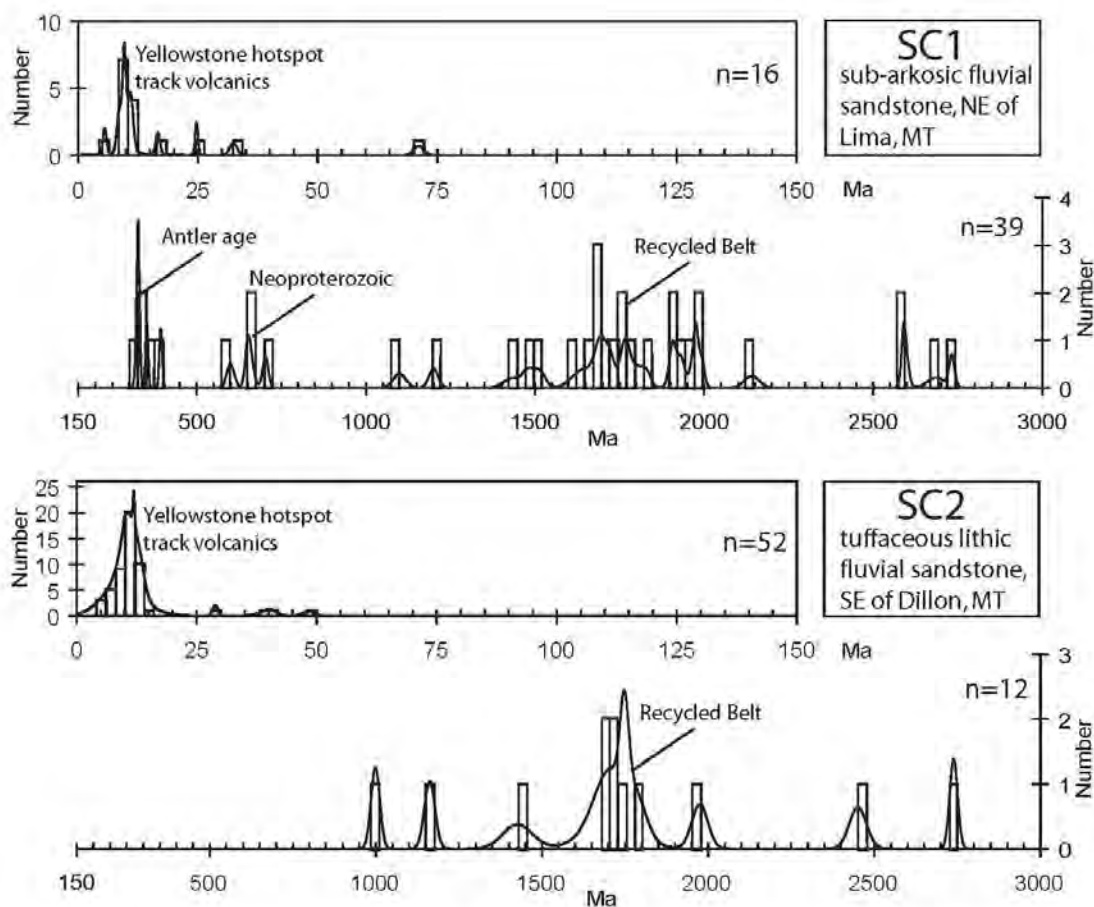


Figure 4: Detrital zircon age spectra of modern late Miocene volcanic-lithic fluvial sandstones deposited in the Ruby Graben, southwest Montana. Both sandstones contain strong components sourced from volcanism on the eastern Snake River Plain and recycled through the Belt Supergroup. Note y-axis is not fixed.

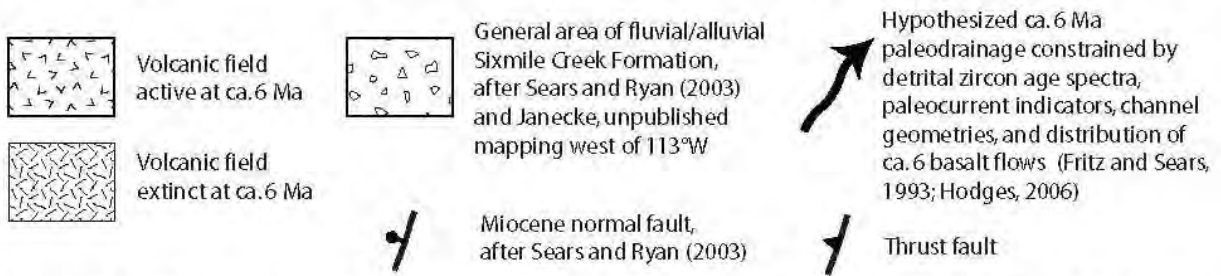
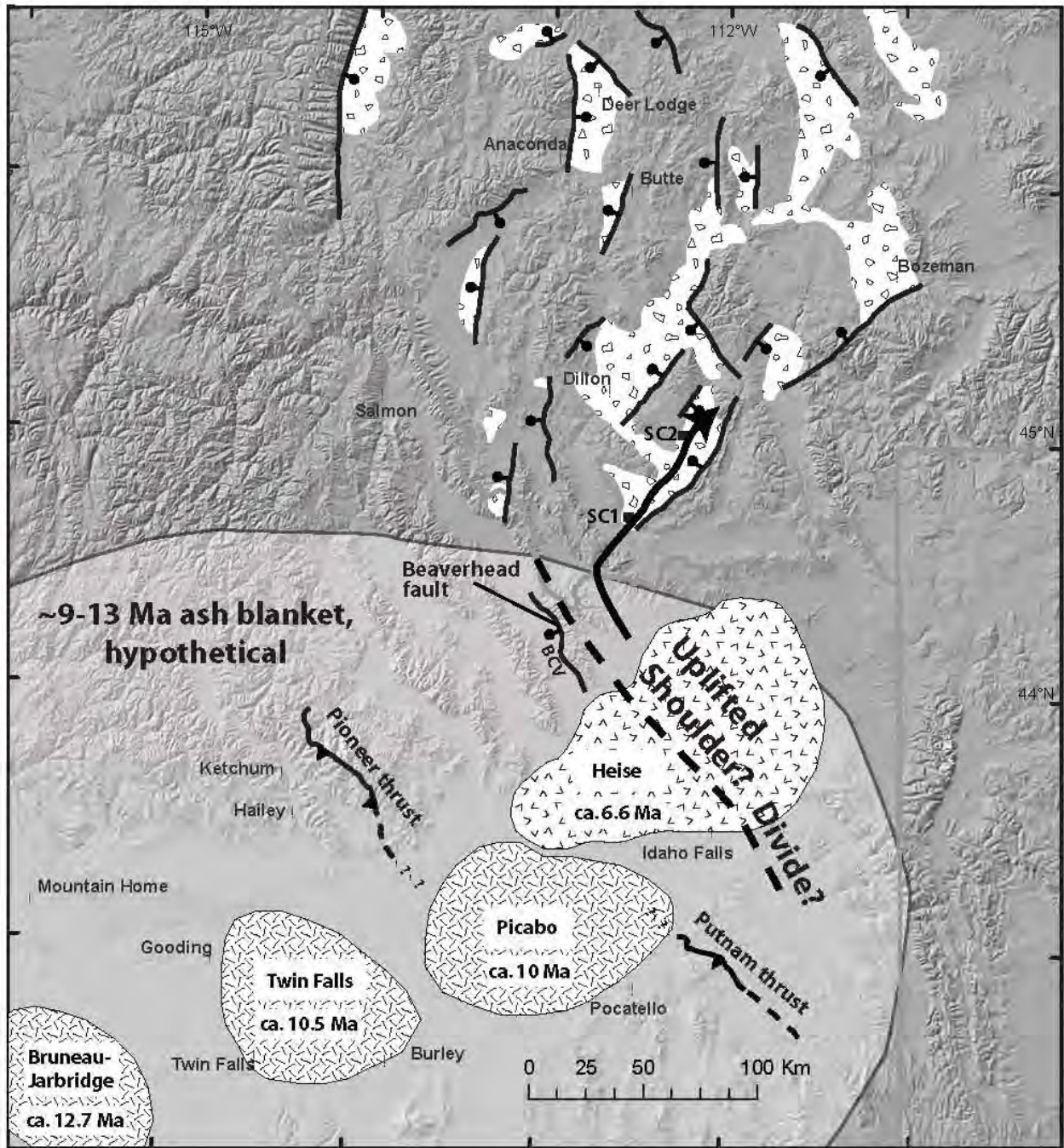


Figure 5: Possible paleogeographic scenario at ca. 6 Ma. Reworked 10-13 Ma ash may have been uplifted on the shoulder of the tumescent Heise volcanic field and been delivered to Late Miocene stream systems in the Ruby graben. BCV = Birch Creek Valley. Volcanic fields distributions and ages from Pierce and Morgan (1992) and Perkins and Nash (2002). Pioneer thrust after Link and Janecke (1999). Putnam thrust after Kellogg et al. (1999).

in the age spectra of these samples have multiple possible sources and precise interpretations of provenance are thus limited. Similarly, some populations have likely been recycled through older sediments.

#### **DETRITAL ZIRCON POPULATIONS AND PROVENANCE OF THE LATE MIOCENE SIXMILE CREEK FORMATION**

Sample SC1 is a subarkosic sandstone from northeast of Lima, Montana (Fig. 1). Thirty-nine of 55 dated zircon grains are pre-Neogene. These demonstrate a variety of older ultimate sources for this sandstone (Fig. 4). These diverse pre-Neogene zircon populations are consistent with the mineralogically mature composition of SC1 as opposed to volcanic lithic composition of the SC2 (Fig. 3). SC2 is a pumiceous volcanic lithic sandstone from the east flank of the Ruby Mountains (Fig. 1), near Timber Hill. Fifty-two of 64 dated zircon grains from this sample compose a major Neogene population; evidence that the stream which deposited this sand was choked by Snake River Plain-Yellowstone hotspot derived tuffaceous detritus (Fig. 4). Sample SC2 contains less information about the diversity of sources. The scattered pre-Neogene grains in both samples cover a wide range of Paleozoic and Precambrian ages (Fig. 4).

##### ***Neogene grain populations***

A dominant ca. 6-14 Ma detrital zircon population is present in both ca. 6 Ma sandstones (SC1 and SC2) sampled here (Fig. 4). The bulk of these grains from both samples are about 9 to 12 Ma. These ages correspond to the ages of silicic volcanism of the Yellowstone hotspot system; specifically, the Twin Falls, Picabo, and Bruneau-Jarbidge volcanic centers (Fig. 5) (Pierce and Morgan, 1992; Perkins and Nash, 2002). Ash fall tuffs from Yellowstone hotspot track volcanism are widespread throughout the western United States (Perkins and Nash, 2002). In the Birch Creek Valley (Fig. 5), for example, Late Miocene tuffs and sandstones are preserved which contain Twin Falls and Picabo volcanic field zircons (Link et al.,

2005). Similar ash fall tuff deposits likely existed to the east and southeast in what is now the eastern Beaverhead Range, prior to Late Miocene-Pliocene uplift and erosion in the footwall of the Beaverhead fault (Rodgers and Anders, 1990) and uplift associated with the passing Yellowstone hotspot system (Fig. 5).

We favor a model whereby much of the hotspot-derived material in the Sixmile Creek Formation originally fell as ash fall and was fluvi-ally reworked (Sears and Ryan, 2003; Fritz and Sears, 2007; M. Perkins, written comm., 2008). The proximate source for this ash was likely much closer than the calderas from which it erupted.

The presence of Twin Falls and Picabo age peaks in southwest Montana sandstones does not require direct drainage from the Twin Falls and Picabo volcanic fields, since the grains could reside in older ash fall tuff or sandstone deposits before being recycled into the 6 Ma Sixmile Creek Formation.

##### ***Paleoproterozoic and Mesoproterozoic grain populations***

Paleoproterozoic and Mesoproterozoic detrital zircon populations (1450-1800 Ma) are also present in both samples from the Anderson Ranch member (Fig. 4). The bulk of these grains were likely ultimately derived from the Yavapai and Mazatzal zones of the Colorado province and proximally recycled through Mesoproterozoic rocks of the Belt Supergroup and correlative strata (Link et al., 2007a). Further recycling through Cretaceous conglomeratic sandstones derived from the Belt Supergroup is likely (Janecke et al., 2000). This interpretation is consistent with ultimate derivation of quartzite cobbles of the Sixmile Creek Formation from Belt Supergroup and Lemhi Group rocks (Fritz and Sears, 1993; Sears and Ryan, 2003; Fritz et al., 2007).

Six Paleoproterozoic grains in sample SC1 form an older population (ca. 1800-2000 Ma) that is distinct from the 1750 to 1600 and 1500 to 1450 Ma populations expected from recycled Belt Supergroup (Link et al., 2007a) (Fig. 4).

The Ordovician Kinnikinic Quartzite and correlative units are composed dominantly of 1.8-2.0 Ga grains derived from the Peace River Arch in British Columbia (Smith and Gehrels, 1994; Gehrels and Dickinson, 1995; Pope, 2008). The grains in SC1 could have been recycled through the Kinnikinic in southwest Montana or Idaho. It is also possible that the 1.8-2.0 grains were derived first-cycle from Paleoproterozoic basement of the Selway terrane exposed in the Beaverhead and Tendoy Ranges of southwest Montana (Foster et al., 2006).

### ***Western Assemblage Grains***

Five anomalous Mississippian-Devonian Antler-age zircon grains are present in sample SC1 and range from about 324-394 Ma (Fig. 4). No sources of this age have been identified in southwest Montana. The closest source for these grains would have been western assemblage rocks in the Antler allochthon, west of the Pioneer thrust in central Idaho (Link et al., 1987; Turner and Otto, 1995; Link et al., 2005).

The presence of these Antler-age grains is compatible with the hypothesis that veined black chert clasts in the Sixmile Creek Formation were ultimately derived from the Milligen Formation in the Antler allochthon (Fritz and Sears, 1993; Sears and Ryan, 2003; Sears and Thomas, 2007; Fritz et al., 2007). Alternatively, these Antler-age zircon grains may have been recycled through conglomerates of the Beaverhead Group or other foreland basin sediments.

Much of the area of southwest Montana was situated in an extensive foreland basin system through much of the Cretaceous, sourced from the west and southwest (DeCelles, 2004). Antler-age grains could have been transported eastward off the Sevier orogenic wedge, deposited, and subsequently reworked.

### ***Neoproterozoic Grains***

Four Neoproterozoic grains are present in sample SC1 and range from about 600-703 Ma (Fig. 4). No known local source exists for these grains. Three of the four grains have ages indistinguishable from ca. 710 to 670 Ma grains identified in tuffs of the Neoproterozoic Pocatello Formation near Pocatello, Idaho (Fig. 5)

(Fanning and Link, 2004). It is possible that the ultimate source of these grains was Pocatello Formation strata in the northward continuation of the Putnam thrust plate (Fig. 5). The limited number of grains, however, limits robust correlation with tuffs of the Pocatello Formation.

Sixty-grain detrital zircon age spectra of Paleogene sandstones in southwest Montana (Stroup et al., in press) commonly contain 1-3 Neoproterozoic grains of unknown origin. These occurrences are yet to be explained but indicate that Neoproterozoic grains are trace components of some pre-Oligocene sedimentary rocks in the region, perhaps Cretaceous foreland basin sediments. Local recycling of Cretaceous sandstones could have provided Neoproterozoic grains to Miocene-Pliocene sediments.

Grains of this broad age range have also been identified in modern streams of central Idaho and are sourced from Neoproterozoic gneiss in the Idaho Pioneer Mountains (Link et al., 2005; Durk et al., 2007). This gneiss was intruded by the Eocene (ca. 50 Ma) Pioneer Pluton during the Challis magmatic episode (Link et al., 2007b) and overlain by a 1-2 km thick sheet of Challis volcanic rocks (Rodgers and Janecke, 1992). Detrital zircon age spectra from modern streams in central Idaho which contain Neoproterozoic grains also systematically contain large populations of Challis-age grains.

Because no Challis grains are present in SC1, the Neoproterozoic grains could not have been supplied first cycle from the Idaho Pioneer Mountains.

### ***Significance of the lack of Challis grains***

The lack of middle Eocene (45 to 50 Ma) Challis grains in both Sixmile Creek samples (Fig. 4) has major implications for the source of all exotic zircon populations and for models of drainage from central Idaho (Fritz and Sears, 1993; Sears and Ryan, 2003; Fritz et al., 2007; Sears and Thomas, 2007). Detrital zircon age spectra from all modern fluvial systems draining central Idaho contain defining Challis peaks (Link et al., 2005). Challis magmatic rocks

cover much of the modern surface of central Idaho and it is clear that Challis grains are a consistent major component of fluvial systems which drain the area today. The lack of these grains in Miocene rocks of southwest Montana precludes the likelihood of first-cycle derivation of exotic clast lithologies and detrital zircon populations from central Idaho.

## DISCUSSION AND CONCLUSIONS

In addition to several minor populations, two major detrital zircon populations are present in Sixmile Creek Formation sandstones analyzed here: (1) a recycled Paleoproterozoic population and (2) a ca. 6-14 Ma population derived ultimately from silicic volcanism of the Yellowstone hotspot track (Fig. 4). Mineralogically mature subarkose (SC1) has diverse minor detrital zircon populations while immature volcanic lithic sandstone SC2 has a single major Snake River Plain-derived zircon population (Fig. 3; Fig. 4).

The Paleoproterozoic 1.5 to 1.7 Ga grains are interpreted as recycled through the Mesoproterozoic Belt Supergroup and Lemhi Group, present in multiple areas near the Idaho-Montana border. In addition, local Cretaceous rocks of the Beaverhead Group are composed dominantly of Belt material, so the detrital zircon populations could have been further recycled through these systems.

The detrital zircon age spectra and sedimentology of the Anderson Ranch member of the Sixmile Creek Formation records a volumetrically significant input of hotspot-age sediment into southwest Montana fluvial systems. A large percentage of the zircons delivered to the system at ca. 6 Ma are significantly older (>3 Ma) than the depositional age. Significant ash fall deposits are not well-preserved in southwest Montana, perhaps due to erosion of the uplifted footwalls of Miocene extensional faults and fluvial reworking of ash deposited in hanging-wall valleys.

In Birch Creek Valley (Fig. 5) in eastern Idaho, however, the ash fall tuff record is well pre-

served (Rodgers and Anders, 1990) and fluvial reworking of this stratigraphy has produced Neogene detrital zircon age spectra in the modern Birch Creek similar to the Sixmile Creek Formation (Link et al., 2005). We suggest regionally extensive, hotspot-related ash fall tuffs were reworked from proximal sources into the Late Miocene Sixmile Creek Formation producing the detrital zircon age spectra observed in samples SC1 and SC2.

Basalt paleovalley-fill and stream-rounded rhyolite pumice clasts, if derived from the Heise volcanic field, require the Late Miocene continental divide to have been farther to the southwest relative to its modern position. This is predicted by the model of a parabola of high relief centered on the active Heise volcanic field (Anders et al., 1989; Pierce and Morgan, 1992) (Fig. 5).

We suggest uplift on the shoulder of the tumescent Heise topographic high produced enough local relief to directly transport Heise-age primary pumice clasts and basalt flows and incise and fluvially rework older ash fall tuffs (Fig. 5). This scenario satisfies necessary conditions for ca. 6 Ma basalt distributions, detrital zircon age spectra, clast lithologies, and sedimentary structures.

The lack of Challis-aged grains in both samples (Fig. 4) contradicts the model of central-Idaho provenance of the Sixmile Creek Formation (Fritz and Sears, 1993; Sears and Ryan, 2003; Fritz et al., 2007; Sears and Ryan, 2007). In contrast, all features of the detrital zircon age spectra of the Sixmile Creek Formation can be explained by mixing of reworked local ash fall tuffs, material shed off the tumescent Heise topographic high, sediment recycled through the Belt Supergroup, and material recycled through local Cretaceous foreland basin sedimentary rocks.

The Antler-age grains and Neoproterozoic grains present in SC1 (Fig. 4), if derived from central Idaho, must have been transported to southwest Montana and stored in sedimentary rocks which predate the Challis magmatic

event. Further detrital zircon geochronology from foreland basin sandstones is required to test this hypothesis. No detrital zircon studies have been conducted on Cretaceous sedimentary rocks of the area.

## ACKNOWLEDGMENTS

This work was funded by NSF EAR-0125756 to Link and several grants to Stroup: 1) Grant-In-Aid of Research from the National Academy of Sciences, administered by Sigma Xi; 2) Grant in Aid from AAPG; and 3) Grant No. FY07-R14 from the Graduate Student Research and Scholarship Committee of Idaho State University, Pocatello, Idaho. Sample location suggestions and discussion with J. Sears, R. Thomas, and S. Janecke were critical for completion of this work. Comments from S. Janecke, D. Rodgers, and B. Crosby improved the quality and clarity of this manuscript.

## REFERENCES

- Anders, M.H., Geissman, J.W., Piety, L.A., and Sullivan, J.T., 1989, Parabolic distribution of circum-eastern Snake River Plain seismicity and latest Quaternary faulting: Migratory pattern and association with the Yellowstone hotspot: *Journal of Geophysical Research*, v. 94, p. 1589-1621.
- Barnosky, A.D., and Labar, W.J., 1989, Mid-Miocene (Barstovian) environmental and tectonic setting near Yellowstone Park, Wyoming and Montana: *Geological Society of America Bulletin*, v. 101, p. 1448-1456.
- Beranek, L.P., Link, P.K., and Fanning, C.M., 2006, Miocene to Holocene landscape evolution of the western Snake River Plain region, Idaho: Using the SHRIMP detrital zircon provenance record to track eastward migration of the Yellowstone hotspot: *Geological Society of America Bulletin*, v. 118, no. 9-10, p. 1027-1050.
- Burbank, D.W., and Barnosky, A.D., 1990, The magnetochronology of Barstovian mammals in southwestern Montana and implications for the initiation of Neogene crustal extension in the northern Rocky Mountains: *Geological Society of America Bulletin*, v. 102, p. 1093-1104.
- DeCelles, P.G., 2004, Late Jurassic to Eocene evolution of the Cordilleran thrust belt and foreland basin system, western U.S.A: *American Journal of Science*, v. 304, p. 105-168.
- Dickinson, W.R., and Gehrels, G.E., 2008, Alternate appraisals of youngest U-Pb grain ages in detrital zircon populations of Mesozoic strata on the Colorado Plateau: *Geological Society of America Abstracts with Programs*, v. 40, no. 1, p. 56.
- Durk, K.M., Link, P.K., Fanning, C.M., 2007, Neoproterozoic 695 Ma felsic orthogneiss, Wildhorse Creek, Pioneer Mountains, South-Central Idaho: New tie point in reconstruction of Rodinian rifting: *Geological Society of America Abstracts with Programs*, v. 39, no. 6, p. 613.
- Fanning, C.M., and Link, P.K., 2004, U-Pb SHRIMP ages of Neoproterozoic (Sturtian) glaciogenic Pocatello Formation, southeastern Idaho: *Geology*, v. 32, no. 10, p. 881-884.
- Fields, R.W., Rasmussen, D.L., Tabrum, A.R., and Nichols, R., 1985, Cenozoic rocks of the intermontane basins of western Montana and eastern Idaho: *in* Flores, R.M., and Kaplan, S.S., eds., *Cenozoic paleogeography of west-central United States*, Pacific Section, Soc. Econ. Paleontologists and Mineralogists, p. 9-30.
- Fritz, W.J., and Sears, J.W., 1993, Tectonics of the Yellowstone hotspot wake in southwestern Montana: *Geology*, v. 21, p. 427-430.
- Fritz, W.J., Sears, J.W., McDowell, R.J., Wampler, J.M., 2007, Cenozoic volcanic rocks of southwestern Montana: *Northwest Geology*, v. 36, 207 p. 91-110.
- Foster, D.A., Mueller, P.A., Mogk, D.W., Wooden, J.L., and Vogl, J.J., 2006, Proterozoic evolution of the western margin of the Wyoming craton: Implications for the tectonic and magmatic evolution of the northern Rocky Mountains: *Canadian Journal of Earth Science*, v. 43, p. 1601-1619.
- Gehrels, G.E., and Dickinson, W.R., 1995, Detrital zircon provenance of Cambrian to Triassic miogeoclinal and eugeoclinal strata in Nevada: *American Journal of Science*, v. 295, p. 18-48.
- Hanneman, D.L., 1989, Cenozoic basin evolution in a part of southwestern Montana: Ph.D. dissertation, Missoula, Montana, University of Montana, 347 p.

- Hodges, M.K.V., 2006, Tertiary stratigraphy of the Idaho Medicine Lodge valley, Clark County, Idaho: Masters thesis, Idaho State University, 163 p.
- Ingersoll, R.V., Bullard, T.F., Ford, R.L., Grimm, J.P., Pickle, J.D., and Sares, S.W., 1984, The effect of grain size on detrital modes: a test of the Gazzi-Dickinson point-counting method: *Journal of Sedimentary Petrology*, v. 54, p. 103-116.
- Ingersoll, R.V., Kretchmer, A.G., Valles, P.K., 1993, The effect of sampling scale on actualistic sandstone petrofacies: *Sedimentology*, v. 40, p. 937-953.
- Janecke, S.U., VanDenburg, C.J., Blankenau, J.J., and M'Gonigle, J.W., 2000, Long-distance longitudinal transport of gravel across the Cordilleran thrust belt of Montana and Idaho: *Geology*, v. 28, no. 5, p. 439-442.
- Kellogg, K.S., Rodgers, D.W., Hladky, F.R., Kiesel, M.A., and Riesterer, J.W., 1999, The Putnam thrust plate, Idaho - dismemberment and tilting by Tertiary normal faults: *in* Hughes, S.S., and Thackray, G.D., eds., *Guidebook to the Geology of Eastern Idaho*: Idaho Museum of Natural History, Pocatello, p. 97-114.
- Kellogg, K.S., Snee, L.W., and Unruh, D.M., 2003, The Mesoproterozoic Beaverhead impact structure and its tectonic setting, Montana-Idaho;  $^{40}\text{Ar}/^{39}\text{Ar}$  and U-Pb isotopic constraints: *Journal of Geology*, v. 111, no. 6, p. 639-652.
- Kuenzi, W.D., and Fields, R.W., 1971, Tertiary stratigraphy, structure, and geologic history, Jefferson basin, Montana: *Geological Society of America Bulletin*, v. 82, p. 3373-3394.
- Link, P.K., Mahoney, J.B., Burton, B.R., Ratchford, M.E., Turner, R.J.W., and Otto, B.R., 1987, Introduction to geology of the central Idaho black shale mineral belt: *Northwest Geology*, v. 16, p. 61-84.
- Link, P.K., and Janecke, S.U., 1999, Geology of east-central Idaho: Geologic roadlogs for the Big and Little Lost River, Lemhi, and Salmon River valleys: *in* Hughes, S.S., and Thackray, G.D., eds., *Guidebook to the geology of Eastern Idaho*: Idaho Museum of Natural History, Pocatello, p. 295-334.
- Link, P.K., Fanning, C.M., and Beranek, L.P., 2005, Reliability and longitudinal change of detrital-zircon age spectra in the Snake River system, Idaho and Wyoming: An example of reproducing the bumpy barcode: *Sedimentary Geology*, v. 182, p. 101-142.
- Link, P.K., Fanning, C.M., Lund, K.I., and Al-einikoff, J.N., 2007a, Detrital zircons, correlation and provenance of Mesoproterozoic Belt Supergroup and correlative strata of east-central Idaho and southwest Montana: *in* Link, P.K., and Lewis, R.S., eds., *SEPM Special Publication 86, Proterozoic geology of western North America and Siberia*, p. 101-128.
- Link, P.K., Durk, K.M., and Fanning, C.M., 2007b, SHRIMP U-Pb ages for Archean orthogneiss, Mesoproterozoic paragneiss, and Eocene Boulder Creek pluton, Pioneer Mountains, south-central Idaho, part of the 2600 Ma Grouse Creek block: *Geological Society of America Abstracts with Programs*, v. 39, no. 6, p. 613.
- Link, P.K., Fanning, C.M., and Stroup, C.S., 2008, Detrital zircon U-Pb geochronologic data for selected Cretaceous, Paleogene, Neogene and Holocene sandstones and river sands in southwest Montana and east-central Idaho: *Montana Bureau of Mines and Geology Open-File Report*, MBMG-569.
- Lonn, J.D., Skipp, B., Ruppel, S.U., Perry, Jr., W.J., Sears, J.W., Bartholomew, M.J., Stickney, M.C., Fritz, W.J., Hurlow, H.A., and Thomas, R.C., 2000, Preliminary geologic map of the Lima 30' x 60' Quadrangle, southwest Montana: *Montana Bureau of Mines and Geology Open File Report* MBMG 408, scale 1:100,000.
- Perkins, M.E., and Nash, B.P., 2002, Explosive silicic volcanism of the Yellowstone hotspot: The ash fall tuff record: *Geological Society of America Bulletin*, v. 114, p. 367-381.
- Pierce, K.L., and Morgan, L.A., 1992, The track of the Yellowstone hot spot: Volcanism, faulting, and uplift: *in* Link, P.K., Kuntz, M.A., and Platt, L.B., eds., *Regional geology of eastern Idaho and western Wyoming*: *Geological Society of America Memoir* 179, p. 1-52.
- Pope, M., 2008, Detrital zircon geochronology of Late Ordovician sandstone in Wyoming suggest Talson-Thelon orogen was a major source of siliciclastic sediment along the transcontinental arch: *Geological Society of America Abstracts with Programs*, v. 40, no. 1, p. 77.

- Rasmussen, D.L., 2003, Tertiary history of western Montana and east-central Idaho: A synopsis: *in* Reynolds, R.G., and Flores, R.M., eds., Cenozoic systems of the Rocky Mountain region: Rocky Mountain Section, Society of Economic Paleontologists and Mineralogists, p. 459-477.
- Rodgers, D.W., and Anders, M.H., 1990, Neogene evolution of Birch Creek Valley near Lone Pine, Idaho: *in* Roberts, S., ed., Geologic field tours of western Wyoming and adjacent parts of Idaho, Montana, and Utah: Geological Survey of Wyoming Public Information Circular 29, p. 27-40.
- Rodgers, D.W., and Janecke, S.U., 1992, Tertiary paleogeologic maps of the western Idaho-Wyoming-Montana thrust belt: *in* Link, P.K., Kuntz, M.A., and Platt, L.B., eds., Regional geology of eastern Idaho and western Wyoming: Geological Society of America Memoir 179, p. 83-94.
- Ruppel, E.T., 1998, Geologic map of the eastern part Leadore 30' x 60' Quadrangle, Montana and Idaho: Montana Bureau of Mines and Geology Open File No. 372, scale 1:100,000.
- Sears, J.W., 1995, Middle Miocene rift system in SW Montana: Implications for the initial outbreak of the Yellowstone hotspot: *Northwest Geology*, v. 25, p. 43-46.
- Sears, J.W., and Fritz, W.J., 1998, Cenozoic tilt domains in southwestern Montana: Interference among three generations of extensional fault systems: *in* Faulds, J.E., and Stewart, J.H., eds., Accommodation zones and transfer zones: The regional segmentation of the Basin and Range province: Geological Society of America Special Paper 323, p. 241-247.
- Sears, J.W., and Ryan, P.C., 2003, Cenozoic evolution of the Montana cordillera: Evidence from paleovalleys: *in* Reynolds, R.G., and Flores, R.M., eds., Cenozoic systems of the Rocky Mountain region: Rocky Mountain Section, Society of Economic Paleontologists and Mineralogists, p. 289-301.
- Sears, J.W., and Thomas, R.C., 2007, Extraordinary Middle Miocene crustal disturbance in southwest Montana: Birth record of the Yellowstone hotspot?: *Northwest Geology*, v. 36, p. 133-142.
- Shane, P.A., and Sears, J.W., 1995, Miocene tephra beds in SW Montana: Geochronology, geochemistry and implications: Geological Society of America, Abstracts with Programs, v. 27, no. 4, p. 55.
- Smith, M., and Gehrels, G., 1994, Detrital zircon geochronology and provenance of the Harmony and Valmy Formations, Roberts Mountains allochthon, Nevada: Geological Society of America Bulletin, v. 106, p. 968-979.
- Stroup, C.N., Sears, J.W., and Link, P.K., 2008, Idaho sources for detrital zircons in Late Miocene Sixmile Creek Formation, SW Montana: Geological Society of America Abstracts with Programs, v. 40, no. 1, p. 78.
- Stroup, C.N., Link, P.K., Janecke, S.U., Fanning, C.M., Yaxley, G., and Beranek, L.P., in press, Eocene to Oligocene provenance and drainage in extensional basins of southwest Montana and east-central Idaho: Evidence from detrital zircon populations in the Renova Formation and equivalent strata: *in* Spencer, J.E., and Titley, S.R., eds., Ores and Orogenesis: Circum-pacific tectonics, geologic evolution, and ore deposits: Arizona Geological Society Digest 22.
- Turner, R.J.W., and Otto, B.R., 1995, Structural and stratigraphic setting of the Triumph stratiform zinc-lead-silver deposit, Devonian Milligen Formation, central Idaho: *in* Worl, R.G., Link, P.K., Winkler, G.R., and Johnson, K.M., eds., Geology and mineral resources of the Hailey 1°x2° quadrangle and the western part of the Idaho Falls 1°x2° Quadrangle, Idaho: U.S. Geological Survey Bulletin 2064-A-R, p. E1-E27.
- Williams, I.S., 1998, U-Th-Pb Geochronology by ion microprobe: *in* McKibben, M.A., Shanks, W.C., III, and Ridley, W.I., eds., Applications of micro-analytical techniques to understanding mineralizing processes: *Reviews in Economic Geology*, v. 7, p. 1-35.
- Woodburne, M.O., and Swisher, C.C., III, 1995, Land mammal high-resolution geochronology, intercontinental overland dispersal, sea level, climate and vicariance: *in* Berggren, W.A., Kent, D.V., Aubry, M.P., and Hardenbol, J., eds., Geochronology, time scales, and global stratigraphic correlations: Unified temporal framework for historical geology, Society of Economic Paleontologists and Mineralogists Special Publication 54, p. 337-364.

*Appendices on following pages*

# Appendix I: Complete detrital zircon SHRIMP U-Pb analytical data

**Table Ia**  
Summary of SHRIMP U-Pb zircon results for sample **SC1** (58PL02)

Grain spot	U (ppm)	Th (ppm)	Th/U	Pb* (ppm)	<sup>204</sup> Pb/ <sup>206</sup> Pb	f <sub>206</sub> %	Total Ratios				Radiogenic Ratios				Age (Ma)			% Disc					
							<sup>238</sup> U/ <sup>206</sup> Pb		<sup>207</sup> Pb/ <sup>206</sup> Pb		<sup>206</sup> Pb/ <sup>238</sup> U		<sup>207</sup> Pb/ <sup>235</sup> U		<sup>207</sup> Pb/ <sup>206</sup> Pb		<sup>206</sup> Pb/ <sup>207</sup> Pb		p				
							±	±	±	±	±	±	±	±	±	±	±			±			
1.1	128	58	0.45	0.2	0.008503	4.41	620.8	30.6	.08109	0.1003	.00154	0.0008				9.9	0.5						
2.1	320	52	0.16	3.1	0.000276	0.28	89.87	1.26	.04965	0.0199	.01110	0.0016				71.1	1.0						
3.1	743	435	0.59	34.4	-	3.48	18.59	0.20	.08091	0.0071	.05192	0.0061				326.3	3.8						
4.1	208	69	0.33	21.0	-	1.95	6.505	0.101	.07890	0.0093	.11529	0.0144				703.4	8.3						
5.1	20	20	1.05	7.8	0.000107	0.15	2.155	0.045	.18491	0.0268	.46341	0.0975	11.731	0.304	0.1836	0.0028	0.811	2455	43	2686	25	9	
6.1	150	137	0.91	37.8	0.000025	0.04	3.406	0.045	.11200	0.0087	.29345	0.0386	4.518	0.070	0.1117	0.0009	0.850	1659	19	1827	15	9	
7.1	124	72	0.58	31.2	-	<0.01	3.416	0.047	.10360	0.0089	.29285	0.0405	4.194	0.069	0.1039	0.0009	0.843	1656	20	1695	16	2	
8.1	2227	545	0.24	7.4	0.000104	0.18	259.8	3.1	.04793	0.0125	.00384	0.0005						24.7	0.3				
9.1	64	36	0.56	16.0	0.000264	0.42	3.435	0.052	.10297	0.0133	.28999	0.0442	3.991	0.082	0.0998	0.0014	0.739	1641	24	1621	26	-1	
10.1	286	129	0.45	85.7	0.000003	0.01	2.870	0.033	.11676	0.0060	.34841	0.0395	5.607	0.070	0.1167	0.0006	0.910	1927	19	1906	9	-1	
11.1	45	27	0.61	15.4	0.000033	0.05	2.495	0.044	.13366	0.0164	.40067	0.0699	7.360	0.159	0.1332	0.0017	0.806	2172	32	2141	22	-1	
12.1	149	74	0.49	39.7	0.000012	0.02	3.227	0.039	.10801	0.0081	.30979	0.0378	4.607	0.066	0.1079	0.0008	0.849	1740	19	1773	14	1	
13.1	49	42	0.86	19.7	-	<0.01	2.152	0.033	.20463	0.0416	.46519	0.0724	13.175	0.336	0.2054	0.0042	0.609	2462	32	2870	33	14	
14.1	106	53	0.50	0.2	-	18.64	573.3	25.3	.19351	0.3876	.00142	0.0011						9.1	0.7				
15.1	207	93	0.45	68.8	0.000008	0.01	2.590	0.033	.17415	0.0098	.38603	0.0486	9.264	0.128	0.1741	0.0010	0.913	2104	23	2597	9	19	
16.1	168	69	0.41	40.6	0.000042	0.07	3.547	0.044	.11030	0.0089	.28173	0.0348	4.262	0.063	0.1097	0.0009	0.831	1600	18	1795	15	11	
17.1	775	102	0.13	118.3	-	0.00	5.625	0.059	.08013	0.0057	.17778	0.0188	1.964	0.025	0.0801	0.0006	0.830	1055	10	1200	14	12	
18.1	374	311	0.83	166.1	-	<0.01	1.934	0.021	.20263	0.0058	.51705	0.0568	14.450	0.164	0.2027	0.0006	0.968	2687	24	2848	5	6	
19.1	300	179	0.60	89.4	-	<0.01	2.881	0.033	.11840	0.0072	.34720	0.0395	5.673	0.073	0.1185	0.0007	0.881	1921	19	1934	11	1	
20.1	201	57	0.28	9.1	-	0.40	19.03	0.25	.05621	0.0124	.05233	0.0069						328.8	4.2				
21.1	239	136	0.57	69.2	0.000035	0.05	2.962	0.038	.18412	0.0166	.33173	0.0427	7.831	0.150	0.1712	0.0024	0.670	1847	23	2570	24	28	
22.1	91	45	0.49	8.2	-	6.34	9.603	0.165	.11174	0.0204	.09753	0.0191						599.9	11.2				
23.1	183	44	0.24	45.2	-	<0.01	3.488	0.043	.10644	0.0090	.28589	0.0353	4.105	0.063	0.1041	0.0009	0.805	1621	18	1699	17	5	
24.1	181	98	0.54	0.2	-	4.24	652.8	23.9	.07973	0.0994	.00147	0.0006						9.4	0.4				
25.1	393	311	0.79	0.5	-	2.07	651.9	16.3	.06256	0.0533	.00150	0.0004						9.7	0.3				
26.1	688	485	0.70	177.6	0.000009	0.01	3.330	0.036	.12149	0.0042	.30026	0.0328	5.025	0.058	0.1214	0.0004	0.951	1693	16	1977	6	14	
27.1	224	50	0.22	41.6	-	<0.01	4.630	0.056	.09266	0.0081	.21601	0.0261	2.760	0.041	0.0927	0.0008	0.810	1261	14	1481	17	15	
28.1	265	175	0.66	48.2	0.000030	0.05	4.725	0.056	.11527	0.0091	.21153	0.0253	3.350	0.049	0.1149	0.0009	0.825	1237	13	1878	15	34	
29.1	94	207	2.21	18.3	-	<0.01	4.413	0.064	.10811	0.0132	.22659	0.0330	3.378	0.064	0.1081	0.0013	0.766	1317	17	1768	22	26	
30.1	124	44	0.35	11.9	0.000158	3.29	8.985	0.154	.08856	0.0252	.10764	0.0198						659.0	11.5				
31.1	200	287	1.44	32.4	-	<0.01	5.301	0.067	.10146	0.0104	.18868	0.0237	2.643	0.043	0.1016	0.0011	0.772	1114	13	1654	19	33	
32.1	203	109	0.54	47.1	-	<0.01	3.702	0.051	.17303	0.0184	.27015	0.0370	6.445	0.112	0.1730	0.0018	0.791	1542	19	2587	18	40	
33.1	295	230	0.78	0.2	-	7.33	1076.7	65.2	.10402	0.1868	.00086	0.0006						5.5	0.4				
34.1	256	77	0.30	23.8	-	1.63	9.246	0.115	.07471	0.0104	.10639	0.0137						651.7	8.0				
35.1	254	134	0.53	50.1	-	<0.01	4.353	0.052	.12068	0.0096	.22974	0.0276	3.823	0.055	0.1207	0.0010	0.833	1333	14	1966	14	32	
36.1	495	194	0.39	26.9	-	0.60	15.786	0.180	.05936	0.0079	.06297	0.0073						393.7	4.4				
37.1	57	27	0.47	17.1	0.000074	0.10	2.855	0.049	.18470	0.0202	.34997	0.0595	8.869	0.181	0.1838	0.0021	0.832	1934	28	2687	19	28	
38.1	156	34	0.22	44.9	0.000002	<0.01	2.987	0.039	.11871	0.0092	.33412	0.0433	5.396	0.082	0.1171	0.0009	0.849	1858	22	1913	14	3	
39.1	142	71	0.50	0.2	-	6.42	541.8	20.5	.09697	0.1069	.00173	0.0007						11.1	0.5				
40.1	213	99	0.46	50.7	0.000022	0.03	3.608	0.043	.10582	0.0072	.27707	0.0329	4.031	0.055	0.1055	0.0007	0.864	1577	17	1723	13	9	
41.1	752	345	0.46	37.0	0.000016	1.94	17.452	0.191	.06918	0.0078	.05619	0.0064						352.4	3.9				
42.1	342	178	0.52	0.8	0.001899	7.42	358.2	8.0	.10501	0.0893	.00258	0.0007						16.6	0.5				
43.1	189	61	0.32	35.9	-	<0.01	4.533	0.055	.09432	0.0083	.22063	0.0270	2.869	0.043	0.0943	0.0008	0.811	1285	14	1515	17	15	
44.1	263	85	0.32	46.1	-	<0.01	4.893	0.057	.09046	0.0129	.20436	0.0238	2.549	0.047	0.0905	0.0013	0.633	1199	13	1435	27	16	
45.1	186	42	0.23	0.5	-	45.98	354.4	9.5	.40954	0.3402	.00152	0.0021						9.8	1.3				
46.1	107	60	0.49	0.3	-	42.20	301.2	14.9	.07966	0.2011	.00152	0.0017						9.0	1.1				
47.1	102	56	0.55	31.8	-	<0.01	2.765	0.039	.18124	0.0154	.36167	0.0516	9.038	0.150	0.1812	0.0015	0.859	1990	24	2664	14	25	
48.1	198	49	0.25	9.0	-	2.77	18.887	0.289	.07519	0.0225	.05148	0.0083						323.6	5.1				
49.1	114	54	0.47	0.9	0.001819	80.19	110.8	3.0	.68005	0.1810	.00179	0.0094						11.5	6.1				
50.1	520	218	0.42	190.2	0.000005	0.01	2.350	0.027	.17334	0.0063	.42548	0.0484	10.165	0.121	0.1733	0.0006	0.953	2285	22	2590	6	12	
51.1	142	79	0.56	59.0	0.000017	0.02	2.066	0.026	.18913	0.0096	.48401	0.0610	12.608	0.172	0.1889	0.0010	0.926	2545	26	2733	8	7	
52.1	132	67	0.51	0.2	0.008151	10.67	526.6	19.5	.13054	0.1187	.00170	0.0007						10.9	0.5				
53.1	234	59	0.25	40.3	0.000024	0.04	4.984	0.063	.10732	0.0169	.20059	0.0252	2.959	0.060	0.1070	0.0017	0.619	1178	14	1749	29	33	
54.1	164	94	0.57	0.2	0.004870	10.21	683.9	27.5	.12686	0.1304	.00131	0.0006						8.5	0.4				
55.1	45	65	1.45	10.1	-	<0.01	3.803	0.065	.10523	0.0240	.26341	0.0447	3.875	0.109	0.1067	0.0024	0.602	1507	23	1744	41	14	
56.1	332	239	0.72	91.5	-	<0.01	3.121	0.035	.12245	0.0059	.32045	0.0362	5.410	0.067	0.1224	0.0006	0.919	1792	18	1992	9	10	
57.1	22	13	0.58	6.3	0.000151	0.20	3.042	0.077	.19229	0.0381	.32801	0.0834	8.614	0.283	0.1905	0.0040	0.774	1829	40	2746	34	33	
58.1	111	52	0.47	0.2	-	27.48	448.4	17.8	.26333	0.3552	.00162	0.0014						10.4	0.9				
59.1	238	37	0.16	59.8	-	<0.01	3.426	0.042	.10797	0.0069	.29191	0.03											

**Table Ib**

Summary of SHRIMP U-Pb zircon results for sample **SC2 (37PL02)**

Grain spot	U (ppm)	Th (ppm)	Th/U	Pb* (ppm)	<sup>204</sup> Pb/ <sup>206</sup> Pb	f <sub>206</sub> %	Total Ratios				Radiogenic Ratios				Age (Ma)							
							<sup>238</sup> U/ <sup>206</sup> Pb		<sup>207</sup> Pb/ <sup>206</sup> Pb		<sup>206</sup> Pb/ <sup>238</sup> U		<sup>207</sup> Pb/ <sup>235</sup> U		<sup>207</sup> Pb/ <sup>206</sup> Pb		<sup>206</sup> Pb/ <sup>238</sup> U		<sup>207</sup> Pb/ <sup>206</sup> Pb		% Disc	
							±	±	±	±	±	±	±	±	±	±	±	±	±	±		
1.1	186	105	0.56	85	0.000060	0.10	1.89	0.03	0.1903	0.0012	0.5289	0.0081	13.828	0.235	0.1896	0.0014	0.903	2737	34	2739	12	0
2.1	220	150	0.68	0.39	0.008267	17.29	486.48	27.56	0.1829	0.0378	0.0017	0.0001						11.0	0.9			
3.1	113	63	0.56	0.25	0.023979	30.63	382.94	23.47	0.2883	0.0417	0.0018	0.0002						11.7	1.3			
4.1	120	94	0.79	0.23	0.028953	40.37	444.37	29.25	0.3651	0.0664	0.0013	0.0002						8.6	1.5			
5.1	186	129	0.70	0.46	0.029750	32.13	349.37	22.38	0.3002	0.0243	0.0019	0.0002						12.5	1.2			
6.1	6063	2650	0.44	9.70	0.000478	0.80	537.13	8.33	0.0526	0.0015	0.0018	0.0000						11.9	0.2			
7.1	123	85	0.69	0.20	0.012912	23.42	515.26	32.07	0.2312	0.0344	0.0015	0.0001						9.6	0.9			
8.1	37	13	0.36	0.20	0.000396	0.67	1.61	0.04	0.2374	0.0027	0.6258	0.0155	20.982	0.574	0.2432	0.0028	0.904	3133	63	3141	19	0
9.1	122	86	0.71	0.24	0.019306	21.14	428.78	29.71	0.2133	0.0240	0.0018	0.0002						11.8	1.0			
10.1	101	53	0.52	0.20	0.056082	39.40	424.58	98.64	0.3575	0.0530	0.0014	0.0004						9.2	2.5			
11.1	91	50	0.55	0.22	0.044062	31.33	358.53	27.22	0.2938	0.0688	0.0019	0.0003						12.3	2.0			
12.1	66	34	0.51	0.13	0.065521	27.50	439.67	34.48	0.2635	0.0345	0.0016	0.0002						10.6	1.2			
13.1	93	49	0.52	0.18	-	28.98	442.81	31.20	0.2752	0.0635	0.0016	0.0002						10.3	1.5			
14.1	610	184	0.30	90	0.000359	0.61	5.81	0.07	0.0765	0.0006	0.1726	0.0021	1.871	0.027	0.0786	0.0006	0.829	1026	12	1162	16	12
15.1	77	57	0.75	0.19	0.025923	40.53	343.59	23.44	0.3665	0.0581	0.0017	0.0003						11.1	1.8			
16.1	100	84	0.84	0.38	0.028502	66.20	228.89	11.69	0.5693	0.0404	0.0015	0.0004						9.5	2.8			
17.1	116	61	0.53	0.35	0.022249	44.27	281.20	14.37	0.3961	0.0293	0.0020	0.0003						12.8	1.7			
18.1	111	49	0.44	0.23	0.051482	25.02	406.29	27.89	0.2440	0.0279	0.0018	0.0002						11.9	1.1			
19.1	127	81	0.64	0.29	0.036032	21.12	376.23	20.72	0.2132	0.0198	0.0021	0.0002						13.5	1.0			
20.1	179	67	0.37	0.33	0.019588	12.44	472.77	23.65	0.1446	0.0329	0.0019	0.0001						11.9	0.9			
21.1	139	78	0.56	0.29	0.030589	15.35	410.18	21.66	0.1676	0.0167	0.0021	0.0001						13.3	0.8			
22.1	133	70	0.53	0.33	0.026416	31.88	348.94	17.95	0.2982	0.0253	0.0020	0.0002						12.6	1.1			
23.1	48	36	0.74	0.17	0.002217	56.93	242.02	19.95	0.4961	0.0518	0.0018	0.0004						11.5	2.8			
24.1	121	57	0.47	0.28	0.030441	33.89	369.91	19.76	0.3141	0.0270	0.0018	0.0002						11.5	1.1			
25.1	110	63	0.58	0.19	0.024795	30.77	502.81	34.58	0.2893	0.0327	0.0014	0.0001						8.9	0.9			
26.1	107	64	0.60	0.25	0.049679	56.23	360.25	64.23	0.4904	0.0454	0.0012	0.0003						7.8	2.1			
27.1	79	48	0.61	0.16	0.059752	32.02	425.24	34.42	0.2992	0.0390	0.0016	0.0002						10.3	1.3			
28.1	72	58	0.80	0.17	0.007395	70.85	367.29	32.66	0.6058	0.0541	0.0008	0.0003						5.1	2.0			
29.1	188	168	0.89	0.49	0.027961	35.68	328.21	17.80	0.3282	0.0505	0.0020	0.0003						12.6	1.7			
30.1	341	194	0.57	0.61	0.021663	26.09	480.52	21.14	0.2524	0.0180	0.0015	0.0001						9.9	0.7			
31.1	1277	642	0.50	5.02	0.003269	1.99	218.49	3.92	0.0624	0.0023	0.0045	0.0001						28.9	0.5			
32.1	179	155	0.86	0.42	0.011708	32.92	362.89	20.93	0.3064	0.0490	0.0018	0.0002						11.9	1.5			
33.1	95	50	0.53	0.27	0.072726	66.35	303.42	23.28	0.5703	0.0830	0.0011	0.0005						7.1	2.9			
34.1	116	59	0.51	0.48	0.039702	67.38	206.34	23.77	0.5787	0.0418	0.0016	0.0005						10.2	3.3			
35.1	89	49	0.56	0.13	0.050049	85.79	74.15	2.70	0.7245	0.0318	0.0019	0.0016						12.3	10.1			
36.1	449	555	1.24	0.70	-	12.85	552.48	22.54	0.1478	0.0110	0.0016	0.0001						10.2	0.5			
37.1	90	38	0.43	0.29	0.040276	56.56	269.78	19.18	0.4931	0.0376	0.0016	0.0003						10.4	2.2			
38.1	142	123	0.87	0.36	0.000028	0.05	3.37	0.05	0.1041	0.0014	0.2970	0.0049	4.247	0.126	0.1037	0.0026	0.552	1676	24	1691	46	1
39.1	108	88	0.81	0.43	0.001410	53.10	217.75	13.76	0.4659	0.0354	0.0022	0.0004						13.9	2.5			
40.1	563	146	0.26	82	0.000924	1.56	5.87	0.08	0.0849	0.0008	0.1675	0.0024	1.656	0.074	0.0717	0.0030	0.325	999	13	977	86	-2
41.1	107	60	0.57	0.54	0.044413	65.20	168.43	32.30	0.5616	0.0780	0.0021	0.0009						13.3	5.5			
42.1	410	251	0.61	2.32	0.001396	4.68	152.18	4.06	0.0839	0.0047	0.0063	0.0002						40.3	1.1			
43.1	118	79	0.67	0.71	0.061702	77.94	142.81	7.16	0.6622	0.0407	0.0015	0.0008						9.9	5.0			
44.1	120	92	0.77	1.04	0.035817	89.05	98.53	4.17	0.7499	0.0378	0.0011	0.0012						7.2	8.0			
45.1	91	105	1.16	0.38	0.040788	64.66	207.51	14.52	0.5572	0.0607	0.0017	0.0006						11.0	3.6			
46.1	168	128	0.76	0.42	0.025675	55.55	344.27	24.73	0.4851	0.0678	0.0013	0.0003						8.3	2.2			
47.1	831	435	0.52	5.55	0.002263	3.18	128.71	2.73	0.0721	0.0092	0.0075	0.0002						48.3	1.2			
48.1	1035	373	0.36	287	0.000235	0.40	3.10	0.04	0.1090	0.0007	0.3220	0.0042	4.747	0.071	0.1069	0.0007	0.885	1799	22	1748	13	-3
49.1	152	72	0.47	0.96	0.000220	0.37	2.31	0.04	0.1623	0.0021	0.4323	0.0078	9.507	0.226	0.1595	0.0025	0.760	2316	35	2450	26	5
50.1	206	186	0.91	0.55	0.040142	41.56	322.24	36.64	0.3746	0.0684	0.0018	0.0004						11.7	2.4			
51.1	116	71	0.61	0.58	0.093897	82.78	173.20	10.51	0.7001	0.0400	0.0010	0.0007						6.4	4.3			
52.1	312	173	0.56	1.97	0.017603	17.00	136.24	4.37	0.1814	0.0337	0.0061	0.0004						39.2	2.6			
53.1	147	72	0.49	0.37	0.000619	1.05	3.41	0.06	0.1070	0.0035	0.2929	0.0051	4.249	0.158	0.1052	0.0035	0.464	1656	28	1718	61	4
54.1	116	53	0.46	0.27	0.035556	56.21	371.66	37.77	0.4902	0.0564	0.0012	0.0003						7.6	1.9			
55.1	95	59	0.62	0.46	0.009813	60.42	176.26	11.89	0.5239	0.0469	0.0022	0.0006						14.5	3.7			
56.1	185	106	0.57	0.47	0.000436	0.74	3.41	0.06	0.1101	0.0014	0.2913	0.0050	4.181	0.202	0.1041	0.0047	0.355	1648	25	1699	83	3
57.1	320	78	0.24	99	0.000741	1.25	2.79	0.04	0.1273	0.0015	0.3564	0.0054	5.958	0.121	0.1213	0.0017	0.740	1965	27	1975	24	1
58.1	134	103	0.77	0.41	0.049402	75.31	278.51	21.01	0.6411	0.0562	0.0009	0.0004						5.7	2.8			
59.1	261	120	0.46	77	0.000125	0.21	2.90	0.05	0.1107	0.0011	0.3438	0.0058	5.166	0.125	0.1090	0.0019	0.695	1905	28	1783	32	-7
60.1	226	77	0.34	60	0.000733	1.24	3.23	0.05	0.1083	0.0023	0.3084	0.0049	4.454	0.124	0.1047	0.0024	0.570	1733	26	1710	42	-1
61.1	516	269	0.52	106	0.000633	1.07	4.19	0.05	0.0989	0.0007	0.2360	0.0030	2.930	0.077	0.0900	0.0021	0.474	1366	15	1427	44	4
62.1	116	88	0.76	0.25	0.017403	36.01	395.36	23.08	0.3308	0.0399</												

<b>Appendix II: Point count data</b>		
Qm	=	monocrystalline quartz
Qp	=	polycrystalline quartz
Chert	=	chert
Plag	=	plagioclase feldspar
Kspar	=	potassium feldspar
Musc	=	muscovite
Biot	=	biotite
Ls	=	sedimentary lithic
Lv	=	volcanic lithic
Lm	=	metamorphic lithic
opq	=	opaque mineral
Qt	=	total quartz
F	=	total feldspar
Lt	=	total lithics

<b>SC1 (58PL02)</b>			<b>SC2 (37PL02)</b>		
	n	%		n	%
Qm	327	65.4	Qm	101	20.2
Qp		0.0	Qp	3	0.6
Chert		0.0	Chert		0.0
Plag	47	9.4	Plag	58	11.6
Kspar	63	12.6	Kspar	46	9.2
Musc		0.0	Musc		0.0
Biot		0.0	Biot		0.0
Ls		0.0	Ls		0.0
Lv	63	12.6	Lv	292	58.4
Lm		0.0	Lm		0.0
opq		0.0	opq		0.0
TOTAL	500	100.0	TOTAL	500	100.0
Qt	327	65.4	Qt	104	20.9
Qm	327	65.4	Qm	3	20.2
F	110	22.0	F	104	20.9
P	47	9.4	P	58	11.7
K	63	12.6	K	46	9.2
Lt	63	12.6	Lt	292	58.3
Lv	63	12.6	Lv	292	58.3
Ls	0	0.0	Ls	0	0.0

# THE BUTCHER CREEK CONGLOMERATE: AN ENIGMATIC PALEOGENE DEPOSIT FROM THE NORTHERN GRAVELLY RANGE OF SOUTHWESTERN MONTANA

**Kevin Lielke**

*Department of Geosciences, The University of Montana, Missoula, MT 59812*

---

## ABSTRACT

The Butcher Creek conglomerate is a new, informally recognized unit within the basal Renova Formation of the northern Gravelly Range. The Butcher Creek conglomerate is exposed in a recently excavated quarry east of Virginia City in the Axolotl Lakes area where Paleogene rocks lie unconformably above Archean basement and isolated remnants of the Paleozoic section. The scarcity of Mesozoic rocks in the surrounding area, the deposit's position relative to the inferred trace of the Greenhorn thrust fault and its clast composition argue against its inclusion within the Cretaceous Beaverhead formation. The modern topography, an approximately north-south trending hill capped by an elongate basalt ridge, is interpreted to be a topographically inverted Eocene paleovalley.

The Butcher Creek conglomerate, at its quarry exposure, is characterized by homogeneous, felsic metamorphic clasts and conspicuously lacks any material derived from the overlying basalt flows of the late Eocene to early Oligocene Virginia City volcanic field. Field relations suggest that it lies beneath, or is interlayered with, the Eocene felsic volcanic tuffs of the lower Virginia City volcanics. These stratigraphic relations suggest that this conglomerate occurs at, or near, the base of the Paleogene section in this area.

Clast counts demonstrate that the conglomerate becomes more heterogeneous south of the quarry outcrop - the probable result of an influx of more locally derived clasts further from the primary metamorphic source terrain. Clast imbrication data from the quarry locality indicate derivation from the northeast (N60E), which along with the predominately felsic metamor-

phic clast composition, suggest a source within the southern Tobacco Root Mountains. Coarse-grained sandstone composed of disintegrated metamorphic material is also present, usually in irregular lens interpreted as fluvial channel deposits. Minor reddish siltstones are also present and are interpreted to be pedogenic in origin.

## GEOLOGIC SETTING

The Butcher Creek conglomerate is located in a topographically low area between the Tobacco Root Mountains to the north and the Gravelly Range to the south (Figure 1). This area is dominated at the surface by the Paleogene volcanics of the Virginia City volcanic field. The Paleogene section is underlain by Archean rocks and isolated remnants of the lower Paleozoic section. This area was clearly subjected to extensive erosion prior to deposition of the Butcher Creek conglomerate and the volcanics of the Virginia City volcanic field. Mesozoic rocks are not present in the immediate vicinity of the Butcher Creek conglomerate, although they exist further to the south in the Gravelly Range.

The Butcher Creek conglomerate itself comprises a conspicuous, generally north-south trending hill directly to the west of the Axolotl Lakes (Figure 2). Exposure is poor except in a few areas along the bed of Butcher Creek and in recently excavated road cuts and a gravel quarry. The gravel hill is directly overlain by an anastomosing, elongate ridge of basalt. The Axolotl Lakes occupy an irregular terrain of unstable felsic tuffs and related sedimentary rocks displaced by modern debris flows. These landslides complicate field observations of the stratigraphic relations of the felsic tuffs and the Butcher Creek conglomerate. The Butcher

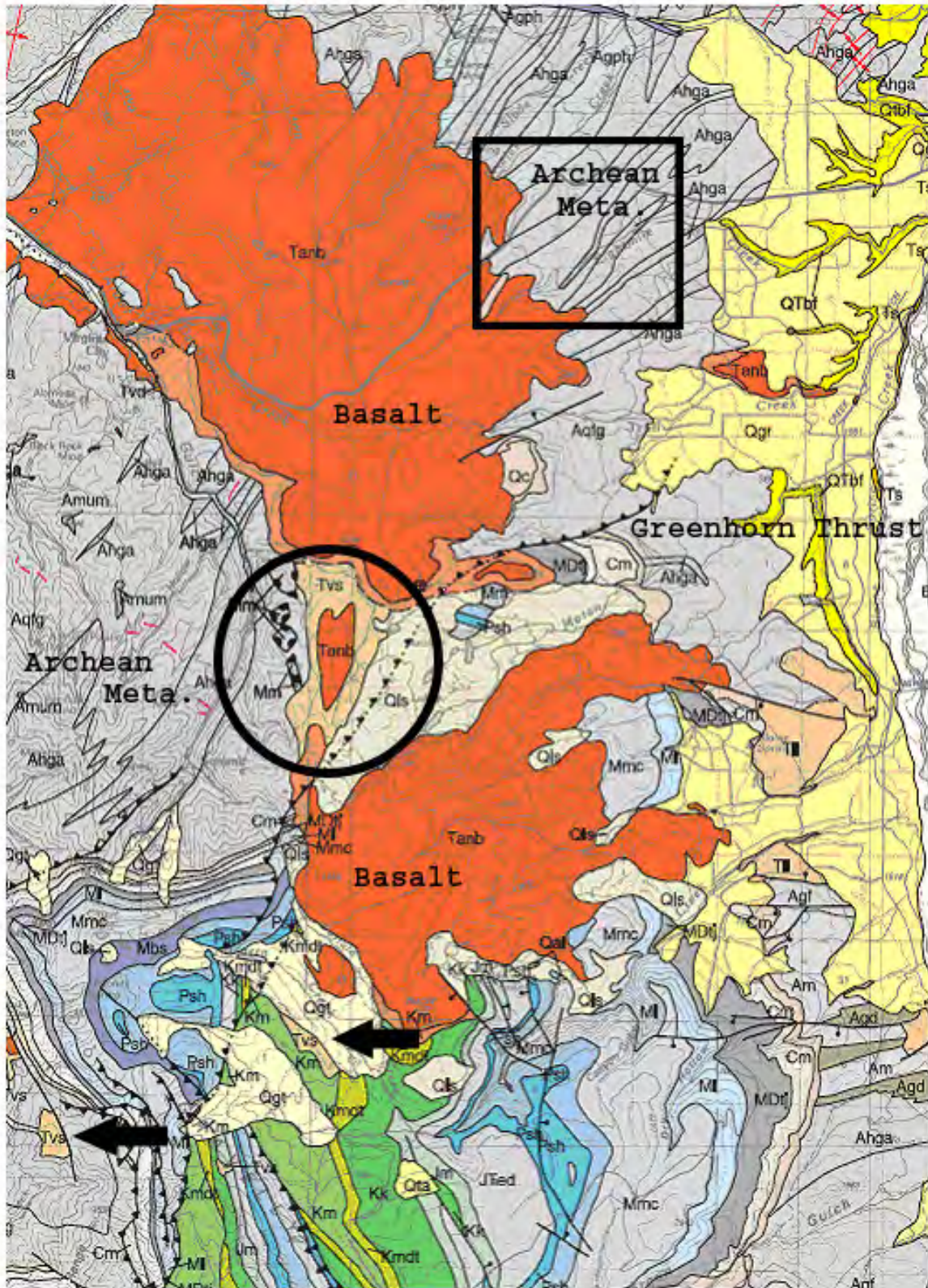


Figure 1. Geologic map of the Butcher Creek area. Main deposit of the Butcher Creek Conglomerate is circled; the square surrounds the area of probable derivation of felsic metamorphic clasts. Black arrows point to two smaller outcrops of unit (Tvs) mapped by Kellogg and Williams which may represent a southern continuation of Paleogene paleo-valley (from Kellogg and Williams, 2006).

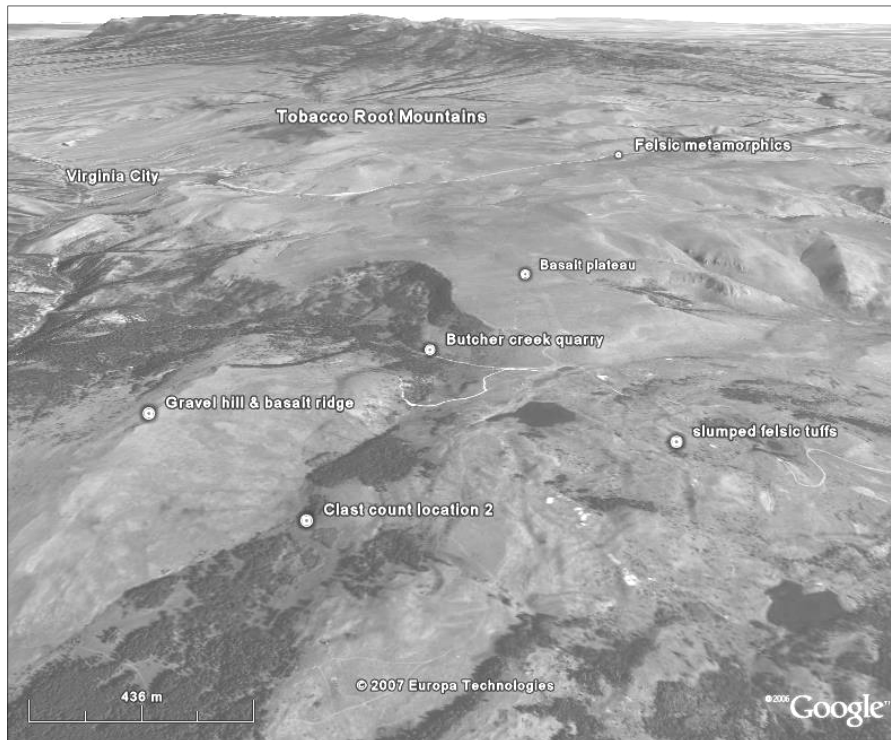


Figure 2. Image of Butcher Creek area looking north towards the Tobacco Root Mountains. Elongate hill of conglomerate capped by linear basalt flow is to left. Modern landslide deposits composed of Eocene felsic volcanic material surround topographic lows containing the Axolotl Lakes to right. Oligocene basalt flows overlie older sedimentary rocks and Archean metamorphics throughout most of this area. Archean felsic metamorphics are exposed in roadcuts underneath the basalt flows along the highway between Virginia City and Ennis. The area labeled 'felsic metamorphics' is approximate location of the sample collected for thin section analysis of probable source rocks for conglomerate and sandstone at quarry location. *Image courtesy of Google Earth™ & Google Inc.™.*

Creek conglomerate is hypothesized, based on stratigraphic and sedimentological considerations summarized below, to represent the base of the Paleogene section in the northern Gravelly Range.

Recent mapping of the Ennis 30'x 60' quadrangle by Kellogg and Williams (2006), lends independent confirmation to this hypothesis. Their map unit (*Tvs*) includes the area referred to here as the Butcher Creek conglomerate and is assigned an Eocene age at the base of the Virginia City volcanic field. Kellogg and Williams (2006), referring to the earlier mapping of Hadley (1969, 1980), describe the unit (*Tvs*) as primarily volcanoclastic in nature - a view incompatible with the homogeneous metamorphic lithologies observed in the Butcher Creek

quarry. It is proposed that the volcanoclastic lithologies described by Kellogg and Williams (2006) probably represent a later phase of basin development and should probably be referred to the lower felsic volcanic unit of the Virginia City volcanic field. The paucity of volcanic clasts in the Butcher Creek conglomerate implies that it predates any activity associated with the Virginia City volcanic field and should be considered as a separate unit within the Renova Formation.

## STRATIGRAPHIC POSITION AND AGE

The Virginia City volcanic field can be subdivided into two units, a lower felsic tuff unit and upper basalt flow unit. Radiometric (K-Ar) dating conducted by Marvin et al. (1974) indicates an Eocene age (51-45 Ma) for the felsic tuffs and a late Eocene/early Oligocene age (30-34 Ma) for the overlying basaltic volcanics. The Butcher Creek conglomerate clearly underlies the younger basalt flows, but its relationship to the older felsic tuffs is uncertain. The conspicuous lack of either basalt or definitive felsic volcanic clasts in samples collected from the conglomerate and in a thin section taken from the interlayered coarse sandstones at the quarry locality strongly suggests that the Butcher Creek conglomerate predates emplacement of the Virginia City volcanic field.

The fact that its clasts are almost entirely derived from Archean metamorphics suggests that the Butcher Creek conglomerate is probably not a Cretaceous synorogenic gravel. Thrust sheets of the Snowcrest /Greenhorn thrusts are

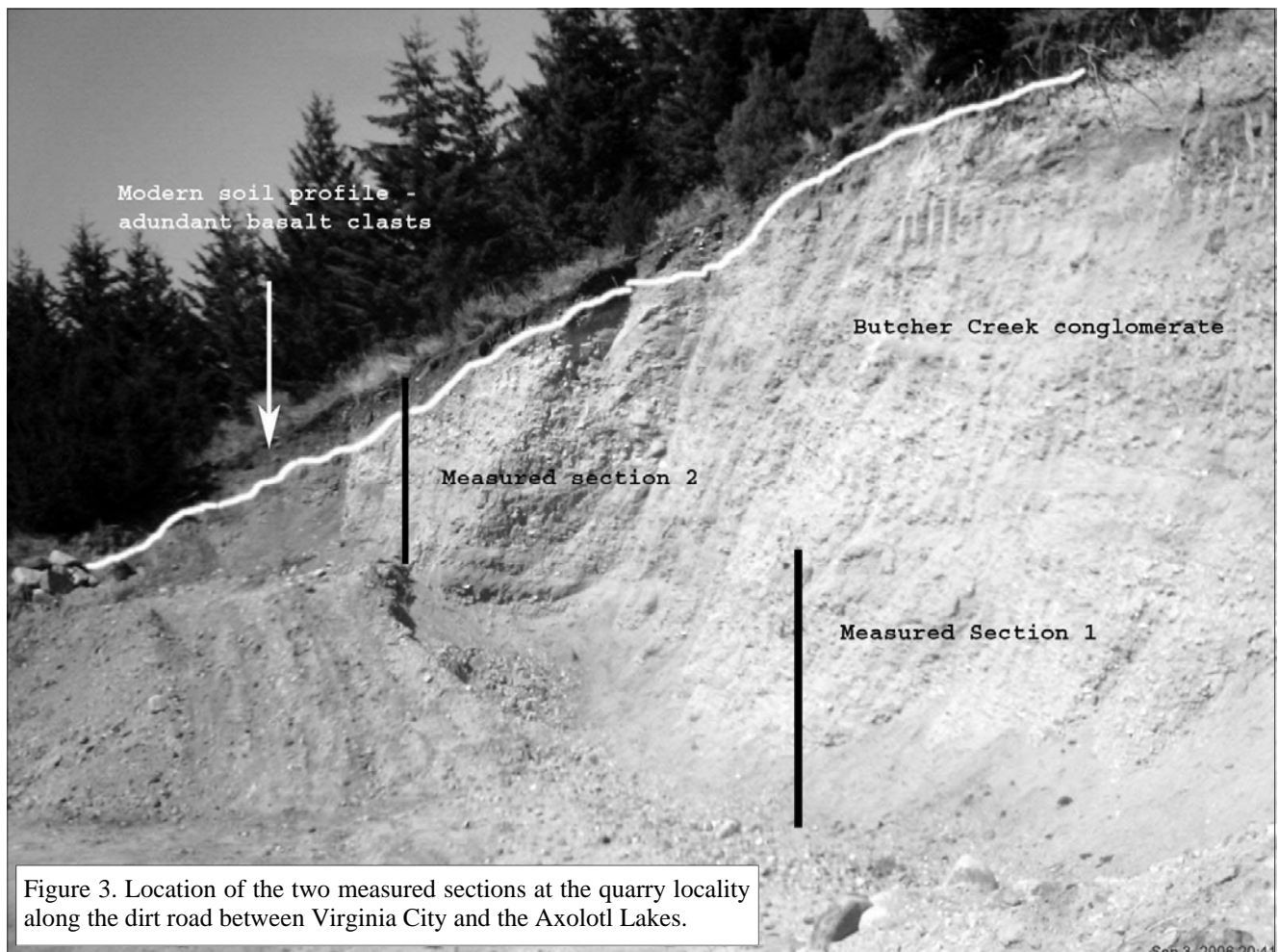
dominated by Paleozoic and Mesozoic lithologies, which are largely absent from the Butcher Creek deposits. Considering the amount of erosion that would have to occur before such a homogeneous metamorphic gravel could form, it seems unlikely that it could be contemporaneous with thrusting in the Snowcrest /Greenhorn fault system. Observed paleocurrent indicators suggest paleoflow was from the northeast, away from the location of Cretaceous thrust sheets. Furthermore, the trace of the Greenhorn Fault inferred by Kellogg and Williams (2006) would place most of the Butcher Creek conglomerate in the hanging-wall of the eroded thrust sheet rather than in the footwall where synorogenic gravel is most likely to form.

One additional feature relevant to the dating of the Butcher Creek conglomerate is the elongate ridge of basalt, which appears to directly overlie the conglomerate south of the quarry locality

without any intervening felsic volcanic material. This suggests the possibility of either an erosive episode between discrete felsic and mafic volcanic events or a more complicated history of bimodal volcanism than has been previously recognized in the Virginia City field. An absolute age for the Butcher Creek conglomerate cannot be confidently assigned until more precise biostratigraphic or radiometric age data becomes available. However, based on relative age criteria, it appears to be no younger than middle to late Eocene.

## SEDIMENTOLOGY

Figure 3 shows the location of two measured sections within the quarry locality. A schematically represented composite measured section is shown in Figure 4. The original sedimentary environment of the rocks exposed in the quarry walls is probably best interpreted as a high energy braided



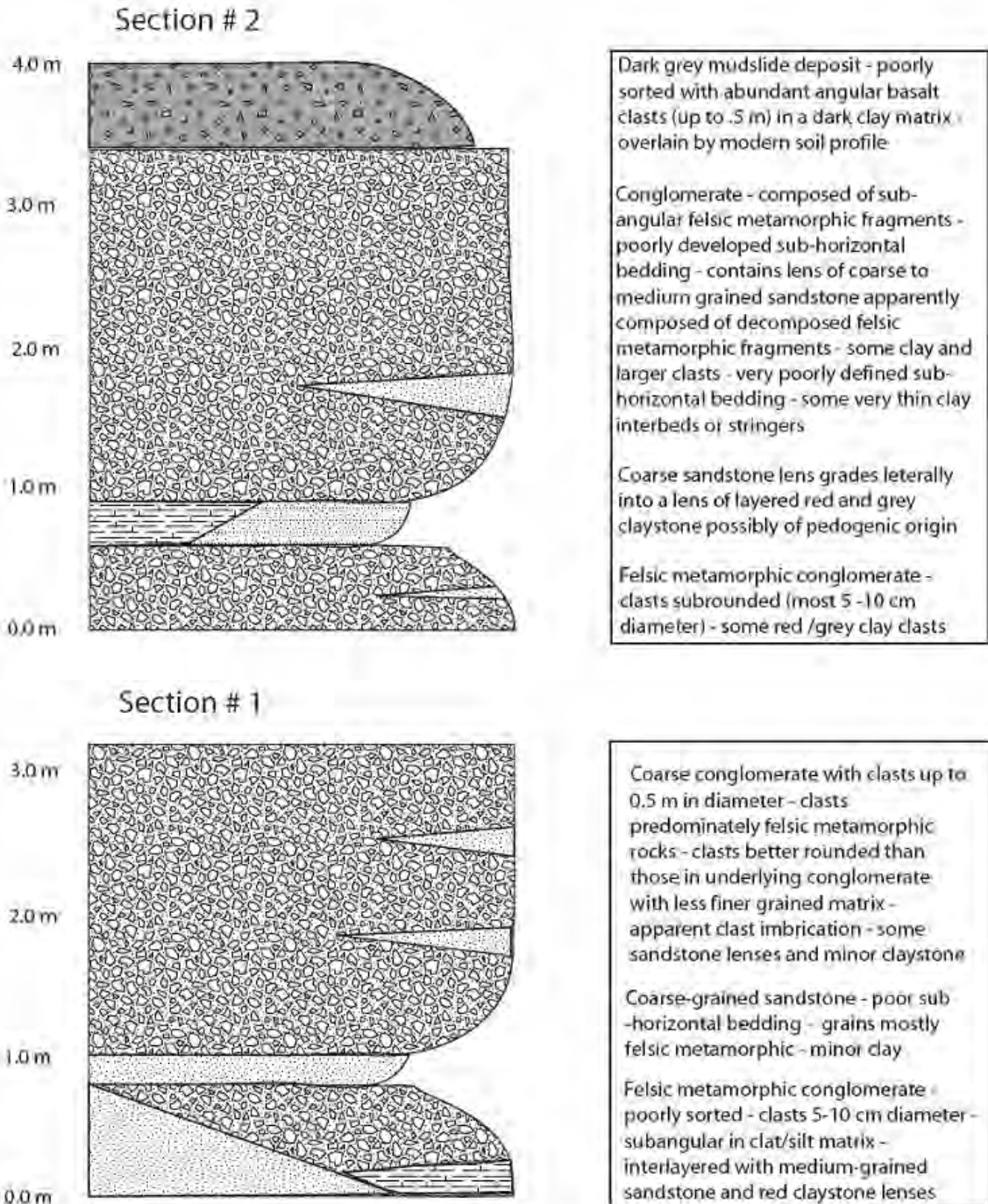


Figure 4. Composite measured section of Butcher Creek quarry locality showing sedimentary facies relationships.

stream or alluvial fan environment. This is suggested by the predominance of relatively large clasts, the crude layering and pebble imbrication, and the presence of both coarse-grained sandstone lenses and minor red and gray/green clay or silt layers (Figure 5). The largely clast-

supported conglomerate layers are moderately well sorted with a predominance of clasts in the 4-8 cm in diameter range. Some larger clasts are also present, especially in the more poorly organized, matrix-rich beds. These probably represent debris flow episodes superimposed on

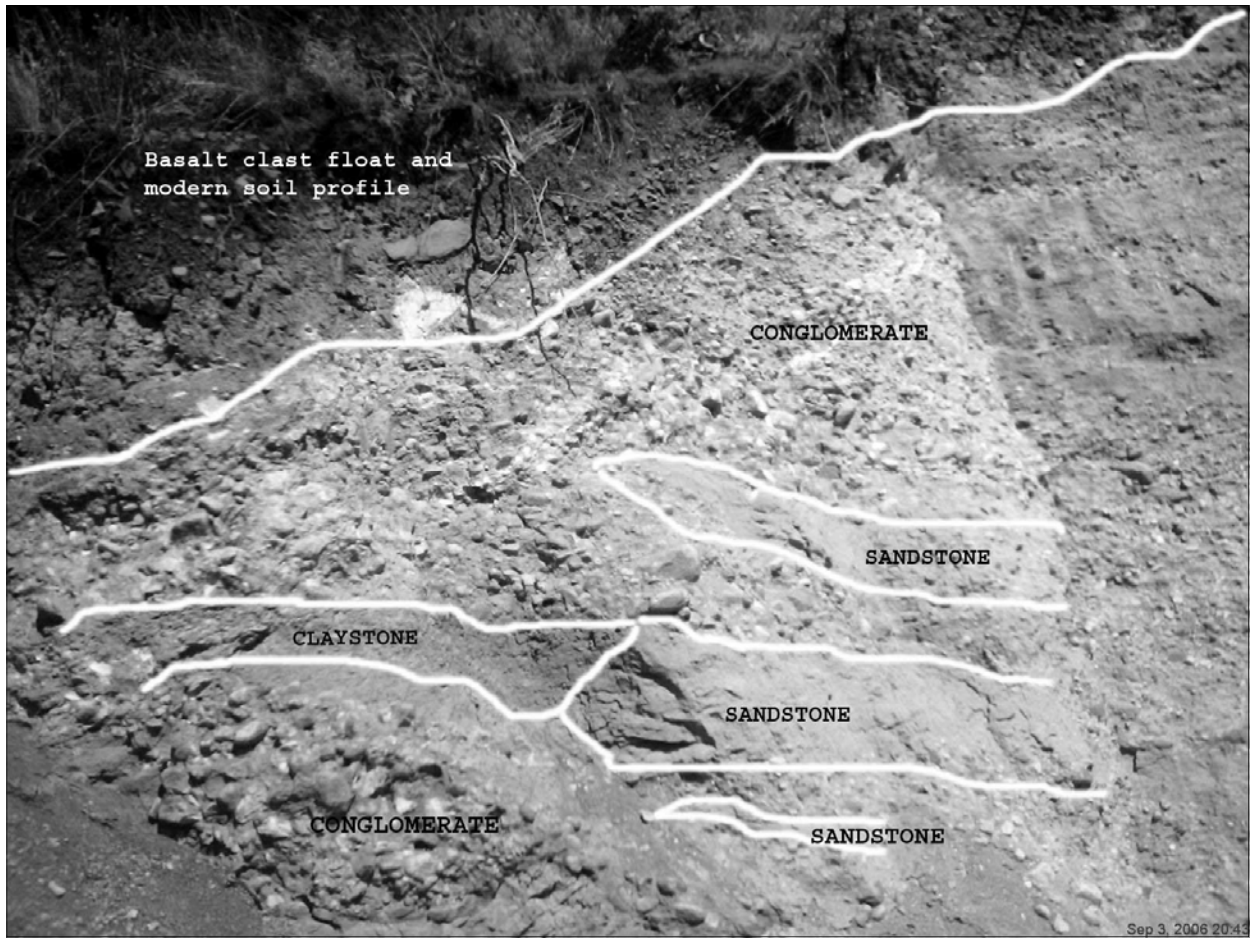


Figure 5. Measured section #2 in Butcher Creek quarry showing relationship of sedimentary facies. Note color difference between conglomerate composed of felsic metamorphic clasts and modern soil profile rich in basaltic material from overlying lava flows.

a dominantly braided stream deposit.

Individual clasts are subangular to subrounded and often highly weathered. Thin, discontinuous layers and individual clasts of reddish or gray/green siltstone and claystone, some with apparent root halos, are interpreted to be the remnants of weathering zones or incipient paleosol horizons probably representing overbank facies. One large (~1.0 m diameter) rounded boulder of reddish claystone was observed, suggesting that many of these fine-grained clasts formed in a stable, subaerial environment and were occasionally remobilized by high energy flows. Analysis of a thin section cut from this boulder shows isolated, weathered quartz grains, usually rimmed by iron oxide, surrounded by porous, amorphous clay and iron oxide minerals. These observations are consis-

tent with a paleosol formed in a warm, moist environment (FitzPatrick, 1984; Retallack, 1996, 2001). This sedimentary package is interpreted to represent deposition in a high-energy mountain stream or in the middle to distal portion of an alluvial fan environment. A local paleodrainage system serving as a watershed for the southern portion of an ancestral Tobacco Root uplift seems the most likely scenario.

### CLAST COUNTS AND PALEOCURRENT MEASUREMENTS

Samples were collected from two sites within the Butcher Creek conglomerate, at the quarry site and along the east bank of Butcher Creek itself (see Figure 2). Clasts at both localities are dominantly felsic metamorphic lithologies.



Figure 6. Imbrication of pebbles in conglomerate near measured section #1 in Butcher Creek quarry. View is towards the west-northwest. Note light-colored felsic metamorphic clasts and interbedded coarse grained sandstone.

Coarse-grained, poorly banded quartz-rich gneiss is the most common constituent. However, some gneiss clasts also contain abundant plagioclase, potassium feldspar, biotite, muscovite, amphiboles and red garnet. At the quarry locality, minor fine-grained quartzites and red to green/gray clay to siltstone clasts are also present. No unambiguous Paleozoic or Mesozoic sedimentary rocks, volcanic fragments or igneous lithologies were observed at the quarry locality. This clast composition is consistent with derivation from the metamorphic lithologies described by Vitaliano et al. (1979) in the southern Tobacco Root Mountains.

Conglomerate layers often show apparent imbrication of elongate clasts (Figure 6). These paleocurrent indicators suggest flow was from the northeast (~N60E), an area on the southern

flanks of the Tobacco Root Mountains characterized by Archean rocks usually overlain by basalt of the upper Virginia City volcanic field. Figure 1 shows the area of probable derivation for the clasts at the quarry locality based on clast lithologies and the measured paleocurrent direction. If derivation of this conglomerate predated the emplacement of the Virginia City volcanics, then a larger area of exposed Archean rocks could have supplied material to the quarry location.

Clast lithologies at the Butcher Creek locality about 0.5 km to the south are more varied but are still dominantly represent felsic metamorphic rock fragments (Figure 7). A more diverse suite of metamorphic lithologies is present, along with apparent fragments of Paleozoic rocks. In particular, several clasts of reddish

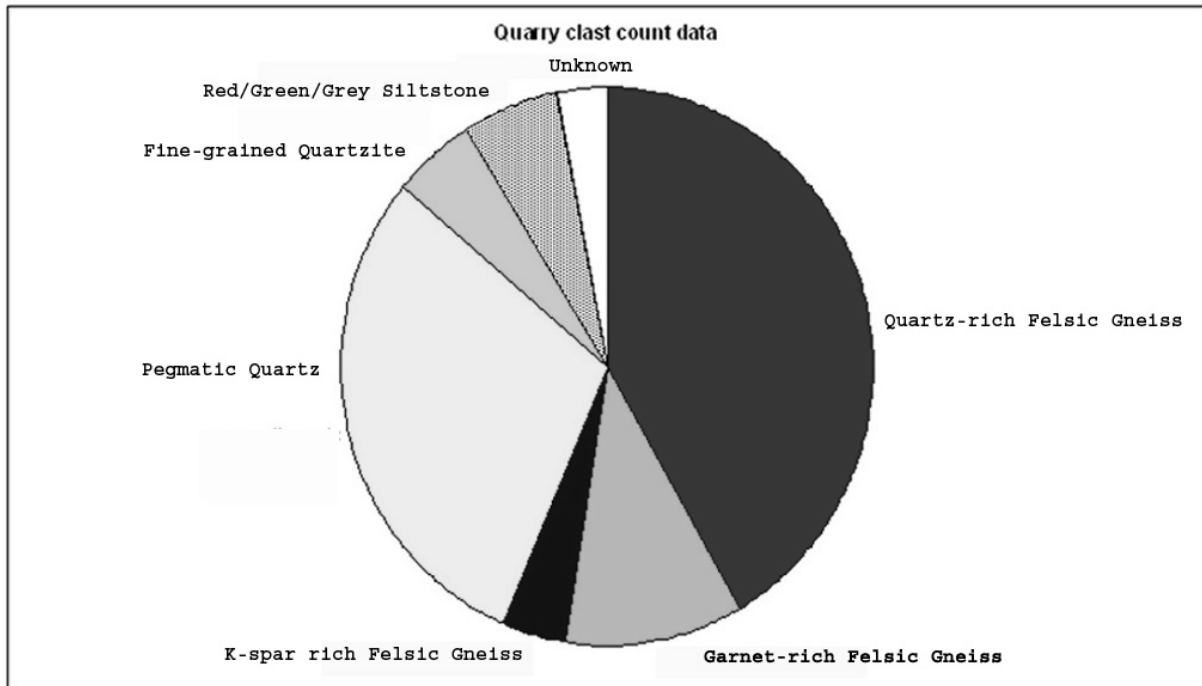
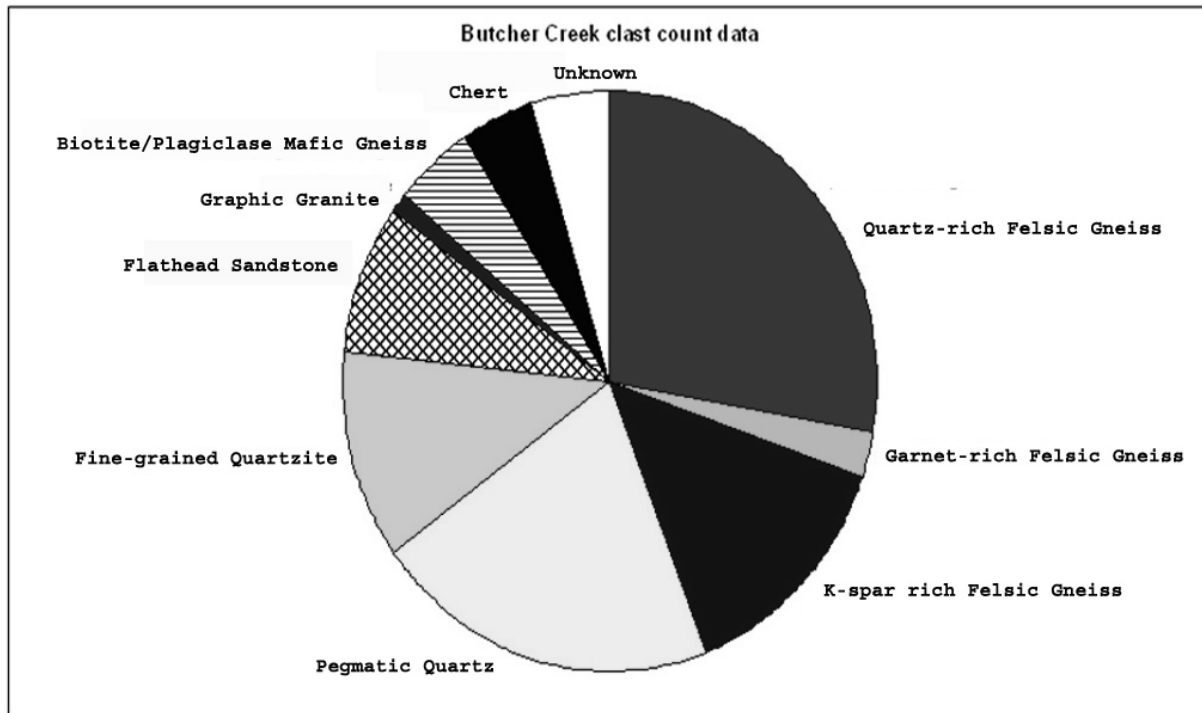


Figure 7. Comparison of clast compositions at quarry site and along the bank of Butcher Creek about 0.5 km to the south of the quarry. Note greater diversity of clast types at southern locality.



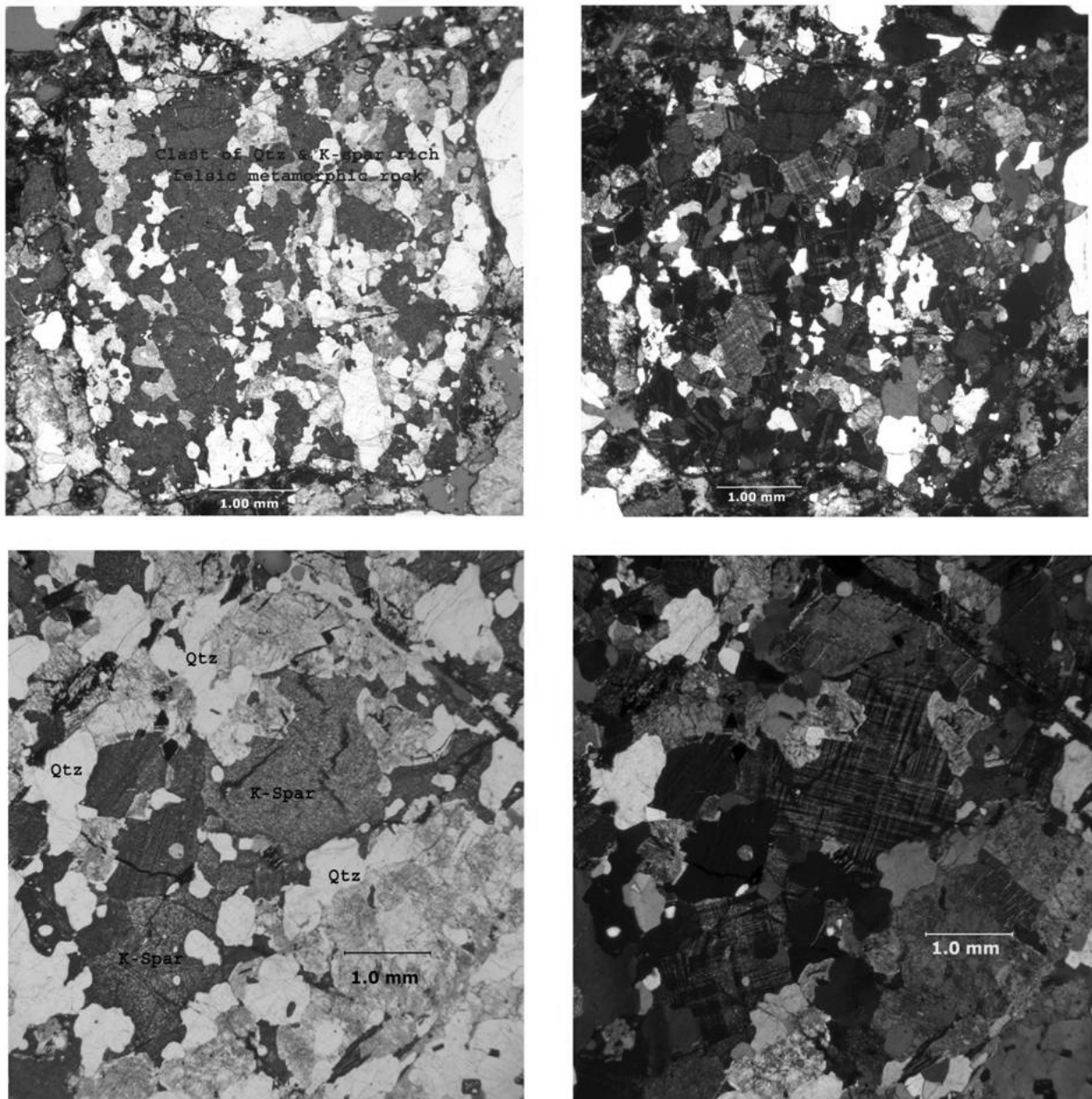


Figure 8. Comparison of thin sections taken from coarse sandstone deposit at quarry locality (top) and from probable source area located to the northeast (bottom). Plane light (left) and crossed polar (right) views are shown for both thin sections. Note the polycrystalline quartz grains showing undulose extinction and the 'tartan twinning' of microcline grains in both sections.

sandstone containing numerous rounded quartz pebbles correspond closely to the description given by Manske (1961) and Bubb (1961) for the lower portion of the Flathead Formation in the northern Gravelly and Greenhorn Ranges. Light colored chert may have ultimately been derived from silica replacement of carbonate in lower Paleozoic limestones. This greater diversity of clast types is interpreted to reflect deri-

vation from local tributaries of the main paleo-valley draining the southern Tobacco Root Mountains. Kellogg and Williams (2006) mapped several remnants of their unit (*Tvs*) south of the Butcher Creek locality (see Figure 1), an observation consistent with a Paleogene, north-south oriented paleo-valley crossing the area which was later uplifted to form the Gravelly Range. The presence of Oligocene age

rocks along the crest of the southern Gravelly Range (Luikart, 1997) provides corroborative evidence that this area was a depositional center, not a high elevation erosional source area, during Paleogene time.

### THIN SECTION ANALYSIS

A sample from one of the coarse-grained sandstone lenses interlayered with the conglomerates near measured section #1 was cut for thin section analysis. The results of this thin section analysis generally support the conclusions of the conglomerate clast count at the quarry location. Fragments composed of polycrystalline quartz and individual quartz and feldspar grains are the most common elements present and probably correspond to the quartz-rich felsic gneiss and quartzite clasts observed in hand samples. Grains composed of approximately equal amounts of quartz and microcline are also observed and probably correspond to the granitic gneiss specimens in the clast counts.

Under crossed polarizers, tartan twinning can be observed in the stained microcline grains along with undulose extinction of polycrystalline quartz grains and minor mica grains which show high interference colors (Figure 8). A groundmass of smaller quartz and feldspar fragments, along with abundant interstitial clay, is also present. Individual garnets and garnet-bearing clasts are conspicuously absent from this thin section and may reflect greater survivability of quartz and feldspar grains in the coarse-grained sandstone deposits. Overall, this mineral assemblage appears to be consistent with derivation from a high-grade, felsic metamorphic terrain such as that described by Vitaliano et al. (1979) for the southern Tobacco Root Mountains. This is corroborated by comparison with a thin section cut from a sample of felsic metamorphic rock obtained from a road cut several kilometers to the northeast of the quarry locality. Polycrystalline quartz and microcline showing distinct tartan twinning, virtually indistinguishable from that observed in the quarry thin section (see Figure 8), strongly suggests that these felsic metamorphic rocks were the primary source locality for the

conglomerate and sandstone clasts in the quarry.

### SUMMARY

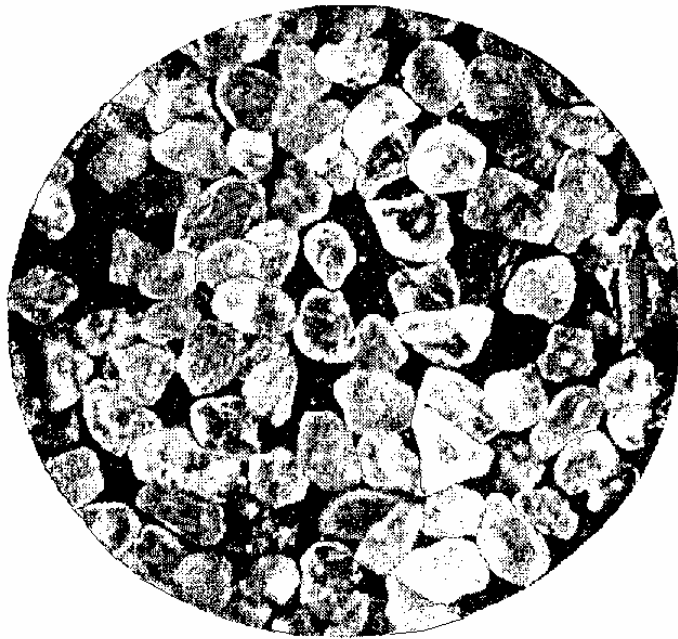
In conclusion, it seems likely that the proposed Butcher Creek member of the Renova Formation represents erosion of the metamorphic rocks of an ancestral Tobacco Root uplift and their subsequent deposition in a north-south trending paleodrainage basin. The portion of the paleovalley exposed in the Butcher Creek quarry locality probably represents deposition relatively near to the source, either in a high-energy mountain stream environment or a braided stream dominated alluvial fan environment. Debris flow deposition probably played an important subsidiary role in the development of the Butcher Creek conglomerate. Whether this ancestral Tobacco Root uplift was active during Paleogene time or represented paleotopography inherited from the Cretaceous orogeny is still an unsettled question.

This gravel may be a southern analog of the basin margin breccias and conglomerates described by Elliott (1998, 2003) within the Oligocene Dunbar Creek Member of the Renova Formation in the Harrison Basin to the north of the Tobacco Root Mountains. As described by Elliott et al. (2003), these basal Paleogene deposits record the initial denudation of the Laramide Tobacco Root Mountains with paleoflow indicators and clast provenance data indicating flow away from the Tobacco Root uplift towards the north. I suggest that the Butcher Creek gravel is a similar paleovalley deposit recording flow off of the southern flank of the same Tobacco Root uplift. The apparent Eocene age of the Butcher Creek deposits implies that they are not precisely time equivalent to the deposits in the Harrison Basin; however, a similar mechanism operating on the flanks of a long-lived topographic high could produce similar deposits over a considerable span of time. The presence of an elongate ridge of basalt along the crest of the hill, which comprises the bulk of the Butcher Creek conglomerate, suggests that the paleovalley possibly continued to exist as a discrete feature at least into

early/middle Oligocene time. However, this feature could simply be an erosional remnant of the larger basalt plateau. Further research will be necessary to determine the answer to this question.

## REFERENCES

- Bubb, J., 1961, Geology of part of the Greenhorn Range and vicinity, Madison county, Montana: M.S. thesis, Oregon State College, 165 p.
- Chamberlain, P., and Poage, M., 2000, Reconstructing the paleotopography of mountain belts from the isotopic composition of authigenic minerals: *Geology*, v. 28, no. 2, p. 115-118.
- Elliott, W., 1998, Tectono-stratigraphic control of Quaternary and Paleogene sediments and structure along the northeast flank of the Tobacco Root mountains, Madison county, Montana: M.S. thesis, Indiana University, 121 p.
- Elliott, W., Douglas, B., and Suttner, L., 2003, Structural control on Quaternary and Paleogene sedimentation in the Harrison basin, Madison county, Montana: *The Mountain Geologist*, v. 40, no. 1, p. 1-18.
- FitzPatrick, E., 1984, *Micromorphology of Soils*: Chapman and Hall, 433 p.
- Hadley, J., 1969, Geologic Map of the Varney quadrangle, Madison county, Montana: United States Geological Survey Map GQ-814.
- Hadley, J., 1980, Geology of the Varney and Cameron Quadrangles, Madison County, Montana: United States Geological Survey Bulletin 1459, 108 p.
- Kellogg, K., and Williams, V., 2006, Geologic map of the Ennis 30' x 60' quadrangle, Madison and Gallatin Counties, Montana, and Park County, Wyoming: Montana Bureau of Mines and Geology Open File Report 529.
- Luikart, E.J., 1997, Syn- and post-Laramide geology of the south-central Gravelly Range, southwestern Montana: M.S. thesis, Bozeman, Montana, Montana State University, 96 p.
- Manske, D., 1961, Geology of the Baldy mountain area, Madison county, Montana: M.S. thesis, Oregon State College, 75 p.
- Marvin, R., Weir, K., Mehnert, H., and Merritt, V., 1974, K-Ar ages of selected Paleogene igneous rocks in southwestern Montana: *Isochron West*, no. 10, p. 17-20.
- Mulch, A., Graham, S., and Chamberlain, P., 2006, Hydrogen isotopes in Eocene river gravels and paleoelevation of the Sierra Nevada: *Science*, v. 313, p. 87-89.
- Retallack, G., 1996, *A Colour Guide to Paleosols*: John Wiley and Sons, 175 p.
- Retallack, G., 2001, *Soils of the Past: an Introduction to Paleopedology*: Blackwell Scientific, 404 p.
- Vitaliano, C., Cordua, W., Burger, H., Hanley, T., Hess, D., and Root, F., 1979, Geology and structure of the southern part of the Tobacco Root Mountains, southwestern Montana: map summary: *Geological Society of America Bulletin*, v. 90, p. 712-715.
- Vitaliano, C., Burger, H., Cordua, W., Hanley, T., Hess, D., and Root, F., 1979 (2004 reprint), Explanatory text to accompany geologic map of the southern Tobacco Root Mountains, Madison County, Montana: *in* Precambrian geology of the Tobacco Root mountains, Montana: Geological Society of America Special Paper 377, p. 247-256.
- Vitaliano, C., Burger, H., Cordua, W., Hanley, T., Hess, D., and Root, F., 1979 (2004 reprint), Geologic map of the southern Tobacco Root Mountains, Madison County, Montana: *in* Precambrian geology of the Tobacco Root mountains, Montana: Geological Society of America Special Paper 377.



# NANODIAMONDS AT THE INDIAN CREEK ARCHEOLOGICAL SITE NEAR TOWNSEND, MONTANA: EVIDENCE OF AN EXTRA-TERRESTRIAL IMPACT EVENT

**David W. Baker**

*Little Belt Consulting Services, Monarch, MT 59463*

**Katelyn E. Gibbs**

*Great Falls High School, Great Falls, MT 59401*

**Allen West**

*GeoScience Consulting, Dewey, AZ 86327*

---

## INTRODUCTION

Firestone et al. (2007) presented exhaustive evidence for an extra-terrestrial impact event in North America about 12,900 calendar years ago that led to the extinction of mammoths and other large ice age mammals. However, in an opinion article Kerr (2008) claimed that definitive proof for this event has not been found, in part, because the presence of nanodiamonds was not proven. This study presents conclusive evidence for nanodiamonds at the Indian Creek Archeological Site west of Townsend, Montana.

## INDIAN CREEK SITE

The Indian Creek Site, located about 10 km west of Townsend, Montana, (Figure 1) is a well-studied archeological site (Davis and Greiser, 1992; Davis and Baumler, 2000) in Quaternary alluvium (Reynolds and Brandt, 2006). Two volcanic ash layers occur here, Mt. Mazama ash layer (6900 C<sup>14</sup> years before present) and the Glacier Peak ash layer (11,200 C<sup>14</sup> years). These volcanic ash beds serve as geological time markers. The beds of interest for the extra-terrestrial impact event are immediately below the Glacier Peak ash layer (Baker et al. 2008; Gibbs, 2008). Davis and Greiser (1992) found a thick organic-rich layer—a black mat—below the Glacier Peak ash layer. Although the Glacier Peak ash layer was exposed at the base of the archeological excavation in the 1980s, it is currently buried.

We sampled a site approximately 600 meters downstream from the lower archeological excavation where the Glacier Peak Volcanic Ash is currently well exposed (Figure 2). As shown in Figure 2, the Glacier Peak Ash is in a stratigraphic sequence of alluvial deposits—high-energy and lower-energy flood deposits. Some clasts are 10 cm in diameter. The ash layer contains abundant clasts approximately 2 cm in diameter. The volcanic ash is gray in color and is interpreted as ash deposited on mountain slopes upstream and then flushed down stream by a heavy rainstorm and redeposited. Figure 2 shows the gamma ray profile in this section. The maximum gamma ray intensity of 13 counts per second occurs at Point 7 in Figure 2, which is 20 cm below the ash layer. The ash layer is a minimum in the gamma ray profile (Point 8).

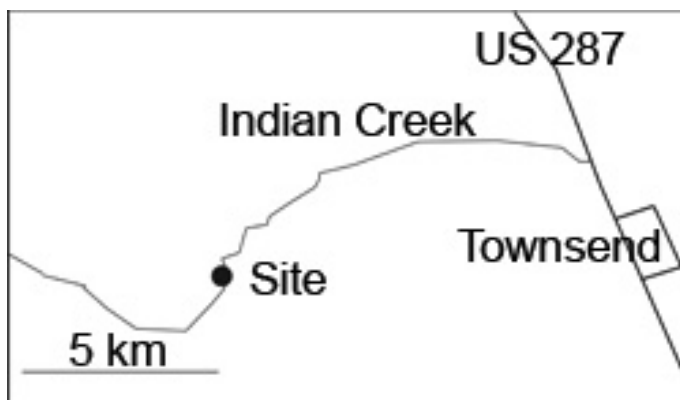


Figure 1. Location map for the Indian Creek Site west of Townsend, Montana.



Figure 2. Outcrop of alluvial beds in Indian Creek that contain the Glacier Peak Volcanic Ash. Gibbs is pointing trowel at a clast in the ash layer. Straight line 1-5 shows location of samples and readings with scintillation counter and is also base line for profiles. Profile of concentration of glass spherules (2, 3 4) has no spherules at Point 2, 360 spherules per kg at Point 3, and a maximum of more than 8,200 spherules per kg in the volcanic ash layer (Point 4). Gamma ray profile (6, 7, 8, 9) has a maximum of 13 counts per second above background at Point 7 and a minimum of 1 cps in the ash layer at Point 8.

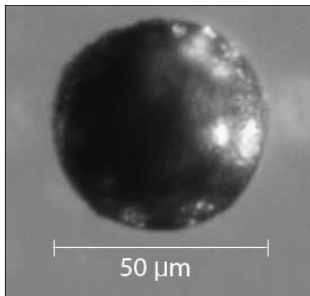


Figure 3. Carbon glass spherules are approximately 50 microns in diameter.

Figure 2 also shows the profile concentration of carbon glass spherules. These spherules (Figure 3) are hollow; they float on water; and the outer shell is full of gas bubbles. Under crossed polarizers in the petrographic microscope, the spherules are isotropic and thus are glass. The maximum concentration of these spherules is found in the volcanic ash layer (Point 4 in Figure 2).

At sites on the Rocky Mountain Front and east of Choteau we found that the maximum radioactivity is below the Glacier Peak Ash and is due to uranium and thorium contained in a phosphate mineral, which acts as a heavy mineral. We suggest that the radioactive particles are heavy minerals at the Indian Creek Site. If

our hypothesis is valid, then we can explain the different stratigraphic levels for the maxima in Figure 2 in terms of the velocity of floodwaters during deposition. Heavy radioactive particles were deposited during a high-energy event and the very light glass spherules and volcanic ash were deposited under a much lower energy flood. As shown in Figure 2 the first occurrence of carbon spherules in the section is between Point 2 and Point 3 approximately 36 cm below the ash layer.

## NANODIAMONDS

Carbon glass spherules were hand picked using the binocular microscope. The spherules were crushed and prepared for the transmission electron microscope (TEM) using the same techniques that were used by West and Goodyear (2008). The TEM photographs were taken at Northern Arizona University. Nanodiamonds 5 to 10 nanometers in diameter are clearly imaged with the TEM (Figure 4). The diffraction pattern (Figure 5) uniquely identifies the mineral as diamond.

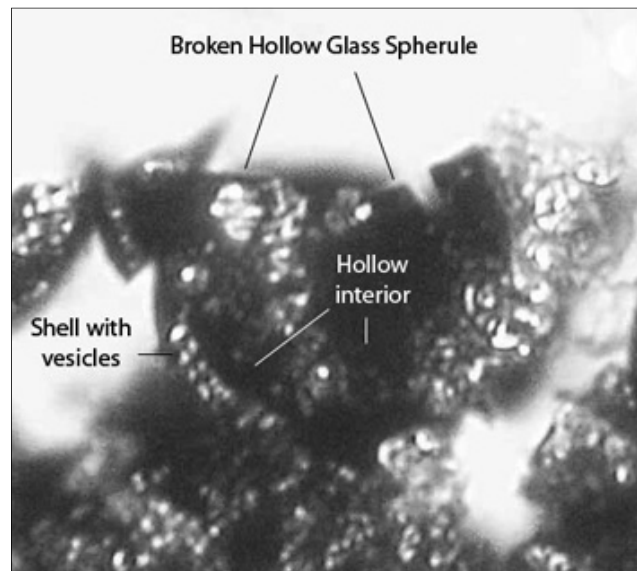


Figure 4. Internal structure of carbon glass spherule: hollow inside with an outer shell containing abundant gas bubbles.

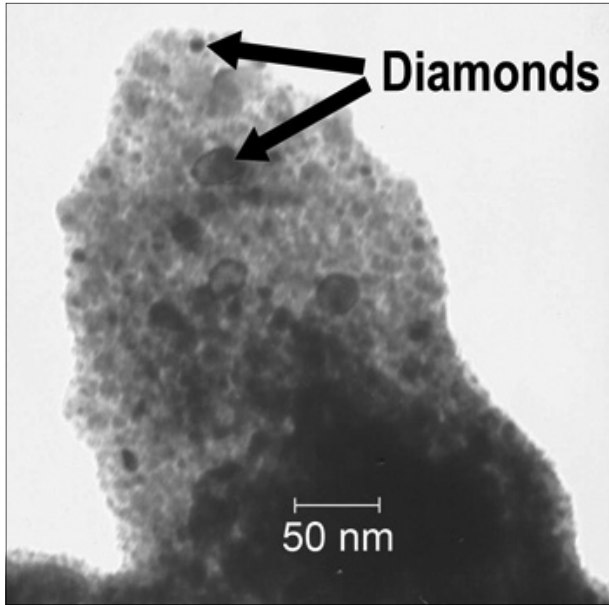


Figure 5. Nanodiamonds as seen with a transmission electron microscope (TEM) are approximately 5 to 10 nanometers (millionths of a meter) in diameter.

## INTERPRETATION

Nanodiamonds are formed commercially using a carbon-rich source such as coal or tar and high explosives and thus can be used to infer the impact of an extra-terrestrial body and a high carbon terrestrial material. On the other hand nanodiamonds are also found in carbonaceous chondrite meteorites and in interstellar dust. In either case the presence of nanodiamonds indicate an origin related to objects from outer space impacting the Earth. It is possible to distinguish between two origins using  $C^{12}/C^{13}$  isotope ratio. A ratio of 42:1 indicates a terrestrial origin for the carbon and ratio 90:1 indicates a extra-terrestrial origin (Carlisle, 1995). However this test has not been run.

## CONCLUSIONS

The presence of nanodiamonds in carbon glass spherules below the Glacier Peak Ash layer at Indian Creek is direct evidence of an extra-terrestrial impact event (West and Goodyear, 2008; Firestone et al., 2006). Our studies of the Indian Creek site, the site at the New Rockport Colony east of Choteau and of sites on the Rocky

Mountain Front all indicate that the impact event occurred stratigraphically below Glacier Peak Volcanic Ash.

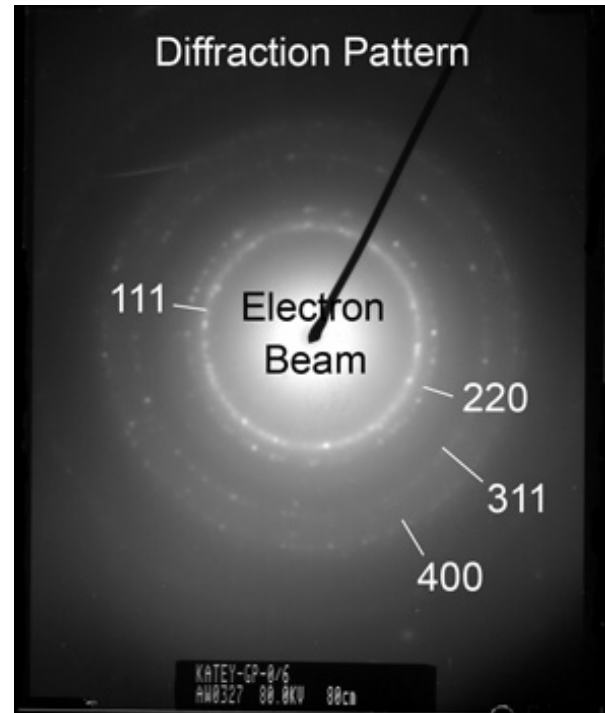


Figure 6. Diffraction pattern for nanodiamonds shows strong peaks for 111, 200, 311, and 400.

## REFERENCES

- Baker, D.W, 2008, Extra-terrestrial impact event about 11,500 years  $C^{14}$  before present--stratigraphic and archeological context of Montana evidence: Montana Archeological Society Annual Meeting, Abstracts with Programs.
- Carlisle, D.B., 1995, Dinosaurs, diamonds, and things from outer space: The great extinction: Stanford University Press, Stanford, Calif., 241 p.
- Davis, L.B., and Baumler, M.F., 2000, Clovis and Folsom occupations at Indian Creek: Current Research in Pleistocene, v. 17, p.17-19.
- Davis, L.B., and Greiser, S.T., 1992, Indian Creek paleoindians: early occupation of the Elkhorn Mountains' southeast flank, west-central Montana: *in* Stanford, D.J., and Day, J.S., eds., Ice Age Hunters of the

Rockies: Denver Museum of Natural History and University Press of Colorado, p.225-283.

Firestone, R.B., West, A., Kennett, J.P., Becker, L., Bunch, T.E., Revay, Z.S., Schultz, P.H., Belgya, T., Kennett, D.J., Erlandson, J.M., Dickenson, O.J., Goodyear, A.C., Harris, R.S., Howard, G.A., Kloosterman, J.B., Lechler, P., Mayewski, P.A., Montgomery, J., Poreda, R., Darrah, T., Que Hee, S.S., Smith, A.R., Stich, A., Topping, W., Wittke, J.H., and Wolbach, W.S., 2007, Evidence for an extraterrestrial impact 12,900 years ago that contributed to the megafaunal extinctions and the Younger Dryas cooling: Proceedings of the National Academy of Sciences, v. 104, p. 16016-16021.

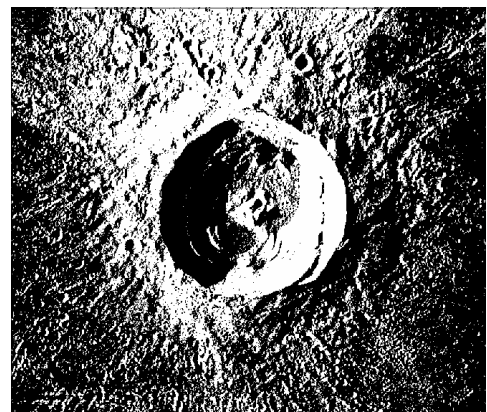
Firestone, R., West, A., and Warwick-Smith, S., 2006, The cycle of cosmic catastrophes: Bear & Co., Rochester, Vermont, 392 p.

Kerr, R.A., 2008, Experts find no evidence for a mammoth-killer impact: Science, v. 319, p. 1331-1332.

Gibbs, K.E., 2008, Direct evidence for extraterrestrial impact event at about 11,500 years C<sup>14</sup> before present: Montana Archeological Society Annual Meeting, Abstracts with Programs.

Reynolds, M.W., and Brandt, T.R., 2006, Preliminary Geological Map of the Townsend 30'x60' Quadrangle, Montana: U.S. Geological Survey, Open-File Report 2006-1138.

West, A., and Goodyear, A., 2008, The Clovis comet: Part I: Evidence for a comet collision 12,900 years ago: Mammoth Trumpet, v. 23, p. 1-4.



# UTILIZING U-PB GEOCHRONOLOGY OF INHERITED ZIRCON IN THE ATLANTA LOBE OF THE IDAHO BATHOLITH AS A PROBE OF THE DEEP CRUST IN SOUTHERN IDAHO: A PROGRESS REPORT

**Rich Gaschnig, Jeff Vervoort**

*School of Earth and Environmental Sciences, Washington State University, Pullman, WA 99164*

**Reed S. Lewis**

*Idaho Geological Survey, University of Idaho, Moscow, ID 83844*

**Andy Dufrane**

*School of Earth and Environmental Sciences, Washington State University, Pullman, WA 99164*

---

## Introduction

Granites have long been used as tools for “imaging” levels of the crust not exposed at the surface (Chappell, 1979) and have provided important and otherwise inaccessible information about the terranes that they intrude (e.g., Farmer and DePaolo, 1983; Bennett and DePaolo, 1987). However, the use of whole-rock radiogenic isotopic data from granites to determine the ages of their host terranes is often complicated by the fact that many granites represent mixtures of multiple components with differing histories (e.g., Collins, 1996) and the fact that some anatectic granites may not have isotopically equilibrated with their sources (Ayres and Harris, 1997; Davies and Tommasini, 2000). Both of these caveats can potentially render whole-rock model ages spurious (Arndt and Goldstein, 1987; Mueller et al., 1996).

Another approach to identifying the sources of granitic magmatism and understanding the nature of the host terranes of granitic plutons is to use resilient inherited minerals, such as zircon. Whereas whole-rock analysis only provides information about the final product of processes such as magma mixing and assimilation, inherited minerals such as zircon can see through these complex processes and provide age and geochemical information about the individual ingredients (e.g., Miller et al., 1992; Keay et al.,

1999). In this contribution, we present preliminary results of the application of this methodology to the Atlanta lobe of the Idaho batholith, which intrudes a complex collage of Precambrian terranes. The pervasive nature of zircon inheritance in the Idaho batholith (e.g., Bickford et al., 1981; Shuster and Bickford, 1985; Toth and Stacey, 1992; Foster and Fanning, 1997; Foster et al., 2001) makes the geochronology of inherited zircon especially useful for identifying and delineating the boundaries of basement terranes, and this may ultimately provide important new constraints for reconstructions of the supercontinent Rodinia and the earlier assembly of Laurentia.

## Geologic Setting

The Idaho batholith was constructed during Late Cretaceous and Paleocene time near the western margin of Laurentia at the junction of several major Precambrian terranes (e.g., Armstrong et al., 1977; Lewis et al., 1987; Toth and Stacey, 1992; Foster and Fanning, 1997) (Figure 1). To the east, the Archean Wyoming Province encompasses most of the state of Wyoming and contains rocks as old as 3.5 Ga (Mueller and Frost, 2006). This is separated from the Medicine Hat block, another poorly understood Archean terrane to the north, by the Great Falls tectonic zone, a Paleoproterozoic suture which experienced magmatism and metamorphism from 1.86 Ga to 1.77 Ga

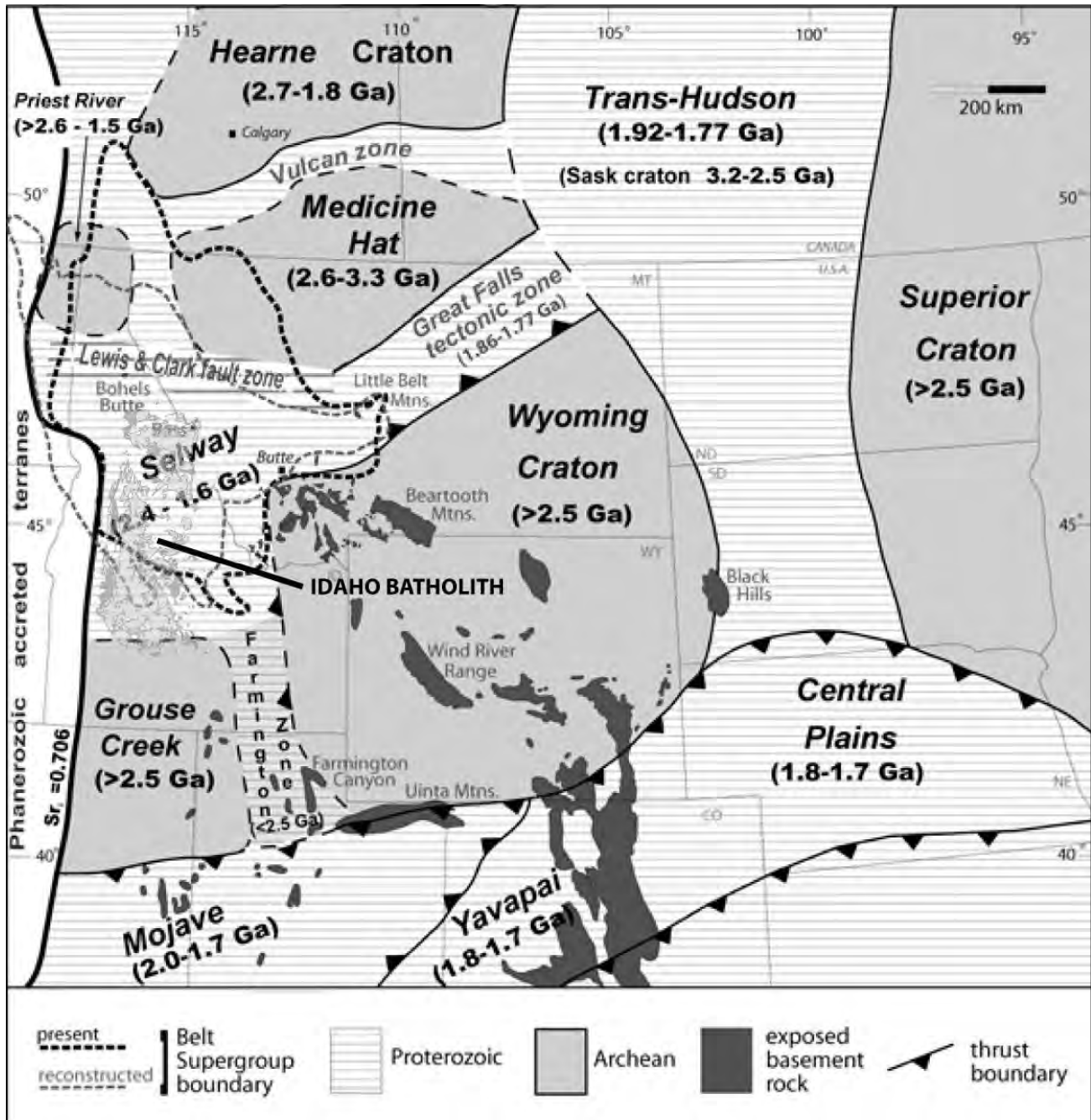


Figure 1. Major Precambrian terranes in the northern U.S. Rockies, with the Idaho batholith shown. Modified from Foster et al. (2006).

(Mueller et al., 2002; Ross, 2002; Cheney et al., 2004). The Great Falls tectonic zone trends southwest across Montana and appears to project under the Bitterroot lobe, the northern half of the Idaho batholith. However, the presence of ages from 2.4 to 1.6 Ga for igneous and metamorphic basement rocks exposed immediately east of the Bitterroot lobe and inherited zircons and model ages from the Bitterroot lobe itself and its eastern satellites prompted Foster et al. (2006) to designate this area as the Selway terrane, which they projected to the southern edge of the Atlanta lobe of the Idaho batholith. The Archean Grouse Creek block is located to the south of the Idaho batholith and the proposed Selway terrane. Lower crustal xenoliths found in Tertiary lavas of the Snake River Plain sample basement of the Grouse Creek block (Leeman et al., 1985; Wolf et al., 2005), which is also exposed at the surface in mountain ranges along the Idaho-Utah border (Wright and Snoke, 1993; Egger et al., 2003).

The Grouse Creek block has an uncertain relationship with the Wyoming Province to the east and is separated from it by the Farmington Canyon complex, a north-trending package of Archean and Paleoproterozoic metasedimentary rocks (Foster et al., 2006).

Major Precambrian events that followed the amalgamation of these terranes were the formation of the Belt basin and its thick sequence of sediments in northern Idaho and Montana and southern British Columbia during the Mesoproterozoic (Evans et al., 2000) and the breakup of Rodinia during the Neoproterozoic, in which a western continental mass rifted away from Laurentia establishing a passive margin (e.g., Ross, 1991). The Windermere Supergroup marks the early stages of this rifting, but there are only a few exposures of it recognized in Idaho (Lund et al., 2003; Fanning and Link, 2004).

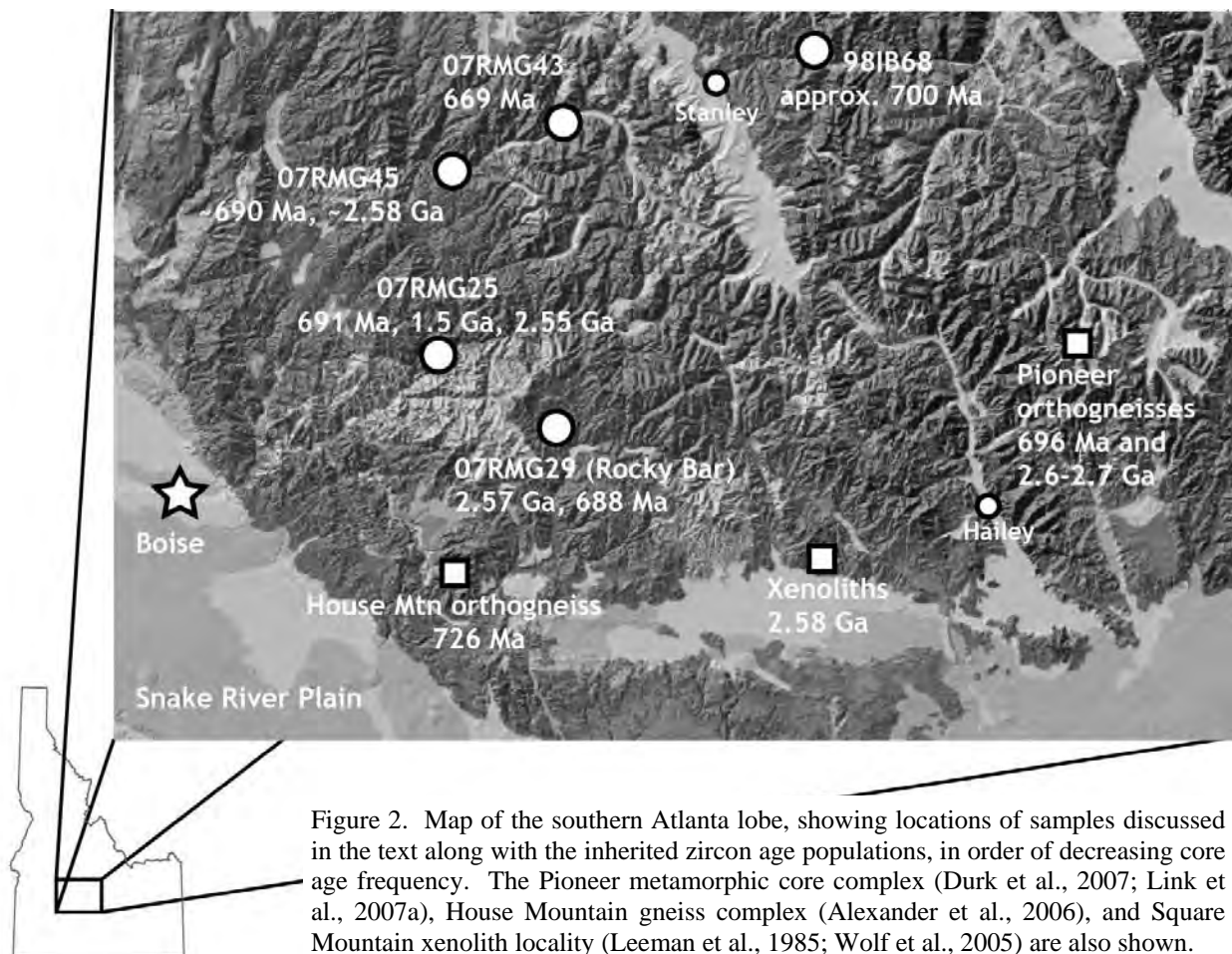


Figure 2. Map of the southern Atlanta lobe, showing locations of samples discussed in the text along with the inherited zircon age populations, in order of decreasing core age frequency. The Pioneer metamorphic core complex (Durk et al., 2007; Link et al., 2007a), House Mountain gneiss complex (Alexander et al., 2006), and Square Mountain xenolith locality (Leeman et al., 1985; Wolf et al., 2005) are also shown.

Recent work in the Pioneer metamorphic core complex and House Mountain gneiss complex in southern Idaho has provided new and important insights into the age and structure of the basement in this part of the state (Figure 2), which are relevant to our work. U-Pb geochronology presented by Link et al. (2007a) and Durk et al. (2007) for the Pioneer metamorphic core complex establish an Archean (2600-2700 Ma) age for a felsic orthogneiss, which is structurally overlain by a series of paragneisses containing detrital zircon age spectra similar to the Belt Supergroup, although the uppermost paragneiss contains isolated Neoproterozoic grains. They also presented a date of 695.6 +/- 9.0 for another felsic orthogneiss, which intrudes the paragneisses. Metamorphic rocks exposed around House Mountain were dated by Alexander et al. (2006) (see also Alexander, 2007), who reported a U-Pb zircon upper intercept age of 726 +/- 5 Ma for a felsic orthogneiss. Detrital zircons from a structurally overlying paragneiss suite were also dated and interpreted to indicate a Neoproterozoic depositional age for the protoliths and possible correlation with the Windermere Supergroup rocks exposed in central Idaho (Lund et al., 2003). We suggest on the basis of the data presented below that the magmas of the Atlanta lobe sampled rocks at depth at depth that are analogous to those exposed in the Pioneer metamorphic core complex and House Mountain gneiss complex.

## Results

Zircons were analyzed in situ using laser ablation-inductively coupled plasma-mass spectrometry (LA-ICP-MS) U-Pb geochronology, following the methods outlined by Chang et al. (2006). Many of the zircons from the Idaho batholith that we have studied contain inherited cores that are only slightly older (< 20 million years) than their magmatic rims, an observation also made by Foster and Fanning (1997) and Foster et al. (2001). Below, we present only data for the Precambrian cores since only these have the potential to provide insight on the *pre-magmatic* deep crustal configuration.

The southernmost sample (07RMG29) containing zircon with inheritance was collected from a biotite granodiorite outside of the ghost town of Rocky Bar (Lat. 43.6840, Lon. -115.2790). Fifteen of the cores analyzed yield late Archean ages, and with the exception of two outliers, they generally cluster around 2570 Ma and define a chord with an upper intercept of 2567 +/- 11 Ma (Figure 3). In addition, we identified five Neoproterozoic cores, four of which overlap and yield a concordia age of 688 +/- 11 Ma.

Sample 07RMG25 was collected from a biotite granodiorite along the Middle Fork of the Boise

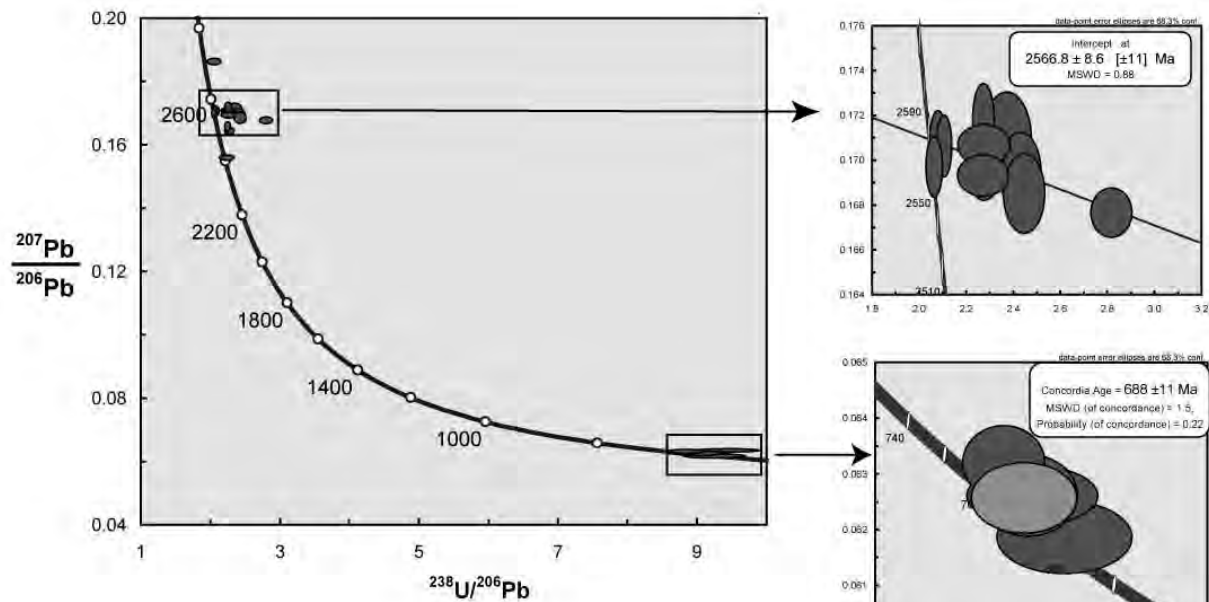


Figure 3. Tera-Wasserburg plot showing U-Pb data for inherited zircon cores from sample 07RMG29. Insets on the right show close-ups of the Archean populations along with the upper intercept age and Neoproterozoic populations with the concordia age.

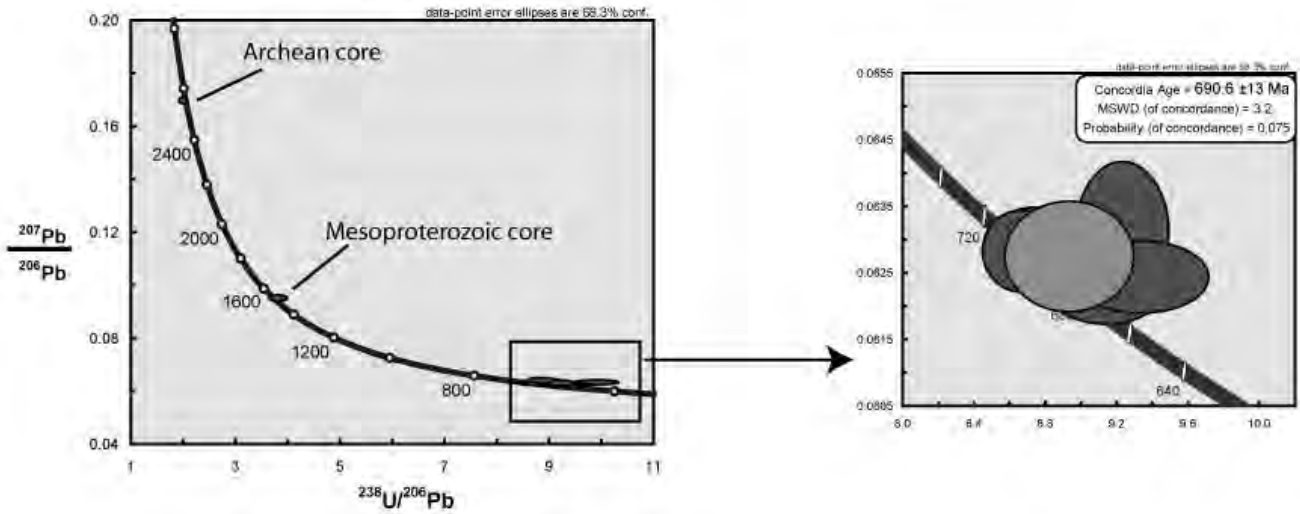


Figure 4. Tera-Wasserburg plot showing U-Pb data for inherited zircon cores from sample 07RMG25. Inset shows Neoproterozoic population with the concordia age.

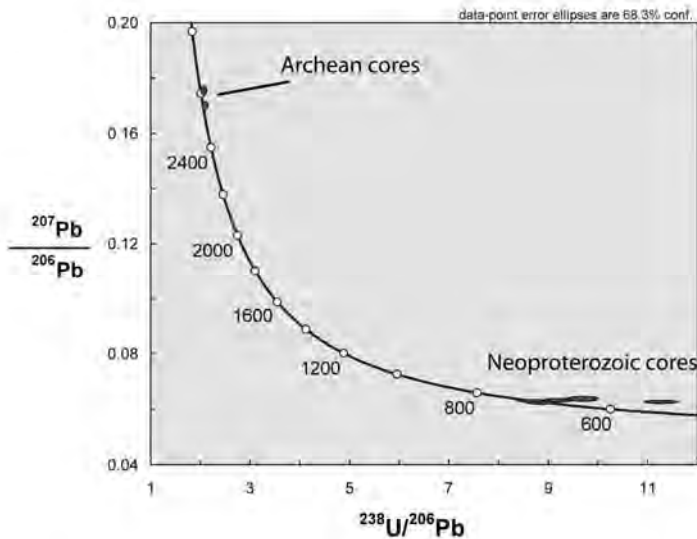
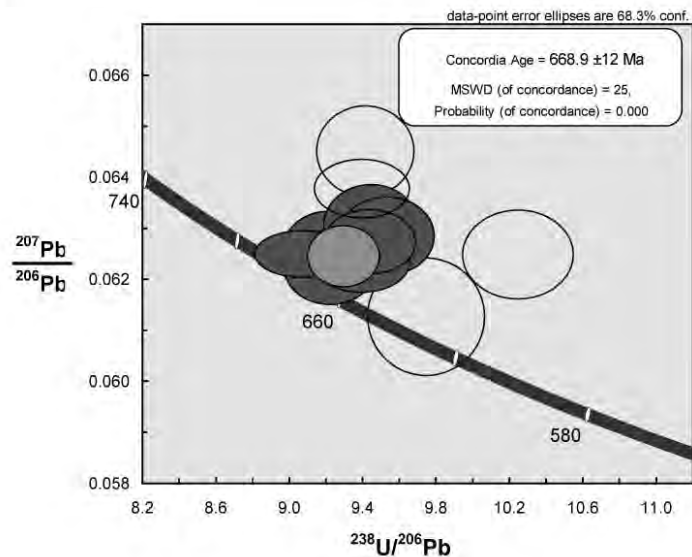


Figure 5. Tera-Wasserburg plot showing U-Pb data for inherited zircon cores from sample 07RMG45.

Figure 6. Tera-Wasserburg plot showing U-Pb data for inherited zircon cores from sample 07RMG43 and concordia age. Unshaded ellipses were not utilized in calculating concordia age. The high MSWD is a reflection of the fact that the concordia age (ellipse with lighter shade) plots slightly to the right of concordia, although the strong overlap of the individual analyses suggests to us that this is a reasonable average age.



River near the Roaring River (43.7805, -115.4927). Nine of the analyzed cores yield similar Neoproterozoic ages (Figure 4), and the five most concordant analyses generate a concordia age of 691 +/- 13 Ma. Two other cores yield ages of 1531 Ma and 2554 Ma.

Sample 07RMG45 was collected from a biotite granodiorite along the South Fork of the Payette River east of Lowman (44.0708, -115.5381). Five of the analyzed cores yield Neoproterozoic ages (Figure 5). Although they fall under the same range as the Neoproterozoic cores in samples 07RMG29 and 07RMG25, they show stronger effects of Pb loss so a reliable mean cannot be calculated. We also identified two Archean cores, with ages of 2557 and 2611 Ma in this sample.

Sample 07RMG43 was collected from a biotite leucogranite along the South Fork of the Payette River near Grandjean (44.1722, -115.2441). All eleven of the inherited cores analyzed have similar Neoproterozoic ages (Figure 6). Eight of these overlap and yield a concordia age of 669 +/- 12 Ma.

Sample 98IB68 was collected by King and Valley (2001) from a dike-like mass of biotite tonalite intruding megacrystic granodiorite east of Stanley (44.2678, -114.7561). We identified only two Precambrian cores. These yield ages of 588 and 604 Ma, but both are more than 10% discordant and have probably suffered from Pb-loss; thus these are minimum ages.

We also studied zircons from several samples of the hornblende-bearing granodiorites in the southeastern corner of the Atlanta lobe near Hailey and a megacrystic granodiorite east of Stanley, but in contrast to the zircons of the peraluminous main phases of the batholith, these zircons lack inherited cores and almost always show simple oscillatory zoning in CL. This may further reflect the distinct chemistry of these plutons, which are typically metaluminous and commonly contain mafic magmatic enclaves.

## Discussion

The use of inherited zircon to determine the age of unexposed basement can be hampered by two major uncertainties. First, it can be difficult to determine whether zircon cores were inherited from the magma source region or were introduced from assimilated wallrock at or near the level of emplacement. Second, if the source or wallrock material is metasedimentary, the inherited zircon population will carry the detrital age spectrum of these rocks but not necessarily the original depositional age of the rocks themselves. This second uncertainty is tempered in this case by the lack of known sedimentary rocks with dominant detrital age peaks of 2.57 Ga and 690 Ma (Link et al., 2007a, b; K. Lund, personal communication) and the presence of exposed metaigneous rocks at House Mountain and the Pioneer metamorphic core complex and xenoliths in Snake River Plain lavas with these same or similar ages (Wolf et al., 2005; Alexander et al., 2006; Durk et al., 2007; Link et al., 2007a). However, we cannot, at this time, easily distinguish between a source and wallrock origin for the inherited zircons described above without more detailed textural and whole-rock geochemical studies.

Zircons from the southern half of the Atlanta lobe of the Idaho batholith show inherited age spectra that are dominated by a Neoproterozoic peak and an Archean peak (Figure 7), and these peaks are so distinct and the ages so similar from sample to sample that they may represent two common magmatic events. With the exception of the single Mesoproterozoic age in sample 07RMG25, this stands in sharp contrast to the inheritance patterns seen in the Bitterroot lobe of northern Idaho (Figure 7), where some samples contain single age populations between 1.7 and 1.8 Ga but many others show a wide range of ages between 1.4 and 1.85 (Foster and Fanning, 1997; Foster et al., 2001; Gaschnig et al., 2007 and unpublished data), similar to the detrital zircon age spectra seen in much of the Belt Supergroup (Ross and Villeneuve, 2003; Link et al., 2007b). This suggests that there may be fundamental differences between the magma source regions of the Atlanta lobe and

Bitterroot lobe of the Idaho batholith (Gaschnig et al., 2007).

The mean Archean core age (2.57 Ga) obtained from the southernmost sample, 07RMG29, is analytically indistinguishable from the U-Pb zircon age (2.58 Ga) reported for a lower crustal xenolith collected from Tertiary Snake River Plain lavas at Square Mountain, 70 km to the southeast (Wolf et al., 2005). In addition, we have obtained hafnium isotopic data by LA-MC-ICP-MS for these inherited cores, which consistently yield present-day epsilon-Hf values of -64, which is generally comparable to range of -58 to -61 reported by Dufrane et al. (2007) for the zircons from the SRP xenoliths. We interpret these similarities to indicate that the Square Mountain lavas and southern Idaho batholith phases around Rocky Bar have sampled the same general deep-crustal material, which is part of the Grouse Creek block. Consequently, the Grouse Creek block may extend (or may have extended during the Late Cretaceous) under the batholith, at least as far north as Rocky Bar, and the southern boundary of the Selway terrane also must be further north. Further support for this hypothesis is provided by whole-rock Nd and Hf isotopes, which are significantly less radiogenic here than elsewhere in the Atlanta lobe (Clarke, 1990; Gaschnig, unpublished data). A lesser Neoproterozoic component to these magmas is also required in order to explain the secondary population of zircon cores of this age and is also permissible with whole-rock isotopic data.

The dominance of Neoproterozoic inherited zircons and subordination or absence of Archean ages in the other samples suggests either different crustal structure, zones of melting, or both to the north of Rocky Bar. Whole-rock Nd data from this part of the batholith (Clarke,

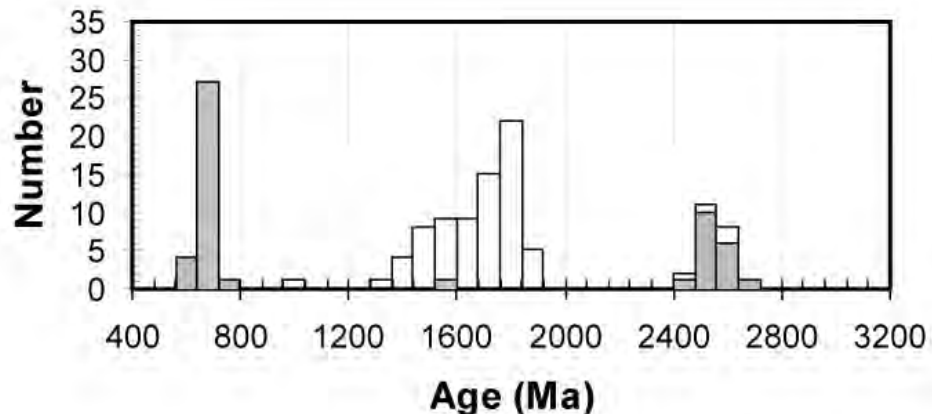


Figure 7. Histogram showing all core ages reported here for the southern Atlanta lobe (shaded) compared to unpublished core dates for the Bitterroot lobe (unshaded).

1990) suggests little or no Archean component. While we cannot dismiss the possibility that Archean crust extends as far north as sample 07RMG45, evidence in favor of its presence is comparatively scarce. What the results from these samples do seem to indicate, however, is that Neoproterozoic rock is extensive in the subsurface and may have originally formed a continuous belt connecting House Mountain and the Pioneers with the Windermere rocks and coeval plutons exposed in central Idaho around Big Creek (Lund et al., 2003).

## Conclusions

Inherited zircons from the southern half of the Atlanta lobe of the Idaho batholith show age spectra dominated by a Neoproterozoic peak around 690 Ma and an Archean one around 2.57 Ga. The Neoproterozoic age is indistinguishable from the age of an orthogneiss exposed in the Pioneer metamorphic core complex (Durk et al., 2007), similar but slightly younger than an orthogneiss exposed in the House Mountain gneiss complex (Alexander et al., 2006), and also indistinguishable from a rhyodacite lava in the Windermere Supergroup in central Idaho (Lund et al., 2003). The Archean age is indistinguishable from the age of lower crustal xenoliths found in Tertiary Snake River Plain lavas at Square Mountain and slightly younger than the range of ages obtained for another orthogneiss in the Pioneer

metamorphic core complex. We conclude that the Archean crust of the Grouse Creek block extends at least 40 km north beyond the Snake River Plain beneath the Atlanta lobe of the Idaho batholith and that Neoproterozoic rocks correlative with the Windermere Supergroup and associated with the breakup of Rodinia are extensive in the subsurface, possibly representing a belt connecting isolated surface exposures in southern and central Idaho. We also suggest that the sharp differences in the inherited zircon age spectra between the Atlanta lobe and Bitterroot lobe reveal that there are fundamental differences in the magma source regions between the lobes, a hypothesis also supported by Nd and zircon-Hf isotopic data (Gaschnig et al., 2007).

### Acknowledgements

We acknowledge support from the Geological Society of America, Praetorius-Exxon Graduate Fellowship, and Tobacco Root Geological Society.

### References

- Alexander, J.T., 2007, Geochronology of the House Mountain gneiss complex in the Atlanta lobe of the Idaho batholith: M.S. thesis, Boise State University, 95 p.
- Alexander, J.T., Schmitz, M.D., and Northrup, C.J., 2006, Preliminary U/Pb zircon data from the House Mountain metamorphic complex in the Atlanta lobe of the Idaho batholith: Geological Society of America, Abstracts with Programs, v. 38, no. 7, p. 483.
- Armstrong, R.L., Taubeneck, W.H., and Hales, P.O., 1977, Rb-Sr and K-Ar geochronometry of Mesozoic granitic rocks and their Sr isotopic composition, Oregon, Washington, and Idaho: Geological Society of America Bulletin, v. 88, p. 397-411.
- Arndt, N.T., and Goldstein, S.L., 1987, Use and abuse of crust-formation ages: Geology, v. 15, no. 10, p. 893-895.
- Ayres, M., and Harris, N., 1997, REE fractionation and Nd-isotope disequilibrium during crustal anatexis: constraints from Himalayan leucogranites: Chemical Geology, v. 139, p. 249-269.
- Bennett, V.C., and DePaolo, D.J., 1987, Proterozoic crustal history of the western United States as determined by neodymium isotopic mapping: Geological Society of America Bulletin, v. 99, no. 5, p. 674-685.
- Bickford, M.E., Chase, R.B., Nelson, B.K., Shuster, R.D., and Arruda, E.C., 1981, U-Pb studies of zircon cores and overgrowths, and monazite; implications for age and petrogenesis of the northeastern Idaho Batholith: Journal of Geology, v. 89, no. 4, p. 433-457.
- Chang, Z., Vervoort, J.D., McClelland, W.C., and Knaack, C., 2006, U-Pb dating of zircon by LA-ICP-MS: Geochemistry, Geophysics, Geosystems, v. 7, no. 1, p. Q05009.
- Chappell, B.W., 1979, Granites as images of their source rocks: Geological Society of America, Abstracts with Programs, v. 11, p. 400.
- Cheney, J.T., Webb, A.A.G., Coath, C.D., and McKeegan, K.D., 2004, In situ ion microprobe  $^{207}\text{Pb}/^{206}\text{Pb}$  dating of monazite from Precambrian metamorphic suites, Tobacco Root Mountains, Montana: in Brady, J.B., Burger, H.R., Cheney, J.T., and Harms, T.A., eds., Precambrian Geology of the Tobacco Root Mountains, Montana: Geological Society of America Special Paper, v. 377, p. 151-179.
- Clarke, C.B., 1990, The geochemistry of the Atlanta lobe of the Idaho batholith in the western United States Cordillera: Ph.D. thesis, The Open University, 357 p.
- Collins, W.J., 1996, Lachlan Fold Belt granitoids: products of three-component mixing: Transactions of the Royal Society of Edinburgh: Earth Sciences, v. 87, p. 171-181.
- Davies, G.R., and Tommasini, S., 2000, Isotopic disequilibrium during rapid crustal anatexis: implications for petrogenetic studies of magmatic processes: Chemical Geology, v. 162, no. 2, p. 169-191.
- Dufrane, S.A., Vervoort, J.D., Leeman, W.P., and Wolf, D.E., 2007, Hafnium isotope composition of Archean zircons from xenoliths of the Snake River Plain, Idaho: EOS, Transactions, American Geophysical Union, Fall Meeting Supplement, v. 88, no. 52, Abstract V43B-1375.

- Durk, K.M., Link, P.K., and Fanning, C.M., 2007, Neoproterozoic 695 Ma felsic orthogneiss, Wildhorse Creek, Pioneer Mountains, south-central Idaho: new tie point in reconstruction of Rodinian rifting: Geological Society of America, Abstracts with Programs, v. 39, no. 6, p. 613.
- Egger, A.E., Dumitru, T.A., Miller, E.L., Savage, C.F.I., and Wooden, J.L., 2003, Timing and nature of Tertiary plutonism and extension in the Grouse Creek Mountains, Utah: International Geology Review, v. 45, no. 6, p. 497-532.
- Evans, K.V., Aleinikoff, J.N., Obradovich, J.D., and Fanning, C.M., 2000, SHRIMP U-Pb geochronology of volcanic rocks, Belt Supergroup, western Montana: evidence for rapid deposition of sedimentary strata: Canadian Journal of Earth Sciences, v. 37, p. 1287-1300.
- Fanning, C.M., and Link, P.K., 2004, U-Pb SHRIMP ages of Neoproterozoic (Sturtian) glaciogenic Pocatello Formation, southeastern Idaho: Geology, v. 32, p. 881-884.
- Farmer, G.L., and DePaolo, D.J., 1983, Origin of Mesozoic and Tertiary granite in the western United States and implications for pre-Mesozoic crustal structure; 1, Nd and Sr isotopic studies in the geocline of the northern Great Basin: Journal of Geophysical Research, v. 88, p. 3379-3401.
- Foster, D.A., and Fanning, C.M., 1997, Geochronology of the northern Idaho Batholith and the Bitterroot metamorphic core complex; magmatism preceding and contemporaneous with extension: Geological Society of America Bulletin, v. 109, no. 4, p. 379-394.
- Foster, D.A., Mueller, P.A., Mogk, D.W., Wooden, J.L., and Vogl, J.J., 2006, Proterozoic evolution of the western margin of the Wyoming craton: implications for the tectonic and magmatic evolution of the northern Rocky Mountains: Canadian Journal of Earth Sciences, v. 43, p. 1601-1619.
- Foster, D.A., Schafer, C., Fanning, C.M., and Hyndman, D.W., 2001, Relationships between crustal partial melting, plutonism, orogeny, and exhumation; Idaho-Bitterroot Batholith: Tectonophysics, v. 342, no. 3-4, p. 313-350.
- Gaschnig, R.M., Vervoort, J.D., Lewis, R.S., and Dufrane, S.A., 2007, Evolution of a long-lived magmatic center in Idaho: EOS, Transactions, American Geophysical Union, Fall Meeting Supplement, v. 88, no. 52, Abstract T14B-07.
- Keay, S., Steele, D., and Compston, W., 1999, Identifying granite sources by SHRIMP U-Pb zircon geochronology: an application to the Lachlan fold-belt: Contributions to Mineralogy and Petrology, v. 137, no. 4, p. 323-341.
- King, E.M., and Valley, J.W., 2001, The source, magmatic contamination, and alteration of the Idaho Batholith: Contributions to Mineralogy and Petrology, v. 142, no. 1, p. 72-88.
- Leeman, W.P., Menzies, M.A., Matty, D.J., and Embree, G.F., 1985, Strontium, neodymium, and lead isotopic compositions of deep crustal xenoliths from the Snake River Plain: evidence for Archean basement: Earth and Planetary Science Letters, v. 75, p. 354-368.
- Lewis, R.S., Kiilsgaard, T.H., Bennett, E.H., and Hall, W.E., 1987, Lithologic and chemical characteristics of the central and southeastern part of the southern lobe of the Idaho Batholith: in Vallier, T.L., and Brooks, H.C., eds., Geology of the Blue Mountains region of Oregon, Idaho, and Washington; the Idaho Batholith and its border zone: U.S. Geological Survey Professional Paper 1436, p. 171-196.
- Link, P.K., Durk, K.M., and Fanning, C.M., 2007a, SHRIMP U-Pb ages for Archean orthogneiss, Mesoproterozoic paragneiss, and Eocene Boulder Creek pluton, Pioneer Mountains, south-central Idaho, part of the 2600 Grouse Creek block: Geological Society of America, Abstracts with Programs, v. 39, no. 6, p. 613.
- Link, P.K., Fanning, C.M., Lund, K.I., and Aleinikoff, J.N., 2007b, Detrital-zircon populations and provenance of Mesoproterozoic strata of east-central Idaho, U.S.A.: correlation with the Belt Supergroup of southwest Montana: in Link, P.K., and Lewis, R.S., eds., Proterozoic Geology of Western North America and Siberia: SEPM Special Publication 86, p. 101-128.
- Lund, K., Aleinikoff, J.N., Evans, K.V., and Fanning, C.M., 2003, SHRIMP U-Pb geochronology of Neoproterozoic Windermere Supergroup, central Idaho: Implications for rifting of western Laurentia and synchronicity of Sturtian glacial deposits: Geological Society of America Bulletin, v. 115, no. 3, p. 349-372.

Miller, C.F., Hanchar, J.M., Wooden, J.L., Bennett, V.C., Harrison, T.M., Wark, D.A., and Foster, D.A., 1992, Source region of a granite batholith: evidence from lower crustal xenoliths and inherited accessory minerals: *Transactions of the Royal Society of Edinburgh: Earth Sciences*, v. 83, p. 49-62.

Mueller, P.A., and Frost, C.D., 2006, The Wyoming Province: a distinctive Archean craton in Laurentian North America: *Canadian Journal of Earth Sciences*, v. 43, p. 1391-1397.

Mueller, P.A., Heatherington, A.L., D'Arcy, K.A., Wooden, J.L., and Nutman, A.P., 1996, Contrasts between Sm-Nd whole-rock and U-Pb zircon systematics in the Tobacco Root batholith, Montana: implications for the determination of crustal age provinces: *Tectonophysics*, v. 265, p. 169-179.

Mueller, P.A., Heatherington, A.L., Kelly, D.M., Wooden, J.L., and Mogk, D.W., 2002, Paleoproterozoic crust within the Great Falls tectonic zone: Implications for the assembly of southern Laurentia: *Geology*, v. 30, no. 2, p. 127-130.

Mueller, P.A., Shuster, R.D., D'Arcy, K.A., Heatherington, A.L., Nutman, A.P., and Williams, I.S., 1995, Source of the northeastern Idaho Batholith; isotopic evidence for a Paleoproterozoic terrane in the Northwestern U.S: *Journal of Geology*, v. 103, no. 1, p. 63-72.

Ross, G.M., 1991, Tectonic setting of the Windermere Supergroup revisited: *Geology*, v. 19, no. 11, p. 1125-1128.

Ross, G.M., 2002, Evolution of Precambrian continental lithosphere in western Canada: results from Lithoprobe studies in Alberta and beyond: *Canadian Journal of Earth Sciences*, v. 39, p. 413-437.

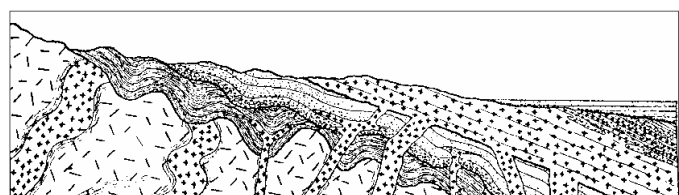
Shuster, R.D., and Bickford, M.E., 1985, Chemical and isotopic evidence for the petrogenesis of the northeastern Idaho Batholith: *Journal of Geology*, v. 93, no. 6, p. 727-742.

Toth, M.I., and Stacey, J.S., 1992, Constraints on the formation of the Bitterroot lobe of the Idaho batholith, Idaho and Montana, from U-Pb zircon geochronology and feldspar Pb isotopic data: *U.S. Geological Survey Bulletin*, v. 2008, 14 p.

Wolf, D.E., Leeman, W.P., and Vervoort, J.D., 2005, U-Pb zircon geochronology of crustal xenoliths confirms presence of Archean basement be-

neath the central and eastern Snake River Plain: *Geological Society of America, Abstracts with Programs*, v. 37, no. 7, p. 60.

Wright, J.E., and Snoke, A.W., 1993, Tertiary magmatism and mylonitization in the Ruby-East Humboldt metamorphic core complex, northeastern Nevada: U-Pb geochronology and Sr, Nd, and Pb isotope geochemistry: *Geological Society of America Bulletin*, v. 105, no. 7, p. 935-952.



# FIELD GUIDE TO THE BENBOW AREA, BEARTOOTH MOUNTAINS FRONT: DEAN TO THE GOLF COURSE, STILLWATER COUNTY, MONTANA

**Ennis P. Geraghty**

*Stillwater Mining Company, P.O. Box 1330, Columbus, Montana 59019  
egeraghty@stillwatermining.com*

## INTRODUCTION

The Benbow area of the Beartooth Mountains front is the “type locale” for Laramide (latest Cretaceous to Paleocene) backthrusting along the Stillwater Complex portion of the front. Here, evidence will be examined for multiple backthrusts, including 6 repetitions of the Great Unconformity (Cambrian Wolsey Shale on Ar-

chean Stillwater Complex). Phanerozoic stratigraphy from Cretaceous Judith River Formation down to Cambrian units is beautifully exposed along the field trip route from Dean (elevation 5,238 feet) to The Golf Course (elevation 9,330 feet). The Archean Stillwater Complex also is exposed along with two (chrome and nickel-copper) of the three associated metal zones. In addition to outcrop visits, we will discuss the

overall Laramide fault architecture of the Beartooth Mountains front as a hinterland-dipping basement duplex (Boyer and Elliott, 1982) with “evolved” triangle-zone characteristics (Sterne, 2006).

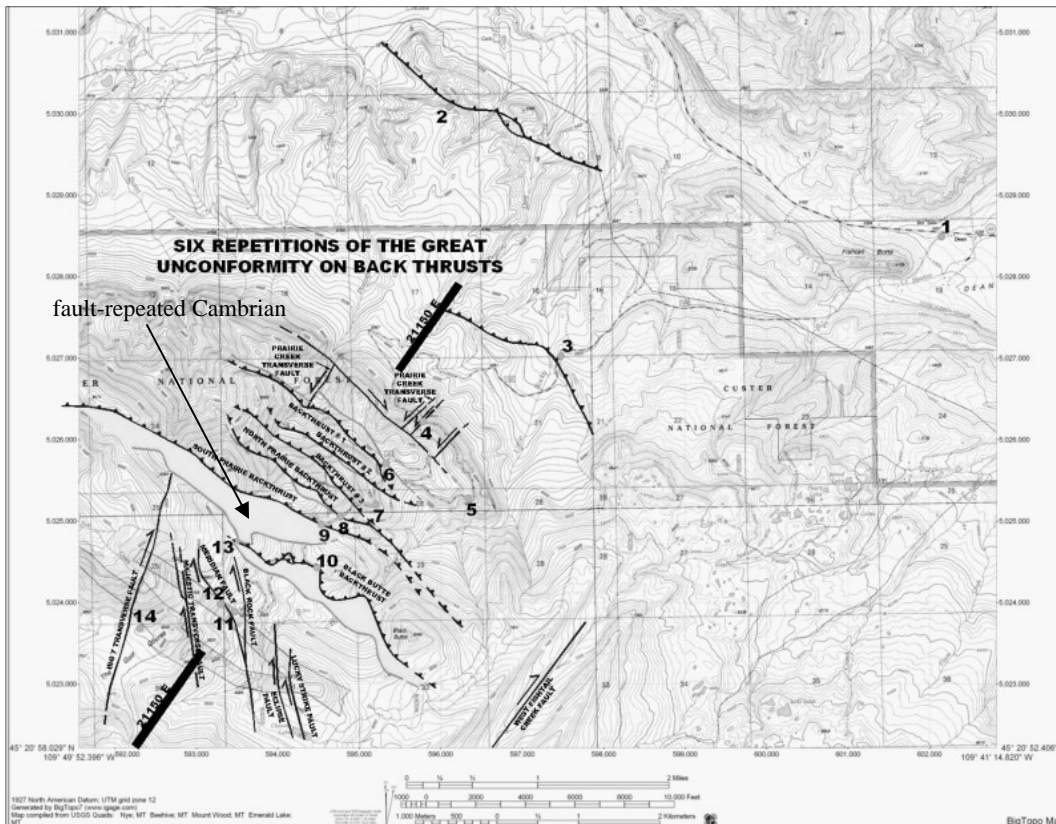


Figure 1. Map of field trip area showing major faults (dark lines). Teeth mark up side of thrust and reverse faults. Light lines are surface trace of Great Unconformity. The labeled zone denotes the distribution of fault-repeated Cambrian rocks. Numbered dots are field trip stops. Line labeled 21150 E shows orientation of cross section. Geologic information modified after Vhay (1934), Jackson et al. (1954), Jones et al. (1960), and Segerstrom and Carlson (1982). Drafted by John Marancik, Stillwater mine.

## Field Trip Road Log (distances in miles)

### Stop 1: Regional Overview

**STOP 1** 0.0 This guide starts at the intersection of Montana Highway # 419 and Benbow Road at the west end of the settlement of Dean, Montana (Fig. 1). We are near the west end of Dean dome, a Laramide structure on the Nye-Bowler lineament (Wilson, 1936), a zone of faulting and folding mapped for a distance of at least 56 mi (90 km) from the Pryor Mountains on the east to the Beartooth mountains front (Fig. 2). To the southwest is a distinctive east-west linear hill, Fishtail Butte, that is underlain by a dike of intrusive igneous breccia, diorite, and minor diorite porphyry of Cretaceous (Judith River; Fig. 3) age. We are standing on shale of Niobrara Formation (Lopez, 2001).

From Dean, we head west on Highway 419.

Crest of Dean Divide; Limestone Butte, straight ahead at 12:00, is cored by diorite porphyry of probable Cretaceous age and capped by Madison Group limestone. Eagle Sandstone cliffs are at 2:00.

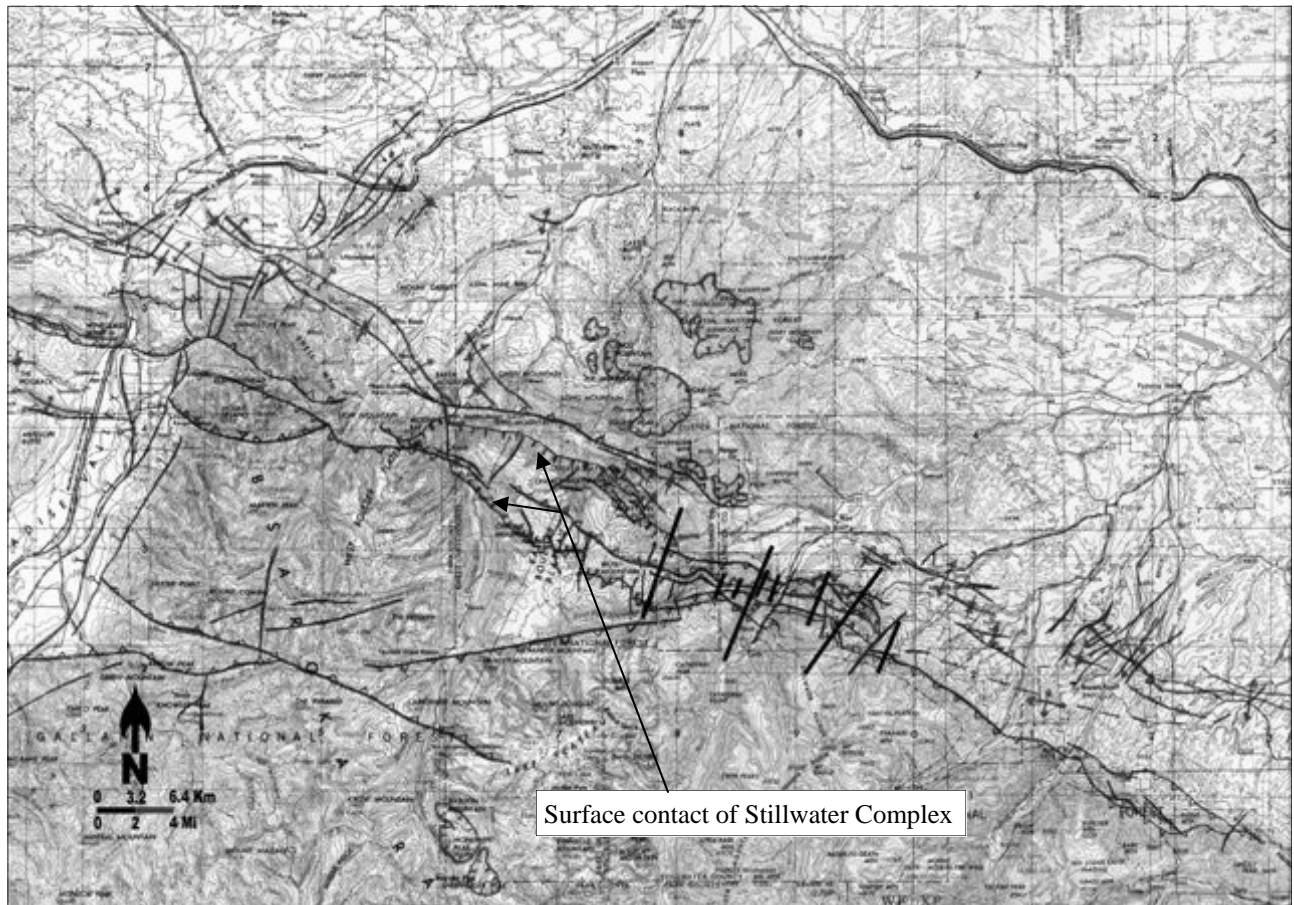
Turn left on Nye Cemetery Road. In front of Limestone Butte notice an asymmetric fold, overturned to the south, in the Sliderock Mountain bedded lahars. Is this caused by a southwest-verging blind backthrust?

Mount Wood, the second highest peak (12,649 feet) in Montana, is straight ahead on the skyline. Note also the prominent palisades (flatirons) of Madison Group limestones on the Beartooth front.

Cross Little Rocky Creek.

Cross Prairie Dog Creek.

Eagle Sandstone at 9:00, dipping south out of Nye dome. Judith River sandstones at 11:00.



Electrical substation on left.

Turn left on Sundance Trail. This is a private road and permission is needed to use it to access Stop 2.

Cross under power line.

Eagle Sandstone on left.

Overtured Clagget Shale in roadcut.

More overtured Clagget Shale in roadcut.

Eagle Sandstone in roadcut.

## **STOP 2** Stop 2: Backthrust Along Nye-Bowler Structural Zone

Overtured north-dipping Clagget Shale; Eagle Sandstone to north, sandstones of Judith River Formation to south. The Eagle has been thrust to the south over Clagget Shale with prominent overtured dips due to thrusting. The fault was originally mapped by Vhay (1934). This structure is also referred to as Stillwater dome (Ames, 1991).

Retrace our way back to Stop 1.

Stop 1 (again): Be sure to reset your odometers to 0.

Eagle Sandstone outcrop to right.

Crossing Meadow Creek.

Crossing Meadow Creek again.

Cattle guard at boundary of Custer National Forest. Benbow Road now is U.S. Forest Service Road # 2414.

Jeep Trail # 2415 on left.

Low outcrops of sandstone in Judith River Formation both sides of road.

Crossing dry Dale Creek.

Intersection with road to right.

Third stop, please pull off onto right shoulder.

## **STOP 3** Stop 3: Eagle Sandstone Roadcut

With this roadcut and the next one at mile marker 3.4, the Eagle Sandstone has a computed thickness of at least 450 feet, much greater than the typical 150 feet. Is there a small backthrust duplicating Eagle section here?

Eagle Sandstone roadcut.

Crossing Little Rocky Creek.

3.8 Ruins of mill that concentrated chromite from Benbow mine in the early 1940's at 12:00. The broken muck was transported to the mill (elevation 6,000 feet) by tramway from the mine (elevation 8,450 feet).

Road to left leads to Benbow millsite. The path of the tramway is visible on the mountainside. Note the prominent palisades (flatirons, hogbacks) of limestones in the Madison Group.

“Salt and pepper” sandstone in the Frontier(?) Formation, now overtured at the mountain front.

Black shale of Colorado Group in road and ditch.

5.1 Kootenai(?) Formation float in bank.

*(opposite page)* Figure 2. Map showing regional geologic features. Dark lines are surface traces of faults (teeth on up side of thrust and reverse faults; line and ball on down side of normal faults). Medium gray lines with fold symbols are surface traces of Laramide anticlines and synclines. Labeled hachured line is surface contact of Stillwater Complex. Other hachured lines are surface extent of Cretaceous intrusions (Eocene at Monument Peak). Dashed line is subsurface extent of Stillwater Complex interpreted by Kleinkopf (1985). Base map is scanned portions of U.S. Geological Survey Billings and Bozeman, Montana; Wyoming 1 X 2 degree quadrangles. Geologic information modified after Butler (1962, 1966); Du Bray et al. (1994); Elliott et al. (1993); Foose, Wise, and Garbarini (1961); Garbarini (1957); Iddings and Weed (1894); Jackson et al. (1954); Jones, Peoples, and Howland (1960); Lammers (1936, 1937); Lopez (2001); Page (1977, 1979); Page and Nokleberg (1974); Phair (1942); Reid, McMannis, and Palmquist (1975); Richards (1957); Robbins and Erslev (1986); Rouse et al. (1937); Segerstrom and Carlson (1982); Todd et al. (1982); Vail (1955); Vhay (1934); C.W. Wilson Jr. (1936); J.T. Wilson (1936) and Wise (2000). Drafted by John Marancik, Stillwater mine.

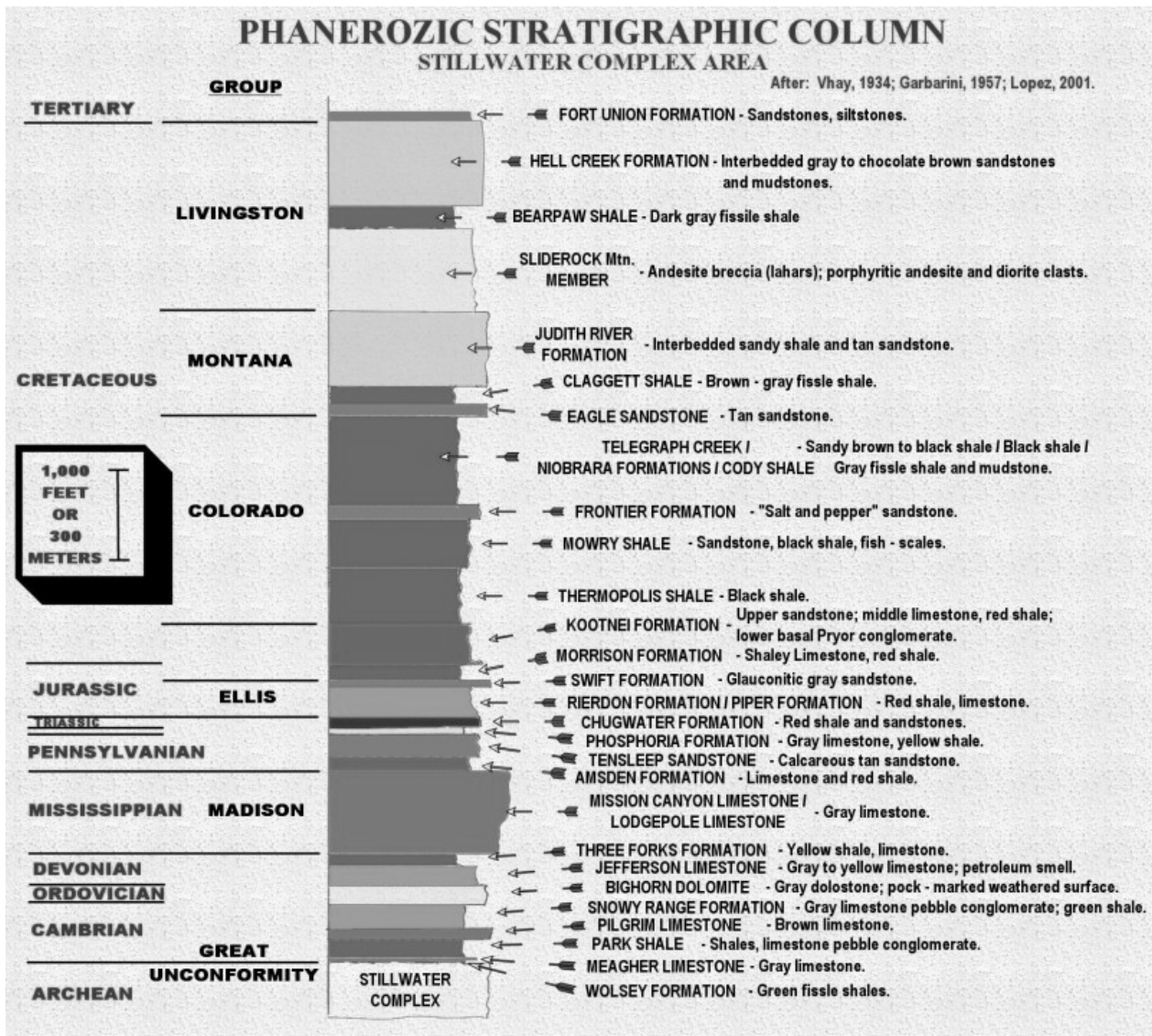


Figure 3. Phanerozoic stratigraphic column, Stillwater Complex area. Drafted by John Marancik, Stillwater mine.

Float of Pryor Conglomerate Member of Kootenai Formation in ditch.

5.3 Switchback in road; outcrop on south side of road is overturned sandstone of Swift Formation, Ellis Group.

Sandstone "pavement" in road, Ellis Group.

5.7 Limestone "pavement" in road, Piper Formation, pink shales in ditch on south side of road.

Red beds of Chugwater Formation.

Tensleep Sandstone.

Amsden Formation outcrop on corner.

Gray limestone of Madison Group; palisade of Mission Canyon Formation.

Amsden Formation again on curve.

6.1 Back into Tensleep Formation.

Contact between Tensleep Formation to south and Chugwater Formation to north, overturned.

Back into Tensleep Formation.

6.35 Fourth stop.

**STOP 4** Stop 4: Transverse Faults

North-trending transverse faults at a high angle to bedding in the sedimentary section and layering in the Stillwater Complex are a prominent fault set along the Beartooth front (Figs. 1, 2). At this stop, 2 transverse faults have left-lateral offsets (pure strike-slip) of 200 and 500 feet, respectively, based on offset of the Madison palisade. They are interpreted as tear faults active during the Laramide Orogeny. These tear faults are in turn offset about 4,000 feet (Fig. 1) on what is interpreted to be an enigmatic, northwest-trending, right lateral strike-slip fault (or extreme oblique-slip forethrust).

Contact between limestone of Mission Canyon Formation to south and Amsden Formation to north.

Amsden/Madison contact again.

6.6 Small northeast-trending transverse fault offsets Madison 100 feet left-lateral. On top of Madison palisade are ruins of aerial tramway that carried broken chromite-bearing rock from East and West Benbow mines to Benbow mill below.

Fifth stop, Madison Group roadcut on curve.

Stop 5: Areal Overlook **STOP 5**

Contact between Lodgepole Limestone of Madison Group on north and Three Forks Formation on south.

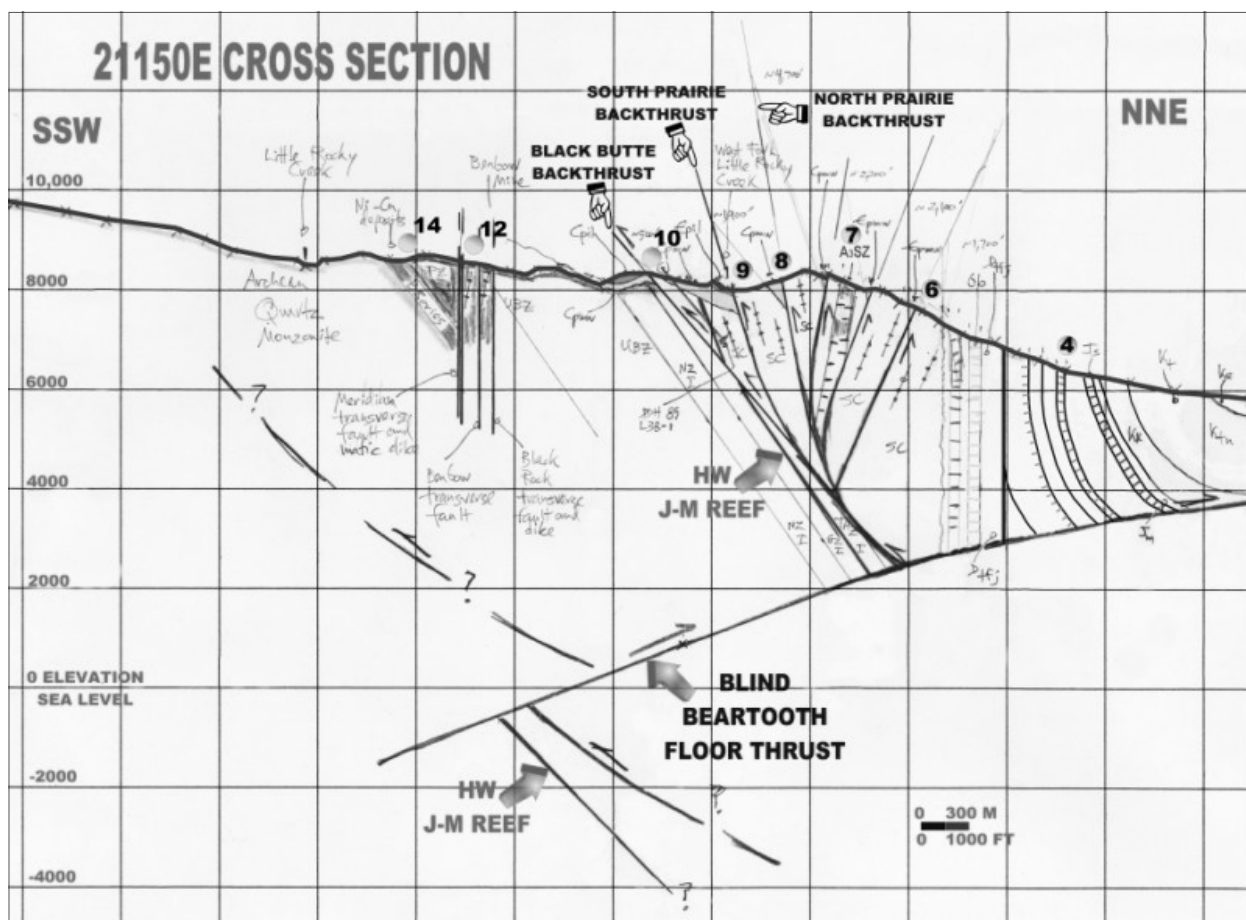


Figure 4. Benbow cross section. See fig. 4 for cross-section location; figure 2 for Phanerozoic stratigraphy; and fig. 5 for Stillwater Complex (SC) stratigraphic nomenclature. Modified after Geraghty (2006). Drafted by John Marancik, Stillwater mine.

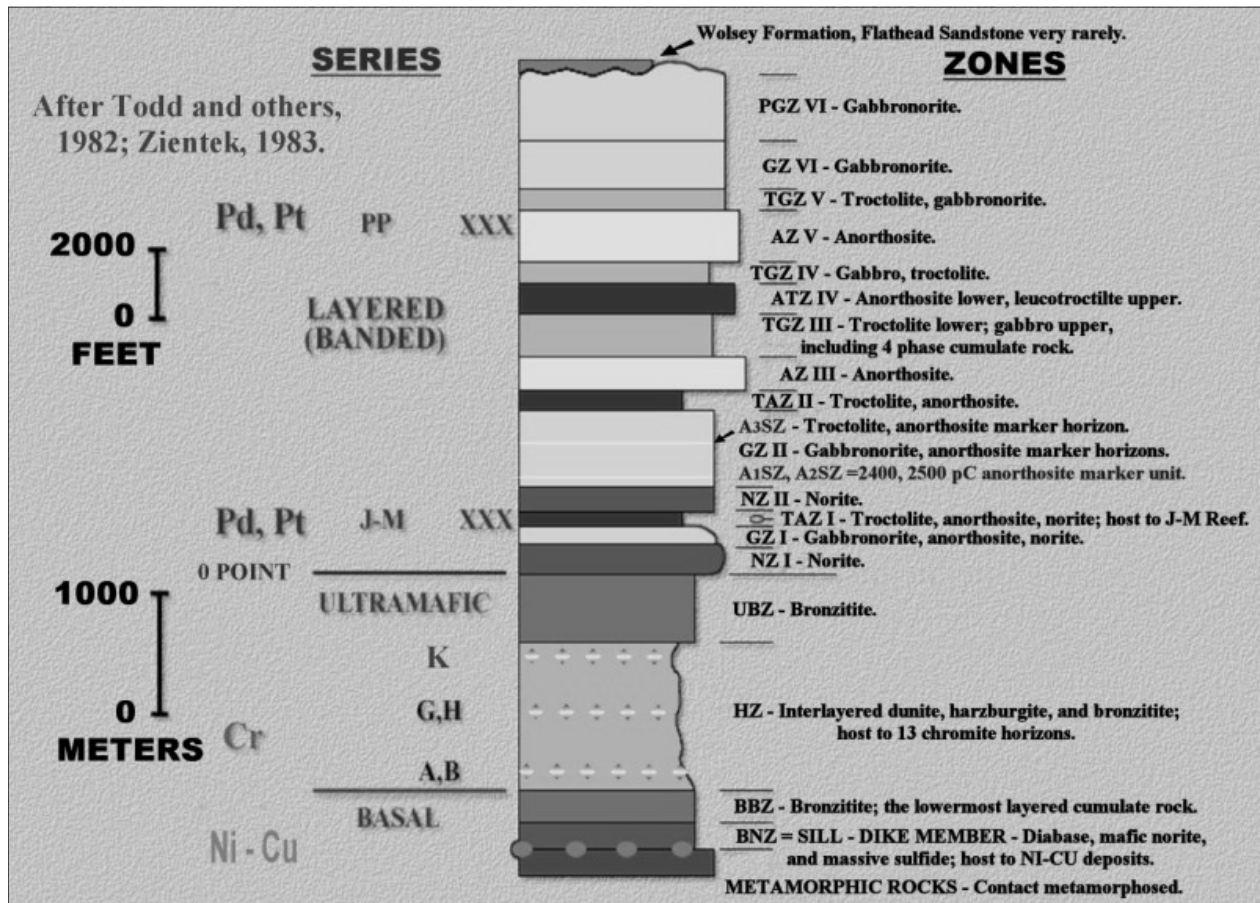


Figure 5. Stratigraphic column for Archean, layered, ultramafic to mafic Stillwater Complex. Drafted by John Marancik, Stillwater mine.

Jefferson Formation.

Pilgrim Limestone roadcut.

Park Formation.

On curve, Great Unconformity (not exposed) between Archean Stillwater Complex to south and Cambrian Wolsey Formation to north.

Pilgrim Limestone roadcut, going back up section.

Bighorn Dolomite with classic pock-marked weathered surface.

Switchback, roadcut of Jefferson Formation.

Bighorn Dolomite.

Pilgrim Limestone.

Sixth stop, on curve.

## **STOP 6** Stop 6: Repetition of Great Unconformity on Backthrust # 1

Hike up hillside through limestone float over Great Unconformity into Stillwater Complex float over backthrust # 1 (Figs. 1, 4) to outcrop of overturned Meagher(?) Limestone. We will discuss the extent of backthrust # 1. This fault was first recognized by Segerstrom and Carlson (1982). Here the overturned backthrust # 1 probably is riding in lower Park Shale (Fig. 3).

Roadcut of Anorthosite Zone III (AZ III, Fig. 5) of the layered, ultramafic to mafic Stillwater Complex. AZ III is the top of the complex at this location. We are missing about the top 8,000 feet of exposed complex here.

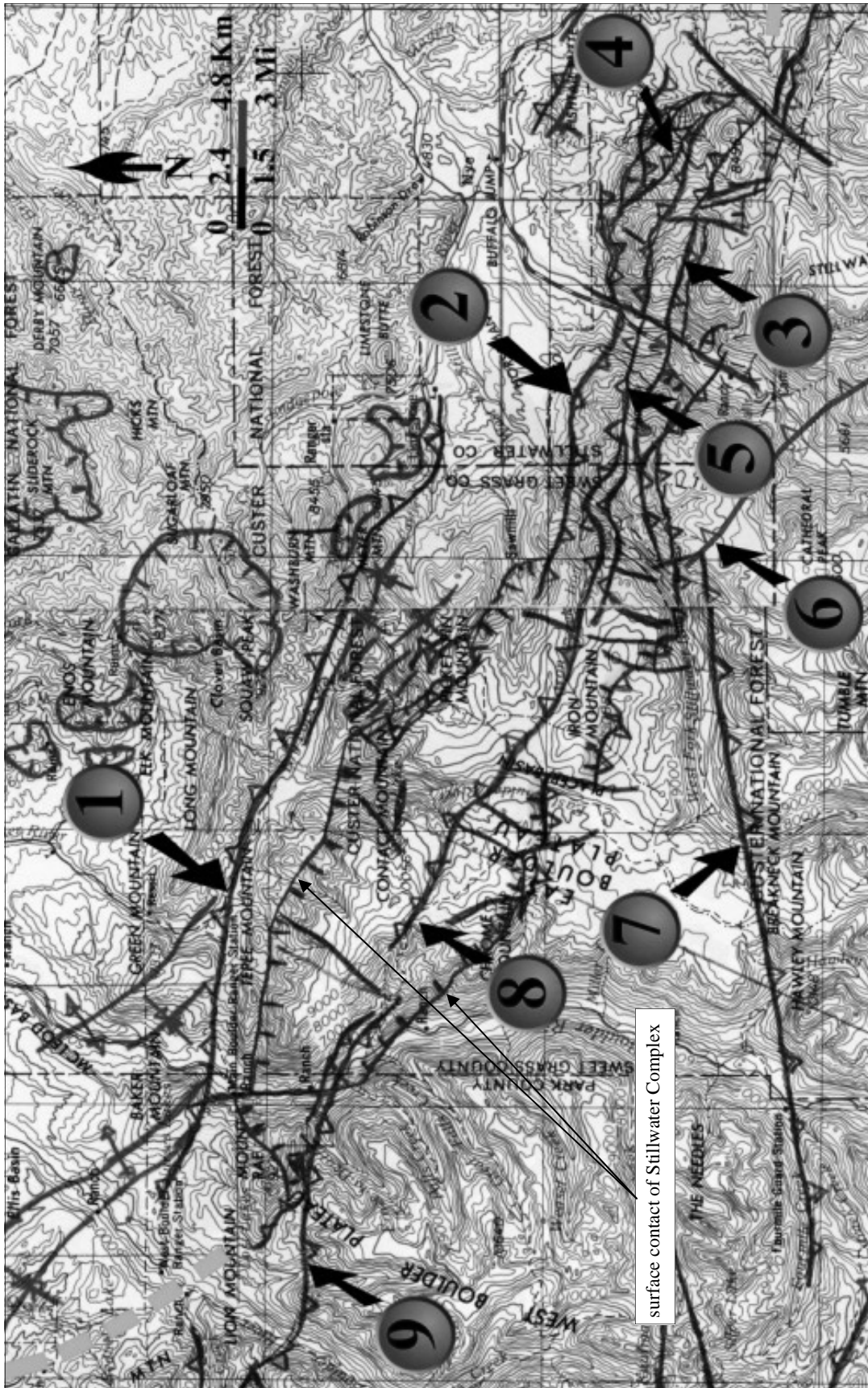


Figure 6. Map of regional faults associated with Stillwater Complex focusing on enlarged portion of figure 2. Dark lines are surface traces of faults (teeth on up side of thrust and reverse faults). Numbered circles correspond to fault names: 1 - Dry Fork fault (Vail, 1955); 2 - Horseman fault (Jones et al., 1960); 3 - Lake/Nye Creek fault (Jones et al., 1960); 4 - North Prairie fault (Jones et al., 1960); 5 - South Prairie fault (Jones et al., 1960); 6 - Sioux Charley Lake fault (Butler, 1962); 7 - Centre fault (J.T. Wilson, 1936); 8 - Iron Creek/Brownlee Creek fault (Jones et al., 1960); 9 - Lost Creek fault (Richards, 1957; Phair, 1942, p. 43 called this fault the Mount Rae thrust). Labeled hachured line is surface contact of Stillwater Complex. Other hachured lines are surface extent of Cretaceous intrusions. Heavy dashed line is subsurface extent of Stillwater Complex interpreted by Kleinkopf (1985). Base map is scanned portions of U.S. Geological Survey Billings and Bozeman, Montana; Wyoming 1 X 2 degree quadrangles. Drafted by John Marancik, Stillwater mine.

Crossing backthrust # 2 in valley at curve in road (Fig. 1). Evidence for this backthrust is exposed on the ridge to the right (west). Backthrust # 2 was first recognized by Jones (Jones et al., 1960, plate 24) and here rides in Park Shale.

Outcrop of gabbro-norite of GZ II (Fig. 5).

Roadcut of anorthosite in here-named Anorthosite 3 Subzone (A3SZ, Fig. 5) of GZ II.

Seventh stop, on corner, overlook to south of Mount Wood, the second highest peak (elevation 12,649 feet) in Montana.

## **STOP 7** Stop 7: Mount Wood Viewpoint

Roadcut is in anorthosite and troctolite of A3SZ of GZ II (Fig. 5). We skipped a stop at backthrust # 2 because it is not exposed at road level.

Roadcuts in GZ II.

9.1 Backthrust # 3 occupies valley (Fig. 1). This fault also is exposed on the ridge to the right (west). Backthrust # 3 was first recognized by Segerstrom and Carlson (1982) and still is riding in Park Shale.

Roadcut in GZ II.

Backthrust # 4, the North Prairie fault (Jones et al., 1960, p. 314; originally mapped by Vhay, 1934) passes through here.

Eighth stop, outcrop of Meagher Limestone again.

## **STOP 8** Stop 8: North Prairie Backthrust

Outcrop is thin-bedded Meagher Limestone, evidence for the fourth repetition of the Great Unconformity. Notice that the dip is no longer overturned. The North Prairie backthrust and its equivalent faults (Iron Creek, Brownlee Creek) are arguably the most continuous of the back-

thrust system of faults and may extend to the main Boulder River Canyon (Fig. 6; Jones et al., 1960, plate 24). The North Prairie backthrust here rides in Park Shale.

Outcrop of gabbro-norite of GZ II.

Ninth stop, backthrust # 5, the South Prairie fault (Jones et al., 1960; originally mapped by Vhay, 1934).

## **STOP 9** Stop 9: South Prairie Backthrust

Here GZ II of the Stillwater Complex (Fig. 5) is thrust south over Cambrian Pilgrim Limestone (Fig. 3). Notice the drag syncline and reversal of dip on Pilgrim beds. Also note that the fault does not occupy the valley; instead the axis of the drag syncline is positioned there. The South Prairie fault also is of regional extent and is interpreted as being present for about 13 miles along strike past the West Fork of the Stillwater River (Fig. 6; Jones et al., 1960, plate 24). At this location the South Prairie backthrust is ramping up section to ride(?) in the Dry Creek Shale, a member of the Snowy Range Formation (Fig. 3).

Axis of east-trending drag syncline is in valley.

Now in Park Formation.

Meagher Limestone, again!! The J-M Reef platinum-palladium zone is directly below us here (Fig. 4).

Great Unconformity again, this time the Cambrian is on Norite Zone I (Fig. 5).

Tenth stop, backthrust# 6, here-named the Black Butte backthrust (originally mapped in part by Vhay, 1934).

## **Stop 10: Black Butte Backthrust**

## **STOP 10** Norite Zone I of the Stillwater Complex is thrust

south over Park(?) Formation. Note the drag syncline.

The Golf Course is straight ahead on the skyline.

Pilgrim Limestone outcrop.

Park Formation below Pilgrim ledge.

Great Unconformity again, Cambrian this time lies on the Upper Bronzite Zone (UBZ) of the Ultramafic Series (Fig.5).

Bronzite of the Upper Bronzite Zone.

T intersection, bear to right.

Eleventh stop.

## STOP 11

### Stop 11: West Benbow Chromite Mine Headframe

Precambrian strike-slip faulting on Central Benbow shift zone (Jones et al., 1960, p. 321) has offset chromite horizons about 2,000 feet right laterally (Fig. 1). These north-trending transverse faults are offset by the west-northwest trending Laramide faults in this area of the Stillwater Complex.

T intersection, bear right. Now in Basal Series of Stillwater Complex (Fig. 5) with associated nickel-copper deposits.

Reclaimed trench associated with nickel-copper exploration by Anaconda Minerals Company, circa 1968.

Intersection, continue straight ahead.

Intersection, bear to left through open gate.

Twelfth stop, mine dumps of chromite-bearing rock.

### Stop 12: West Benbow Chromite Dumps

## STOP 12

Chromite-bearing rock is from the G and H chromite layers mined during 1942 to 1943 (Page et al., 1985).

Intersection, bear to right.

Intersection, bear to right.

Top of Grassy Knob, survey post. After a quick overlook, we will head back down, retracing our path.

Thirteenth stop, Great Unconformity again, Wolsey Formation on Norite Zone I.

### Stop 13: Black Butte Backthrust, Again

## STOP 13

Norite Zone I is thrust south over Meagher (?) Limestone. The Black Butte backthrust seems to tip out laterally just to west of here.

Great Unconformity, again!!

Back at intersection at mile marker 12.7, bear left.

Back at intersection at 12.6, bear right.

Crossing stope on G/H chromite zone, West Benbow mine.

14.1 Intersection, bear to right.

The Golf Course.

Fourteenth stop, Big 7 transverse fault (Jackson et al., 1954).

### Stop 14: Overlook at Big 7 Transverse Fault

## STOP 14

The Big 7 fault is a north-trending, strike-slip fault with about 2,000 feet of right-lateral offset on the Basal Series and associated nickel-copper deposits. A mafic dike occupies the fault trend for part of the strike. Generally, the

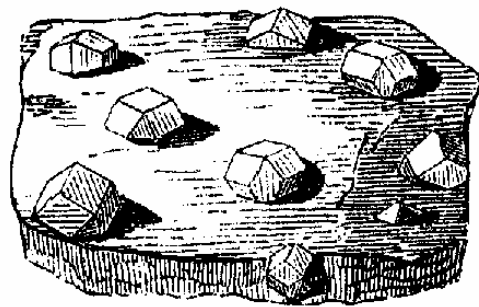
north-south dikes in the Beartooth Mountains date at 2,000 to 2,100 Ma (Mueller and Wooden, 1988, p. 138-139).

**End of field trip, retrace your way back out.**

## REFERENCES CITED

- Ames, V., 1991, Road log Nye-Bowler lineament Billings to Dean, Montana via Red Dome and Red Lodge: American Association of Petroleum Geologists Rocky Mountain Section Meeting Field Trip # 1, p. 1-19.
- Boyer, S.E., and Elliott, D., 1982, Thrust systems: American Association of Petroleum Geologists Bulletin, v. 66, no. 9, p. 1196-1230.
- Butler, J.R., 1962, Geology of the Cathedral Peak area, Beartooth Mountains, Montana: PhD dissertation, Columbia University, New York, 108 p.
- Butler, J.R., 1966, Geologic evolution of the Beartooth Mountains, Montana and Wyoming: Part 6: Cathedral Peak area, Montana: Geological Society of America Bulletin, v. 77, no. 1, p. 45-63.
- Du Bray, E.A., Elliott, J.E., Van Gosen, B.S., La-Rock, E.J., and West, A.W., 1994, Reconnaissance geologic map of the Sliderock Mountain area, Sweet Grass and Stillwater Counties, Montana: U.S. Geological Survey Miscellaneous Field Studies Map MF-2259.
- Elliott, J.E., Van Gosen, B.S., Du Bray, E.A., La-Rock, E.J., and Zientek, M.L., 1993, Geology of the Absaroka-Beartooth study area: *in* Hammarstrom, J.M., Zientek, M.L., and Elliott, J.E., eds., Mineral resource assessment of the Absaroka-Beartooth study area, Custer and Gallatin National Forests, Montana: U.S. Geological Survey Open-File Report 93-207, p. B1-B23.
- Foose, R.M., Wise, D.U., and Garbarini, G.S., 1961, Structural geology of the Beartooth Mountains, Montana and Wyoming: Geological Society of America Bulletin, v. 72, no. 8, p. 143-1172.
- Garbarini, G.S., 1957, Geology of the McLeod area, Beartooth range, Montana: PhD dissertation, Princeton University, Princeton, New Jersey, 235 p.
- Geraghty, E.P., 2006, Laramide structural evolution of the Stillwater Complex portion of Beartooth Mountains front, southcentral Montana: Integration of surface and underground mapping and drilling: American Association of Petroleum Geologists Rocky Mountain Section Program, p. 29.
- Iddings, J.P., and Weed, W.H., 1894, Geologic atlas of the Livingston folio, Montana: U.S. Geological Survey Geologic Atlas of the United States, 12 p.
- Jackson, E.D., Howland, A.L., Peoples, J.W., and Jones, W.R., 1954, Geologic maps and sections of the eastern part of the Stillwater Complex in Stillwater County, Montana: U.S. Geological Survey Open File Report 54-133.
- Jones, W.R., Peoples, J.W., and Howland, A.L., 1960, Igneous and tectonic structures of the Stillwater Complex, Montana: U.S. Geological Survey Bulletin 1071-H, 340 p.
- Kleinkopf, M.D., 1985, Regional gravity and magnetic anomalies of the Stillwater Complex area in Czamanske, G.K., and Zientek, M.L., eds., The Stillwater Complex, Montana: geology and guide: Montana Bureau of Mines and Geology Special Publication 92, p. 33-38.
- Lammers, E.C.H., 1936, The structural geology of the Livingston Peak area, Montana: PhD dissertation, The University of Chicago, Chicago, Illinois, 42 p.
- Lammers, E.C.H., 1937, The structural geology of the Livingston Peak area, Montana: J. of Geology, v. XLV, no. 3, p. 268-295.
- Lopez, D.A., 2001, Preliminary geologic map of the Red Lodge 30' X 60' quadrangle, south-central Montana: Montana Bureau of Mines and Geology Open File Report MBMG-423.
- Mueller, P.A., and Wooden, J.L., 1988, Field guide to an Archean transect, eastern Beartooth Mountains, Montana-Wyoming: *in* Lewis, S.E., and Berg, R.B., eds., Precambrian and Mesozoic plate margins: Montana, Idaho, and Wyoming with field guides for the 8th International Conference on Basement Tectonics: Montana Bureau of Mines and Geology Special Publication 96, p. 131-140.
- Page, N.J., 1977, Stillwater Complex, Montana: Rock succession, metamorphism and structure of the Complex and adjacent rocks: U.S. Geological Survey Professional Paper 999, 79 p.

- Page, N.J., 1979, Stillwater Complex, Montana – structure, mineralogy, and petrology of the Basal Zone with emphasis on the occurrence of sulfides: U.S. Geological Survey Professional Paper 1038, 69 p.
- Page, N.J., and Nokleberg, W.J., 1974, Geologic map of the Stillwater Complex, Montana: U.S. Geological Survey Miscellaneous Investigations Series Map I-797.
- Page, N.J., Zientek, M.L., Lipin, B.R., Mann, E.L., Schmidt, E.A., Turner, A.R., Czamanske, G.K., and Raedeke, L.D., 1985, Exploration and mining history of the Stillwater Complex and adjacent rocks: *in* Czamanske, G.K., and Zientek, M.L., eds., *The Stillwater Complex, Montana: geology and guide*: Montana Bureau of Mines and Geology Special Publication 92, p. 77–117.
- Phair, G., 1942, The geology of the Shell Mountain area, Park County, Montana: MSc thesis, Rutgers University, New Brunswick, New Jersey, 54 p.
- Reid, R.R., McMannis, W.J., and Palmquist, J.C., 1975, Precambrian geology of North Snowy block, Beartooth Mountains, Montana: Geological Society of America Special Paper 157, 135 p.
- Richards, P.W., 1957, Geology of the area east and southeast of Livingston, Park County, Montana: U.S. Geological Survey Bulletin 1021-L, p. 385-438.
- Robbins, E.A., and Erslev, E.A., Basement wedges, back-thrusting and thin-skinned deformation in the northwest Beartooth Mountains near Livingston, Montana: *in* Garrison, P.B., ed., *Geology of the Beartooth uplift and adjacent basins*: Montana Geological Society and Yellowstone Bighorn Research Association Joint Field Conference and Symposium, p. 111-123.
- Rouse, J.T., Hess, H.H., Foote, F., Vhay, J.S., and Wilson, K.P., 1937, Petrology, structure, and relation to tectonics of porphyry intrusions in the Beartooth Mountains, Montana: *J. of Geology*, v. 15, no. 7, p. 717-740.
- Seegerstrom, K., and Carlson, R.R., 1982, Geologic map of the banded upper zone of the Stillwater Complex and adjacent rocks, Stillwater, Sweet Grass, and Park Counties, Montana: U.S. Geological Survey Miscellaneous Investigations Series Map I-1383.
- Sterne, E.J., 2006, Stacked, “evolved” triangle zones along the southeastern flank of the Colorado Front Range: *in* Reynolds, R.G., and Sterne, E.J., eds., *Structural geology of the Colorado Front Range*: *Mountain Geologist*, v. 43, no. 1, p. 65-92.
- Todd, S.G., Keith, D.W., LeRoy, L.W., Schissel, D.J., Mann, E.L., and Irvine, T.N., 1982, The J-M platinum-palladium reef of the Stillwater Complex, Montana: I: stratigraphy and petrology: *Economic Geology*, v. 77, no. 6, p. 1454-1480.
- Vail, P.R., 1955, The igneous and metamorphic complex of East Boulder River area, Montana: MSc thesis, Northwestern University, Evanston, Illinois, 69 p.
- Vhay, J.S., 1934, The Geology of a part of the Beartooth front near Nye, Montana: PhD dissertation, Princeton University, Princeton, New Jersey, 123 p.
- Wilson Jr., C.W., 1936, Geology of the Nye-Bowler lineament, Stillwater and Carbon Counties, Montana: *Bulletin American Association of Petroleum Geologists*, v. 20, no. 9, p. 1161- 1188.
- Wilson, J.T., 1936, The geology of the Mill Creek – Stillwater area, Montana: PhD dissertation, Princeton University, Princeton, New Jersey, 131 p.
- Wise, D.U., 2000, Laramide structures in basement and cover of the Beartooth uplift near Red Lodge, Montana: *American Association of Petroleum Geologists Bulletin*, v. 84, no. 3, p. 360-375.
- Zientek, M.L., 1983, Petrogenesis of the Basal Zone of the Stillwater Complex, Montana: PhD dissertation, Stanford University, Stanford, California, 229 p.



# GENERAL GEOLOGY AND MINING PRACTICES ON THE J-M REEF, STILLWATER MINE, NYE, MT

## **Mike Koski**

*Senior Development Geologist, Stillwater Mining Company*

## **Mike Pasecznyk**

*Senior Grade Control Geologist, Stillwater Mining Company*

## **Matt Knight**

*Production Engineer, Stillwater Mining Company*

## **Ennis Geraghty**

*Stillwater Mining Company*

---

## INTRODUCTION

The Stillwater Mining Company is currently mining the platinum group metal (PGM)-bearing J-M Reef at two locations: the Stillwater Mine, with access along the Stillwater River on the eastern section of the Stillwater Complex, and the East Boulder Mine, with access to the western section along the East Boulder drainage. Both mines target the same stratigraphic horizon associated with the Palladium Platinum J-M Reef, the first package of Troctolite/Anorthosite layers (TAZ1) above the ultramafic series (Todd and others, 1982). In the broad sense, the J-M Reef is very continuous and is traceable for the entire exposed 28 miles of Stillwater Complex. At the mining scale, the Reef exhibits dramatic variations in ore continuity, geometry, and structural complexity. This paper will attempt to give the reader a glimpse of these variations and how they affect mining method selection, waste dilution control, and metal recovery procedures at the Stillwater mines.

## HISTORY

Economic interest in the Stillwater Complex began in the late 1800's on the basal nickel-copper zone, which is exposed on surface as a gossan. Further exploration of the Stillwater soon revealed chromite seams that could be

mined underground and stockpiled as a strategic domestic source of chromium for the various war efforts up to 1961. In the 1930's Ed Sampson recognized and published (Peoples and others, 1936) the similarities of the Stillwater complex to the PGM-rich Bushveld Complex and found traces of Pt/Pd in what was to become known as the upper-banded series. It wasn't until the 1960's that Keith Conn, exploration manager for Johns-Manville Corporation, organized a concerted exploration effort to find a Bushveld-type Merensky Reef equivalent in the Stillwater Complex. The field work for this effort started in 1967 and this work, in addition to major advancements in fire assays techniques for PGM made by Bondar-Clegg and the USGS, allowed for part-per-billion concentrations of PGM to be detected in soil geochemistry sampling. Enough interest was generated to keep exploration money coming for six years until 1973 when a consistent PGM-bearing horizon was identified and its relationship to TAZ1 was recognized. Once this relationship was understood, Manville geologists quickly targeted TAZ1 for drilling and surface mapping, which was crucial to Manville laying claim to most of the Reef horizon. Chevron Resources joint ventured with Manville in 1979, and a tri-venture with the Anaconda Company, who controlled the rest of the Reef horizon, was formed in 1983.

Production on the JM Reef began in October of

1985 after extensive test mining in three exploration adits: the West Fork Adit in the Stillwater Valley (1975), the Frog Pond Adit above the East Boulder Mine (1980), and Anaconda's Minneapolis Adit in the Stillwater Valley (1979). The Minneapolis Adit was selected as the most suitable access point, and a major pre-production feasibility study was undertaken in 1983. Talented technical staff from all three companies came together and numerous pre-production test stopes, drifts, and raises were mined to determine if the Reef had the continuity and grade to be mined at a profit. Dilution-control procedures currently used in mining on the Reef evolved directly from what was learned during this period of test mining.

The company continued to evolve with Lac Minerals buying out Anaconda in 1985, followed by Chevron Resources and Manville buying out Lac to form a joint venture in 1993. Stillwater Mining Company became a stand-alone publicly traded company in 1994, and, most recently, MMC Norilsk Nickel of Russia bought a controlling percentage of stock in 2003.

Production has increased from a 250 TPD mine with three adits to two mines: The Stillwater Mine, currently at 1750 ore tons per day with 20 levels, over 70 miles of footwall lateral and a shaft (1995), and the East Boulder Mine (2000), currently at 1400 TPD, accessed with a 20,000 foot rail adit through the mountain front. Figures 1 and 2 summarize annual production at both mines.

## GENERAL GEOLOGY

The Stillwater Complex is an Archean, mafic to ultramafic, (Figure 3 and Figure 4) layered, sagging lopolithic igneous intrusion with an exposed thickness of 21,000 feet (Figure 5). The complex is divided into three major lithologic series. The first is the Basal Series, which is subdivided into two zones. The lower zone, referred to as the Sill-Dike Complex by Zientek (1983), and the upper zone is the Basal Bronzite (Page and Nokleberg, 1974). The Sill-Dike complex and adjacent regional metamorphic rocks (strongly contact-metamorphosed by the Stillwater Complex) host the Ni-Cu deposits. Next in the stratigraphic sequence is the Ultramafic Series which is also subdivided into two zones. The lower zone is the Peridotite or Harzburgite Zone (Page & Nokleberg) and the upper zone is the Upper Bronzite Cumulate. The Peridotite Zone hosts the thirteen chromite

Fig. 1. STILLWATER MINE TOTAL ANNUAL OUNCE PRODUCTION

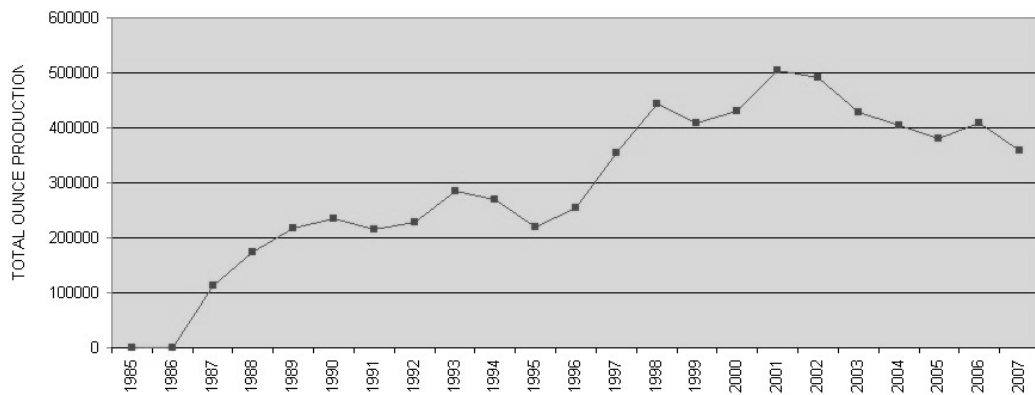
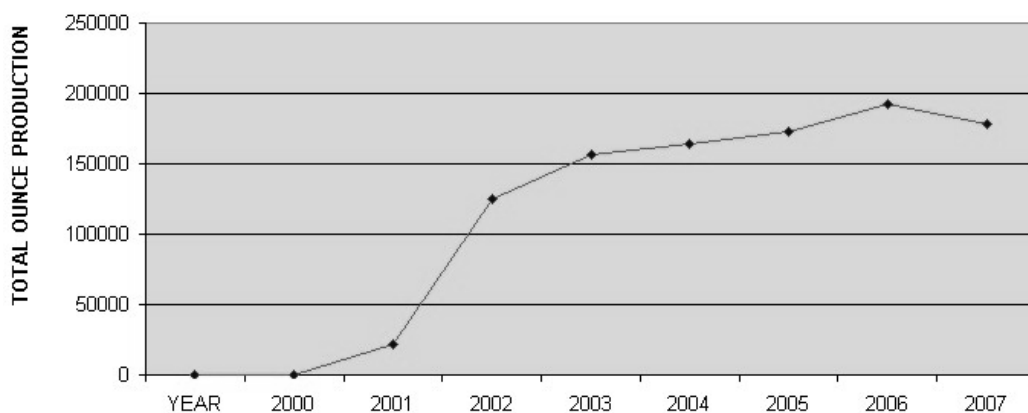


Fig. 2. EAST BOULDER MINE TOTAL ANNUAL OUNCE PRODUCTION



Stillwater Mining Company			
Proven & Probable Reserve Summary as of December 31, 2007			
	Tons	Ounces	Grade
<b>Stillwater Mine</b>			
Proven	2,783,572	1,795,640	0.65
Probable	14,360,013	8,790,632	0.61
<b>Proven &amp; Probable</b>	<b>17,143,585</b>	<b>10,586,272</b>	<b>0.62</b>
<b>East Boulder</b>			
Proven	2,016,758	920,931	0.46
Probable	20,867,838	9,660,252	0.46
<b>Proven &amp; Probable</b>	<b>22,884,596</b>	<b>10,581,183</b>	<b>0.46</b>
<b>Stillwater Mining Company</b>			
<b>Total Proven &amp; Probable</b>	<b>40,028,182</b>	<b>21,167,455</b>	<b>0.53</b>

Figure 3. 2007 proven and probable reserves

horizons that are mapped alphabetically as layers A through M. Most of the production has come from the G and H seams. The Banded Series comprises the remaining known 14,000 feet of Stillwater Complex, and hosts the PGM-rich J-M Reef as well as the sub-economic, PGM enriched Picket Pin Zone. The Banded series is marked by the first occurrence of cumulate plagioclase above the Basal series and has several large-scale repeated cycles of Norite/Gabbronorite/Olivine cumulates.

The J-M Reef is associated with TAZ1 (Troctolite-Anorthosite Zone 1), the first olivine-bearing rocks found above the Ultramafic Series (Todd and others, 1982). This package of rocks varies in thickness throughout the Complex. It can be very thin to absent, and up to over 400' thick with multiple layers of anorthosite and troctolite. It lies "unconformably" on gabbronorites and norites of the Lower Banded Series and is overlain by more norites. The base-metal sulfide content in TAZ1 ranges from non-existent to two percent and rarely up to five percent. The sulfide mineralization is always interstitial to the cumulate silicate minerals and can be very coarse-grained to extremely fine-grained, depending on the lithologic host. Often, a relatively fine-grained leucocratic troctolite/anorthosite within TAZ1 marks the upper stratigraphic extent (or "hanging wall") of the Reef mineralization. The base of TAZ1 is often very pegmatoidal and contains minerals such as phlogopite which are indicative of increased volatile content in the cumulate pile. The down dip extension of the Reef is cut off by a Laramide age floor thrust. Laramide age back-thrusts and high angle reverse faults also affect our mining.

Typically, the PGM mineralized portion of TAZ1 is marked by visible concentrations of the base metal sulfides pentlandite, pyrrhotite, and chalcopyrite. The major PGM-bearing minerals are the Pt/Pd/Ni sulfides braggite, cooperite, and vysotskite. The majority of the palladium, however, (approximately 80%) occurs as substitution into the pentlandite crystal lattice. Isoferroplatinum and the Pt/Pd telluride moncheite are also contributors. These PGM minerals are typically microscopic and are rarely seen in hand-specimen. The in-situ Pd:Pt ratio is very consistent throughout the explored extent of the J-M Reef at 3.5:1 at the Stillwater Mine and 3.6:1 at the East Boulder Mine. PGM mineralization, with accompanying base metal sulfides, can be found throughout TAZ1, but is most commonly found very near the "hanging wall" contact. Generally the PGM sulfide horizon is higher grade with less continuity at the Stillwater Mine versus the East Boulder Mine. Mineralization above the "hanging wall" contact is rare and usually sub-ore grade. Other than minor disseminated zones, hanging wall mineralization is usually confined to thin discontinuous olivine cumulates

#### Fig. 4. J-M Reef Mineralogy

##### Major Minerals

- Plagioclase Feldspar (bytownite)
- Orthopyroxene (bronzite)
- Clinopyroxene (augite)
- Olivine (chrysolite serpentinized with magnetite)

##### Minor Minerals

- Sulfides: pentlandite, pyrrhotite, chalcopyrite, and many Pd-Pt-bearing sulfides
- Phlogopite
- Chromite

#### Fig. 5. J-M Reef Rock Types

- **Norite**—plagioclase and brozite cumulate
- **Gabbronorite**—plagioclase, augite, and bronzite cumulate
- **Troctolite**—plagioclase and olivine cumulate
- **Anorthosite**—plagioclase cumulate
- **Dunite**—olivine cumulate

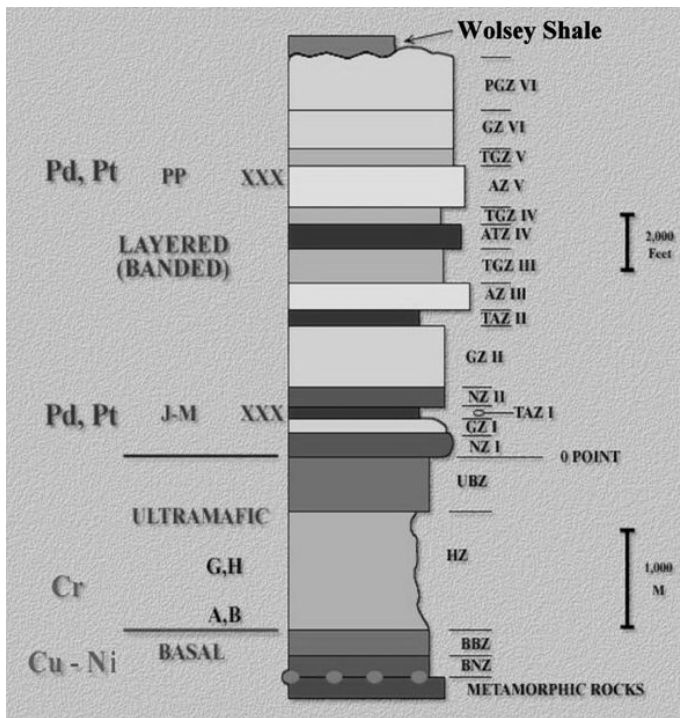


Figure 6. Stillwater Complex generalized stratigraphic column

known locally as “buckshot”, referring to the texture of the olivine cumulates grains. Sulfide mineralization can extend from the hanging wall up to 120 feet toward the “footwall” and can cross from the olivine bearing rocks of TAZ1 into the gabbronorite footwall lithologies. Sulfide mineralization is often stratiform, but rarely stratabound, and often crosscuts the igneous layered lithologies. Olivine bearing lithologies are the favored lithology for hosting ore, but significant amounts of ore are found in anorthosite, as well. The largest ore bodies (known locally as “ballrooms”) are often hosted dominantly in footwall gabbronorite (Figure 6).

## THE GEOLOGY DEPARTMENT AT THE STILLWATER MINE

The Geology Department at the Stillwater Mine has several roles. The Geology Department works with the Engineering Department in directing primary development and the design of production headings. The department works with Mine Operations, directing the diamond drilling for development and production drilling programs, monitoring material handling,

and grade control (directing the production miners at each production heading).

The Geology Department at the Stillwater Mine currently employs 24 geologists. There are four development geologists in charge of footwall infrastructure, diamond drilling and reserve definition. There are 20 underground mine geologists. The mine is divided into three areas that have development and production geologists associated with them.

## DEVELOPMENT GEOLOGY

The development geologists have many responsibilities at the Stillwater Mine that include both development and production.

Primary development at the Stillwater Mine involves mining the main travel ways, known as Footwall Laterals, throughout the mine. Footwall laterals are designed to be one hundred feet south of the Reef. The Development geologists design diamond drill programs that guide the primary development at the Stillwater Mine. These diamond drill programs drill ahead of the face at the end of the Footwall Laterals (probes), and at oblique angles to the Reef (Reef touches). The purpose of these drilling programs is to determine the position of the Reef and look for geologic surprises before the Footwall Lateral advances, which would necessitate a redesign of the Footwall Lateral (Figure 7).

In conjunction with development drilling programs the development geologists conduct geologic mapping along the Footwall Laterals. The main purpose of geologic mapping the Footwall laterals is to look for major geologic structures that could impact the position of the Reef (Figure 8).

On the production side, the development geologists are responsible for identifying mineable reserves. This is accomplished with definition drilling programs. Definition drilling at the Stillwater Mine is designed at fifty-foot intervals horizontally and to intercept the Reef at fifty-foot intervals vertically to define reserve



Figure 7. Grade –Thickness (opt-ft) contour of J-M Reef at Stillwater Mine (10'x 10' blocks)

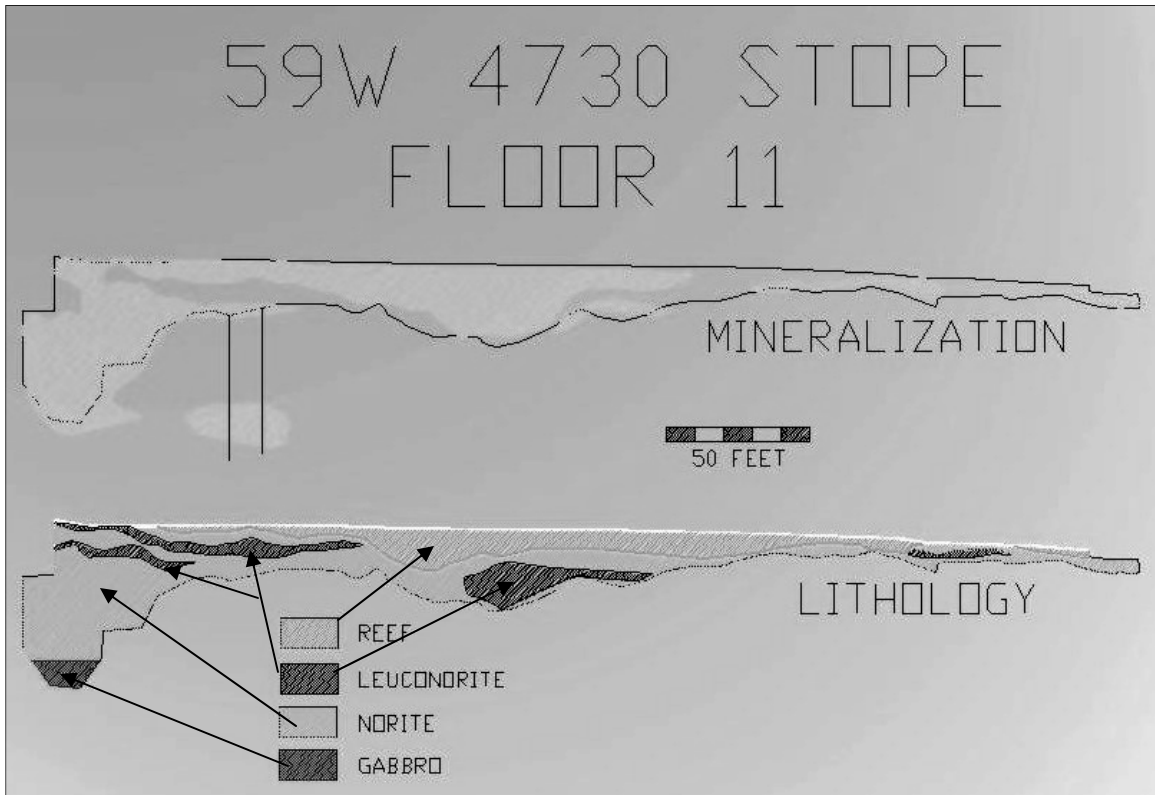


Figure 8. Comparison of lithology and mineralization

blocks (Figures 9 and 10). Total drilling footages are approximately 400,000 feet per year at The Stillwater Mine and approximately 180,000 feet at the East Boulder Mine. Forty to sixty percent of the definition diamond drill holes at the Stillwater Mine make cutoff grade producing stopes at an in-situ grade of 1.0 opt compared to the East Boulder Mine where seventy to eighty percent of the definition holes make cutoff grade at an in-situ grade of 0.65opt.

The development geologists log the majority of the core generated by both development and definition drilling programs and the production geologists log the remainder. Core is logged for lithology, mineralization, structure, and geotechnical properties. The drilling data is entered into a database and downloaded into a three-dimensional modeling program. The development geologists are responsible for the geologic interpretation and production of cross sections. A geologic model is generated from the cross sections, and from the model, reserves are calculated.

## **PRODUCTION GEOLOGY**

The production and mine geologists are intimately involved in the planning and mining of the Reef.

Once a mineable reserve, or stope block is defined, the production geologists, in conjunction with production engineers, design the mining plan for the reserve block. Based on the model and the individual diamond drill holes, the production geologists determine the ore width and grade of the block. The production engineers determine the most economical mining method to be used based on this information. From this information production forecasting can be accomplished (Figure 11).

Within the production group are the mine geologists, also known as grade control geologists. The primary function of these geologists is to directly guide the mining of the Reef. They are responsible for keeping each working

heading in the mineralized zone, in the correct stratigraphic position through waste gaps and structural offsets, define the geometry of the ore zone, minimize waste, and maximize recovery of the reserve (Figures 12 and 13.)

This is accomplished with knowledge of the definition diamond drilling and previous mining within the stope block as a guide. The decision of ore versus waste is based on visual observations of the volume and distribution of Cu/Ni sulfides, stratigraphy, and dilution at the face. The ore is very visual at both mines and has a very sharp cut off (it is either there or it's not). We use an underground visual cutoff of 0.3 opt.

At current rates of ore production (1750 tons per day (tpd)), the grade control geologists at the Stillwater Mine service seventy to ninety working mining faces. At the face the grade control geologist will make measurements of face dimensions, identify lithologies, mineralization and ore width, structures, and sample the face. From these observations, a visual estimate of the grade of the face is made and a decision is made to ship the round as ore or waste. Additional decisions made at the face include how wide to mine the face, which direction to continue mining, determining if the correct mining profile is being achieved, and whether or not the end of the stope block has been reached. Samples are primarily used for historic information since most of the important decisions are made instantly at the face.

## **ORE GEOMETRY, DILUTION, ORE DELETION, AND METAL RECOVERY CONTROL ON THE JM REEF**

The JM Reef averages six feet in horizontal width overall and, depending on mining method, up to 35% of the volume in a mining block along the strike of the Reef can be internal waste. The underground mine geologist is focused on identifying this waste and separating it from the ore stream, ensuring that it does not go to the mill. The Reef material that is mined and shipped to the mill averages eight feet wide with a grade of approximately 0.60

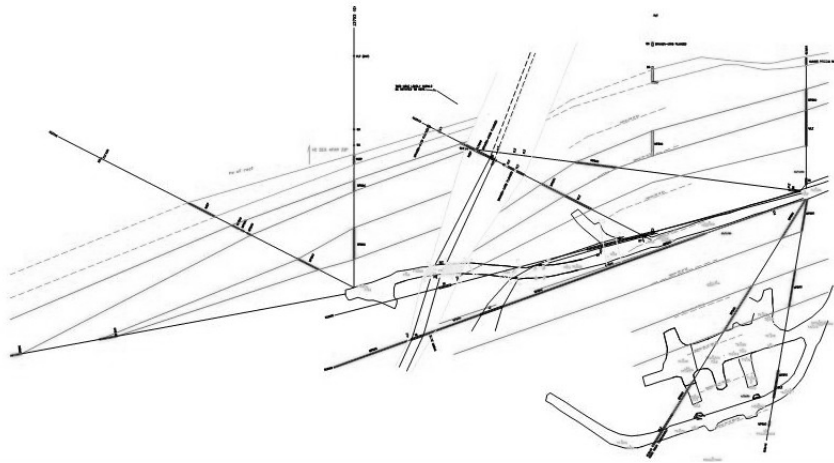


Figure 9. Probe drilling pattern

Figure 10. Combined probe and mapping results

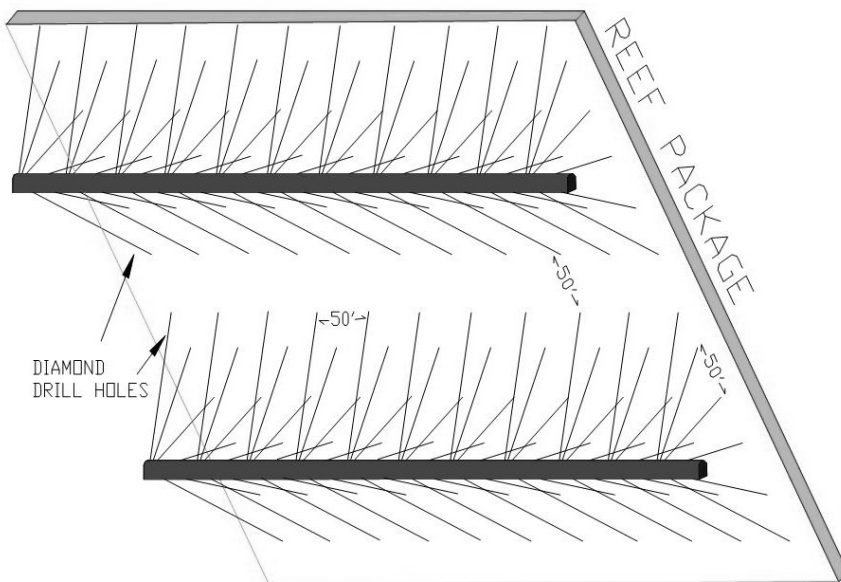
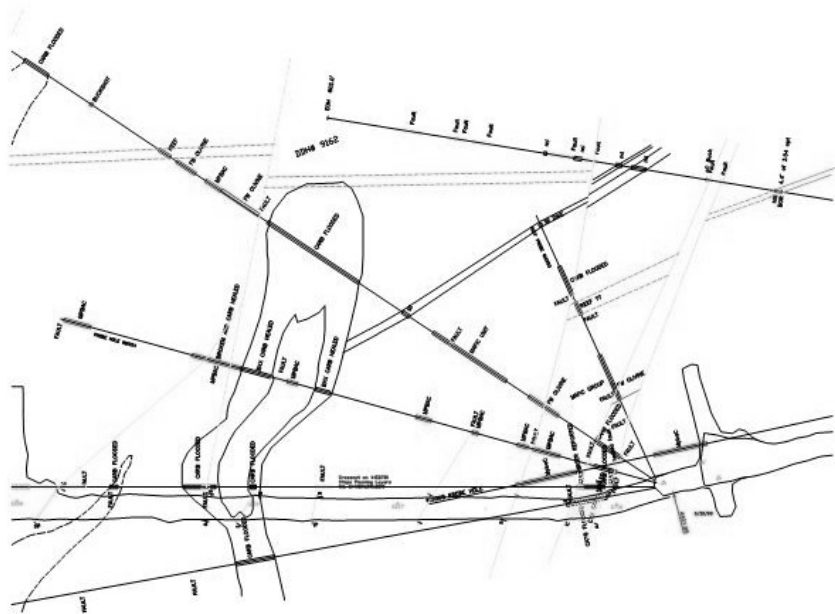


Figure 11. Typical Stillwater Mine definition drill layout

Figure 12. Typical drilling cross section

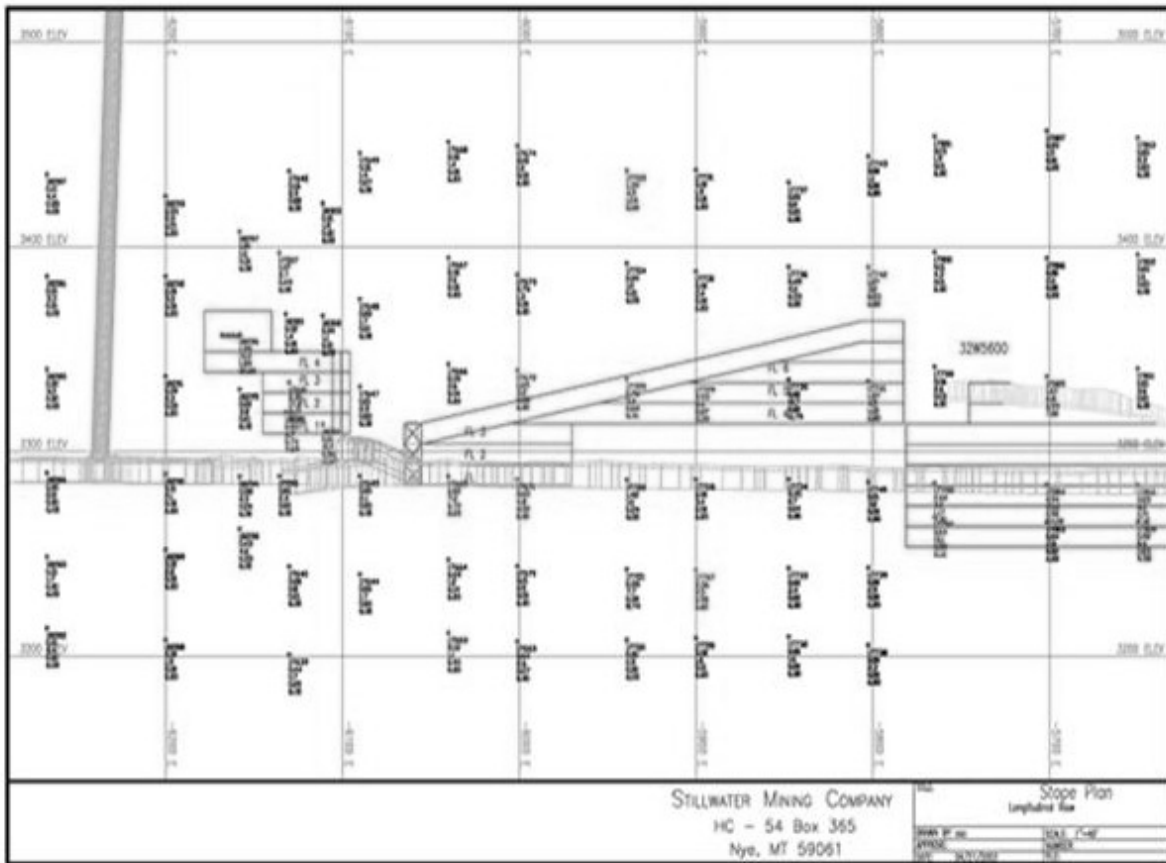
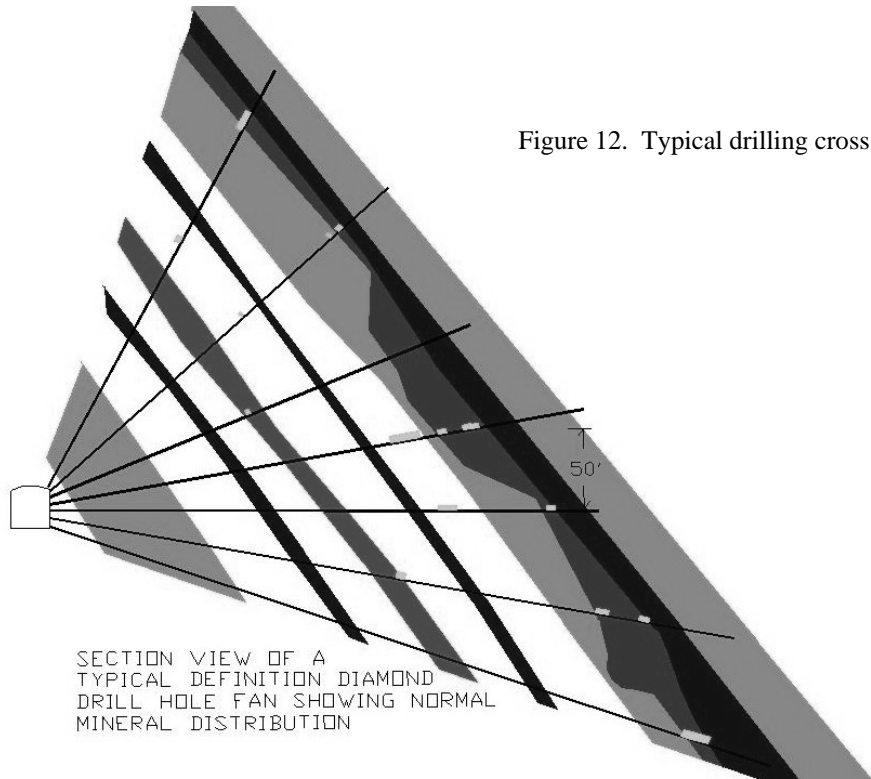


Figure 13. Example of a slope plan with drill composites

ounces per ton (opt) at the Stillwater Mine.

The geometry of the ore zone varies dramatically at the Stillwater Mine. The mined zones are very diverse structurally, lithologically, and even grade versus sulfide percentage can be complex, depending on the area of the deposit. The host lithologies and proximity to major structures will often determine the structural competency of the zone of interest, which will effect dilution (and thus grade), and mining costs.

Locally, ore zone(s) pinch and swell from less than one foot wide up to 120 feet wide. Some ore zones are very thin and have a fairly consistent, linear hanging wall, requiring maximum dilution control while others will pinch and swell radically into keel-shaped, thick deposits (Figure 14). Typically, ore zones at the Stillwater Mine do not extend more than 300 feet along strike without a waste gap of 100 feet or more.

The East Boulder ore displays more continuity, but at a lower grade. Structural complication, related to Laramide age thrusting, creates both difficulty and opportunity for successful mining. Locally the Reef can be severely sheared and displaced; in other areas the Reef can be stacked by a regional backthrust, the South Prairie Fault (Jones, et al., 1966), to create multiple stope targets. Archean diabase dikes, slightly younger than the main Stillwater Complex, will also crosscut stratigraphy and the mineralized Reef, often creating offset through simple dilution.

Dilution within a specific stope block is very ore-width dependent, and selection of the correct mining method and equipment to match all geologic parameters is crucial to extracting a high-quality ore.

Two types of dilution are routinely monitored on a daily basis, both mine-wide and within the specific stopes: mining dilution and total dilution. Mining dilution is the percentage of waste measurable at the face that is mined with the ore based on approved minimum-mining

widths for the assigned equipment. Mining dilution is somewhat controllable and is dependent on mining practices. Total dilution is the amount of in-situ waste measured at the face compared to the ore width. Total dilution is not controllable and is dependent on the width of the orebody. Dilution targets are six percent mining dilution and eighteen percent total dilution. If the mining dilution is low, but the total dilution is high, consideration is given to reducing the equipment size. Mine plans must stay flexible to accommodate unforeseen changes in the geology.

Controlling dilution and maximizing ounce recovery is the primary economic focus. Numerous factors can affect dilution when mining. These range from the correct choice of equipment size for the orebody, geologic factors that destabilize lithologic units outside of the orebody, to poor mining practices. Even geologists can contribute to dilution by not recognizing stratigraphy or sulfide mineralization present in the face. Other factors that affect dilution downstream from the mining face are improper material handling such as mixing of muckpiles, ore shipped as waste or vice versa, improper stope clean out - either leaving ore behind (especially against hanging wall) or taking excessive backfill.

Deletion - leaving ore - is a concern with sublevel panels, mining at the incorrect stope profile, and stopes where the hanging wall dips at a shallow angle. In the sublevel panels the actual ore distribution cannot be evaluated as they are spaced approximately thirty-five feet apart vertically. Stopes that are not mined to the correct profile - at the dip of the hanging wall, can cause deletion and dilution (see Figure 12). Where the hanging wall has a shallow dip, the stope cannot be mined at the dip of the hanging wall due to equipment restraints.

## **MINING METHOD SELECTION**

The selection of mining methods is based on geology, geometry of the orebody, and ground conditions. Many factors play a part in mining method selection such as ore widths, lateral

extent of the ore, dip of the hanging wall, ground conditions, and even the skill of the miners, which tends to change over time. Engineering will design two alternatives and run the costs of those mining methods against the reserved ounces. The intent is to select the most appropriate method for economic exploitation of the orebody.

The JM Reef is a narrow-vein type of orebody. Mining originally started out (1985-1990) being very selective with 100% slusher stopes (cut and fill). In the early days, most of the miners were from the Silver Valley in Idaho and were very skilled at captured cut-and-fill overhand (slusher) mining (Figure 15). More productive methods were tested and utilized as the mine evolved. Sublevel open stoping (Figure 16), ramp-and-fill (Figure 17), and underhand methods utilizing paste (Figure 18), have been added to the mining methods utilized when needed. With the addition of these other methods, mining widths increased. The result is more tons are mined with a subsequent decrease in ore grade at the mill, as the in-situ grade does not change dramatically. This also causes an increase in the waste to ore ratio and possibly deletion of the resource depending on the economics of the mining method. However, the trade-off is an increase in overall productivity due to higher individual stope production and quicker cash flow.

Secondary waste development for access ramps associated with the various mining methods also increases mining costs.

## **MINING METHODS**

Stillwater mining method percentages based on 2007 production numbers:

- 51% ramp-and-fill – designed for larger ore bodies that will support a ramp system
- 32% sublevel extraction – designed for flatter hanging wall dips and fairly consistent ore type
- 17% captured cut and fill - targeting narrow ore bodies without large extent.

In summary, the J-M reef provides many challenges and opportunities, both for the underground mine geologist and production staff.

## **REFERENCES**

Todd, S.G., Keith, D.W., LeRoy, L.W., Schissel, D.J., Mann, E.L., and Irvine, T.N., 1982, The J-M platinum-palladium reef of the Stillwater Complex, Montana: I: stratigraphy and petrology: *Economic Geology*, v. 77, no. 6, p. 1454-1480.

Page, N.J., and Nokleberg, W.J., 1974, Geologic map of the Stillwater Complex, Montana: U.S. Geological Survey Miscellaneous Investigations Series Map I-797.

Peoples, J.W., Howland, A.L., and Sampson, E., 1936, The Stillwater Igneous Complex and associated occurrences of nickel and platinum group metals: Montana Bureau of Mines and Geology, *Miscellaneous Contributions No. 7*.

Zientek, M.L., 1983, Petrogenesis of the Basal Zone of the Stillwater Complex, Montana: PhD dissertation, Stanford University, Stanford, California, 229 p.

*Figs. 14-20 are on following pages.*

Figure 14. Typical mining face showing mineralization and dilution

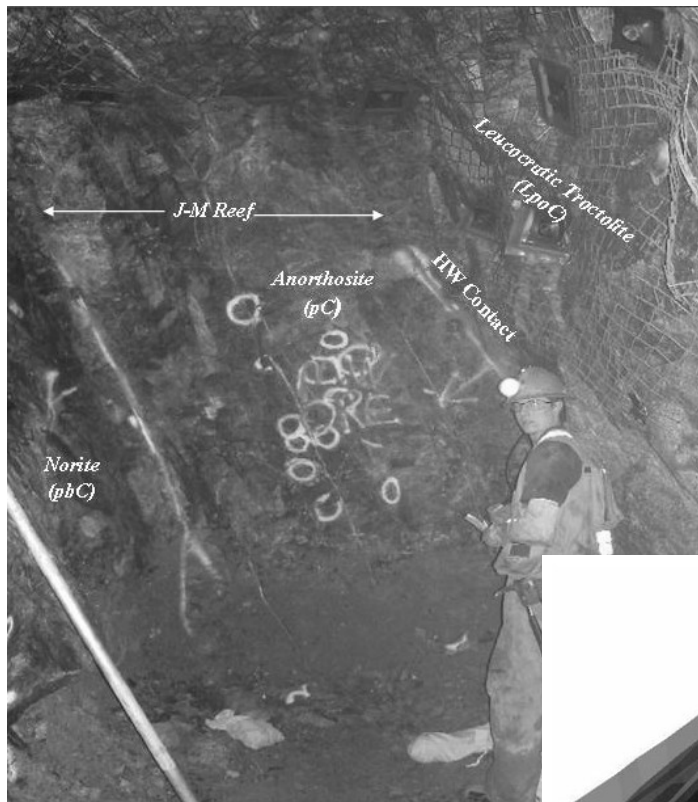
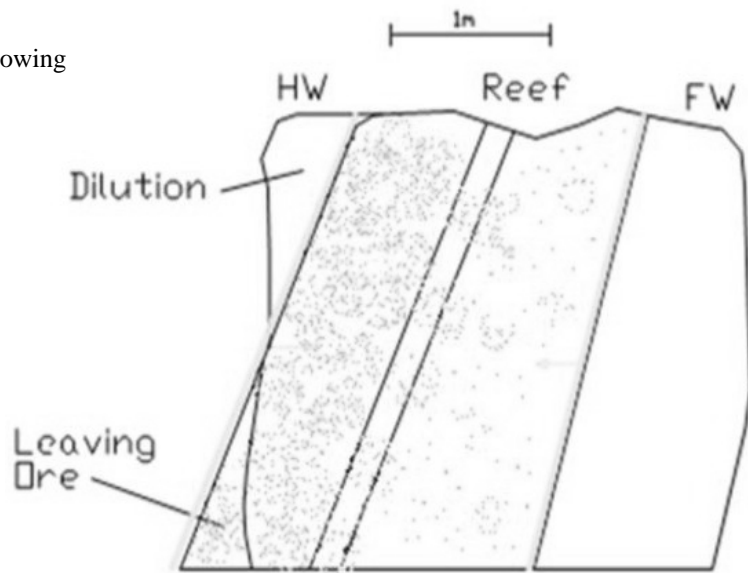


Figure 15. Photo of underground geology mark up of J-M Reef

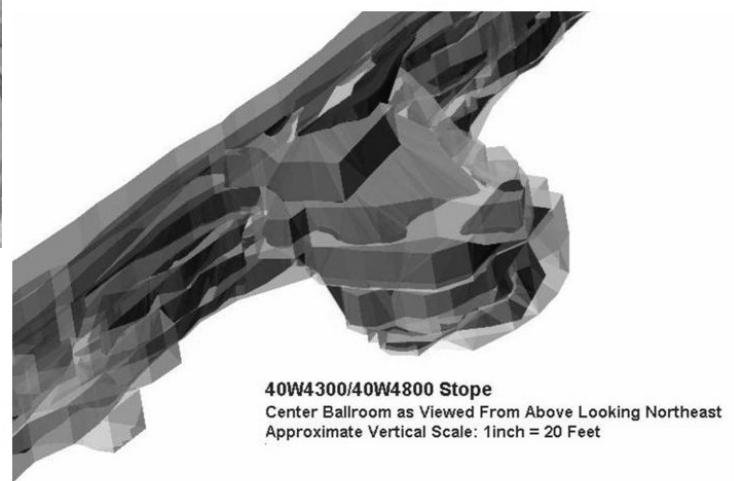


Figure 16. 3-D model of "Ballroom" on J-M Reef

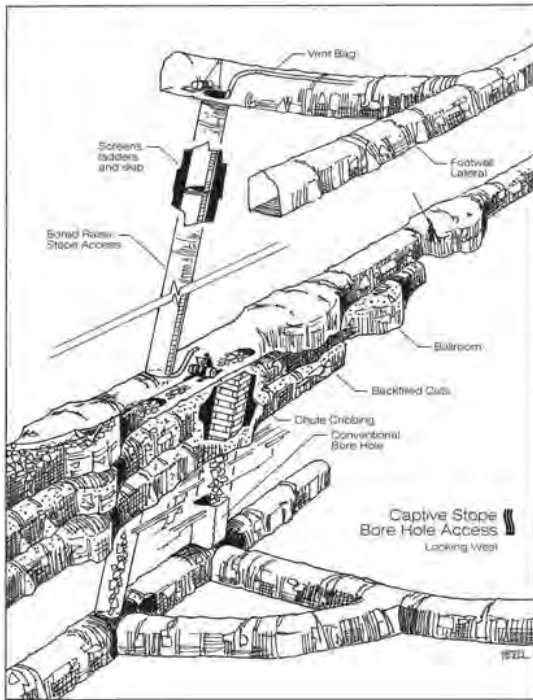


Figure 17. Captive mining method

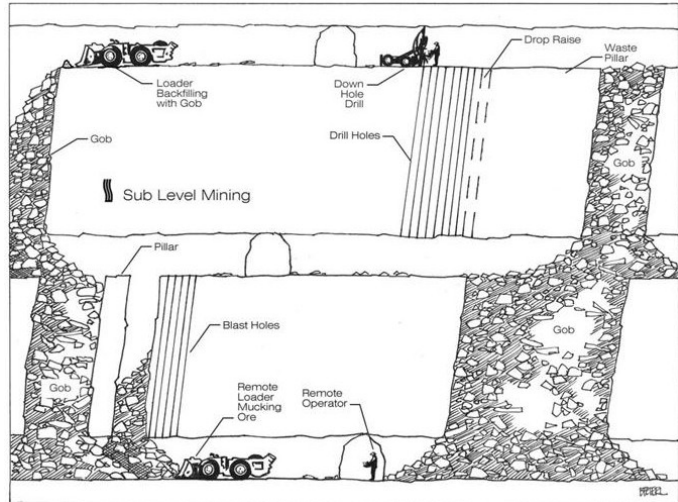


Figure 18. Sub-level mining method

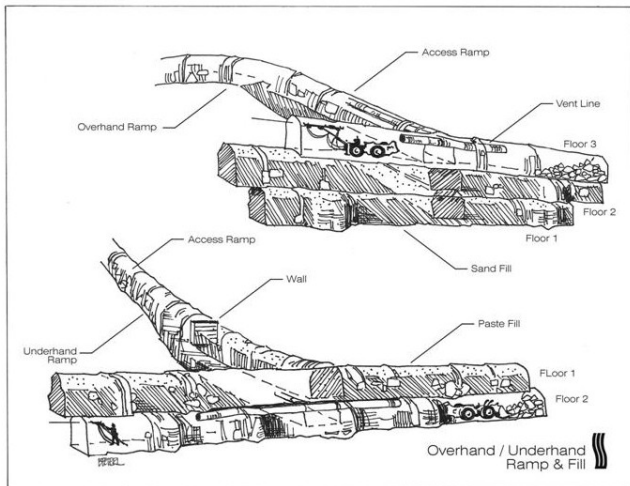


Figure 19. Overhand ramp and fill mining method

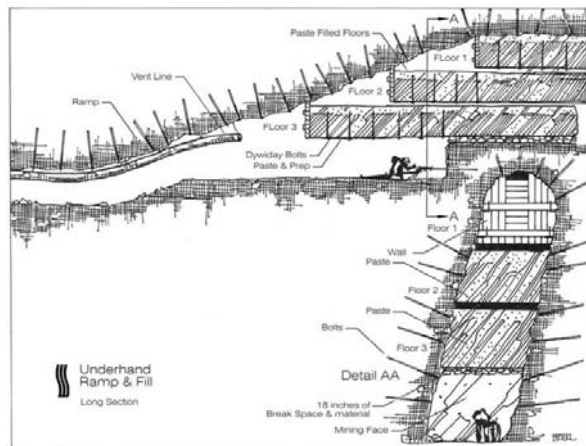


Figure 20. Underhand ramp and fill mining method

# **FIELD GUIDE: PALEOSEISMITES: INDICATORS OF LARAMIDE TECTONISM AND OTHER EVENTS NEAR THE BIGHORN BASIN, MONTANA AND WYOMING**

**Mervin J. Bartholomew**

*Department of Earth Sciences, University of Memphis, Memphis, Tennessee 38152*

**Kevin G. Stewart**

*Dept. of Geological Sciences, Univ. of North Carolina at Chapel Hill, Chapel Hill, NC 27599*

**Donald U. Wise**

*Department of Geosciences, University of Massachusetts, Amherst, MA 01003*

**Heather A. Ballantyne**

*Dept. of Geological Sciences, Univ. of North Carolina at Chapel Hill, Chapel Hill, NC 27599*

---

## **ABSTRACT**

Paleoseismites within the Linley Conglomerate and Tongue River members of the Fort Union Formation of the Bighorn Basin are records of individual tectonic events related primarily to late Paleocene uplift of the Beartooth Mountains. Older paleoseismites within the Elk Basin anticline reflect late Cretaceous tectonism there and some younger seismites reflect Eocene tectonism north of Heart Mountain. Clastic dikes are perhaps the most widely recognized sedimentary feature which is easily associated with paleo-earthquakes, but different types of paleoseismites are related to two factors: the distance from the earthquake; and the sedimentary facies in which the seismites were generated. This field trip will visit sites with different types of paleoseismites (e.g., big-slab debris flows, convolute bedding, diapirs, and ball and pillow structures) and discussions will include their relationships with sedimentary facies as well as the likely source areas of paleo-earthquakes that produced them during uplift of the Beartooth Mountains and the Elk Basin anticline.

## **INTRODUCTION**

This field trip and our field trip for the 2007 Geological Society of America annual meeting (Stewart et al., 2008) represent our first publica-

tions about ancient seismites of the Bighorn Basin which are associated with Laramide uplift of the Beartooth Plateau and Elk Basin anticline. We previously discussed aspects of this ongoing work at a GSA meeting (Ballantyne et al., 2004; Bartholomew et al., 2004; Stewart et al., 2004). Some of these ancient seismites occur in areas mapped by students at the YBRA, although they were not the focus of student work. Hence, they came to our attention while working at the YBRA. Part of that work involved seeing new exposures of the Linley Conglomerate and the Tongue River Member of the Fort Union Formation in the YBRA-Red Lodge area, visiting localities described by DeCelles et al. (1991), and recognizing the diverse types of ancient seismites in different sedimentary facies of these units (Table 1). This work builds our work on ancient seismites in other areas (Bartholomew and Rich, 2007; Bartholomew and Stewart, 2001; Bartholomew et al., 2002a, b; Stewart et al., 2002; Wooten et al., 2001). Part of that work also involved numerous discussions of the structure of the Red Lodge corner (e.g., Foose et al., 1961; Wise, 2000) of the Beartooth uplift, which is an integral part to the understanding of how some of these paleoseismites formed. Eventually we hope to be able to correlate specific sets of paleoseismites across large areas which will enable us to determine the frequency of events

Type of soft-sediment deformation feature	Age/Formation	Lithology	Location	Facies
<b>Debris flows</b>	Paleocene Fort Union Formation-Linley conglomerate member.	Poorly sorted, matrix-supported carbonate cobbles and boulders.	Adjacent to mountain front, field trip stops # ?	Proximal alluvial fan
<b>Clastic dikes and sills</b>	Paleocene Fort Union Formation-Tongue River Member; Cretaceous Eagle Formation.	Interbedded sandstone, mudstone, and conglomerate (Fort Union Fm.) Interbedded shale, sandstone, and coal (Eagle Fm.)	Field Trip stops ?? (Fort Union Fm.); Field trip stops ?? (Eagle Fm.)	Mid-fan (Fort Union); Alluvial plain (Eagle Fm.)
<b>Convolute bedding, ball-and-pillow structures, diapirs</b>	Paleocene Fort Union Formation-Tongue River Member; Cretaceous Eagle Formation.	Interbedded sandstone, siltstone, and shale.	Field trip stops ???	Distal fan (Fort Union Fm.); alluvial plain (Eagle Fm.)

Table 1. Types of paleoseismites found in different lithologies of rock units.

and the “felt” regions for specific paleo-earthquakes and thus constraining the epicentral areas for different groups of paleo-earthquakes (McCalpin, 1996; Wheeler, 2002; Obermeier et al., 2002).

Our recent GSA field trip (Stewart et al., 2008) in this area focused on the relationship of different types of paleoseismites to the sedimentary facies in which they occur. On this field trip we shall also discuss that topic along with the relationship between the seismites and the Beartooth fault and its ramp, which is the suspected paleohypocenter-region when the fault was active. We will examine paleoseismites at sites in south-central Montana and northwestern Wyoming in the: 1) late Paleocene Linley Conglomerate and Tongue River members of

the Fort Union Formation, which are associated with the Laramide uplift of the Beartooth Mountains (DeCelles et al., 1991; Foose et al., 1961; Wise, 2000; Stewart et al., 2008); 2) Late Cretaceous (Campanian) Virgille sandstone in the Eagle Formation in the core of the Laramide Elk Basin anticline (Engelder et al., 1997; Stewart et al., 2008); and 3) Eocene Willwood Formation (Stewart et al., 2008).

## PALEOSEISMITES

Paleoseismites are features formed in soft sediments (e.g., liquefaction features, slumps and landslides) which are caused by shaking during paleo-earthquakes (Obermeier, 1996a, Seilacher, 1984) and hence are indicators of the “felt” area of ancient earthquakes (McCalpin,

1996; Wheeler, 2002). Distinguishing paleoseismites from similar features produced by nontectonic processes such as loading or slumping can be difficult (Wheeler, 2002; Mills, 1983; Obermeier, 1996a; Pope et al., 1997). We prefer to use the term paleoseismites for “suspect” soft-sediment deformational features when they are in regional and/or stratigraphic association with partially fluidized beds and/or clastic dikes (e.g., Stewart et al., 2002) which are generally regarded as the best evidence of strong seismic shaking (Tuttle and Seeber, 1991; Bourgeois and Johnson, 2001; Obermeier, 1996a). Clastic dikes (Figure 1A, B) are often associated with sandblows (Figure 1A) which are a common indicator of the epicentral area of a large earthquake. After eruption, sandblows are typically unconformably truncated by overlying sediments that post-date the seismic event. A few Cretaceous features within the Elk Basin anticline likely represent sandblows (Figure 1C), but ancient sandblows are generally lacking in Paleocene strata proximal to the Beartooth uplift.

Some dikes are planar with preferred orientations (Figure 1A, B). In extensional tectonic settings, these dikes can be interpreted as having been injected along pre-existing joints and, coupled with other fracture data, can provide an excellent

indicator of the orientation of the regional horizontal extension direction (e.g., Bartholomew et al., 2002a, b; Stewart et al., 2002). However, many Paleocene dikes that we have observed near the Beartooth uplift, did not follow planar fractures upward, did not break the paleosurface as sandblows, and commonly taper upward (Figure 1D). Their orientations may exhibit preferred di-

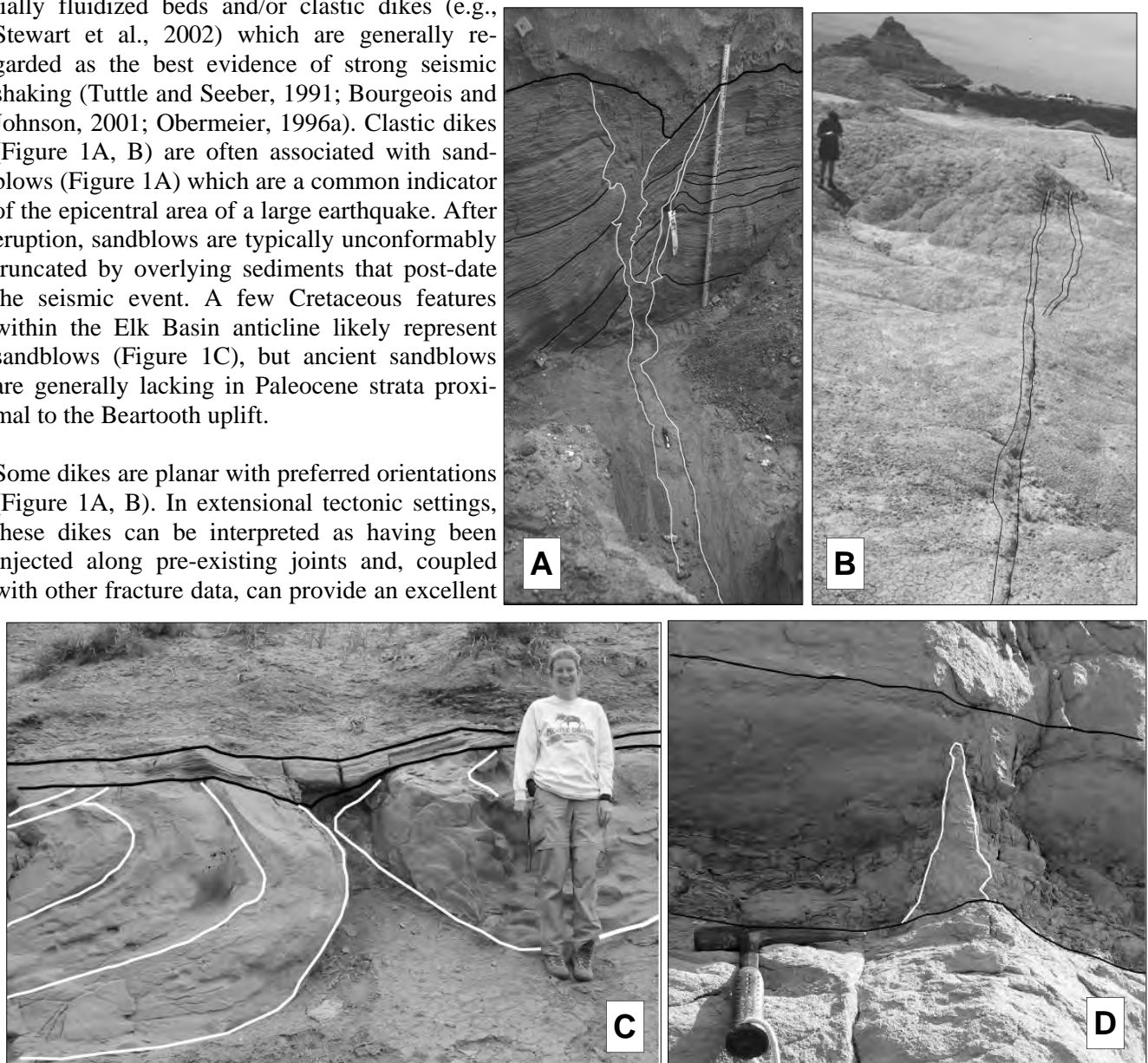


Figure 1. **A:** Planar clastic dike intruded through folded strata at the base of a small Late Pleistocene sandblow-vent near the main fault in trench across the Lima Reservoir fault in the Centennial Valley, MT (6 on Figure 2) (Bartholomew et al., 2002); **B:** Planar clastic dikes intruded along joints in the Oligocene White River Formation in the Badlands, SD first noted by Lawler (1923); **C:** Soft-sediment folds flanking a sandblow-vent in the Late Cretaceous Virgille sandstone in the Eagle Formation in the Elk Basin anticline (2 on Figure 2); **D:** Typical upwardly tapering, Paleocene clastic dike in the Tongue River Member of the Fort Union Formation (4 on Figure 2) near the Beartooth uplift.



Figure 2. Location map (modified from physiographic map in Renfro and Feray, 1972) showing some paleoseismite locations in southern Montana and northern Wyoming. Shading indicates relative age from black (older) to white (younger). 1—Pennsylvanian; 2—Late Cretaceous; 3 and 4—Late Paleocene; 5—Late Eocene; 6—Late Quaternary; 7—historic, 1959 Madison Canyon slide.

reactions locally within one or more beds, but do not appear to be systematic over a large area. These dikes can be interpreted as evidence of hydrofracturing, i.e., high fluid pressure in a bed forcefully injecting sand into the overlying sediment. Stewart et al. (2008) suggest that these orientations may have a relationship to fan-geometry, i.e. a large-scale sedimentary feature. Hence, these dikes may be more like sandblows whose distribution and orientations were influenced by features such as ancient beaches during the 1886 Charlestown, SC, earthquake, or by stream banks and ancient meander-patterns along the Mississippi River during the 1811-1812 New Madrid earthquakes (Obermeier, 1996b) and therefore, these dikes and sandblows may not reflect the regional stress field. If fan-slope and fan-geometry influence dike-orientations, then we may be able

to decipher some relationship between dikes and fan-location by comparing dike-orientations and flow-directions in liquefied beds (Figure 3A) which should reflect slopes in different parts of the fan.

Soft-sediment folds (convolute bedding) and/or disrupted chaotic deposits can result from liquefaction or seismic shaking as well as from non-tectonic causes. Obviously, there are flow or slide features that we know are seismites because they actually formed during a historic earthquake, e.g., the Madison slide (Figure 3B) which formed Quake Lake during the 1959 Hebgen Lake earthquake (7 on Figure 2), but recognition of such a single landslide or one bed with convolute bedding (Figure 3C) as a paleoseismite in the stratigraphic record is difficult if it is not associated with other features

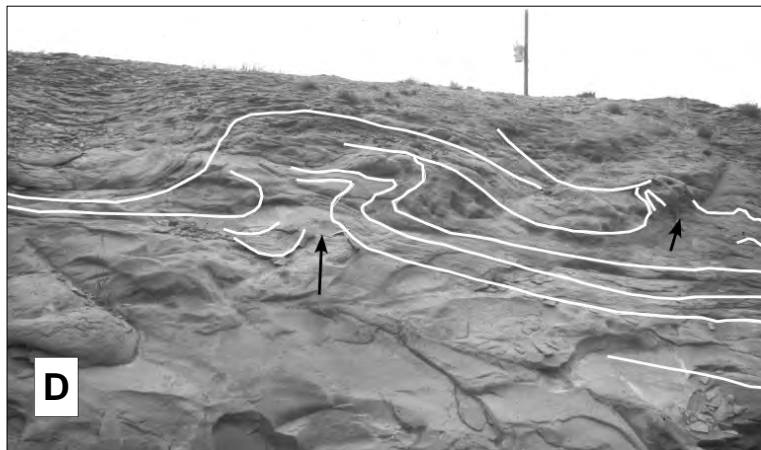
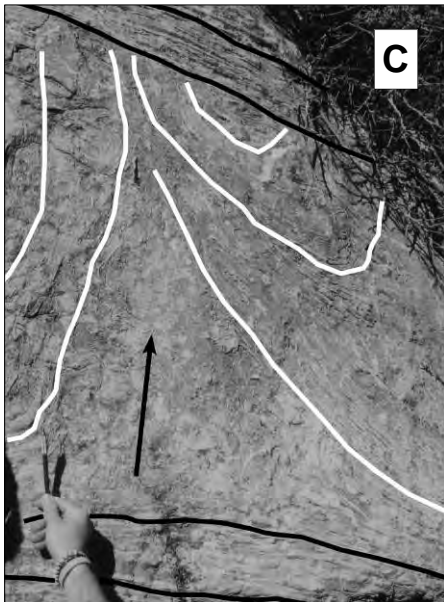


Figure 3. **A:** small soft-sediment folds exhibiting a consistent direction of flow of top-to-north flow in overturned crossbedded sandstone in the Tongue River Member of the Fort Union Formation (4 on Figure 2); only top part of bed (right of dashed line) was liquefied; **B:** Madison Canyon landslide which blocked the Madison River to form Quake Lake in 1959 (7 on Figure 2); **C:** Soft-sediment deformation (paleoseismite?) in crossbedded layer of Tensleep sandstone, Crazy Woman Canyon, Big Horn Mountains, Wyoming (1 on Figure 2); arrow indicates upward flow (photograph by Randy Cox); **D:** Large soft-sediment folds in Bull Mountains (3 on Figure 2); arrow indicates upward flow; telephone pole in background for scale.

(e.g., clastic dikes). Some paleoseismites (e.g., convolute bedding, ball and pillow structure) might not be associated with clastic dikes, but are features found repeatedly in a stratigraphic sequence, such as in the Tongue River Member of the Fort Union Formation of the Bull Mountains (Figure 3D). Regionally this same unit contains abundant paleoseismites associated with the Beartooth uplift (Stewart et al., 2008), hence, similar features in the Bull Mountains suggest that large earthquakes occurred there as well. The absence, so far at least, of recognized paleoseismites between the Bull Mountains and the Beartooth Mountains precludes interpreting Bull Mountains paleoseismites as being caused by Beartooth Mountains earthquakes. Thus, the Bull Mountains area must be near a fault that was active during the Late Paleocene.

Convolute bedding and debris flows (or landslides) are the most common paleoseismites within the Tongue River Member, but they occur in different sedimentary environments (Stewart et al., 2004, 2008; Ballantyne and others, 2004) relative to the source-region of paleo-earthquakes on faults beneath the Beartooth uplift (Bartholomew and others, 2004). Debris flows and landslides are in the upper portions of alluvial fans proximal to the rising mountain front and convolute bedding is common in the distal portions of alluvial fans (Table 1). Not all liquefaction results in significant lateral flow. Within the distal portion of fans as well as in fluvial deposits of the main valley, well away from the earthquake source region and from steep slopes of the upper fans, liquefaction typically produces small in situ diapirs (Figure 4A) and ball and pillow structure (Figure 4B) – features formed by vertical flow with little lateral flow.

We have documented their occurrence in syntectonic alluvial fans, described by DeCelles et al. (1991), who suggested that they were caused by paleo-earthquakes. Paleoseismites occur from the mouth of Clark Canyon northward to Red Lodge and then northwestward to near Nye (Figure 2). Three types of paleoseismites occur in this area: 1) clastic dikes and sills, which are indicative of forceful

injection of liquefied sediments; 2) large and small convolute-bedding features (flow-folds but also including diapirs and ball-and-pillow), which are indicative of dewatering and lateral flow; 3) debris flows (or landslides) with large blocks, which are indicative of mobilization by severe seismic shaking.

## **TECTONICS OF THE RED LODGE CORNER**

Mapping the Fort Union Formation in the foot-wall of the Beartooth fault in the Red Lodge corner (Figure 5) helps to constrain structural interpretations of the emplacement of structures associated with that fault. It also helps to constrain the location of the complex ramp structure which would have been where hypocenters may have been the source for strong paleo-earthquakes would have been located during the late Paleocene. Wise (2000) outlined many structural characteristics of this corner, some of which date back to the classic mapping done by Foose et al. (1961). These include:

1. northwest of the Willow Creek fault, the near-vertical Paleozoic sedimentary section is “pinned” to basement;
2. south of the Maurice fault, the steeply dipping Paleozoic sedimentary section is also “pinned” to basement;
3. between the Willow Creek and Maurice faults, the internally faulted Paleozoic sedimentary section is bounded by faults (herein called the Towne Point duplex) which separate it from the structurally overlying basement and the structurally underlying Tongue River Member of the Fort Union Formation (or laterally equivalent Linley Conglomerate Member);
4. a fracture zone to the southwest of the Towne Point duplex between the faults marks a hinge in the basement hanging wall above the duplex;
5. the steeply NW-dipping Willow Creek fault is characterized by normal displacement rather than right-lateral strike-slip displacement as

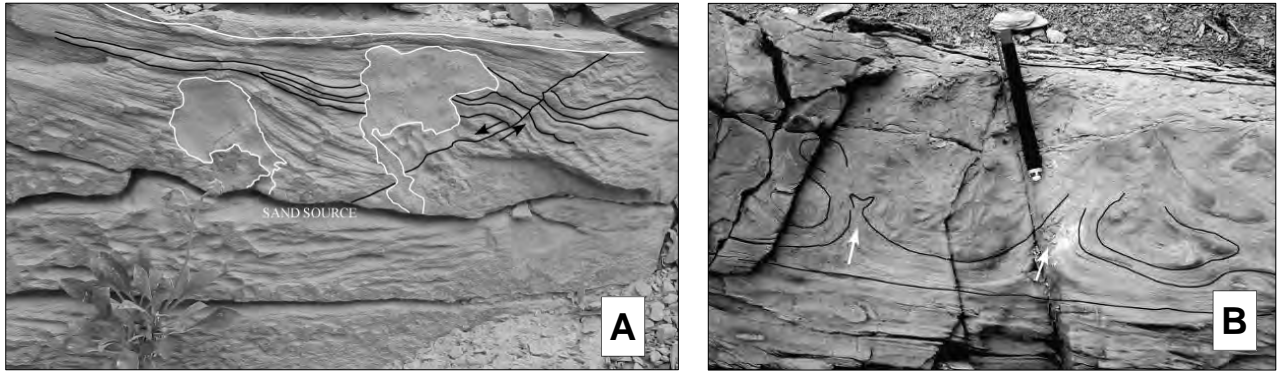


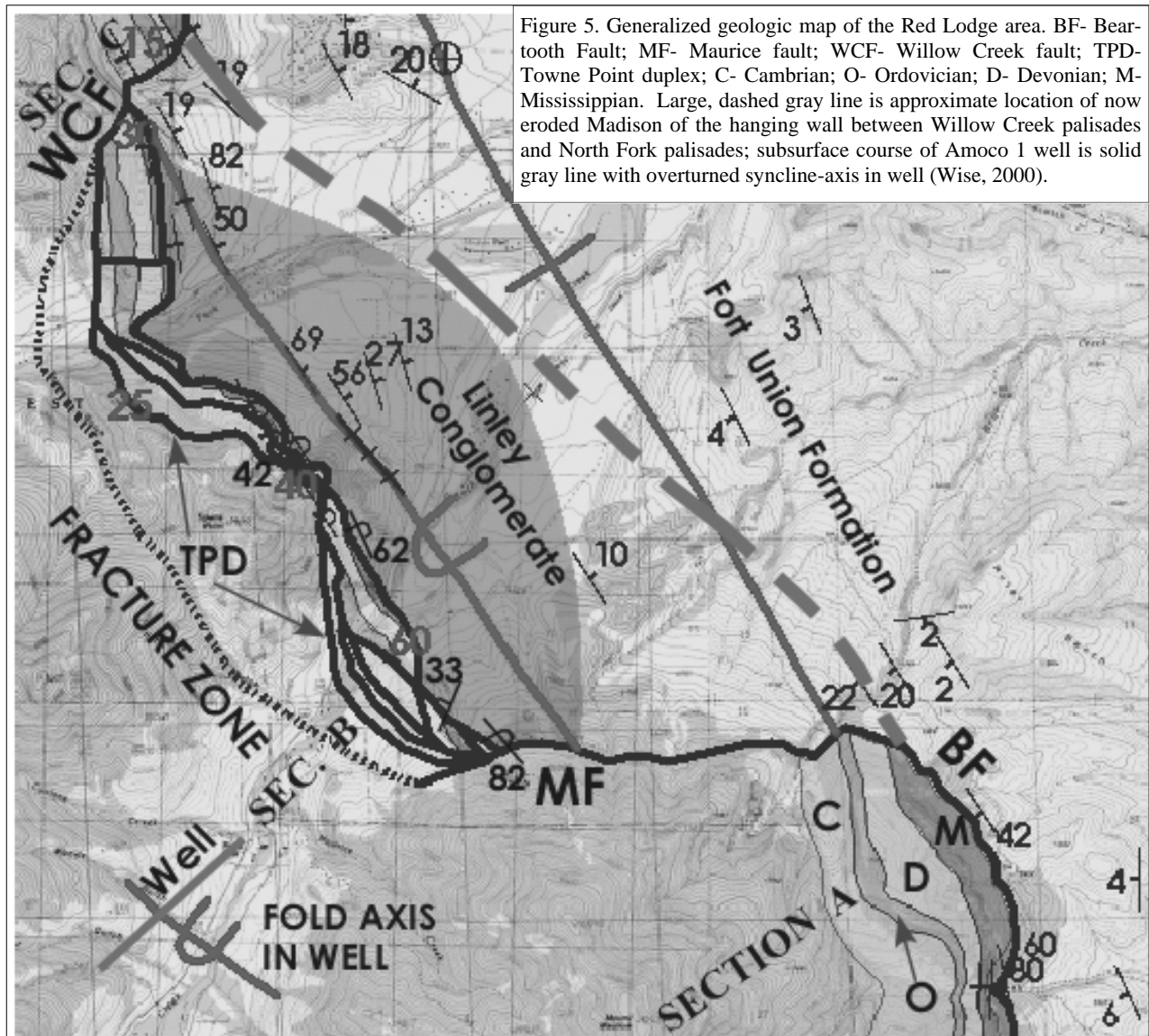
Figure 4. **A:** Small irregularly shaped clastic dikes of fine grained sand which both originated from the same source bed. These were injected with little evidence of deformation of the surrounding strata. A syndepositional normal fault is terminated upward by bedding and is cut by one diaper. **B:** Ball and pillow structure with arrows showing upward injection of fine grained sand. **C:** Outcrop of fine grained sandstone with 3 beds containing paleoseismites separated by non-deformed beds. Folds are outlined by white lines and diaper (D) is outlined in black; only the upper part of bed 1 is deformed (above dashed line).

originally inferred by Foose et al. (1961) from the apparent offset of Paleozoic strata on opposite sides of the fault;

6. by analogy, the Maurice fault is also interpreted as a steeply SE-dipping normal fault instead of a left-lateral strike slip fault as originally inferred;

7. the 1986 Amoco 1 well was drilled through basement and a fault-bounded interval of sheared, overturned sedimentary strata into a recumbent footwall syncline of Mesozoic and Paleozoic rocks; the footwall syncline has a NE-dipping axial surface which trends  $\sim N60^\circ W$ .

Bedding defines an axis of the overturned footwall syncline in the Paleocene sediments with a trend of  $\sim N30^\circ W$ , which is parallel to the axis of a broad synclinal trough farther northeast toward Red Lodge (Figure 5). Such overturned footwall synclines typically develop perpendicular to the direction of shortening, hence slip on the Beartooth fault near Red Lodge trended  $\sim N60^\circ E$  during the Late Paleocene when synorogenic alluvial fans (DeCelles et al., 1991) developed and were over ridden by the advancing Beartooth thrust (Wise, 2000). Our diagrammatic cross sections (Figure 6) depict the relationships of the alluvial fans of the footwall syncline to the exposed part of the Towne Point duplex as well as speculation on what the structure might look like beneath Mount Maurice



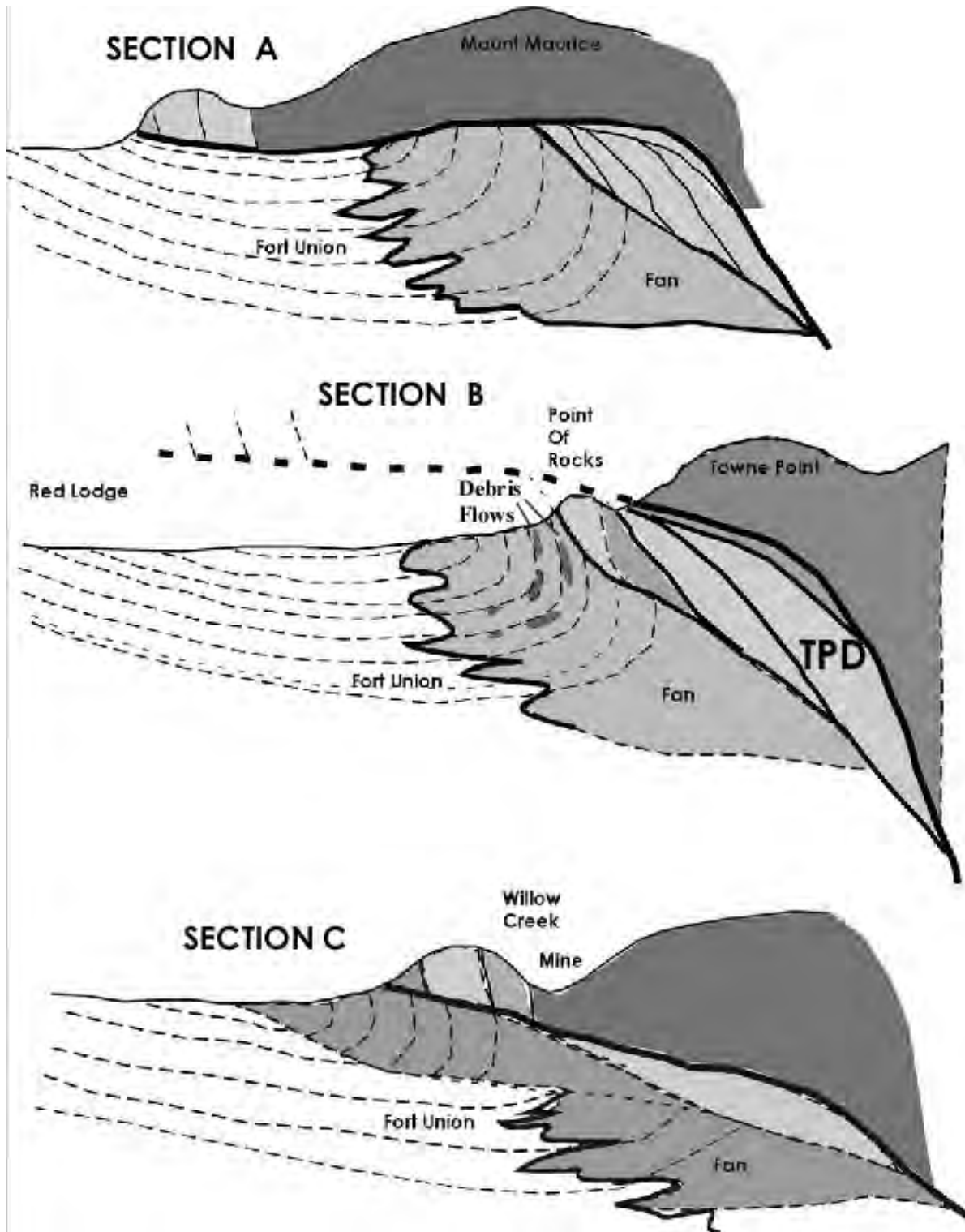


Figure 6. Diagrammatic cross sections (approximate locations shown on Figure 7) of the Red Lodge area depicting relationships among the Footwall syncline in the Fort Union Formation, the Towne Point duplex, and the hanging wall of the Beartooth fault.

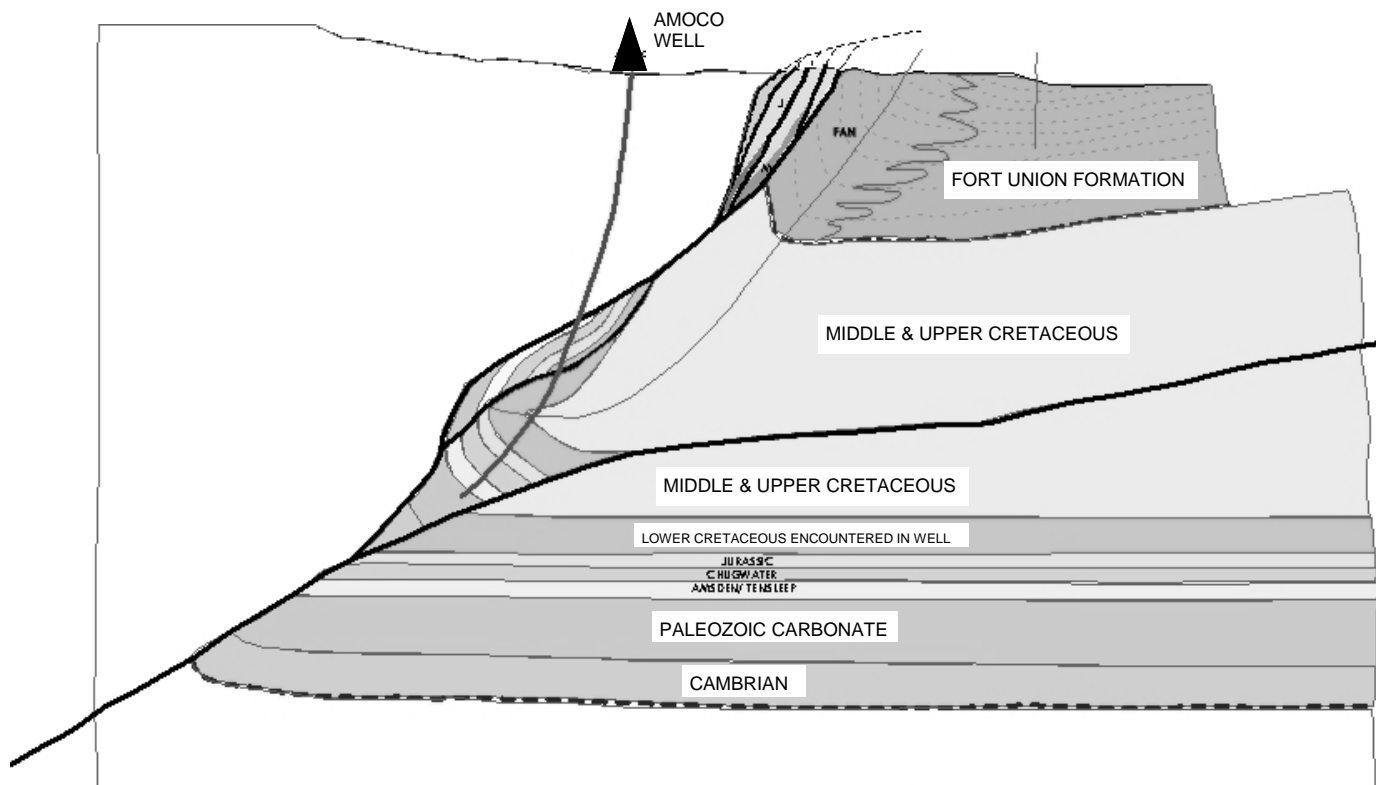


Figure 7. Cross section along the line of well-course (Figure 5).

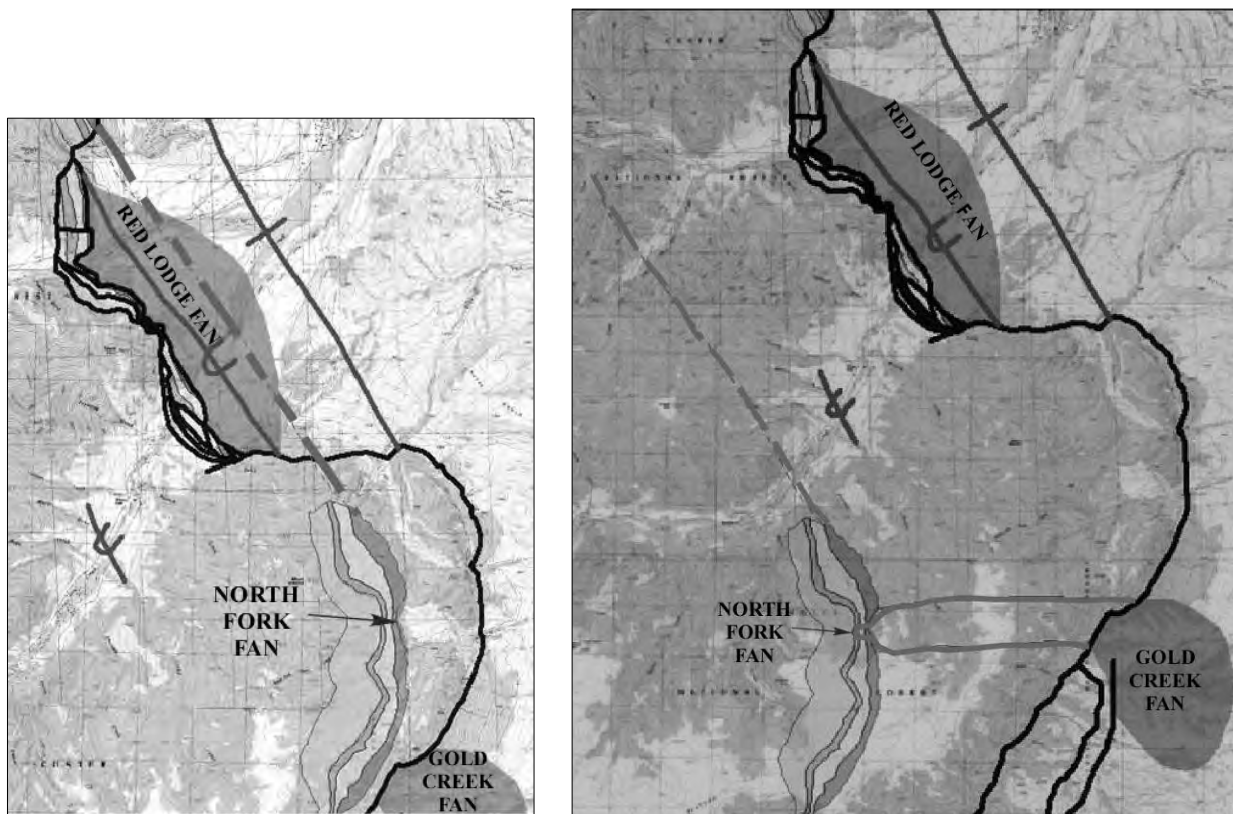


Figure 8. Maps showing palinspastic restoration of North Fork palisades (STOP 4) to its approximate position during deposition of Paleocene alluvial fans.

Figure 9. Diagram showing the distribution of Paleocene alluvial fans and seismite features to the irregularly shaped, approximate ramp (light gray dashed line) of the Beartooth Fault (BF) with approximate restored locations of the Towne Point duplex, the cliff-forming Paleozoic strata at Clark Canyon, North Fork, and Willow Creek, the Clark Fork fault (CFF) and footwall synclines (FWS).

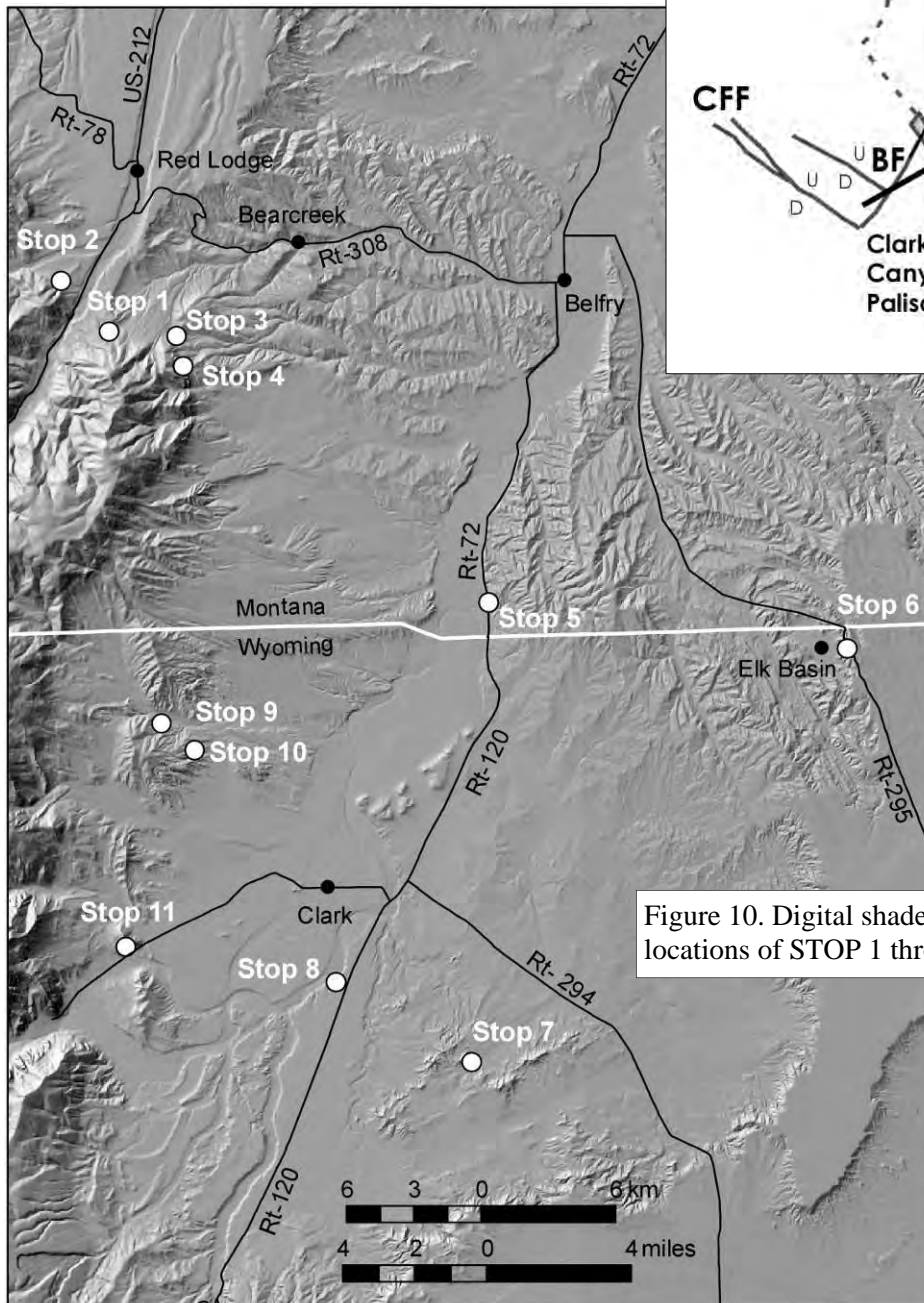
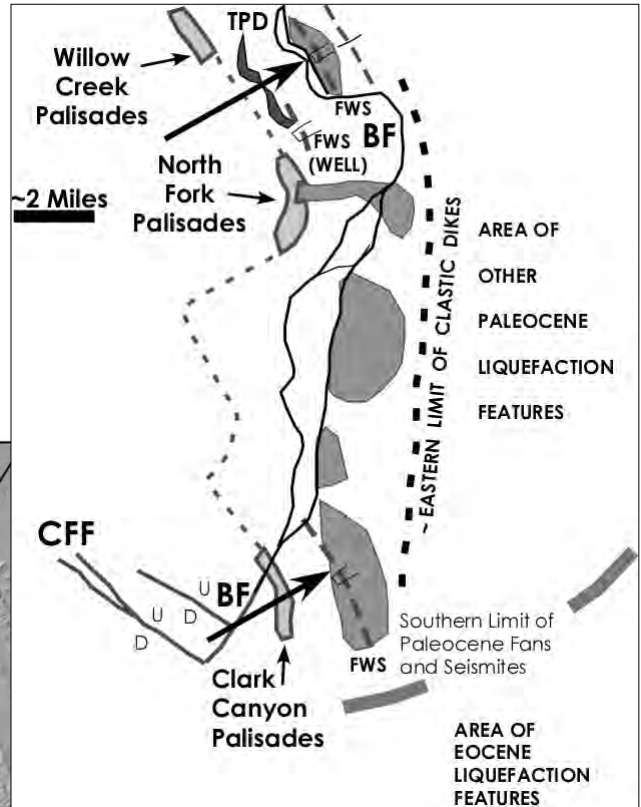


Figure 10. Digital shaded relief map showing locations of STOP 1 through STOP 11.

and Willow Creek if the duplex extends laterally.

The trend of the footwall-syncline axis differs by  $\sim 30^\circ$  from the axial surface deduced from the dipmeter log in the well (Wise, 2000). To reconcile these differences and to approximate the palinspastic location of the hanging-wall palisades of Paleozoic strata, we drew a balanced cross section along the line of the well course (Figure 7). One way to balance the section is with a thrust that detaches the footwall syncline from relatively flat-lying Paleozoic strata “pinned” to basement. A subsurface ramp along this thrust accounts for the dip of bedding toward the thrust in the Fort Union Formation near Red Lodge. The recumbent syncline at depth (where the well is located) is thus rotated along the ramp during later stages of thrusting.

The axis of the syncline in the well is, however, parallel to inferred trace of the Paleozoic section connecting the Willow Creek palisades with those along the North Fork on the Mount Maurice block. Thus the Mount Maurice area and the well axis appear to have been rotated counterclockwise (relative to the Willow Creek block) during thrusting on the fault beneath the recumbent syncline. In order to learn more about where the ramp was located relative to the synorogenic alluvial fans during Paleocene faulting, we first rotated both the axis in the well and the Mount Maurice area clockwise to align the axis with the mapped axes (Figure 5; cf. Figure 8A). This results in an alignment of the hanging-wall Paleozoic strata of Willow Creek area with that of the Mount Maurice block. Next we restored the section in the well (Figure 7) back down the ramp to match its footwall cutoff positions. This moves the frontal hanging-wall palisades (Figure 8 – dashed lines on section B) back the minimum distance needed

to balance the cross section. This restoration places the hanging-wall debris flows of the upper alluvial fan (STOP 4) in proximity to the Gold Creek fan. Perhaps this was indeed the head of the Gold Creek fan, but in any case, it does place the Madison Formation at a minimum distance from both the Gold Creek and Red Lodge fans at a time when it was being actively eroded and supplying material to the fans.

At Clark Canyon, the axis of the overturned footwall syncline also trends  $\sim N30^\circ W$ , indicating the same direction of shortening as at Red Lodge (Figure 9). Foose et al. (1961) indicated that the Clark Fork and Beartooth faults intersected and formed a corner of the Beartooth uplift at Clark Canyon. Their interpretation is consistent with the absence of Paleocene alluvial fans south of the Clark Fork fan (Figure 9 and STOP 11 on Figure 10). Unfolding the footwall Paleozoic section at Clark Canyon gives us another cutoff point on the Beartooth fault. Thus the approximate location of the footwall cutoff of the Paleozoic section can be inferred if intervening alluvial fans (DeCelles et al., 1991) were all approximately the same distance from the ramp. This would suggest that the ramp was irregularly shaped or had tear faults along it (Figure 9). This suggests that clastic dikes occur about 5-10 miles away from the ramp (likely hypocenter locations) and other small-scale seismites out as far as 20 miles from the ramp.

While agreeing with the new Linley Conglomerate and related surface observations near the Red Lodge Corner, one of us (DUW) prefers his (Wise, 2000) interpretation based on a two-stage uplift of the Beartooth Range. The axis of the range as a whole as well as many regional  $N45^\circ-60^\circ W$  trending structures are slightly older than the N-S range front south of Red Lodge, a feature that uplifts, truncates and tilts many of these older structures. This younger southern section of the front moved more easterly

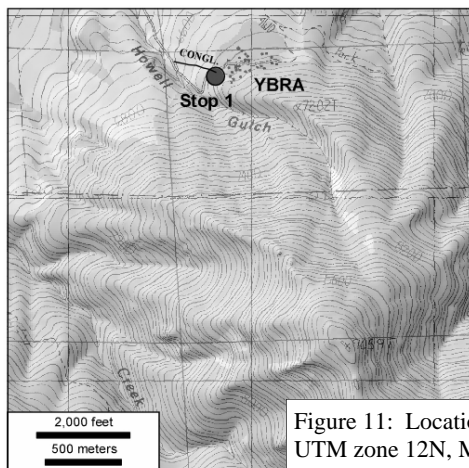


Figure 11: Location map for STOP 1. 635,813m E 4,997,691m N, UTM zone 12N, Mount Maurice, MT-WY quadrangle

than the older structures north of Red Lodge but had much less horizontal displacement than suggested on Figure 9.

This is especially the case where these more steeply dipping frontal structures must truncate the footwall syncline in a very limited distance just to the SE of the AMOCO well. In this scenario the Linley Conglomerate and Gold Creek Fan might be parts of the same conglomerate body connected at depth. Farther south at Bennett Creek an uplifted and truncated NW-trending basement fault may have added another complication to fan evolution as indicated by interfingering of lenses of basement cobbles in fans just to its south with those of carbonate and porphyry clasts to its north. Farther south, the master thrust of the Beartooth Front does increase displacement as it splays southeastward within the basin sediments to produce the second footwall syncline structure east of the Clarks Fork Canyon shown on Figure 9.

STOP 1. Although it may have been obvious what rocks cropped out along the road in the early days of the YBRA camp when the road was first made, in more recent years it was unknown what rocks were downhill from the camp beneath the area which is littered with cobbles and boulders and has a red soil. A few years ago at this stop, the bank of the road was scraped and near-vertical bedding

**STOP 1**

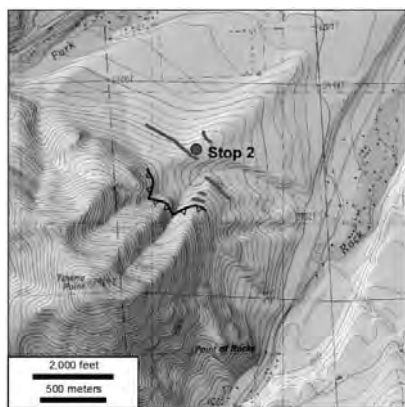


Figure 12: Location map for STOP 2. Red Lodge West, MT 7.5 minute quadrangle. UTM coordinates: 634,352 m E 5,000,548m N zone 12N.



Figure 13: Steeply inclined Slab of Madison limestone (foreground) is parallel to bedding in near-vertical red conglomerate on hill to southeast of STOP 2 (Figure 12). More gently dipping (white lines) deposit of boulder conglomerate at STOP 2 (background) is not continuous with conglomerate in foreground.

gently dipping bedding was exposed in the drainage ditch along the road downhill of the cattle gate in red, cross bedded, conglomeratic coarse grained sandstone. Thus the area on the east side of the upper part of the Howell Gulch road is inferred to be Linley Conglomerate in the footwall syncline beneath the Towne Point duplex (Figures 5 and 6). About a half-mile below the sharp bend, the fault contact between the duplex and conglomerate can be approximated at  $\sim 60^\circ$  (Figure 7).

STOP 2. The carbonates at the ledge at STOP 2 (Figure 12) consist of large, generally angular blocks enveloped in a poorly sorted, matrix-supported conglomerate of smaller angular clasts of carbonate with a red to pinkish-gray, sandy clay matrix. Bedding is poorly defined except by large beds of conglomerate and infrequently by minor thin beds of sandstone. The very large slabs of Madison Formation at several locations on the hill to the southeast (Figures 12 and 13), were originally interpreted as exposures along backthrusts beneath the Beartooth thrust (e.g., Foose et al., 1961). We

**STOP 2**

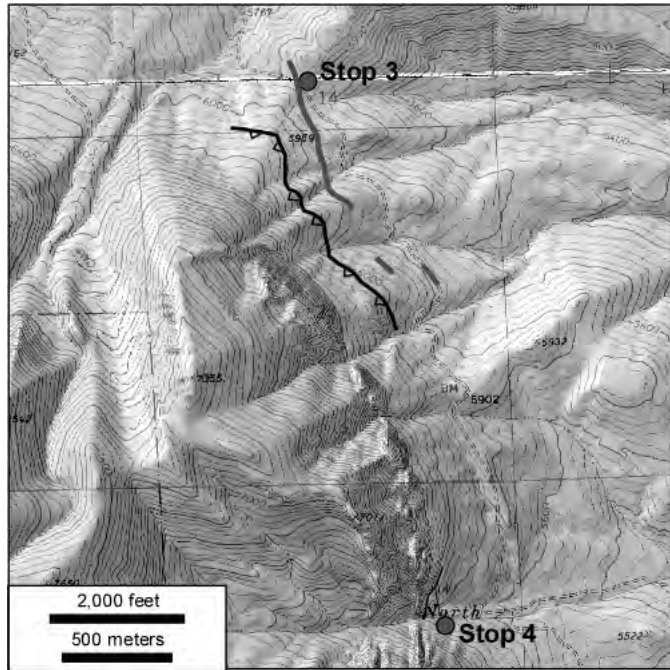


Figure 14. Location map for STOP 3, Red Lodge East, MT and Tolman Flat, MT 7.5 minute quadrangles. UTM coordinates 639,468m E 4,998,211m N, zone 12N. STOP 4. Red Lodge East, MT and Tolman Flat, MT 7.5 minute quadrangles. UTM coordinates 640,149m E 4,995,675m N, zone 12N.

interpret these deposits as debris flows which happen to contain some very large slabs (Figure 6, section B). By themselves, these deposits would not be obvious paleoseismites. But within the context of abundant clastic dikes and other liquefaction features in the Fort Union, we interpret these large-slab deposits as debris flows that were likely seismically induced. Slabs break off of cliffs and get concentrated at the head of fans. Major earthquakes (e.g., 1959 Hebgen Lake earthquake) can then trigger a landslide or debris flow which encompasses such slabs. The recent example of many landslides produced by the 12 May, 2008 Mw 7.9 Sichuan, China earthquake, simply reinforces the concepts that large mass-movement deposits are an integral part of the seismite picture in an area of significant relief.

**STOP 3** STOP 3. Structurally (at this stop), the Beartooth thrust has moved along a flat that is stratigraphically high (Figure 15) in the Fort Union Formation (Figure 6, section A). As a

result, the thrust over rode the coarse alluvial fan equivalents of the Fort Union Formation and now rests on top of more distal facies. Here a 3-to-4-m-thick, coarse-grained, cross-bedded sandstone containing paleoseismites can be traced for ~0.5 miles south. It contains small diapirs (Figure 16 A) and abundant convoluted cross bedding (Figure 16B) (Stewart et al., 2008). This sandstone is one of many which are interbedded with thicker mudstone and siltstone beds in this upper part of the Tongue River Formation. We interpret these sandstones primarily as channel sands in a distal, fluvial-dominated fan. Other channel sands with convoluted crossbedding also occur above and below the prominent bed at STOP 3. Repetition within a stratigraphic sequence like this supports the interpretation that these are paleoseismites caused by periodic large paleo-earthquakes.

STOP 4. Here along the North Fork trail, the steeply dipping, angular unconformity between debris-flow deposits of the Linley Conglomerate and the underlying Madison Formation in the hanging wall of the Beartooth thrust is quite visible (Figure 17A). The Madison is near-vertical and bedding in the debris flows dips steeply northeast. Obviously at the time of deposition of the Linley, the Madison was exposed. In order to determine the approximate dip of the Madison at that time, we have rotated the photograph (Figure 17B) so that bedding in the Linley is ~15°-20°. This gives the Madison a dip of ~50°. The Beartooth thrust is likely along a flat beneath the near-vertical Madison here (Figure 6) and the dip of ~50° at the time of deposition of the Linley would imply that the Madison was located on a ramp (Figure 7), perhaps in a position approximately equivalent to where the well was drilled.

STOP 5. This stop is above a new road cut (grassed over naturally). As a result, some pictures (Figure 4), which are from the old road cut may not match exposures today. Above the road cut, in the natural exposure are

	Age (Ma)	North American Land Mammal Age	Magnetostratigraphy	Lithostratigraphy	seismites	
<b>Eocene</b>	50.7	<b>Wasatchian</b>	Wa7	<b>Willwood Formation</b>	?	
	51.7		Wa6			23R
			Wa5			23N
	52.4		Wa4			24R
			Wa3			24R
	53.4		Wa2			24N
			Wa1			24N
	55	<b>Clarkforkian</b>	Cf3	25R		
			Cf2			
			Cf1			
55.9	<b>Tiffanian</b>	Ti5	25N	Tongue River Member		
56.4		Ti4	26R			
		57.6	Ti3	26N	Linley Cong. ---?---	
57.9		Ti2	27R	Lebo Member		
60		Ti1				
	60.9	<b>Torrejonian</b>		To4	Fort Union Formation	
To3			27N			
To2			28R			
61.3	To1	28R	Tullock Member			
62.5	<b>Puercan</b>	Pu3		28N		
63.6		Pu2	29R			
63.9		Pu1	29N			
65						
<b>Cretaceous</b>			30R	Lance Fm.		

Figure 15. Stratigraphic section of the Fort Union and Willwood formations with accompanying biostratigraphy, paleomagnetostratigraphy, and approximate paleoseismites intervals (Gingerich, 1983; Butler et al., 1981; Krause and Wells, 1999; Brown, 1993; Cande and Kent, 1995).

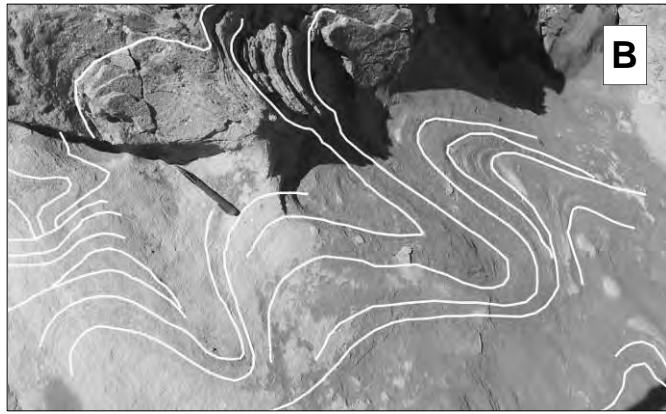


Figure 16. Diapir of coarse-grained sand (A) and convolute bedding in a cross bedded sandstone (B) at STOP 3 (Figure 13).

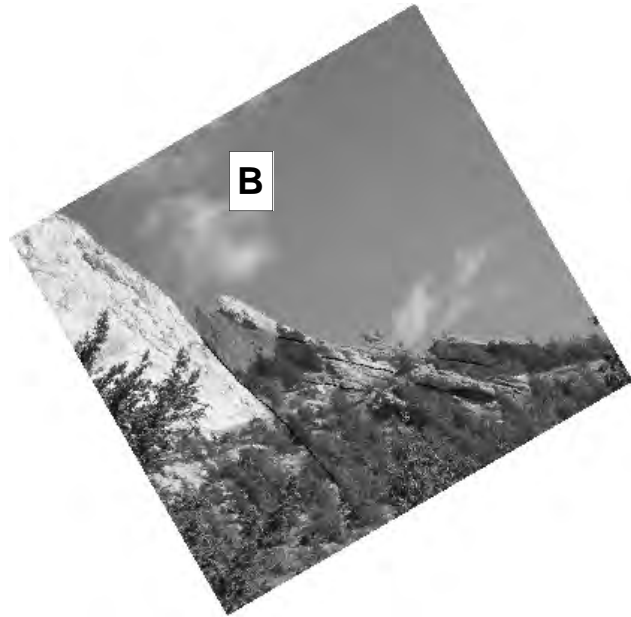


Figure 17. **A:** Unconformity between steeply dipping Madison limestone (left) and NE-dipping debris flows of the Linley Conglomerate (right); **B:** fan is rotated  $\sim 30^\circ$  so that bedding in fan has an  $\sim 15^\circ$ - $20^\circ$  dip, then the unconformity and bedding in the Madison dip  $\sim 50^\circ$  NW.



Figure 18. Location map for STOP 5. Hollenbeck Draw, MT-WY 7.5 minute quadrangle. UTM coordinates 653,468m E 4,986,343m N, zone 12N.

good examples of convoluted cross bedding within channel sands of the Tongue Fork Member. Thinly bedded sandstones typically contain diapirs and ball-and-pillow structures (Figure 4A, B), whereas thickly bedded channel sandstones contain convolute bedding (Figure 19).

## STOP 6

STOP 6. Only a few clastic dikes (Figure 21) occur in the Virgille sandstone of the Cretaceous (Campanian) Eagle Formation in the Elk Basin anticline. These Cretaceous dikes are generally wider, longer, and more planar than the Paleocene ones, hence they are likely injections along pre-existing joints. These NE-SW-trending dikes are parallel to the cross-strike set of tectonic joints, which Engelder et al., (1997) concluded formed after the strike-parallel set of tectonic joints in the Elk Basin anticline. Both large-scale (Figure 1C) and small-scale (Figure 21B) convolute bedding also occur in the Virgille and the presence of probable sandblow-vents (Figure 1C) suggests that the then-active fault, which produced these paleoseismites, was the fault beneath the Elk Basin anticline. The lack of Cretaceous paleoseismites near the Beartooth uplift and the Bull Mountains suggests that Laramide



Figure 19. Convolute bedding in the Tongue River Member.

faults that were active in Cretaceous time were not widespread.

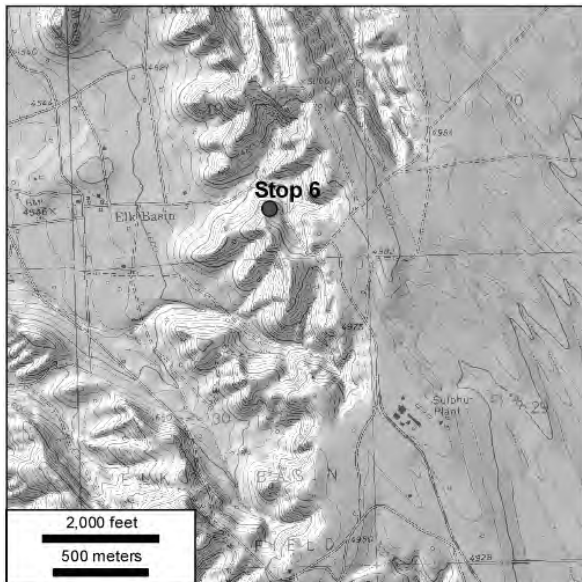


Figure 20. Location map for STOP 6. Elk Basin, WY 7.5 minute quadrangle. UTM coordinates 669,419m E 4,983,851m N, zone 12N.

STOP 7. The Willwood Formation is a thick sequence of mudstones with wide channels cut into the mudstones. The channels are filled with crossbedded coarse-grained sandstone. It is in these channel sands, north of Heart Mountain, where we have found convolute bedding. So far we have not identified any paleoseismites in the Willwood to the south or east of Heart Mountain. Even to the north of Heart Mountain, there is a dearth of paleoseismites in the upper Tongue River Member and the lower Willwood Formation. Stop 7 (Figure 22) is at the one place where we have seen a subhorizontal bedding in the channel sand abruptly change to convolute bedding (Figure 23). Such an abrupt lateral change from normal bedding to liquefaction suggests seismic shaking as the cause.

## STOP 7

## STOP 8

STOP 8. Cross bedded sandstone with convolute bedding (Figure 25) make up the ledges below the parking to the west and southwest. From this point, we can gain an appreciation of what the distribution of Paleocene alluvial fans with their paleoseismites versus the distribution of Eocene paleoseismites in the Willwood Formation means in terms of regional tectonics. The absence of late Paleocene alluvial fans and late Paleocene seismites south of the Clark Canyon fan (Figures 9 and 10) indicates that no substantial late Paleocene uplift existed south of Clark Canyon in the Rattlesnake Mountain area. In contrast, the Eocene Willwood Formation unconformably truncates older strata between Rattlesnake Mountain and Heart Mountain (which rests structurally on top of the Willwood Formation, e.g., Pierce, 1957, 1980; Hauge, 1985, 1990) and contains abundant paleoseismites in the area north and northwest of Heart Mountain. The presence of Eocene paleoseismites in channel deposits of ancient streams suggests perhaps that uplift of Rattlesnake Mountain occurred in the Eocene.



## STOP 9

STOP 9. This wide, ~2-m-high Paleocene clastic dike (Figure 27A) appears to have originated from the sandy matrix of a bed of sandy conglomerate at the base of the dike. The coarse-sand dikes cuts across red sandstone and mudstone as well as green mudstone. Sandy conglomerate overlies the beds containing the dike. These reddish beds of conglomerate, sand, and mudstone are characteristic of the transitional facies between the Tongue River Member and the Linley Conglomerate of the alluvial fans described by DeCelles et al. 1991). As noted by Stewart et al. (2008), the red color may have the reason that Pierce (1965) misidentified these beds as the Eocene Willwood Formation.

This bank had been cut back since the previous photograph was taken in 2003 (Stewart et al., 2008, their Figure 14). Small-scale folds (Figure 27B) are present in thinner bedded claystones and siltstones.

## STOP 10

STOP 10. This is one of the best areas to see many clastic dikes (Figure 28), sills, and small syndepositional normal faults which characterize the fluvial-dominated parts lower parts of the alluvial fans. This transitional part of the fans is dominated by thick brownish-gray sandstones interbedded



Figure 21. **A:** Typical planar sandstone dike in Cretaceous strata in the Elk Basin anticline; **B:** recumbent, isoclinal fold in cross bedded Virgille sandstone. Convolute bedding is truncated (dashed line) by normal bedding.

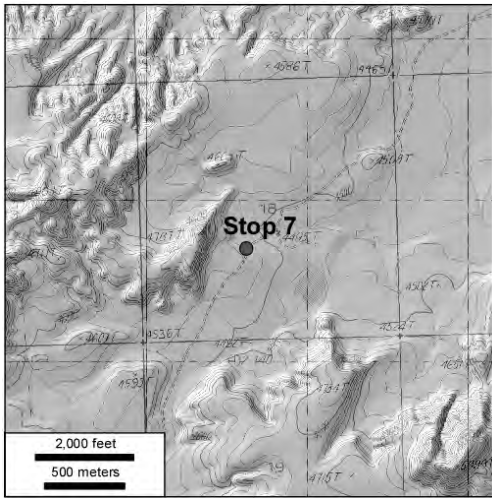


Figure 22. Location map for STOP 7 Badlands Hills, WY 7.5 minute quadrangle. UTM coordinates 652,630m E 4,965,690m N, zone 12N.

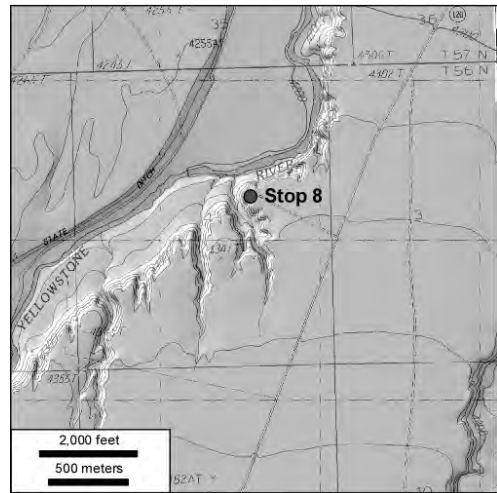


Figure 24. Location map for STOP 8. Chapman Bench, WY 7.5 minute quadrangle. UTM coordinates 646,578m E 4,969,264m N, zone 12N.



Figure 23. Convolute bedding in channel sandstone of the Willwood Formation. Bedding becomes subhorizontal in the same bed in the background to the right (west).

Figure 25. Typical convolute bedding in coarse-grained sandstone of the Tongue River Member.



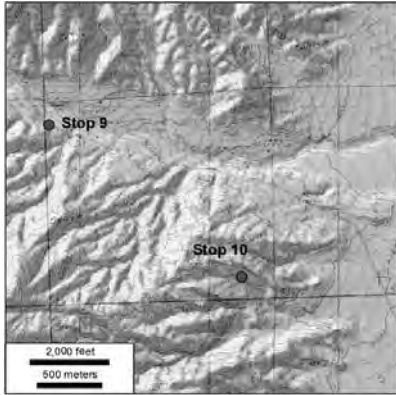


Figure 26. Location map for STOP 9. Clark, WY 7.5 minute quadrangle. UTM coordinates 638,772m E 4,980,844m N, zone 12N. STOP 10. Clark, WY 7.5-minute quadrangle. UTM coordinates, all zone 12N - 640,851m E 4,979,615m N



Figure 27. **A:** Coarse sand dike at STOP 9 as it appeared in 2007 (photograph by John Whitmore); **B:** small-scale folds in thinly bedded mudstone and siltstone.

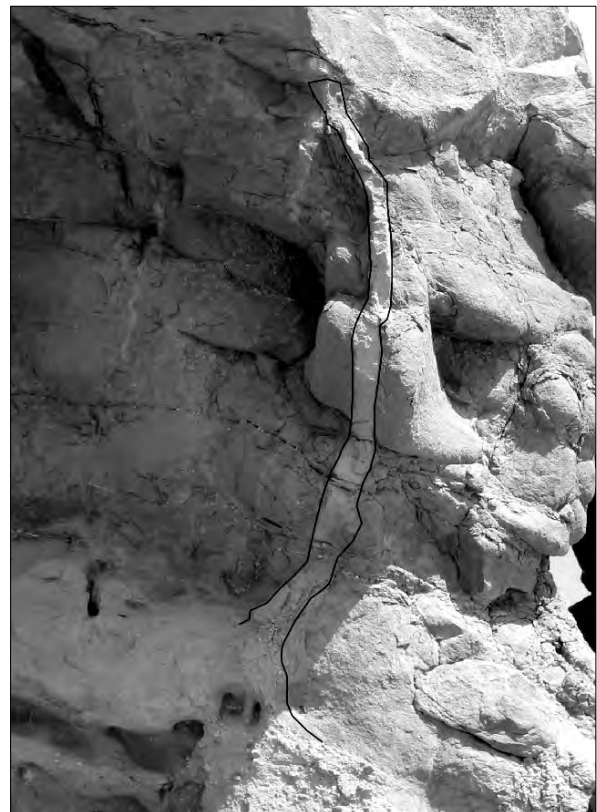


Figure 28. Typical clastic dike which widens and merges downward with underlying sandstone and terminates upward against overlying sandstone.

with greenish-gray siltstone/mudstones. Interspersed and increasing up the fans are thick reddish-gray conglomerates. Upwardly terminating (and commonly tapering) dikes (Figure 1D) are common in the Tongue River Member and are excellent evidence of forceful hydraulic injection (Obermeier, 1996a, b). The dikes commonly originate from underlying sandstone beds and intrude upward across the siltstone/

or before reaching the overlying thick sandstone or conglomerate beds. Some are sill-like, a few bifurcate, and others fill sinuous cracks. This mode of occurrence suggests few dikes erupted on to the land surface (cf. Figure 1A, 1C), but is consistent with their development at some depth below the surface. Fluid pressure was sufficient to penetrate fine-grained clay-rich rock, but was insufficient to penetrate overlying thick beds of sand which capped the fine grained sediment. A dearth of surface-filled cracks versus the abundance of upwardly terminating and tapering dikes in the Tongue River Member is also indicative of seismically induced dike-emplacment (Stewart et al., 2008).

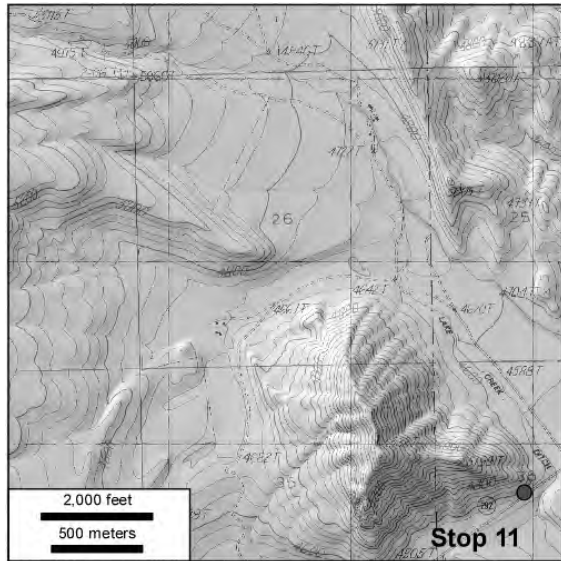


Figure 29. Location map for STOP 11. 637,955m E 4,970,736m N UTM zone 12, North Bennett Creek, WY quadrangle

**STOP 11** STOP 11. This stop is the classic conglomeratic beds of the alluvial fans described by DeCelles et al. (1991). Even in the very coarse-grained rocks here careful examination shows some examples of paleoseismites (convolute bedding; Figure 30) as noted by DeCelles et al. (1991).

sandstone intervals and either terminate against

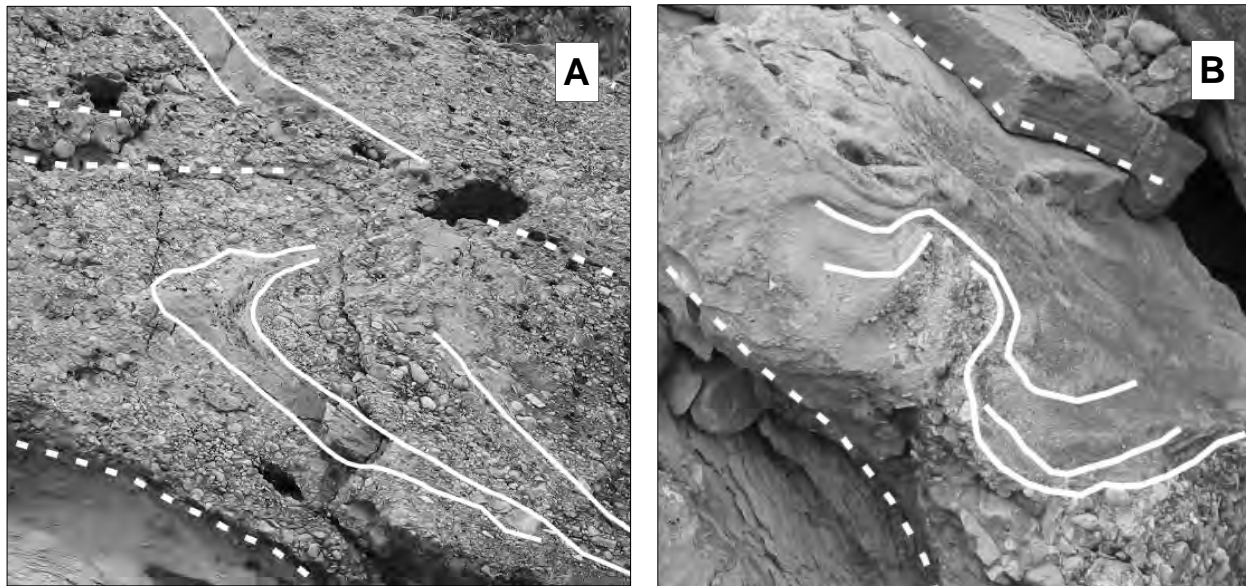


Figure 30. **A and B:** Soft-sediment folds in sandstone beds in Linley Conglomerate; dashed lines are bedding in outcrops.



## ACKNOWLEDGEMENTS

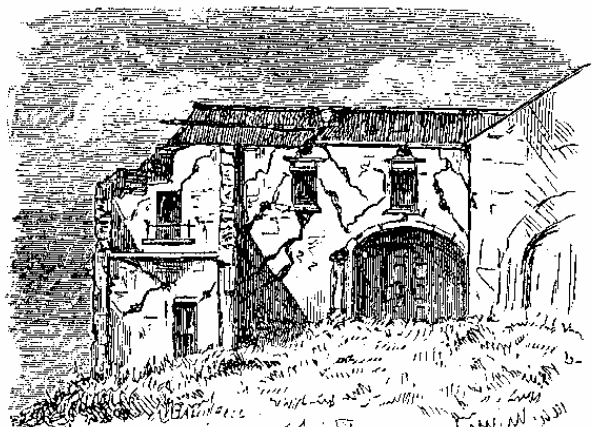
Marv Kauffman provided us with paleoseismic locations in Elk Basin.

## REFERENCES

- Ballantyne, H., Stewart, K.G., and Bartholomew, M.J., 2004, Laramide paleoseismites in the Clarks Fork Basin, Montana and Wyoming: Geological Society of America Abstracts with Programs, v. 36, no. 4, p. 36.
- Bartholomew, M.J., and Rich, F.J., 2007, The walls of colonial Fort Dorchester: A record of structures caused by the August 31, 1886, Charleston, South Carolina, earthquake and its subsequent earthquake history: *Southeastern Geology*, v. 44, no. 4, p. 147–169.
- Bartholomew, M.J., and Stewart, K.G., 2001, Paleoseismites and tectonics of the Deep River Triassic basin, North Carolina: Geological Society of America Abstracts with Programs, v. 33, no. 3, p. A-27.
- Bartholomew, M.J., Brodie, B.M., Willoughby, R.H., Lewis, S.E., and Syms, F.H., 2002a, Mid-Tertiary paleoseismites: Syndepositional features and section restoration used to indicate paleoseismicity, Atlantic Coastal Plain, South Carolina and Georgia: *in* Ettensohn, F.R., Rast, N., and Brett, C.E., eds., *Ancient Seismites: Geological Society of America Special Paper 359*, p. 63–74.
- Bartholomew, M.J., Stickney, M.C., Wilde, E.M., and Dundas, R.G., 2002b, Late Quaternary paleoseismites: Syndepositional features and section restoration used to indicate paleoseismicity and stress-field orientations during faulting along the main Lima Reservoir fault, southwestern Montana: *in* Ettensohn, F.R., Rast, N., and Brett, C.E., eds., *Ancient Seismites: Geological Society of America Special Paper 359*, p. 29–47.
- Bartholomew, M.J., Wise, D.U., and Stewart, K.G., 2004, Structural refinement of the northeastern corner of the Laramide Beartooth uplift, Montana: Geological Society of America Abstracts with Programs, v. 36, no. 5, p. 268.
- Bourgeois, J., and Johnson, S.Y., 2001, Geologic evidence of earthquakes at the Snohomish Delta, Washington, in the past 1200 yr.: Geological Society of America Bulletin, v. 113, p. 482–494.
- Brown, J.L., 1993, Sedimentology and Depositional History of the Lower Paleocene Tullock Member of the Fort Union Formation, Powder River Basin, Wyoming and Montana: US Geological Survey Bulletin 1917-L, p. L1-L42.
- Butler, R.F., Gingerich, P.D., and Lindsay, E.H., 1981, Magnetic Polarity Stratigraphy and Biostratigraphy of Paleocene and Lower Eocene continental deposits, Clark's Fork Basin, Wyoming: *Journal of Geology*, v. 89, p. 299-316.
- Cande, S.C., and Kent, D.V., 1995, Revised calibration of the geomagnetic polarity timescale for the Late Cretaceous and Cenozoic: *Journal of Geophysical Research*, v. 100, no. B4, p. 6093-6095.
- DeCelles, P.G., Gray, M.B., Ridgeway, K.D., Cole, R.B., Pivnik, D.A., Pequera, N., and Srivistava, P., 1991, Controls on synorogenic alluvial fan architecture, Beartooth conglomerate (Paleocene), Wyoming and Montana: *Sedimentology*, v. 38, p. 567–590, doi: 10.1111/j.1365-3091.1991.tb01009.x.
- Engelder, T., Gross, M.R., and Pinkerton, P., 1997, An analysis of joint development in thick sandstone beds of the Elk Basin anticline, Montana-Wyoming: *in* Hoak, T.E., Klawitter, A., and Blomquist, P.K., eds., *Fractured Reservoirs: Characterization and Modeling Guidebook*, Rocky Mountain Association of Geologists, p. 1–18.
- Foose, R.M., Wise, D.U., and Garbarini, G.S., 1961, Structural geology of the Beartooth Mountains, Montana and Wyoming: Geological Society of America Bulletin, v. 72, p. 1143–1172.
- Gingerich, Phillip D., 1983, Paleocene-Eocene faunal zones and a preliminary analysis of Laramide structure deformation in the Clark's Fork Basin, Wyoming: *in* Boberg, W.W., ed., *Geology of the Bighorn Basin: Wyoming Geological Association Guidebook*, p.185-197.
- Hauge, T.A., 1985, Gravity-spreading origin of the Heart Mountain allochthon, northwestern Wyoming:

- Geological Society of America Bulletin, v. 96, p.1440-1456.
- Hauge, T.A., 1990, Continuous-allochthon model of Heart Mountain faulting: Geological Society of America Bulletin, v. 102, p. 1174-1188.
- Kraus, M.J., and Wells, T.M., 1999, Facies and facies architecture of Paleocene floodplain deposits, Fort Union Formation, Bighorn Basin, Wyoming: The Mountain Geologist, v. 36, no.2, p.57-70.
- Lawler, T.B., 1923, On the occurrence of sandstone dikes and chalcedony veins in the White River Oligocene: American Journal of Science, v. 5, p. 160-172.
- McCalpin, J.P., ed., 1996, Paleoseismology: Academic Press, New York, New York, 588 p.
- Mills, P.C., 1983, Genesis and diagnostic value of soft-sediment deformation structures: A review: Sedimentary Geology, v. 35, p. 83-104.
- Obermeier, S.F., 1996a, Use of liquefaction-induced features for paleoseismic analysis: An overview of how seismic liquefaction features can be distinguished from other features and how their regional distribution and properties of source sediment can be used to infer the location and strength of Holocene paleo-earthquakes: Engineering Geology, v. 44, p. 1-76, doi: 10.1016/S0013-7952(96)00040-3.
- Obermeier, S.F., 1996b, Using liquefaction-induced features for paleoseismic analysis: Chapter 7 in McCalpin, J.P., ed., Paleoseismology: Academic Press, New York, New York, p. 331-396.
- Obermeier, S.F., Pond, E. C., Olson, S. M., and Green, R. A., 2002, Paleoliquefaction studies in continental settings: in Ettensohn, F.R., Rast, N., and Brett, C.E., eds., Ancient Seismites: Geological Society of America Special Paper 359, p. 13-27.
- Pierce, W.G., 1957, Heart Mountain and South Fork detachment thrusts of Wyoming: American Association of Petroleum Geologists Bulletin, v. 41, no. 4, p. 591-626.
- Pierce, W.G., 1965, Geologic map of the Clark Quadrangle, Park County, Wyoming: U.S. Geological Survey Geologic Quadrangle Map GQ-0477.
- Pierce, W.G., 1980, The Heart Mountain break-away fault, northwestern Wyoming: Geological Society of America Bulletin, v. 91, p. 272-281.
- Pope, M.C., Read, J.F., Bambach, R.K., and Hofmann, H.J., 1997, Late Middle to Late Ordovician seismites of Kentucky, Southwest Ohio and Virginia: Sedimentary recorders of earthquakes in the Appalachian Basin: Geological Society of America Bulletin, v. 109, p. 489-503.
- Renfro, H.B., and Feray, D.E., compilers, 1972, Geological highway map of the northern Rocky Mountain region, Idaho, Montana, Wyoming: American Association of Petroleum Geologists, Map No. 5, Tulsa, Oklahoma.
- Seilacher, A., 1984, Sedimentary structures tentatively attributed to seismic events: Marine Geology, v. 55, p.1-12.
- Stewart, K.G., Dennison, J.M., and Bartholomew, M.J., 2002, Late Mississippian paleoseismites from southeastern West Virginia and southwestern Virginia: in Ettensohn, F.R., Rast, N., and Brett, C.E., eds., Ancient Seismites: Geological Society of America Special Paper 359, p.127-144.
- Stewart, K.G., Ballantyne, H., and Bartholomew, M.J., 2004, Reconstructing the timing and structural evolution of the eastern Beartooth uplift using paleoseismites and synkinematic alluvial fans: Geological Society of America Abstracts with Programs, v. 36, no. 5, p. 268.
- Stewart, K.G., Bartholomew, M.J., and Ballantyne, H.A., 2008, Laramide paleoseismites of the Bighorn Basin: in Reynolds, R.G., ed., Roaming the Rocky Mountains and Environs: Geological Field Trips: Geological Society of America, Field Guide 10, (15 p., in press).
- Tuttle, M., and Seeber, L., 1991, Historic and pre-historic earthquake-induced liquefaction in Newbury, Massachusetts: Geology, v. 19, p. 594-597.
- Wheeler, R.L., 2002, Distinguishing seismic from nonseismic soft-sediment structures: Criteria from seismic-hazard analysis: in Ettensohn, F.R., Rast, N., and Brett, C.E., eds., Ancient Seismites: Geological Society of America Special Paper 359, p. 1-11.
- Wise, D.U., 2000, Laramide structures in basement and cover of the Beartooth uplift near Red Lodge, Montana: American Association of Petroleum Geologists Bulletin, v. 84, no. 3, p. 360-375.

Wooten, R.M., Bartholomew, M.J., and Malin, P.E., 2001, Structural features exposed in Triassic sedimentary rocks near the proposed low-level radioactive waste disposal site, southwestern Wake County, North Carolina: *in* Hoffman, W., editor, Guidebook for 2001 Geological Society of America Southeastern Section Meeting, April 5-6, 2001, North Carolina State University, Raleigh, North Carolina, p. 51-74.



# A FIELD GUIDE TO THE CAMBRIAN SECTION AT BEARTOOTH BUTTE, NORTHWESTERN WYOMING

**Robert C. Thomas**

*Department of Environmental Sciences, The University of Montana Western, Dillon, MT 59725  
r\_thomas@umwestern.edu*

## INTRODUCTION

The rocks atop the Beartooth Plateau in southern Montana and northern Wyoming primarily consist of Archean metamorphic rocks and Proterozoic intrusive rocks (Mueller et al., this volume). However, a prominent island of lower Paleozoic rocks can be found on the south side of the Beartooth Plateau along the Beartooth Highway at Beartooth Butte in Wyoming (Figure 1). This butte rises to a total elevation of 10,514 feet above sea level, and approximately 1,613 feet above the surrounding plateau surface.

The focus of this paper is the Cambrian section at Beartooth Butte, although the entire stratigraphic package is worthy of study. Because the topography of Beartooth Butte is steep and the formations difficult to access, a closer look at the Cambrian formations is easier to get along the switchbacks of the dirt road to Clay Butte fire lookout tower, just to the west of Beartooth Butte. However, for a breathtaking overview of lower Paleozoic stratigraphy, there are few places on Earth that are more stunning than the view of Beartooth Butte from the south shore of Beartooth Lake (Figure 3).

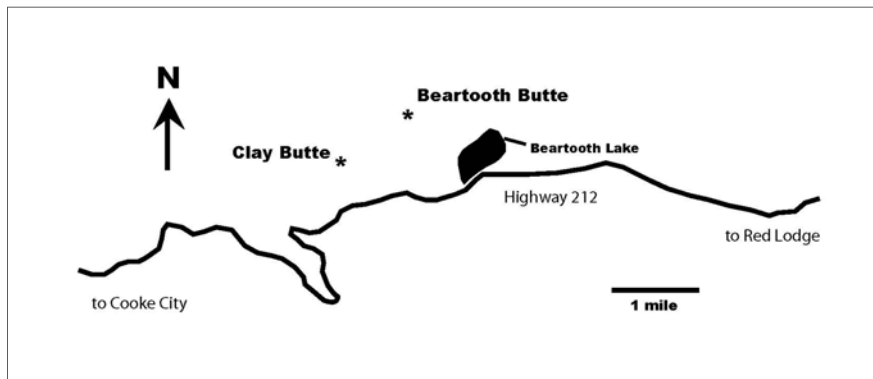


Figure 1. Location map for Beartooth Butte, Wyoming.

The Cambrian section at Beartooth Butte spans Middle to Late Cambrian time, and includes important features such as the Great Unconformity, the Sauk transgression, grand cycles and the repeated mass extinctions that characterize Cambrian shallow-shelf environments around the world. These features are covered in some detail in this paper.

This remnant of lower Paleozoic rock is preserved in the hangingwall of a northwest-trending (N80W) normal fault called the Top of the World Fault. Beartooth Butte is properly termed a nunatak, or an isolated hill that once projected above the surface of glacial ice that surrounded it during the Pleistocene. Both the wedge shape of the butte and the absence of glacial deposits at its summit attest to the flow of ice from the northeast to the southwest, around Beartooth Butte (Figure 2; James, 1995).



Figure 2. The wedge-shaped “nunatak” of Beartooth Butte looking east from Clay Butte.

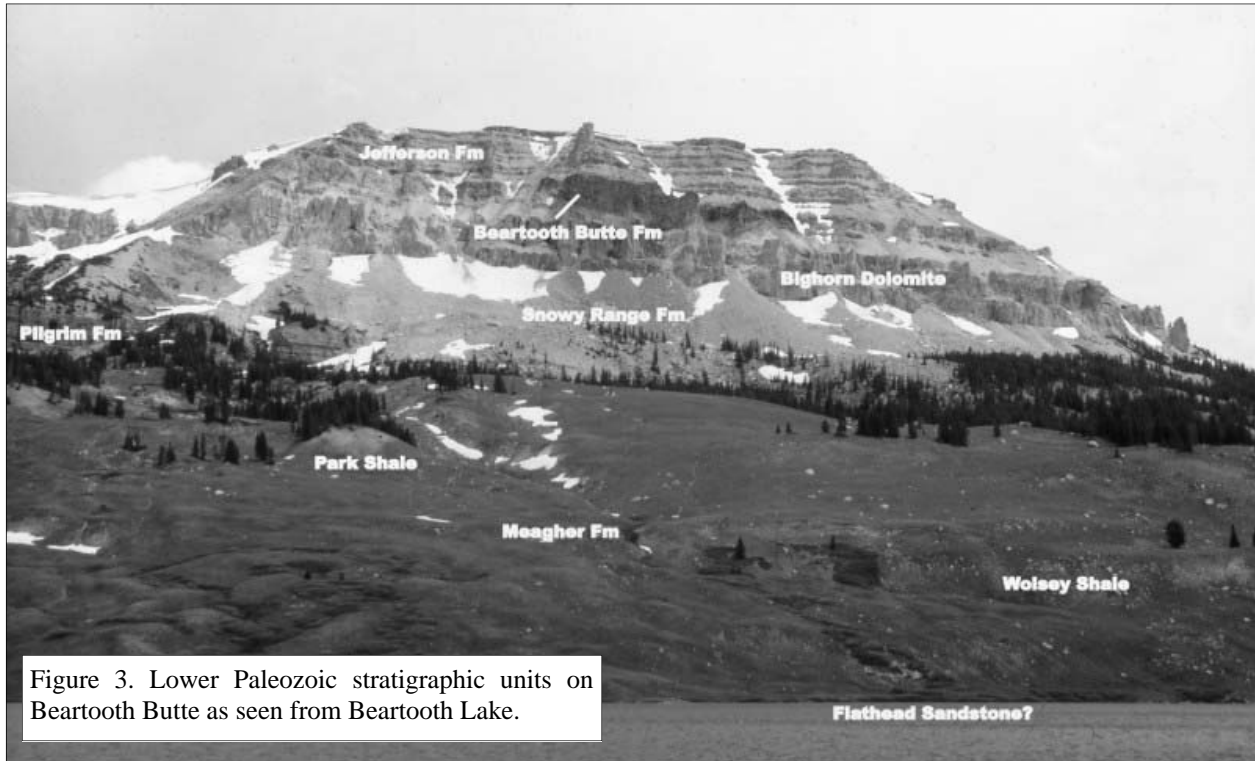


Figure 3. Lower Paleozoic stratigraphic units on Beartooth Butte as seen from Beartooth Lake.

During the Cambrian, the North American continent was in an equatorial position and sedimentation occurred in distinctive belts that surrounded a topographic high called the Transcontinental Arch (Palmer, 1960). The depositional systems (onshore to offshore) consisted of fluvial and beach environments, an intrashelf basin and a carbonate platform that spanned the Cordilleran Hingeline (i.e., the boundary between stable cratonic and rift-stage crust). Oceanward of the carbonate platform was a sediment-starved region of the shelf that accumulated subtidal, carbonate mud, siliciclastic mud and chert. During low stands in sea level, this area was inundated with land-derived sediment that resulted in the onlap of siliciclastics onto the carbonate platform (Thomas, 1993).

### STRATIGRAPHIC OVERVIEW OF BEARTOOTH BUTTE

Aside from surficial deposits, the Paleozoic stratigraphy of Beartooth Butte includes Cambrian through Devonian sedimentary rocks (Figure 4). Near the base of the butte, the Middle Cambrian Flathead Sandstone rests unconformably on Archean metamorphic rocks,

forming a stratigraphic hiatus of over two billion years. This nonconformity is known as the “Great Unconformity”, and stands as the most prominent gap in the geologic history of North America.

The basal Cambrian section (Flathead Sandstone, Wolsey Shale and Meagher Formation) records the Sauk Transgression of the North American craton (Sloss, 1963, 1988). The remainder of the Cambrian section (Park Shale, Pilgrim Formation and Snowy Range Formation) record sea-level fluctuations that produced carbonate-siliciclastic cycles called Grand Cycles (Aitken, 1981). Within these rocks are recorded several biotic crises that punctuated the rapid and expansive evolution of life on the planet during the Cambrian (Thomas, 1995).

The Cambrian rocks are unconformably overlain by the Ordovician Bighorn Dolomite, which was deposited during a eustatic sea-level rise that marks the Tippecanoe Sequence of Sloss (1963, 1988) and is probably of late Middle Ordovician age at Beartooth Butte. The spectacular “red spot” on the butte is the Beartooth Butte Formation, a lower Devonian estuarine channel deposit that contains well-

Middle Devonian	Jefferson Formation
Early Devonian	Beartooth Butte Formation
Middle Ordovician	Big Horn Dolomite
Late Cambrian	Snowy Range Formation: Grove Creek Member Sage Member Dry Creek Shale
	Pilgrim Formation
Middle Cambrian	Park Shale
	Meagher Formation
	Wolsey Shale
	Flathead Sandstone
Archean	Granite Gneiss

Figure 4. Lower Paleozoic stratigraphy of Beartooth Butte.

preserved fossil flora, eurypterids and fish (Bryant, 1932; Dorf, 1934; Tetlie, 2007). The fossil flora (*psilopsid* flora) found in this formation, was discovered in the early 1930s by Erling Dorf and at the time was the oldest known record of terrestrial vegetation in the United States (Dorf, 1934).

Following a major erosional event during the Early Devonian, regional transgression resumed during Middle to Late Devonian time, resulting in the deposition of stromatoporoid dolostone of the Jefferson Formation over the estuarine deposits of the Beartooth Butte Formation. This transgression initiates the Kaskaskia Sequence of Sloss (1963), which is a very well documented, global event.

### THE GREAT UNCONFORMITY

Poorly exposed at the base of Beartooth Butte are outcrops of the Cambrian Flathead Sandstone, the basal transgressive sand of the Sauk Sequence. Although not exposed on Beartooth Butte, this formation rests unconformably on Archean metamorphic rocks with a gap of at least 2.2 billion years! The nonconformity is called the Great Unconformity, and it can be found throughout western North America.

The flat surface of the Beartooth Plateau is a conspicuous feature that probably formed as a result of erosional processes that, in part, produced the Great Unconformity. The metamorphic rocks were formed during the Archean as a result of continental collisions that produced very large mountains in this part of Montana and Wyoming. These mountains were deeply eroded and the topography reduced to a nearly planar surface during the Proterozoic and to some extent during the Cambrian transgression as well (Poldervaart and Bentley, 1958).

### THE SAUK TRANSGRESSION

The first three formations overlying the Archean metamorphic rocks at Beartooth Butte (Flathead Sandstone, Wolsey Shale and Meagher Formation) mark the beginning of the well-known Sauk Sequence or Paleozoic transgression of the North American Craton (see Figure 4). The Sauk Sequence is diachronous from west to east and is the first of four major marine incursions onto the craton during the Paleozoic (Sauk, Tippecanoe, Kaskaskia and Absaroka Sequences; Sloss, 1963, 1988). At Beartooth Butte, the Sauk transgression probably reached the area in the Middle Cambrian (*Albertella* Zone) and ended with Early Ordovician regression (Lochman-Balk, 1971).

The Flathead Sandstone is poorly exposed on Beartooth Butte, but where it is exposed in the area (e.g., Sunlight Basin), it consists of trough cross-bedded quartz sandstone that was deposited in nearshore marine environments. The sandstone is gradationally overlain by micaceous siltstone and claystone of the Wolsey Shale. These siliciclastic deposits contain numerous burrows and trilobite tracks (*Cruziana* and *Rusophycus*), and were deposited in lower-energy environments of the intrashelf basin as the Sauk transgression continued to onlap the craton.

At some distance away from the North American craton, the influx of siliciclastic sediment was sufficiently reduced to allow for calcite-secreting organisms to flourish. As a result, a very large (100s of kilometers wide) carbonate platform developed outboard of the intrashelf basin. The Meagher Formation marks the landward transgression and pro-

gradation of this platform over the intrashelf basin deposits of the Wolsey Shale.

The Sauk transgression of the craton reached its initial maximum extent in this area by Middle Cambrian (*Bathyriscus-Elrathia* Zone) time based on trilobites collected from the Meagher Formation (Lochman-Balk, 1971). During the remainder of the Cambrian, sea level fluctuated and deposited thick (>100 meters) couplets of platform carbonates and intrashelf basin siliciclastics. These carbonate-siliciclastic packages are called “grand cycles”.

## GRAND CYCLES

The top of the Meagher Formation at Beartooth Butte forms a sharp contact with the dominantly siliciclastic deposits of the Park Shale. This boundary marks the boundary between two thick (hundreds of meters) siliciclastic-carbonate cycles called grand cycles by Aitken (1966, 1978, 1981). Because of the similarity of grand cycles and the associated mass extinctions events at Beartooth Butte with other exposures in Montana and Wyoming, the following discussions of grand cycles and Cambrian mass extinctions have been modified from a previously published discussion published by the author in a field guide to the Cambrian section at Camp Creek in southwest Montana (Thomas, 2007).

Grand cycles are equivalent to the second-order cycles of Vail et al. (1977), and some of the cycles can be correlated between the Cordilleran and the Appalachian passive margins (Aitken, 1981; Palmer, 1981; Chow and James, 1987; Westrop, 1992). According to Palmer (1960), the cycles are the products of lateral shifts in the facies belts that surrounded the craton during the Cambrian.

Grand cycles are couplets that consist of a lower, siliciclastic-dominated half-cycle (Park Shale) that passes gradationally upward into an upper, carbonate-dominated half-cycle (Pilgrim Formation). At the top of each grand cycle, the abrupt reappearance of siliciclastic deposits marks the beginning of the next grand cycle

(Dry Creek Shale Member of the Snowy Range Formation). The boundaries of grand cycles are mostly conformable in oceanward sections, but they tend to pass into disconformable contacts towards the craton (Aitken, 1981). It has been difficult to determine if grand cycle tops are isochronous or diachronous. However, by using a mass extinction boundary as a time line for correlation, it is possible to show that at least one of the grand cycle tops is not time synchronous (Thomas, 1992, 1993).

Three basic features are observed in most grand cycles: (1) initiation of siliciclastic deposition at the base of a grand cycle is associated with a relative deepening of the shelf; (2) the transition between the siliciclastic half-cycle and the overlying carbonate half-cycle is diachronous, tending to be younger toward the craton; and (3) the top of the carbonate half-cycle consists of progradational, peritidal lithofacies that record maximum shallowing within the grand cycle (Mount and Rowland, 1981).

Internally, grand cycles are composed of repeated, smaller-scale (fourth and fifth-order) upward-shallowing cycles, especially oceanward of the Cordilleran Hingeline) where the rate of subsidence is greater (Lohman, 1977; Osleger and Read, 1991). Lohmann (1977) concluded that the meter-scale cycles within carbonate-platform deposits in Utah formed through progradational shallowing, followed either by tectonic subsidence or eustatic sea-level rise. According to Osleger and Read (1991), these meter-scale cycles are a part of a stacked sequence of third, fourth and fifth-order cycles that reflect Milankovitch-forced eustatic fluctuations.

A number of mechanisms have been proposed for the formation of grand cycles. Aitken (1966) originally proposed that grand cycles were caused by the periodic tilting of the cratonic margin coupled with a resultant slight uplift of the craton. He (1966) argued that tilting of the cratonic margin deepened the outer edge of the carbonate platform and permitted the incursion of outer-ramp siliciclastics over the carbonate platform. Coeval uplift of the

craton provided a westward flood of terrigenous sediment that merged with the transgressing outer ramp siliciclastics to form a complete siliciclastic half-cycle of the new grand cycle.

Lochman-Balk (1957, 1970, 1971) argued alternatively that the carbonate-siliciclastic alternations were produced by glacio-eustatic sea-level fluctuations rather than tectonic upwarps of the craton. She proposed that terrigenous sediments were deposited on the craton during low-stands in sea level, and then were reworked during the subsequent sea-level rise into the siliciclastic half-cycle of the next grand cycle. Erosional unconformities at the tops of some grand cycle boundaries that are overlain by transgressive siliciclastics support this conclusion (Lochman-Balk and Hu, 1960; Thomas, 1993).

Many authors have speculated that grand cycles are a product of changes in the rate of relative sea-level rise rather than eustatic sea-level rise and fall (R. Price in Aitken, 1966; Sepkoski, 1977; Palmer and Halley, 1979; Mount and Rowland, 1981; Chow and James, 1987; Palmer and Rowland, 1989; Westrop, 1989). Palmer and Halley (1979) proposed that grand cycles form as a result of differential rates of either basinal subsidence or sea-level rise. In their model, a decreasing rate of relative sea-level rise triggers landward progradation of peritidal carbonates and oceanward progradation of nearshore siliciclastics. Eventually, carbonate genesis is terminated, and continued oceanward progradation of the siliciclastic sediments across the slowly subsiding shelf buries the carbonate platform and initiates the next grand cycle.

This model was slightly modified by Mount and Rowland (1981) by proposing that oceanward transport of the nearshore siliciclastic sediments was initiated by a sudden rise in relative sea level, rather than a slow decline in the rate of relative sea-level rise as Palmer and Halley (1979) proposed. Mount and Rowland (1981) argued that during maximum progradation of the carbonate platform, siliciclastic sedi-

ments were ponded in paralic and coastal reservoirs. A sudden rise in relative sea level increased the wave energy in those nearshore environments and initiated the offshore transport of the coastal siliciclastic sediments through storm-surge ebb. They favored a eustatic mechanism over regional uplift, regional subsidence, or variations in the sediment supply, because of the correlatability of individual grand cycles.

Thomas (1993) utilized the Marjumiid-Pterocephaliid mass extinction event to correlate one grand cycle boundary (grand cycle top 10) across the entire shelf in the western United States. At Beartooth Butte, this grand cycle boundary correlates with the abrupt transition from sandy limestone of the Pilgrim Formation to siltstone and fine sandstone of the overlying Snowy Range Formation. He found that on the craton, the grand cycle boundary correlates with exposure and the development of a wide-

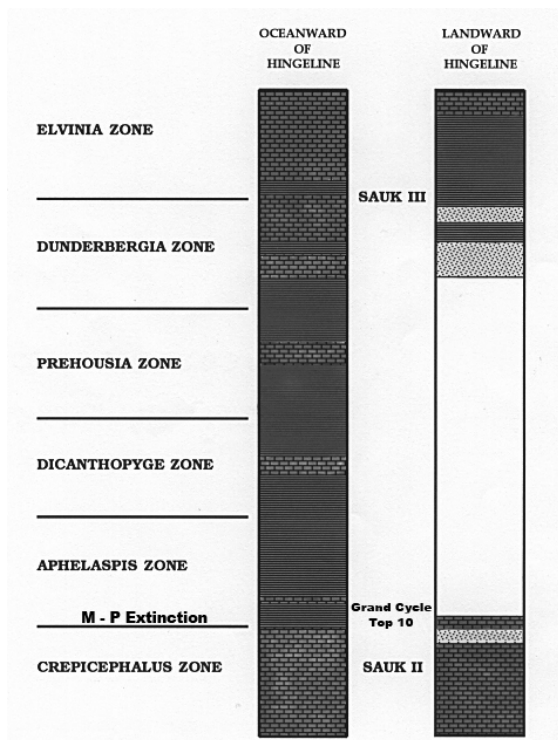


Figure 5. Relationship between sedimentary deposition across the Cordilleran Hingeline and the position of the Marjumiid-Pterocephaliid (M-P) extinction, grand cycle boundary top #10, the Sauk II – Sauk III subsequence boundary and Late Cambrian trilobite zonation in the western United States.

spread unconformity. Oceanward of the Cordilleran Hingeline, the grand cycle boundary correlates with deepening and a conformable transition from carbonate to siliciclastic deposition (Figure 5).

Thomas (1993) concluded that eustatic drop exposed the craton, resulting in a flood of cratonally-derived siliciclastic sediment onto the carbonate platform oceanward of the hingeline. The result was a gradual termination of carbonate production, associated deepening of the shelf and a conformable transition from carbonate to siliciclastic deposition. When the ocean transgressed back onto the craton (over two biozones later), it buried the erosional surface with cratonally-derived siliciclastic sediment (Dry Creek Shale Member of the Snowy Range Formation). This unconformity is the Sauk II – Sauk III subsequence boundary on the craton (see Figure 5; Sloss, 1988; Saltzman et al., 2004).

SERIES	FAUNAL ZONE	BIOMERE	SUBSEQUENCE		
			ocean	craton	
Lower Ordovician	Missisquoia				
	Saukia	Ptychaspid Biomere	<b>Mass Extinction</b>	SAUK III	
Saratogia					
Taenicephalus					
Upper Cambrian	Elvinia	Pterocephaliid Biomere	<b>Mass Extinction</b>	SAUK II	
	Dunderbergia				
	Aphelaspis				
	Crepicephalus			HIATUS	
	Middle Cambrian	Cedaria	Marjumiid Biomere	<b>Mass Extinction</b>	SAUK I
		Bolaspidella			
Bathyriscus-Eltrathina					
Glossopleura		Corynexochid Biomere	<b>Mass Extinction</b>	SAUK I	
Albertella					
Plagiura-Poliella					
Lower Cambrian	Olenellus	Olenellid Biomere			

Figure 6. The five mass extinction events that punctuate the Cambrian faunal sequence in North America (modified from Palmer, 1981).

## CAMBRIAN MASS EXTINCTIONS

The Cambrian section at Beartooth Butte records at least three mass extinction events (Corynexochid-Marjumiid, Marjumiid-Pterocephaliid and Pterocephaliid-Ptychaspid extinctions) that punctuate the rapid evolution of the shelf faunas (Figure 6). Probably the best studied of these mass extinction events is the Marjumiid-Pterocephaliid extinction, which is well exposed at many locations throughout North America, including the spectacular exposure at Beartooth Butte (Thomas, 1993).

The Marjumiid-Pterocephaliid extinction event is recognized by the abrupt disappearance of nearly all of the highly specialized, tropical shelf trilobites, and the subsequent appearance of large numbers of one or two genera of deep-ocean trilobites that migrated onto the shelf after the extinction event (Palmer, 1965). At Beartooth Butte, careful fossil collecting allowed the extinction boundary to be narrowed down to a line in the field, and so this locale, like many others in western North America, provides detailed data about the extinction event horizon.

The proposed mechanisms for Cambrian mass extinctions are varied. Some of the proposed causes include global warming, global cooling, shelf-wide cooling and/or anoxia caused by a rise in the thermocline, habitat loss due to sea-level drop, expansion of the oxygen minimum zone due to sea-level rise, increases in solar radiation, volcanism and anoxia, biofacies shifts and bolide impacts. (Lochman and Duncan, 1944; Palmer, 1965; Öpik, 1966; Lochman-Balk, 1970, 1971; Johnson, 1974; Stitt, 1977; Palmer, 1982; Westrop and Ludvigsen, 1987; Wright et al., 1987; Thomas, 1993, 1995; Saltzman et al., 1995, 1998; Cuggy, 1996; Westrop and Cuggy, 1999; Montanez et al., 2000; Maoyan, 2004; Miller and Evans, 2004; Hough et al., 2005).

Thomas (1993) studied the Marjumiid-Pterocephaliid extinction over the entire shelf in the western United States for his dissertation. The focus of the work was to better understand

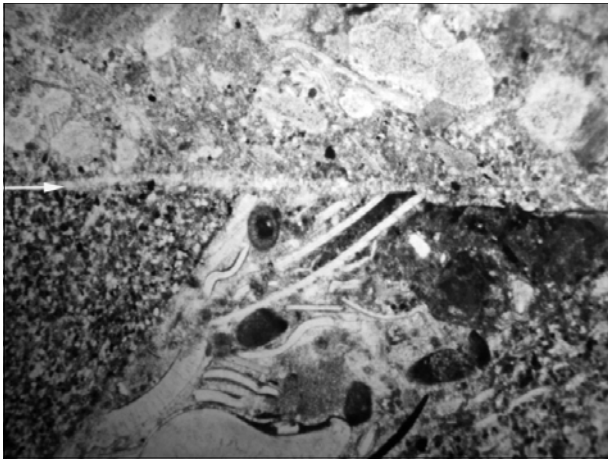


Figure 7. Dissolution surface (white arrow) at the Marjumiid-Pterocephaliid mass extinction boundary (North Fork Grove Creek locality, Montana). Notice the truncated grains. The field of view is approximately 3 cm.



Figure 8. The Marjumiid-Pterocephaliid mass extinction boundary at Beartooth Butte. The head of the hammer is resting on the boundary.

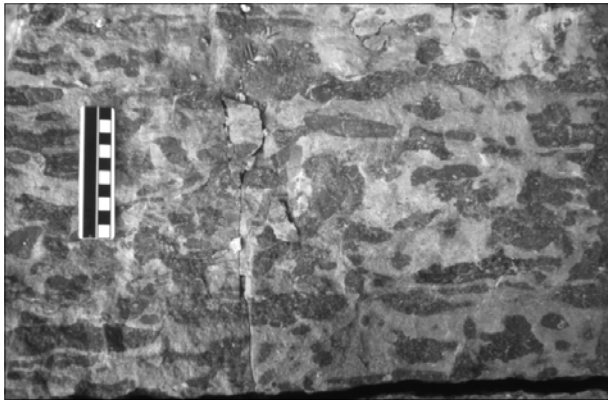


Figure 9. Field photo of oolitic grainstone in the Pilgrim Formation at Beartooth Butte, Wyoming.

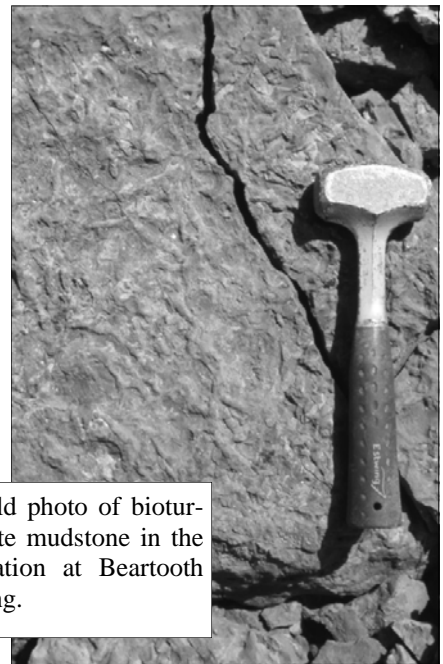


Figure 10. Field photo of bioturbated, carbonate mudstone in the Pilgrim Formation at Beartooth Butte, Wyoming.



Figure 11. Trough, cross-bedded, quartz sandstone in the Pilgrim Formation at Beartooth Butte, Wyoming.



Figure 12. *Aphelaspis* coquinite in the Pilgrim Formation at Beartooth Butte, Wyoming. Field of view is approximately 15 centimeters across.

the paleoenvironmental setting of the extinction event. The results of the work was the discovery that the extinction occurred during the sea-level drop that ultimately resulted in the Sauk II – Sauk III unconformity on the craton (see Figure 5). He concluded that the sea-level drop was a eustatic event related to global cooling, and that the cooling event killed off the warm-water adapted shelf trilobites, while initiating the migration of the cold-water adapted, deep-ocean trilobites onto the shelf.

The cause of global cooling is a difficult problem to resolve. The traditional view is that the Cambrian is an extraordinarily warm period of time with no significant planetary ice (Saltzman et al., 2000). In addition, studies of Pleistocene temperature variations in the tropics show that ocean water remained warm during glacial maxima (Crowley and North, 1991). Seemingly, the only way to cause a global cooling event in the Cambrian is to directly cool the atmosphere, possibly through a reduction in greenhouse gases.

An intriguing and important piece of evidence comes from the extinction boundary itself. It turns out that the extinction boundary can be narrowed down to a line through careful trilobite collecting (including at the Beartooth Butte locality). At all localities on the carbonate platform where the extinction boundary was narrowed down to a line, it coincided with a dissolution surface (Figure 7). In most cases, it can be proven that the dissolution surface formed subaqueously, and was not the result of exposure. This surface indicates that ocean water was more acidic at the time of the extinction. Since cold water tends to be more acidic than warm water, the dissolution surface may indicate oceanic cooling, possibly related to climatic cooling or an incursion of deep, cold water onto the platform (Wilde et al., 1990; Glumac et al., 1998; Perfetta et al., 1999).

It is unlikely that deep, cold water moved across the carbonate platform, because the platform was shallowing on the cratonal side of the Cordilleran Hingeline at the time of the extinction. It is more likely that the atmosphere

cooled, possibly due to a reduction in atmospheric carbon dioxide. The carbonate platforms were major sinks for atmospheric carbon dioxide in the Cambrian. They grew larger during times of marine transgression and absorbed progressively more atmospheric carbon dioxide with growth. It is possible that enough CO<sub>2</sub> was absorbed by the carbonate platforms to cause a CO<sub>2</sub> minimum crisis in the atmosphere with a resulting global cooling of ocean water, increased ocean acidity and possibly even eustatic sea-level drop if glaciers formed in the process.

Conversely, data collected from global oceanic surface water during the 21st century indicate that ocean acidification is occurring in association with global warming, not global cooling (Orr et al., 2005). As the anthropogenic carbon dioxide concentrations increase, oceanic pH is going down, causing the carbonate ion concentration to go down as well. Evidence shows that ocean acidification is having a negative impact on calcite and aragonite-secreting organisms. By comparison, a non-anthropogenic increase in atmospheric CO<sub>2</sub> during the Cambrian might have produced lethal levels of oceanic acidification and left a dissolution surface at the Marjumiid-Pterocephaliid extinction boundary as evidence of the environmental change. Whatever caused this extinction the dissolution surface at the boundary must be accounted for in the model.

The Marjumiid-Pterocephaliid extinction boundary at Beartooth Butte is an excellent place to see evidence for environmental change at the time of the extinction (Figure 8). Well before the extinction, as represented by 10s of meters of strata, shallow-shelf organisms lived in well-circulated, subtidal carbonate platform environments that are now represented by deposits of oolitic grainstone and bioturbated mudstone in the Pilgrim Formation (Figures 9 and 10). Within approximately 1.0 meter of the extinction boundary, trough-cross-bedded quartz sandstone and peloidal grainstone is dominant (Figure 11). The influx of quartz sand is evidence for the encroachment of the cratonal shoreline due to eustatic drop at the time of the extinction.

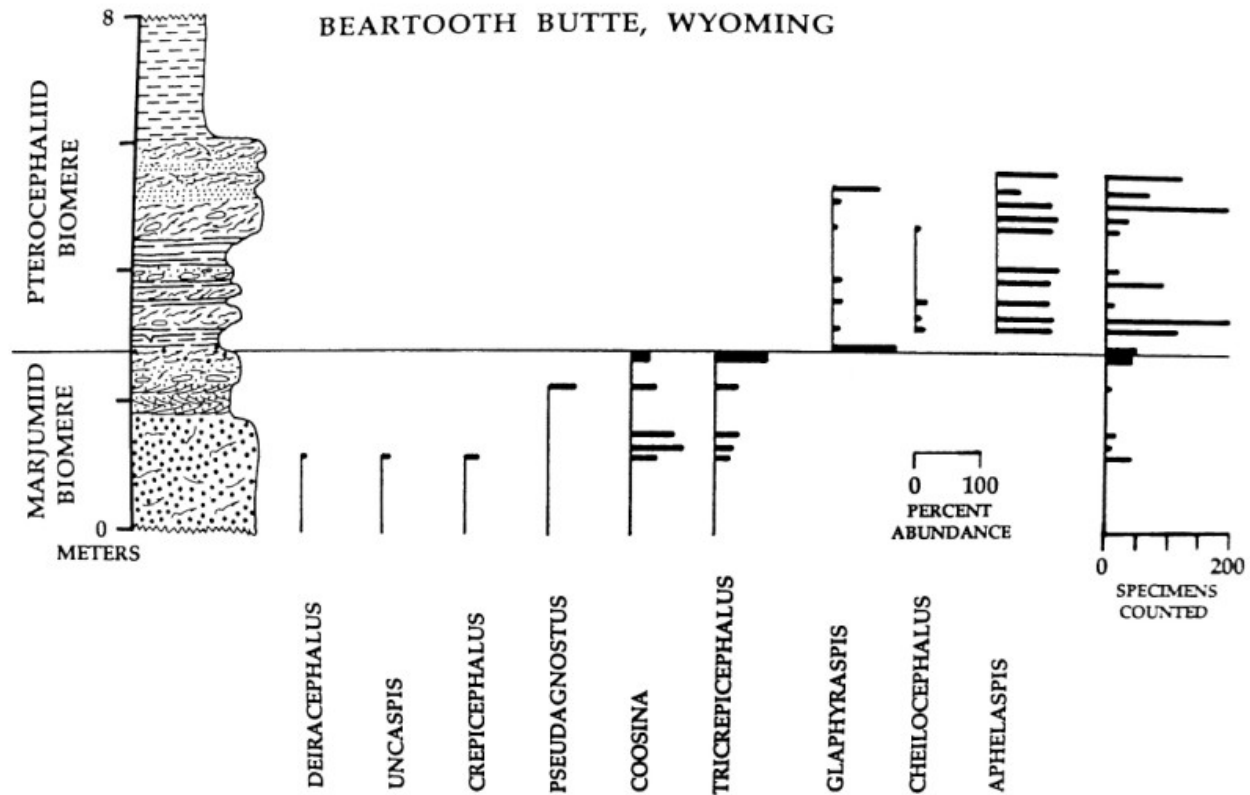


Figure 13. Biostratigraphic range chart showing the occurrence and abundance of trilobite genera across the Marjumiid-Pterocephaliid extinction boundary at Beartooth Butte.

Following the extinction, carbonate platform deposition continued for a short period of time (represented by about 3.0 meters of strata), but the deposits changed from healthy, subtidal environments to unhealthy, shallow, restricted, peritidal environments. These peritidal environments are represented by mud-cracked, peloidal grainstone, quartz sandstone and siltstone, and storm deposited beds of *Aphelaspis* coquinite (Figure 12) that were deposited as the shelf continued to shallow prior to the exposure of the North American craton.

The faunal changes at Beartooth Butte also indicate deteriorating environmental conditions at the time of the extinction. The biostratigraphy at this locale (primarily trilobites) shows a gradual die-off of the well-established shelf faunas prior to the extinction boundary. This is most likely due to changing environments that would no longer sustain organisms adapted to well-circulated shelf conditions. Post extinc-

tion, invading trilobites from off-shelf environments take over the empty niche spaces on the shelf and survive in large numbers. The success of the invading trilobites is shown by the large number of body fossils of a small number of trilobite species in the deposits immediately after the extinction (Figure 13).

The overlying Dry Creek Shale Member of the Snowy Range Formation consists of tan, fissile siltstone that was deposited in subtidal, siliclastic shelf environments as the sea transgressed over the eroded carbonate platform (Figure 14). Fossils found in the basal beds of the Dry Creek Shale near Red Lodge, Montana indicate that transgression occurred in this area during *Dunderbergia* Zone time (Thomas, unpublished data), which is approximately 2.5 biozones younger than the uppermost beds of the Pilgrim Formation. The biostratigraphic data argue for an unconformity between the Pilgrim Formation and the Dry Creek Shale,



Figure 14. Subtidal siltstone in the basal part of the Dry Creek Shale Member of the Snowy Range Formation.

probably as a result of sea-level drop that eventually exposed the carbonate platform. At Bear-tooth Butte, the basal bed of the Dry Creek Shale consists of a glauconitic, carbonate rudstone composed of pebbles of Pilgrim Limestone. This is likely a basal lag deposited on the unconformity between the Pilgrim Formation and the Dry Creek Shale Member of the Snowy Range Formation.

As sea-level continued to rise during the deposition of the Snowy Range Formation, a carbonate platform formed as sea level rise moved the source of land-derived sediment far enough away for carbonate production to begin once again (Sage and Grove Creek Members of the Snowy Range Formation). The Sage Member contains a good exposure of the Pterocephaliid-Ptychaspid extinction boundary at Bear-tooth Butte, which was studied in detail by Dave Backus (Backus, 1994). The Cambrian-Ordovician boundary, which is another mass extinction boundary, has been removed at Bear-tooth Butte by erosion, and so Middle and Upper Ordovician dolostone of the Big Horn Dolomite rest unconformably on the Snowy Range Formation.

## ACKNOWLEDGMENTS

The section at Bear-tooth Butte was measured, described and collected by the author and his field assistant, Jason Paur, during the summer of 1990. I am grateful to Jason, who was an undergraduate student at the University of Washington at the time, for braving the mosquitoes and lightning storms to get the job done. The graph showing the stratigraphy of Bear-tooth Butte (Figure 4) was provided by Dick Gibson.

## REFERENCES CITED

- Aitken, J.D., 1966, Middle Cambrian to Middle Ordovician cyclic sedimentation, southern Rocky Mountains of Alberta: *Canadian Petroleum Geologists Bulletin*, v. 14, p. 405-441.
- Aitken, J.D., 1978, Revised models for depositional grand cycles, Cambrian of the southern Rocky Mountains, Canada: *Canadian Petroleum Geologists Bulletin*, v. 26, p. 515-542.
- Aitken, J.D., 1981, Generalizations about grand cycles, in Taylor, M.E., ed., *Short papers for the second international symposium on the Cambrian System: U.S. Geological Survey Open-File Report 81-743*, p. 8-14.
- Backus, D.H., 1994, The sedimentological record at the Pterocephaliid-Ptychaspid biomere boundary: Implications for Upper Cambrian extinction events: Master's thesis, University of Washington, Seattle, 49 p.
- Bryant, W.L., 1932, Lower Devonian facies of the Bear-tooth Butte, Wyoming: *Proceedings of the American Philosophical Society*, v. 71, p. 225-254.
- Chow, N., and James, N.P., 1987, Cambrian grand cycles: a northern Appalachian perspective: *Geological Society of America Bulletin*, v. 98, p. 418-429.
- Crowley, T.J., and North, G.R., 1991, *Paleoclimatology*: Oxford Univ. Press, New York, 339 p.
- Cuggy, M.B., 1996, Patterns of faunal change at an Upper Cambrian trilobite extinction event, Nolichucky Formation, Tennessee and Virginia: Master's thesis, Brock University, Saint Catharines, ON, 142 p.

- Dorf, Erling, 1934, Lower Devonian flora from Bear-tooth Butte, Wyoming: Geological Society of America Bulletin, v. 45, p. 425-440.
- Glumac, B., and Walker, K.R., 1998, A Late Cambrian positive carbon-isotope excursion in the southern Appalachians: Relation to biostratigraphy, sequence stratigraphy, environments of deposition, and diagenesis: Journal of Sedimentary Research, v. 68, n. 6, p. 1212-1222.
- Hough, M., Shields, G.A., Strauss, H., Evins, L.Z., Henderson, R.A., and Mackenzie, S., 2005, Linking Cambrian volcanism to marine anoxia and mass extinction; clues from sulphur isotope geochemistry: Geological Society of Australia program and abstracts, v. 81, p. 50.
- James, H.L., 1995, Geologic and historic guide to the Beartooth Highway, Montana and Wyoming: Montana Bureau of Mines and Geology Special Publication 110, 134 p.
- Johnson, J.G., 1974, Extinction of perched faunas: Geology, v. 2, p. 479-482.
- Lochman-Balk, C., 1970, Upper Cambrian faunal patterns on the craton: Geological Society of America Bulletin, v. 81, p. 3197-3224.
- Lochman-Balk, C., 1971, The Cambrian of the Craton of the United States: *in* Holland, C.H., ed., Cambrian of the New World: John Wiley and Sons, Ltd., p. 79-167.
- Lochman-Balk, C., and Hu, C.H., 1960, Upper Cambrian faunas from the northwest Wind River Mountains, Wyoming Pt. 1: Journal of Paleontology, v. 34, p. 793-834.
- Lochman, C., 1957, Paleocology of the Cambrian in Montana and Wyoming: Geological Society of America Memoir, no. 67, v. 2, p. 117-162.
- Lochman, C., and Duncan, D., 1944, Early Upper Cambrian faunas of central Montana: Geological Society of America Special Paper, no. 54, 181 p.
- Lohmann, K.C., 1977, Causative factors of the outer detrital belt House embayment--A sedimentologic examination of a terrigenous-carbonate depositional system, early Upper Cambrian (Dresbachian), east-central Utah and west-central Nevada: Ph.D. thesis, State University of New York, Stony Brook, 301 p.
- Maoyan, Z., Junming, Z., Guoxiang, L., and Aihua, Y., 2004, Evolution of C isotopes in the Cambrian of China; implications for Cambrian subdivision and trilobite mass extinctions: Geobios, v. 37, p. 287-301.
- Miller, J.F., and Evans, K.R., Appearances and extinctions of Upper Cambrian-Lower Ordovician species commonly coincide with sequence-stratigraphic boundaries: Geological Society of America Abstracts with Programs, v. 36, p. 165.
- Montanez, I.P., Osleger, D.A., Banner, J.L., Mack, L.E., and Musgrove, M., 2000, Evolution of the Sr and C isotope composition of Cambrian oceans: GSA Today, v. 10, n. 5, p. 1-7.
- Mount, J.F., and Rowland, S.M., 1981, Grand cycle A (Lower Cambrian) of the southern Great Basin: A product of differential rates of relative sea-level rise: *in* Taylor, M.E., ed., Short papers for the Second International Symposium on the Cambrian System: U.S. Geological Survey Open-File Report, no. 81-743, p. 160-162.
- Öpik, A.A., 1966, The early Upper Cambrian crisis and its correlation: Royal Society of New South Wales Journal and Proceedings, v. 100, p. 9-14.
- Orr, J.C., Fabry, V.J., Aumont, O., Bopp, L., Doney, S.C., Feely, R.A., Gnanadesikan, A., Gruber, N., Ishida, A., Joos, F., Key, R.M., Lindsay, K., Majer-Reimer, E., Matear, R., Monfray, P., Mouchet, A., Najjar, R.G., Plattner, G.K., Rodgers, K.B., Sabine, C.L., Sarmiento, J.L., Schlitzer, R., Slater, R.D., Totterdell, I.J., Weirig, M.F., Yamanaka, Y., and Yool, A., 2005, Anthropogenic ocean acidification over the twenty-first century and its impact on calcifying organisms: Nature, v. 437, p. 681-686.
- Osleger, D.A., and Read, J.F., 1991, Relation of eustasy to stacking patterns of meter-scale carbonate cycles, Late Cambrian, U.S.A.: Journal of Sedimentary Petrology, v. 61, p. 1225-1252.
- Palmer, A.R., 1960, Some aspects of the Upper Cambrian stratigraphy of White Pine County, Nevada and vicinity: Intermountain Association of Petroleum Geologists, Eastern Nevada Geological Society Guidebook, 11th Annual Joint Field Conference, p. 53-58.
- Palmer, A.R., 1965, Biomere, a new kind of biostratigraphic unit: Journal of Paleontology, v. 39, p. 149-153.

- Palmer, A.R., 1981, On the correlatability of grand cycle tops: *in* Taylor, M.E., ed., Short papers for the Second International Symposium on the Cambrian System: U.S. Geological Survey Open-File Report, no. 81-743, p. 156-159.
- Palmer, A.R., 1982, Biome boundaries: a possible test for extraterrestrial perturbations of the biosphere.: *in* Silver, L.T., and Schultz, P.H., eds., Geologic implications of impacts of large asteroids and comets on the earth: Geological Society of America Special Paper, no. 190, p. 469-476.
- Palmer, A.R., and Halley, R.B., 1979, The physical stratigraphy and biostratigraphy of the Lower and Middle Cambrian Carrara Formation in the southern Great Basin (western United States): U.S. Geological Survey Professional Paper, no. 1047, 131 p.
- Palmer, A.R., and Rowland, S., 1989, Early Cambrian stratigraphy and paleontology, southern Great Basin, California-Nevada: *in* Taylor, M.E., ed., 1989, Cambrian and Early Ordovician stratigraphy and paleontology of the Basin and Range Province, western United States: Field Trip Guidebook T125, 28th International Geological Congress, American Geophysical Union, Washington, D.C., p. 17-27.
- Perfetta, P.J., Shelton, K.L., and Stitt, J.M., 1999, Carbon isotope evidence for deep-water invasion at the Marjumiid-Pterocephaliid biome boundary, Black Hills, USA: A common origin for biotic crises on Late Cambrian shelves: *Geology*, v. 27, p. 403-406.
- Poldervaart, A., and Bentley, R.D., 1958, Precambrian and later evolution of the Beartooth Mountains, Montana and Wyoming: Billings Geological Society Guidebook, p. 7-15.
- Saltzman, M.R., Davidson, J. P., Holden, P., Runnegar, B., and Lohmann, K.C., 1995, Sea-level-driven changes in ocean chemistry at an Upper Cambrian extinction horizon: *Geology*, v. 23, p. 893-896.
- Saltzman, M.R., Runnegar, B., and Lohmann, K.C., 1998, Carbon isotope stratigraphy of Upper Cambrian (Steptean Stage) sequences of the eastern Great Basin: Record of a global oceanographic event: *Geological Society of America Bulletin*, v. 110, n. 3, p. 285-297.
- Saltzman, M.R., Ripperdan, R.L., Brasier, M.D., Lohmann, K.C., Robison, R.A., Chang, W. T., Peng, S., Ergaliev, E.K., and Runnegar, B., 2000, A global carbon isotope excursion (SPICE) during the Late Cambrian: relation to trilobite extinctions, organic-matter burial and sea level: *Palaeogeography, Palaeoclimatology, Palaeoecology*, v. 162, no. 3, p. 211-223.
- Saltzman, M.R., Cowan, C.A., Runkel, A.C., Runnegar, B., Stewart, M.C., and Palmer, A.R., 2004, The Late Cambrian Spice Event and the Sauk II-Sauk III regression: New evidence from Laurentian basins in Utah, Iowa, and Newfoundland: *Journal of Sedimentary Research*, v. 74, p. 366-377.
- Sepkoski, J.J., Jr., 1977, Dresbachian (Upper Cambrian) stratigraphy in Montana, Wyoming and South Dakota: Ph.D. thesis, Harvard University, Boston, Massachusetts, 505 p.
- Sloss, L.L., 1963, Sequences in the cratonic interior of North America: *Geological Society of America Bulletin*, v. 74, p. 93-114.
- Sloss, L.L., 1988, Tectonic evolution of the craton in Phanerozoic time: *in* Sloss, L.L., ed., *Sedimentary Cover-North American Craton*; U.S.: Geological Society of America, The Geology of North America, v. D-2, p. 83-107.
- Stitt, J.H., 1977, Late Cambrian and earliest Ordovician trilobites, Wichita Mountains area, Oklahoma: *Oklahoma Geological Survey Bulletin*, no. 124, 79 p.
- Tetlie, E.O., 2007, Like father, like son? Not amongst the Eurypterids (Chelicerata) from Beartooth Butte, Wyoming: *Journal of Paleontology*, v. 81, no. 6, p. 1423-1431.
- Thomas, R.C., 1992, The utility of Cambrian mass extinction boundaries for the correlation of grand-cycle boundaries: *Geological Society of America Abstracts with Programs*, v. 24, p. 65.
- Thomas, R.C., 1993, The Marjumiid-Pterocephaliid (Upper Cambrian) mass extinction event in the Western United States: Ph.D. thesis], University of Washington, Seattle, 352 p.
- Thomas, R.C., 1995, Cambrian mass extinction ("biome") boundaries: A summary of thirty years of research: *Northwest Geology*, v. 24, p. 67-75.
- Thomas, R.C., 2007, A field guide to the Cambrian section at Camp Creek, southwest Montana: *in* Tho-

mas, R.C., and Gibson, R.I., eds., Introduction to the Geology of the Dillon Area: Northwest Geology, v. 36, p. 231-244.

Vail, P.R., Mitchum, R.M., Jr., and Thompson, S., 1977, Seismic stratigraphy and global changes of sea level, Part 4: Global cycles of relative changes in sea level: *in* Payton, C.E., ed., Seismic stratigraphy - applications to hydrocarbon exploration: American Association of Petroleum Geologists Memoir, no. 26, p. 83-97.

Westrop, S.R., 1989, Facies anatomy of an Upper Cambrian grand cycle: Bison Creek and Mistaya formations, southern Alberta: Canadian Journal of Earth Science, v. 26, p. 2292-2304.

Westrop, S.R., 1992, Upper Cambrian (Marjuman-Steptoean) trilobites from the Port Au Port Group, western Newfoundland: Journal of Paleontology, v. 66, p. 228-255.

Westrop, S.R., and Ludvigsen, R., 1987, Biogeographic control of trilobite mass extinction at an Upper Cambrian "biomere" boundary: Paleobiology, v. 13, p. 84-99.

Westrop, S.R., and Cuggy, M.B., 1999, Comparative paleoecology of Cambrian trilobite extinctions: Journal of Paleontology, v. 73, n. 2, p. 337-354.

Wilde, P., Quimby-Hunt, M.S., Berry, W.B.N., 1990, Vertical advection from oxic or anoxic water from the main pycnocline as a cause of rapid extinction or rapid radiations: *in* Kauffman, E.G., and Walliser, O.H., eds., Extinction events in Earth history: Berlin, Springer-Verlag, p. 85-97.

Wright, J., Miller, J.F., and Holser, W.T., 1987b, Conodont chemostratigraphy across the Cambrian-Ordovician boundary: western U.S.A. and southeast China: *in* Austin, R.L., ed., Conodonts, investigative techniques and applications: Chichester, England, Ellis Horwood Limited, p. 256-283.

